University of Southampton

Space Charge Measurement in Polymer Insulated Power Cables Using the PEA Method

By

Mingli Fu

A thesis submitted for the Degree of

Doctor of Philosophy

In

The Department of Electronics and Computer Science

April 2002

UNIVERSITY OF SOUTHAMPTON

DEPARTMENT OF ELECTRONICS AND COMPUTRER SCIENCE

Doctor of Philosophy

SPACE CHARGE MEASUREMETN IN POLYMER INSUALTED POWER CABLES USING THE PEA METHOD

By Mingli Fu

Abstract

The Pulsed Electro-Acoustic (PEA) technique has been widely used to measure space charge distribution in solid dielectrics. A considerable amount of work has been done on the charge dynamics in plaque samples. Recently, there have been several attempts to apply the technique to polymeric power cables, but it has been hampered by experimental difficulties in achieving a universal electrode system to maintain an intimate contact between the curved ground electrode, transducer and absorber.

In this research, a modified system employing a flat ground electrode, transducer and acoustic absorber has been introduced. By thoroughly analysing the propagation of the acoustic pressure in the new electrode arrangement, it is concluded that the revised electrode system will give the same detection sensitivity and spatial resolution as that of the old version. The new PEA system not only achieves an intimate contact acoustically but also has advantages of easy assembly of cable sample and is suitable for different sizes of cables without any modification.

The basic principle of space charge measurement in cable geometry with the new system is fully outlined. To remove the influences of the geometry factor, the acoustic propagation attenuation and dispersion through the polymer material, a compensation algorithm has been developed to improve the measurement accuracy both on charge density and position.

A comprehensive program with the functions of data acquisition, deconvolution of original signal, calibration and compensation both to geometry and propagation factors has been developed in the LabView^{TM} environment. The method to calculate the electric stress distribution from the results of the space charge profile in cable geometries has been proposed.

For practical application, space charge distribution measurements were carried out on several prototype cable samples which adopt modified XLPEs (undegassed and degassed) as insulating materials. The comparisons were conducted on both the space charge accumulation and its influence on the electric stress distribution. The results showed that the modification to the XLPE material is profitable from the point of view of space charge suppression. Moreover, the thermal treatment to the sample showed that the removal of the volatile residue had a significant influence on the space charge behaviour.

To study the effects of the modification of the XLPE and its residual impurities on the space charge accumulation, a PEA system capable of measuring the space charge distribution in thick plaque samples was built. Space charge measurements were carried out on different XLPE samples and with a variety of residue contents.

In the voltage polarity reversal operation of a dc system, the previously accumulated stationary space charge may not promptly respond to the polarity inversion. This situation may result in a very complex electric stress distribution and raise the risk of insulation failure due to the localised electric stress being too high. The space charge evolution during and after the voltage polarity reversal was experimentally studied in two commercial XLPE cables.

Finally, reasons were sought experimentally for the sheet charge at the outer surface of the semiconducting sheath and the shift of the peak of induced charge at inner interface. Some appropriate measures have been suggested to eliminate their effects.

Content

Acknowledgements

I would like to thank Dr George Chen for his guidance, support and encouragement throughout the whole process of this work, without which the completion of this thesis would be impossible. My gratitude must also go to Professor Tony Davies for providing me this precious opportunity to do research in the High Voltage Laboratory and for his supervision in every part of this project.

My thanks also go to my colleagues in the group, particularly Mr Roland Caldecutt, Mr Neil Palmer and Mr Richard Howell for the invaluable assistance in the technical work. The frequent and helpful discussion from Mr Mathew Brown and Fred Ho is highly appreciated.

I would like to acknowledge Pirelli Cables UK and Italy for the financial and material support to the project. I am indebted to Mr. Julian Head and Dr. Gabriele Perego, all of them with Pirelli Cables, for their invaluable advice and discussion throughout the project. I would also particularly like to thank my friend Prof. Denys Mead who have carefully read and revised my thesis.

I am most grateful to my wife Shuping and my daughter Angela (Anqi) for their love, encouragement and patience throughout the duration of my study in UK.

All of the members in the group were shocked by Roland's sudden death just at the moment when this thesis was nearly completed. His contribution to the research is highly appreciated.

List of Symbols and Abbreviations

Symbols

A	Richardson-Duchman constant
A_1, A_2	Capture and excitation constants of an electron at trap site
a	Inner radius of cable insulation
b	Outer radius of cable insulation
C	Capacitance of coupling capacitor bank of the pulsed voltage
C_p	Acoustic transducer's capacitance
d	The thickness of the transducer
E	Electric stress
$E(a)$, $E(b)$	Electric stress at the inner and outer interface of the cable insulation
$E_{total}(r)$	Total electric stress distribution
$E_{applied}(r)$	Externally applied electric stress distribution (space charge free)
$E_{charge}(r)$	Electric stress distribution due to space charge
E_g	Band gap
$e_p(t, r)$	Pulsed electric stresses distribution across the cable insulation
f	Frequency
$f(t, a)$, $f(t, b)$	Pulsed forces acting on the charge layers at inner and outer interfaces of cable sample
G	The gain of the electronic amplifier
$H(\omega)$	The transfer function of whole PEA system for cable geometry
$h(t)$	The unit impulse response of a continuous system
J	Electrical current density in the dielectric material
K_1, K_2	The coefficients of acoustic wave at inner and outer interfaces of cable sample propagating towards the transducer, in XLPE cable with polymer semiconducting layer, they are 0.5

K_3, K_4, K_5	The transmission coefficients of acoustic wave at the interfaces of insulation/semi-con, semi-con/ground electrode and ground electrode/transducer, in XLPE cable with polymer semiconducting layer, $K_3=2K_1=2K_2=1$
k	The piezoelectric strain constant of the transducer
k	Boltzmann constant, 8.62×10^{-5} eV/K
k	Wave number of the acoustic pressure wave
N_t	Trap concentration in the dielectric
n_t	The concentration of filled traps in the dielectric
n	The number of free electrons in the dielectric
$P(\omega)$	Acoustic pressure wave in frequency domain
p	Electric stress coefficient of conductivity
$p_a(t)$	Pressure wave generated by induced charge at a
$p_b(b)$	Pressure wave generated by induced charge at b
$p_s(t)$	Pressure wave generated by space charge in the bulk material
p_i	Incident pressure wave at the interface
p_r	Reflected pressure wave from the interface
P_t	Transmitted pressure wave through the interface
$p(t)$	The total pressure generated by space charge and induced surface charge
$q(t)$	Induced charge on the surface of transducer due to piezoelectric effect
R_a	The resistive input impedance of the amplifier
r	The radius of the cable insulation
S	The area of the transducer
T	Temperature
ΔT	The width of the pulsed voltage
t	Time
U	Electric potential
$U_{applied}$	External applied voltage
$u(t)$	Step function
u_{sa}	The velocity of the acoustic wave propagation in the dielectric
u_p	The velocity of the acoustic wave propagation in the transducer

τ_a	Acoustic wave time constant of the transducer, $\tau_a=d/u_p$
τ_e	Time constant of the high pass filter, $\tau_e=R_aC_p$
ω	Angular frequency, $\omega=2\pi f$

Abbreviations

Al	Aluminium
AC or ac	Alternating current
DC or dc	Direct current
DCP	Dicumyl peroxide
HDPE	High density polyethylene
HVDC	High voltage direct current
GPIB	General purpose interface board
LDPE	Low density polyethylene
LIMM	Laser intensity modulation method
LIPP	Laser induced pressure pulse
PE	Polyethylene
PEA	Pulsed electro-acoustic
PIPS	Piezoelectrically induced pressure step
PMMA	Polyethyl methacrylate
PVDF	Polyvinylidene fluoride
PWP	Pressure wave propagation method
SCLC	Space charge limited conduction
TSC	Thermally stimulated current
TSL	Thermally simulated luminescence
XLPE	Cross-linked polyethylene

Chapter 1

Introduction

1.1 Research background

Nowadays, a considerable amount of transmission and distribution of electricity, especially in urban areas, is carried out by means of underground power cables. Growing public awareness of environmental issues and the need to maintain a highly reliable system have led to polymeric materials progressively replacing oil impregnated paper insulation in underground cables. On the other hand, with large energy pools and separate load centres, the control of the large reactive power becomes difficult in alternating current (ac) underground transmission system. Owing to the absence of periodic charging current with direct voltage, high voltage direct current (hvdc) cable would be an attractive option and could play an increasingly important role in direct current (dc) transmission links. Therefore, dc transmission by cables is not only frequently applied in cross-channel project, but also may be expected to take place in inland schemes where the greater utility of underground cables is required whilst the use of overhead lines are increasingly restricted because of the amenity consideration. Furthermore, the ease of fault current control and low dielectric loss are other merits in comparison with the alternating current system [1]. This renewed interest in high voltage dc transmission has led to many manufacturers worldwide investing in dc polymeric power cable development.

Among the polymeric materials used as insulation both in ac and dc power cables, the most prominent has been polyethylene (PE), either pure or its cross-linked form (XLPE). This is due to their high dielectric strengths and electrical resistivities

combined with some good physical properties, such as resistance to cracking and moisture penetration [2].

However, under certain operating conditions, their good electrical insulation properties may become degraded. For example, trapped or low mobility electrically charged species within the bulk could give rise to space charges. This is particularly true when the dielectric is subjected to a dc stress. If some space charge is formed in the extruded insulation of a polymer power cable, the electric stress distribution may be greatly distorted. This can result in localised electric stress enhancement leading to premature failure of the cable at stresses well below the anticipated or designed values. Prediction by conventional numerical techniques (e.g. finite element) of the trapped charge and subsequent stress distributions only give limited information. Although the models of charge mobility, transportation and trapping phenomena have also been established [3] lack of information on realistic parameters has limited their application in practice. Therefore, there is a need for a better understanding of space charge accumulation characteristics in polymeric materials under dc electric stresses.

For these reasons, space charge measurement has attracted the attention of many researchers over the past two decades, and several new techniques based on the acoustic wave propagation through the material have been developed for non-destructive measurement of both the location and the density of space charge in dielectrics. They are the pressure wave propagation method (PWP), the laser induced pressure wave propagation method (LIPP) and pulsed electro-acoustic method (PEA). Among them, the PEA technique is the most commonly used method because of its lower cost and satisfactory sensitivity and resolution [4-6].

Until now, a considerable amount of research has been concentrated not only on developing the detecting technique but also on studying the mechanism of space charge formation, migration and accumulation in sheet samples. Fruitful results have consequently been achieved [7-20]. After several years of successful space charge research in film samples, attempts had been made to apply these techniques (particularly the PEA method) to measure space charge in extruded polymeric insulation power cables [21-24]. However, the step of moving on from planar to cable geometry systems has shown up some problems with the PEA technique and the associated signal processing. This has hindered its application in practice both in industry and academia. Firstly, in all studies on cable samples, a curved ground electrode, transducer and absorber have been used in the PEA system. This

configuration is problematic due to the difficulty of obtaining good acoustic contact at the interfaces between the following different media, the outer sheath of the cable sample, the ground electrode, the transducer and the acoustic absorber block. This arrangement limits itself to a particular cable size. Obviously, the modification of the system for various cable diameters is complex and the assembly of the apparatus and sample is time consuming.

Secondly, for a full sized cable sample, the attenuation and dispersion of acoustic wave propagation through the cable insulation due to the lossy and dispersive properties of polymeric material may be significant and is no longer negligible if a more accurate measurement result is required. Additionally, the cylindrical geometry of the cable causes a variation on the pulsed electric stress distribution throughout the insulation thickness and the divergence of the acoustic pressure wave intensity when it travels along the radial direction from the inside part of the cable insulation. All these effects of the material and the geometry can impair the measurement of the space charge distribution in charge density and position resolution. This influence depends on the cable size and structure. To ensure an accurate measurement of the space charge distribution, these factors have to be considered in the data processing.

Thirdly, the electric stress enhancement due to the space charge accumulation plays a key role in electrical failure of the cable insulation. However, the method of calculating the electric stress across the cable insulation on the basis of the space charge distribution is not so far available. A literature review reveals that the main attention has been placed only on the electric stress at the interface. The interfacial stress variation under different ageing conditions has been extensively discussed in relation to the space charge [21, 24]. It is obviously true that the interfacial stress can be easily obtained from the induced charge density at the interface of insulation and electrode, and it is also important in the situation where a heterocharge appears in the sample as the electric stress at the interface is strengthened. On the other hand, it may also be possible for the maximum electric stress to appear in the bulk insulation in the case of homocharge or packet charge formation somewhere in the central part of the insulating material. Therefore, it may be meaningful to obtain the detailed electric stress distribution across the cable insulation from the space charge measurement.

The principle objective of the research is to solve the previously mentioned problems in space charge measurement in cable geometry both by introducing a flat electrode design and a proper signal and data processing algorithm.

Thanks to the extensive research on space charge phenomena in polymer materials, several modifications have been made to the XLPE for the purpose of suppressing the space charge accumulation. The effectiveness of these attempts needs to be tested both on cable samples and thick plaque samples.

1.2 Project overview

The above mentioned issues concerned with the space charge detection in different cable geometries have been fully taken into account and the following objectives have been achieved:

- A modified PEA system was built employing a flat ground electrode, transducer and absorber, enabling the space charge distribution for different sizes of polymer insulated cables to be measured. A theory has been developed for the modified PEA system and experimental results have validated the system;
- A data processing algorithm has been developed to obtain a true representation of space charge distribution across the thickness of the cable insulation. This takes account of the possible errors due to acoustic wave attenuation and dispersion, as well as divergent electric pulse stress and acoustic pressure in coaxial geometry;
- A quantitative appraisal of the electric stress profile across the insulation has been developed, taking the applied stress and the contribution from the space charge into consideration.

Based on the above achievements in advancing techniques of space charge measurement of polymer power cables, space charge distributions in several power cables employing different modified XLPE materials as insulation were measured using the newly modified PEA system. A comparison was made between these cables and the reference cable which had XLPE as insulation, both under fresh and degassed conditions. The results from the aspects of space charge formation and the new electric field strength distribution showed that some of modifications to the XLPE material are preferable in the polymer dc cable insulation.

To closely study the effects of the modification of the material and residue on the space charge characteristics, a group of thick plaque samples made of different types of XLPEs and with a variety of impurity contents were tested to measure the space charge

distribution. The differences in the space charge accumulation amongst the different amended materials are quite significant. The experiment revealed that the residue of the material plays a key role in space charge behaviour.

When the polarity of a dc transmission system is reversed, the space charge formed corresponding to the initial polarity does not change instantaneously to that of the new polarity. This can be very dangerous to the cable insulation because some localised stress may be extremely enhanced. Space charge evolution in the process of voltage conversion was measured in two XLPE cables and their electric stress distributions were correspondingly obtained. The highest stress can reach about 50kV/mm from its applied value of 32kV/mm.

This thesis is divided into 11 chapters with appendices. As fundamental background, the basic concepts concerning with the mechanisms of space charge formation, migration and accumulation in dielectrics (particularly in polymer insulations) is presented in Chapter 2. For a better understanding of the results obtained in the project, the chemical and physical structure of polyethylene (PE) and cross-linked polyethylene (XLPE) are also briefly introduced.

Chapter 3 reviews the techniques of space charge measurement in dielectrics and their applications in plaque and cable samples, including the evolution of the techniques, brief principles of each method and a simple comparison between them. The background of space charge detection in cable samples and current achievements are briefly presented.

A modified PEA system for coaxial samples, which adopts a flat ground electrode, is introduced and the acoustic wave propagation in the new electrode configuration is briefed in chapter 4. The basic principle based on the modified PEA system, and the essential techniques such as the raw signal deconvolution and charge density calibration is fully discussed. Chapter 5 deals with the data processing technique on geometry and acoustic propagation compensation. Chapter 6 details the method to calculate the electric stress distribution from the space charge measurement. An overall program capable of carrying out the above data acquisition and processing algorithm is developed in LabView^{TM} environment. The interface (front panel) and the block diagram of the program are listed in an appendix.

As a practical application of the techniques developed in this thesis, the space charge measurement results in cable samples and thick plaque samples (all made on

different XLPEs) are presented and discussed in chapter 7 and 8. Comparisons are made between different modified materials with different residue contents.

Space charge evolution during and after voltage polarity reversal is experimentally investigated and the results are presented in chapter 9. From the electric stress profile derived from the space charge distribution, very high localised stress has been identified at the moment of the polarity switching.

In chapter 10, some of the problems encountered in the space charge measurement in cable samples, such as the interference peak caused by the pulse voltage at the outer surface of outer semiconducting sheath and the shift of the induced charge at the inner electrode and insulation surface are experimentally studied. Results are presented and discussed.

Finally, the whole project is summarised in chapter 11 and some further work is suggested.

Chapter 2

PE, XLPE Insulation and Space Charge Formation

2.1 Introduction

Space charge is the term given to the electrical charge that becomes trapped within the bulk of a dielectric and can occur as a result of electron beam irradiation [25], or an electric potential application across the insulation sandwiched between two electrodes [26, 27]. In many cases the trapped space charge will be extremely stable and may exist in the dielectric for many months or even longer after the electrodes have been shorted together. A stable charge distribution in a dielectric is of great use in the area of electrets, where the incident pressure will interact with the space charge and cause a current to flow in an external circuit [28]. However, when the space charge is present in high voltage insulation systems (e.g. polymeric insulation in power cables), the electric stress distribution may be greatly distorted. This can eventually result in localised stress enhancement leading to premature failure at stresses well below the anticipated or designed values.

In these two completely different situations, it is desirable to understand the physical processes involved for the purpose of being able to control them. For instance, it may be necessary to obtain long life-time space charge distributions in electrets or, in contrast, to prevent the formation of space charge in insulation materials.

In this chapter, the basic concepts concerning the mechanisms of space charge formation, migration and accumulation in dielectrics, particularly in polymer materials will be presented. As fundamental knowledge, the chemical and physical structure of the most popular polymers used in power cable insulation, polyethylene (PE) and cross-

linked polyethylene (XLPE) are briefly reviewed. Furthermore, other relevant theories are also briefly introduced, such as the conduction of the polymer that is inclusive of ionic and electronic conduction and disassociation of impurity dipoles.

2.2 Polyethylene (PE) and cross-linked polyethylene (XLPE) used in power cables

2.2.1 Chemical and physical structure of polyethylene (PE)

Most of the synthetic high polymers are organic compounds consisting of long, chain-like molecules where repeated molecular units are linked by covalent bonds. A single molecular chain commonly contains a thousand or more repeated units and reaches a total length in excess of 1 μm [29]. Polyethylene is produced from ethylene gas by a process known as "polymerisation", in which the monomer molecules (i.e. CH_2 =CH_2 groups) are linked together to produce the polymer chains. To synthesise a polymer chain the monomer must be at least bi-functional. That means it must be able to react on two sites of the molecules (i.e. bi-functionality of ethylene is achieved by opening the carbon to carbon double bond). Figure 2.1 shows the monomer ethylene and repeated monomer in polyethylene, where "n" is the number of monomer units (i.e. CH_2 -CH_2 groups) in the polymer chain, which is known as the "degree of polymerisation".

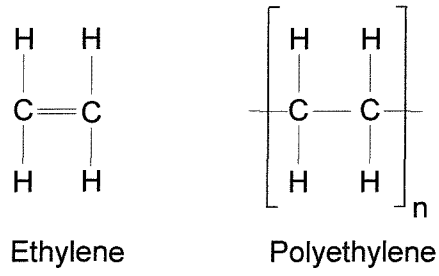

Figure 2.1 Chemical structures of ethylene and polyethylene

These chains run partly parallel to themselves or to other chains, see the illustration in figure 2.2. These parallel regions form the crystalline part of the polymer. For another part of their length, the chains follow an arbitrary path and create amorphous regions. These regions where impurities would accumulate are susceptible to the formation of space charge [30, 31].

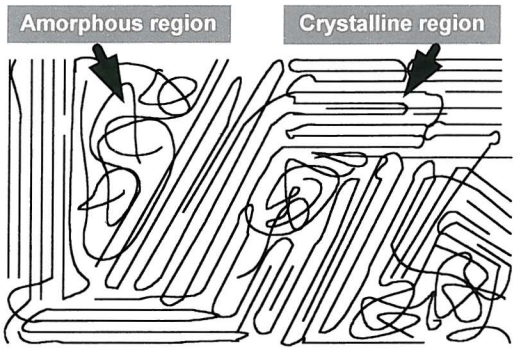

Figure 2.2 Diagram of polymer crystallinity model

The percentage of the volume that is occupied by the crystalline region is called the "crystallinity" or "crystalline ratio", and affects some of the mechanical characteristics of the material, such as density and Young's modulus. The high density of polyethylene is a direct consequence of higher crystallinity, which results in the reduction of the chain branching. Polyethylene with 70-80% crystallinity is called "high-density polyethylene (HDPE)", and its density is around 945-960 kg/m^3. It has fewer and shorter chain branches than "low-density polyethylene (LDPE)" with typically 45-55% crystallinity and a density of 916-930 kg/m^3. Among other physical properties, the melting point of the polymer increases with the crystallinity. The crystalline melting point of polyethylene increases from 110 °C (LDPE) to 130 °C (HDPE) as the density is increased from 916 to 960 kg/m^3 [30].

Generally speaking, the conduction of charges in the amorphous region is far better than that in the crystalline area in polymer material, and the former is likely to collect impurities and traps. There will therefore be more chances for charge carriers being initiated and trapped in the amorphous regions [30, 31].

2.2.2 Evolution of PE for cable insulation

a. LDPE

In the late1930s, low density polyethylene (LDPE) exhibited "a unique combination of electrical and mechanical properties" in power cable insulation, which enabled cables to be light, flexible, clean and easy to install [2]. It was believed that LDPE was an ideal insulating material, because of its exceptionally high intrinsic dielectric strength, low permittivity, negligible dielectric losses, good thermal conductivity and an apparent watertightness, etc.

However, it had quite a low crystalline melting temperature (105 to 115°C), and was sensitive to oxidation, and electrical discharge. It had poor resistance to mechanical and electric stress cracking. Another problem of using LDPE is its high expansion coefficient with increasing temperature.

b. HDPE

The development of HDPE insulated power cable was parallel to that of LDPE with a time lag of 8 to 10 years. HDPE is more difficult to implement than LDPE, but it was still preferred by some manufacturers because of its better mechanical and thermal characteristics. It has a higher crystalline melting temperature (125 to 135°C), which increases the operational temperature of the cable from about 70°C for LDPE to 80°C for HDPE, and 90°C instead of 80°C under short time overloaded conditions [2].

c. XLPE

Despite their excellent electrical properties, their thermoplastic properties have limited the wide use of LDPE and HDPE in power cable insulation. At the end of 1950s, cross-linked polyethylene (XLPE) was developed which had an impact on the extruded polymer insulated power cable industry. Cross-linking results in bridging the molecular chains between carbons and changing the thermoplastic polyethylene into a thermo-set counterpart. Because of this, XLPE conserves some mechanical resistance when it gets hot, enabling the operating temperature of XLPE insulated cables to go to 90°C under steady state conditions, 100 to 105°C or even higher in an emergency, and even to 250°C under short circuit conditions [2].

Moreover the chemical stability and dielectric properties of PE are preserved, as well as its mechanical resistance under cold conditions. The tendency to stress cracking is significantly eliminated. In addition to anti-oxidants, various additives can be introduced in the cross-linking operation to improve some specific properties of XLPE.

2.2.3 Cross-linking processes and byproducts

In fact, XLPE may be considered to be composed of three parts: a cross-linked part, a non-cross-linked part and a part with molecules of lower molecular weight. The cross-linked part has a three-dimensional network structure formed by the curing reaction.

The non-cross-linked part is essentially LDPE. The low molecular weight part includes residual byproducts of the cross-linking process and some additives [32]. XLPE is therefore semi-crystalline and may have a variety of morphologies.

The cross-linking processing of polyethylene is generally finished in two types of chemical reactions; they are Dicumyl peroxide cross-linking process and Silane cross-linking process [33].

Dicumyl peroxide (DCP) is the most widely used peroxide in the cable industry to give fast cross-linking. A fairly low proportion (i.e. about 2.5%) of the peroxide is added to the base polymer. Due to the temperature used for the cable extrusion (between 130 to 150^{O}C), the dicumyl peroxide remains inactive. However, when the temperature is raised to about 180^{O}C the dicumyl peroxide quickly decomposes and initiates the cross-linking reaction.

Another cross-linking process, "Silane cross-linking" proposed by Dow Corning, is progressively replacing the conventional peroxide cross-linking method to manufacture low voltage XLPE cables. This process is classified as a "two component system" for two materials such as cross-linkable graft polymer and a catalyst master batch need to be prepared before the cross-linking process. The two materials are blended together at the fabricating machine and the mixed product is subsequently cross-linked by immersion in water or low-pressure steam.

The cross-linking operation is much more complex than that explained here. However, we are only interested in the by-products which are formed and reside in the material after the manufacturing process. These residues, such as acetophenone, cumyl alcohol, methyl styrene, and methanol together with some extra additives are the main source of space charge formation and accumulation [32-35]. It is also known that DCP cross-linked XLPE contains significantly higher concentrations of byproducts than silane XLPE [33].

2.3 Space charge formation in polymer insulation

When the polymer insulating material is subjected to high electric stress, it tends to become charged and the charges may remain in the material for a certain period of time. These charges or charge carriers can be supplied from the electrodes or can be generated within the bulk of the material. Generally, the charge generation and accumulation can be categorized as in the following process:

- **Injection and extraction**, which controls the emission or extraction of electrons or holes at the polymer/electrode interface. These processes are strongly dependent on the conditions of the interfaces such as materials, surface defects and impurities.
- **Ionisation,** is associated with the electric field assisted dissociation of chemical species such as residues of cross-linking byproducts, additives.
- **Hopping** controls the charge migration within the polymeric bulk insulation.
- **Trapping**, the charges or charge carriers created by the above processes accumulate somewhere within the insulating material. This is dependent on the availability (concentration) of the trapper, the depth and the nature of the trap site inside the bulk of the material.

2.3.1 Homocharge and heterocharge

For the convenience of easy description, the space charge accumulated in insulation materials is often classified as homocharge and heterocharge according to its polarity and the polarity of the adjacent electrode. Homocharge has the same polarity as the electrode, while heterocharge has the opposite polarity of the electrode, as shown in figure 2.3.

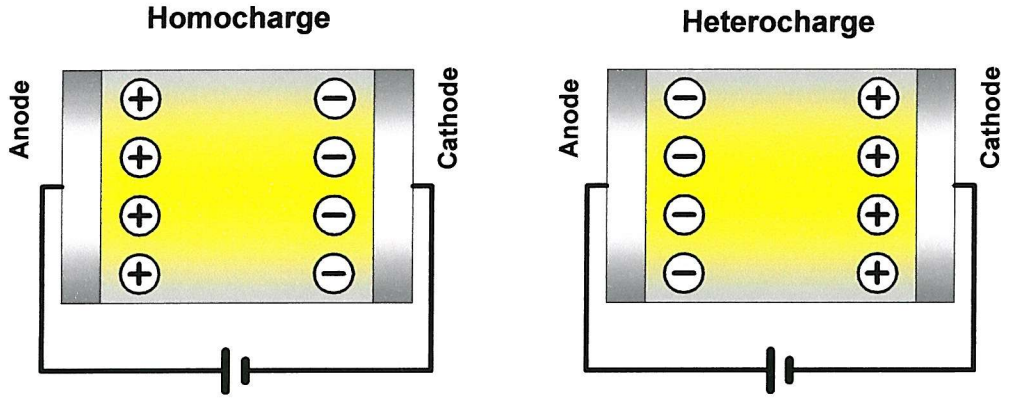

Figure 2.3 Illustration of homocharge and heterocharge near the electrodes

Generally speaking, trapping of an injected charge may form homocharge near the electrodes. Consider a dielectric-metal sandwich system in which electrons can be injected into the dielectric from the cathode. The same argument can also be reasonably applied to positive holes. The consequence of homocharge formation will be to reduce

the interfacial electric stress between the insulation and electrode and enhance the stress in the middle of the sample.

Heterocharge can be generated by field-assisted ionisation of dissociable species in the material. Under the external applied electric stress, negative charges or charge carriers will migrate toward the electrode of opposite polarity (positive) and may become trapped there. In contrast, heterocharge will result in an enhancement of the electric stress at the interfaces and a reduction in the middle of the material.

It should be emphasized that homocharge or heterocharge do not necessarily arise at both electrodes at the same time [31].

2.3.2. Charge injection (surface effect)

Consider now the interface between a metal electrode and a dielectric material. Electrons in the metal are free to move throughout the bulk, but when they reach the surface, they are subjected to a constraint imposed by the noncontinuity of the solid. In order to move beyond the surface, they require excess energy. The work done in removing an electron to infinity is called the work function. With the contact with the dielectric, the potential barrier at the interface will be modified and both electrons (at the cathode) and holes (at the anode) may be injected, depending upon the energy level in the dielectric.

Figure 2.4 shows the typical energy-band diagram for the metal-polymer interface. Under this situation, charge flow will take place so as to equalize the Fermi level of the two materials and will therefore give rise to either a negatively or a positively charged barrier according to the difference between their work functions. Thus the barrier heights or the energy required for electron and hole injection are

$$\phi_e = \phi_m - \chi \tag{2.1}$$

and

$$\phi_h = E_g - \phi_m + \chi \tag{2.2}$$

where ϕ_m is the work function of metal electrode, and χ is the electron affinity of polymer, and E_g is the band gap.

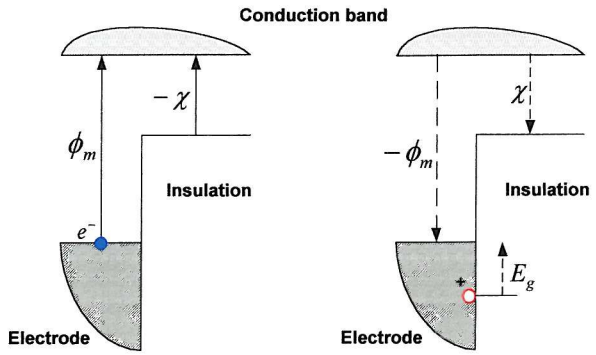

Figure 2.4 Potential barriers between metal electrode and polymer

There are three ways by which the energy required for an electron to escape from the metal may be supplied:

(1) by a thermal process known as thermionic emission,

(2) by the application of high electric fields in field emission, and

(3) by photon absorption at sufficiently short wavelength in the photonemission process.

In mechanisms (1) and (2), charge injection from electrode to an insulator may take place by field-assisted thermionic emission known as the Richardson-Schottky effect or simply Schottky emission [36].

Schottky emission governs the conduction current, which is connected with temperature T and electric stress E, and is given by the following equation

$$J = AT^2 \exp\left[\frac{-\phi_e + \beta_s E^{1/2}}{kT}\right] \tag{2.3}$$

and

$$\beta_s = \left(e^3/4\pi\varepsilon_r\varepsilon_0\right)^{1/2} \tag{2.4}$$

where J is the injection current density, A is the Richardson – Dushman constant, k is the Boltzmann constant, ε_0 is the permittivity of free space and ε_r is the relative permittivity of the dielectric.

The interface between the metal and dielectric presents an essentially ohmic contact at electric field below about 1kV/mm, while at the field greater than 100kV/mm electron tunnelling through the barrier becomes the more probable process. However, electron injection into polymers has been observed at electric stresses between 4kV/mm and 300kV/mm for PE and at 20kV/mm for PET. There is a tremendous variation on the emission stress [36].

Generally speaking, electrical conduction of a polymer depends strongly upon the nature of the electrode-polymer interface as well as that of the polymer bulk [37, 38]. Injection of electrons at the cathode and extraction of electrons at the anode are the main mechanisms for the emission of charges in most polymers. However, this is not necessarily the case for all polymers, as some polymers emit and conduct "holes" [30]. Ieda [39] has summarized dominant carrier injections in different polymers, as shown in Table 1. Of course, the electrode material plays a critical role in the issue of whether an electron or a hole is injected.

Table 1. Injected carriers in different polymers

Injected carrier	*Polymer*
Electrons	PE, PET, PEN
Holes	EVA, PPX, PTFE, FEP

PET – *polyethylene terephthalate*
PEN – *polyethylene naphthalene*
EVA – *ethyl vinyl acetate*
PPX – *poly-xylylene*
PTFE – *Teflon*
FEP – *fluor ethylene propylene*

Due to the complex physical and chemical structure of the polymer, the determination of the type of injected charge carrier is not clear at the moment. The extraction of electrons from the polymer, or in other words injection of "holes" to the polymer is even less well understood than the injection of electrons [36].

For the charge accumulation under electron injection, there are two possible situations classified by injection capability which result in different net charges in the locations adjacent to the electrodes. First, when the electrons move faster through the polymer than they are supplied from the cathode, a layer with insufficient electrons is present and a positive charge (holes) is formed adjacent the cathode, see figure 2.5 (a). Meanwhile, the electric stress at the cathode is strengthened and the electron emission increases as shown in equation (2.3). The positive charge decreases and becomes more evenly distributed.

Similarly, if the extraction speed of electrons at the anode is lower than that of electrons from the cathode and the bulk of the polymer, there will be an electron layer formed in front of the anode and can be regarded as heterocharge. On both sides of the

polymer dielectric, the charges are trapped within the amorphous state, the imperfections, and the impurities or at interfaces of different morphologies [40].

Another situation occurs when more electrons are injected in the dielectric than that can be carried away, as shown in figure 2.5 (b) and a homocharge layer is formed at the cathode. A similar process may occur at the anode if more electrons are extracted from the polymer leaving positive holes adjacent to the anode.

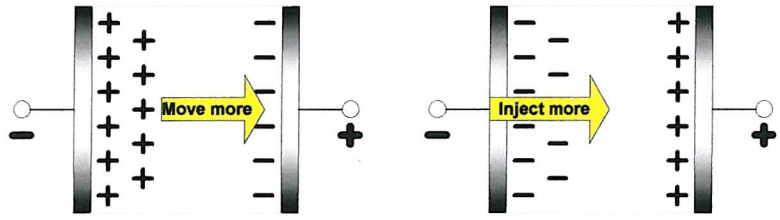

Figure 2.5 Formation of hetero and homocharge in electron injection

2.3.3 Contribution of electronic conduction to space charge (bulk effect)

With regard to the basic conduction mechanism, it is immaterial whether the material is a metal, semiconductor or dielectric, the energized electrons always constitute the major part of the conduction current. When the moving electrons become trapped in the dielectric, space charge appears. Despite the fact that the electronic conduction in organic molecular compounds differs in several important ways from metals and inorganic semi-conductors; the well-known band theory of atomic lattices has provided the basic concept for the discussion of conduction in polymer insulations [29].

a. Band theory

In the atom model, a number of electrons move in separate orbits around the nucleus of the atom. Not every orbit and only a limited number situated at discrete distances from the nucleus are available for the acceptance of electrons. An electron can leap from one orbit to another, which represents a discrete energy level. There will be no electrons in between. In an insulator, as shown in figure 2.6, the lower energy band, called a valence band is completely filled with electrons. A separation, known as an energy gap E_g lies between the valence band and the higher level band, called a conduction band.

No states or orbits are available for electrons in the energy gap. The highest energised electrons in the ground state must gain additional energy, equal to E_g, before they can reach empty orbits and become mobile to take part in electrical conduction [36].

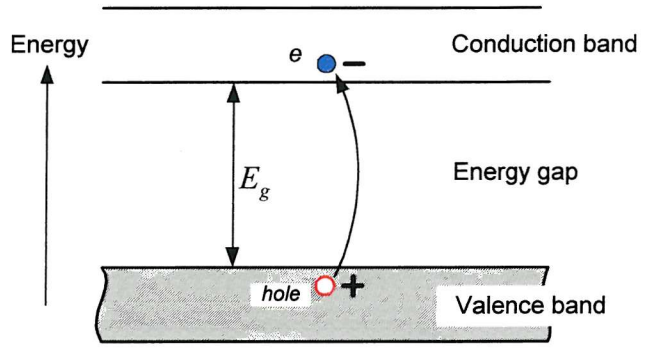

Figure 2.6 Illustration of energy bands in insulator

An insulator is characterized by its band gap E_g. At absolute zero temperature, any solid with an energy gap is non-conducting. However, at any finite temperature, there is a probability that some electrons may be thermally excited across the energy gap into the lowest unoccupied molecular orbital band (conduction band), leaving behind unoccupied positive holes in the valence band. Since the electrons in the bottom of the conduction band and the positive holes in the top of the valence band are molecular orbits that extend throughout the entire material, both can contribute to the conduction process.

b. <u>Electronic process in polymer</u>

Basically, the transport of charge within the macromolecule itself and the transport between molecules are the two main factors that affect conduction in polymers [41]. The intermolecule transport of charge is generally poor due to its weak interaction between the polymeric chains. Moreover, the partially crystallized phase possesses only a small range of order resulting in low carrier mobility.

The Poole-Frenkel mechanism can be regarded as the bulk-limited analogue of the Schottky effect [42]. For the Pool-Frenkel mechanism to occur the insulator must have a wide band gap and must contain donors and acceptors. In this analysis we only consider the case of an insulator containing donors with energy kT below the conduction band to simplify the treatment.

An electron trapped in a donor state is surrounded by a potential barrier with height ϕ. When energised, the Columbic force between the electron and the donor will modify this energy barrier, as shown in figure 2.7. With an applied external electric field, the reduction of the barrier becomes proportional to the square root of the applied field. The relationship between the conductivity and the applied field is given by

$$\sigma = \sigma_a \exp\left[\frac{\beta_{PF} E^{1/2}}{2kT}\right] \tag{2.5}$$

where $\beta_{PF} = \left(e^3/\pi\varepsilon_0\varepsilon_r\right)^{1/2}$, and σ_a is a constant.

Generally, it is difficult to distinguish between the Schottky and the Pool-Frenkel mechanisms as the data from both cases may fit the mechanism equally well. However, the proper distinction may be made according to the mechanism to see whether the effect is bulk or electrode dominated, The Schottky effect should depend upon the electrode material while the Pool-Frenkel does not [41, 42].

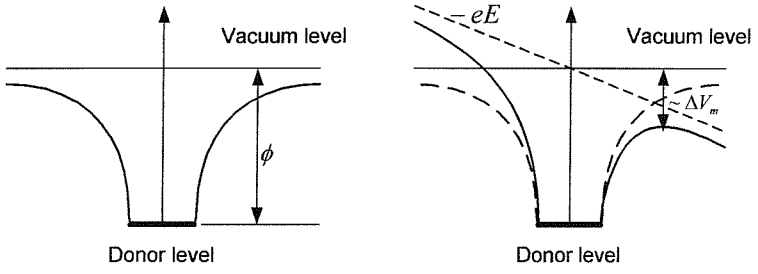

Figure 2.7 Charge in electron potential near donor site due to the external electric field

2.3.4 Ionization (bulk effect)

According to Suh [31], in most cases space charge limited conduction (SCLC) is the major conduction mechanism in polyethylene. This means the conductance of the polymer is governed mostly by the electron injection from the electrode. This situation may be easy to understand for most polymers, particularly, in that they have long molecules which are saturated in the chemical sense (no double bonds), such as PE and XLPE. There will be no significant electronic conductivity because of a lack of energised electrons. So the constituents of the polymer, specifically in XLPE are believed to be another mechanism causing conduction and subsequently space charge accumulation if the charge carriers are trapped [32, 34].

Low field conduction in polymers is frequently found to obey the Arrhenius-type relationship [41, 42]

$$\sigma(T) = \sigma_b \exp\left[-\frac{\phi}{kT}\right] = \sum q_i n_i \mu_i \qquad (2.6)$$

where σ_b is a material constant, ϕ is the activation energy, k is the Boltzmann constant, T is the temperature, q_i, n_i and μ_i are the ith charge, density and mobility of conducting species respectively. This usually is attributed to an ionic conduction mechanism. Although it is not possible to identify the ions experimentally, it is reasonable to assume that they are derived mainly from fragments of the polymerisation catalyst, degradation and dissociation products of the polymer itself and residues after the material processing [37].

As stated in the section 2.2, the available PE and XLPE materials for power cable insulation contain various impurities such as catalysts, antioxidants, voltage stabilizers and by-products from the cross-linking reaction [43, 44]. Under the application of external electric stress these impurities may be separated into ion pairs by the dissociation process as expressed in the following reaction

$$AB \Leftrightarrow A^+ + B^- \qquad (2.7)$$

This determines the ion concentration in the polymer and is of course, directly related to the initial concentration of ionic compound. If the mobility of ions is very limited, this will simply appear as additional atomic polarization. However, when the ion mobility is appreciable, the ion would move towards the electrode of opposite polarity under the applied stress by the "hopping process", and would lead to the build up of the heterocharge [39].

2.3.5 Charge trapping and detrapping

In the previous section, on the basis of the theory of conduction in polymer insulation, the origination and transport of charge and charge carrier has been briefly introduced. When the charges are produced in the dielectric, a portion of them contributes to electrical conduction and some may become trapped as space charge. At the same time, the moving charge or charge carriers may also be trapped elsewhere. Therefore the space charge accumulation in the dielectric material is dependent on the availability and the nature of the traps. The residence time of a charge carrier in a trap will be dependent on the depth of the trap, (*i.e.* the energy required to activate the carrier free

of the trap) and the temperature and the external applied electric field. It is well known that the trapping ability is closely related to the structure of the polymer, such as the crystallinity, molecular weight and morphology. The chemical modification of the polymer also plays a key role in the charging activities [45-48].

Actually, the process of detrapping (*e.g.* the escape of some of the trapped charge from the trap site) will occur simultaneously if the charges possess enough energy. Therefore, it is easy to understand that the space charge formation in the material results from a competition between a trapping rate and a detrapping rate.

As stated previously, charge carriers in an insulating material can be trapped at impurities or physical defects. Immobilization of the carriers reduces conductivity and so contributes to the space charge formation. The capture rate for free electrons by a single trapping level can be described in term of a time constant τ_{trap}.

$$\left(\frac{dn}{dt}\right)_{capture} = -\left(\frac{n}{\tau_{trap}}\right) \tag{2.8}$$

where n is the number of free electrons. Here for a given material, the lifetime toward trapping can be regarded as constant. More precisely, the above equation should be expressed in kinetics formulation with a rate constant A_1, as

$$\left(\frac{dn_t}{dt}\right)_{capture} = A_1 n(N_t - n_t) \tag{2.9}$$

where N_t is the trap concentration, n_t is the concentration of filled traps. This processing is schematically illustrated in figure 2.8. If $n_t << N_t$, the detrapping reaction takes place at a rate constant of A_2 at a rate given by

$$\left(\frac{dn_t}{dt}\right)_{excitation} = A_2 n_t(N_t - n) \tag{2.10}$$

In the thermal equilibrium conditions of Fermi statistics, it follows that

$$A_2 = A_1 \exp\left[\frac{-(E_c - E_t)}{kT}\right] \tag{2.11}$$

In the above equation, the trap depth (E_c-E_t) is simply the binding energy of the charge in the trapping centre [36].

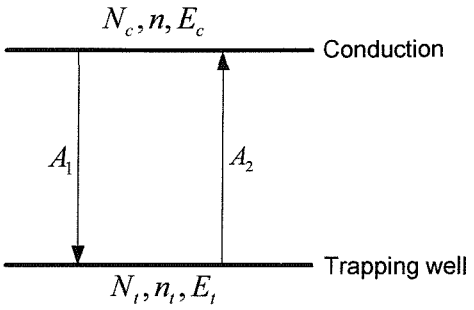

Figure 2.8 Trapping and detrapping processes of an electron

Thermally stimulated current (TSC) and thermally stimulated luminescence (TSL) are two typical applications of proving the trapping and detrapping process in dielectrics. They are more sensitive techniques for studying traps and their depths in dielectrics [39, 49].

2.3.5 Charge trapping in PE

Several traps have been reported as existing in the polyethylene [37, 50], and are summarised in Table 2, including their nature and origins.

Table 2. The nature and origins of the charge traps in PE

Origin	*Region*	*Trap depth (eV)*
Defect		0.1-0.3
	Lamellar surface	0.3
	Amorphous	0.24
	Amorphous	0.8-1.0
	Amorphous-crystalline interface	1.0-1.4
	Crystalline	1.2-1.7
Unstable oxidation products	Amorphous	
Stable oxidation products	Amorphous-crystalline interface	1.4
Cross-link	Amorphous	1.0
Antistatic agent	Amorphous	1.2

From Table 2, it is noticed that polyethylene has a wide range of trap depths which may be classified into two broad groups as shallow traps and deep traps. Shallow traps stand for the traps having depths ranging from 0.1 to $0.3eV$, and normally have a high concentration in polyethylene, whereas deep traps have depths in the range between 0.8

and $1.7eV$ and are relatively few in polyethylene. From the previous description, it is known that the deeper the trap the greater the energy required to release a trapped charge. Therefore, the trapping level is an important characteristic for the insulating material used in dc polymer power cables. For the dc cable, an insulating material containing shallow traps will ensure that any charge that accumulates within the bulk can easily be conducted away.

Despite the considerable amount of research on the effects of the impurities and morphology on space charge behaviour in insulating polymers; e.g. in PE and XLPE [32, 34, 35, 51-53], the detailed mechanism is still ambiguously defined. Nevertheless, a polymers' morphology and thermal history may be as important as its molecular structure in determining the trapping effect.

2.4 Summary

As a fundamental background to space charge characteristics in polymer insulations, the physical and chemical structure and the processing technology of PE and XLPE has been briefly illustrated in this chapter.

The space charge origination in the dielectric material is generally attributed to two mechanisms. The first one is based on Schottky emission, in which the electrons or holes may be injected through the electrode - polymer interface when they acquire adequate energy to overcome the potential barrier. This process is strongly dependent on the conditions at the interfaces that include material, surface defects and impurities. The second mechanism is the generation of charge within the polymer itself. This has been discussed from the viewpoint of the conduction of the dielectric material. However, because the polymer lacks free electrons, the charge or charge carrier taking part in the conduction is believed to be associated with ionisation of chemical species in the polymer. These may be the by-products introduced during the manufacture of the material, such as residues of the cross-linking reaction, antioxidant and other impurities.

The injected charges or other kinds of charge carrier initiated in the bulk of the material are trapped in sites where inhomogenities appear, such as crystalline/amorphous interfaces, impurities, at which space charge develops. This process is dependent on the availability of traps (or trap density) and the nature of traps. The charge resident time is directly connected with the trap depth, which is expressed

by the energy required to activate the charge carrier free from the trap. In polyethylene, for instance, both shallow and deep traps were found with trap depths of the range $0.1\sim1.7eV$. Obviously, the factors of material crystallinity ratio, concentration of residues, additives after manufacturing and other impurities will also affect the insulations charging ability. The detrapping of charge carriers always occurs at the same time as trapping, thus the appearance of the space charge within the material is the resultant of trapping and detrapping. This may be influenced by the temperature and external applied electric field.

Chapter 3

Review of Space Charge Measurement in Plaque and Cable Geometries

3.1 The necessity of space charge measurement in polymer insulation

When a polymer insulator is subjected to a high dc electric stress, it will tend to become charged and the charge may remain in the material for a quite long time. As described in the foregoing chapter, these charges may be supplied from the electrode injection or the ionisation of the impurities in the bulk material itself.

Specifically for PE and XLPE, previous researchers have shown that the electric stresses are not the only parameters involved in the space charge formation. The cross-linking, melting, softening and permeation processes can also result in space charge accumulation [38, 54]. Once the space charge is accumulated in the insulation of an XLPE power cable, the profile of the original designed electric field intensity may be greatly distorted. This can result in localised stress enhancement leading to premature failure of the cable insulation at a stress well below the anticipated or designed values [55-59].

Even for ac XLPE power cables, it is a common practice to use a dc testing voltage instead of ac voltage to check the insulation integrity after manufacture or on site after installation or in routine tests during system operation. This is because the large charging current under ac voltage requires a bulky or even unrealistic ac supply for the test. An EPRI sponsored project has shown that dc testing results in a loss of life for ac XLPE cables [57]. In this situation, the space charge induced during the dc voltage test

is believed to have played a critical role in the deterioration. It has also been reported that the space charge is responsible for dielectric ageing through the initiation and growth of so-called electrical trees [58-61].

The above hazards brought about by space charges in polymer insulation, particularly in PE and XLPE, have prompted a considerable number of studies on space charge accumulation and their effects on insulation characteristics [58-64]. Initially, most of these were only qualitative discussions as the lack of space charge position distribution information. Therefore, the measurement of space charge distributions, in particular with an adequate spatial resolution, is required in order to give an informative insight into space charge formation, migration and accumulation inside polymer insulating materials. Consequently, the knowledge of the modified electric stress profile due to the generation of space charges will lead to a better understanding of the electric breakdown and treeing phenomena in polymer insulation. All the knowledge obtained from this measurement together with on-going material research may fulfil the long-standing endeavour to finally control the space charge accumulation in the insulating materials.

3.2 The techniques of space charge measurement

Space charge measurement in insulating materials had previously been performed through the use of conventional techniques such as the thermally stimulated current (TSC) and thermal pulse methods. TSC had been a popular method for studying all the fundamental mechanisms of charge storage and release in insulators, but it is unable to supply position information of space charge distribution [64]. The thermal pulse method and its modified type, such as the thermal step method [66] and the laser intensity modulation method (LIMM)[67] can be used to determine the location of space charges. However, the position resolution is high near the exciting electrodes but decreases with the increasing depth due to thermal expansion.

Over the last two decades, several new techniques based on the principle of pulsed pressure waves have been developed for non-destructive measurement of both the location and the density of space charge in dielectrics. They are the pressure wave propagation method (PWP) [68-70] and pulsed electro-acoustic method (PEA) [4-6]. The category of PWP can be subdivided into the laser induced pressure pulse (LIPP)

and the piezoelectrically induced pressure step (PIPS) according to the mechanisms of pressure wave generation.

The basic principles and their features of the above-mentioned techniques are briefly explained in the following sections.

3.2.1 PIPS method

The principle of the PIPS method [4, 71] is illustrated in figure 3.1. A mechanical pressure pulse is exerted by a piezo-electric device on a ground electrode contacting with the sample to be tested. The resulting perturbation of the charge layer on the sample induces a change of the surface charge on the electrodes. The time dependent signal of displacement current in the external circuit contains the information about the space charge distribution in the sample. By detecting this current, the charge profile is obtained.

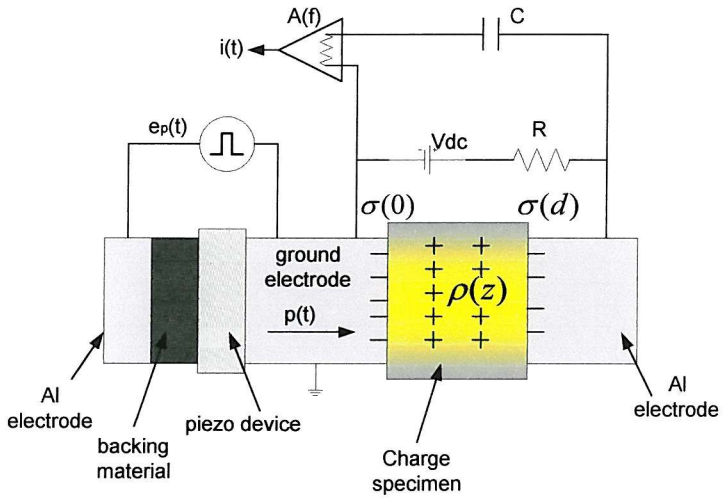

Figure 3.1 Principle diagram of the PWP method

The pulsed pressure wave $p(t)$ is generated when an impulse voltage $v_p(t)$ is applied to a piezoelectric device. In order to maintain the shape of the pressure pulse, a proper acoustic impedance match between the piezoelectric device and the electrode is necessary.

When the pressure wave propagates through the charged sample, the time dependence of the surface charge $dq(t)/dt$ leads to a current $i(t)$ in the external detecting circuit. According to this principle, it is known that the current signal is given by the convolution of the space charge $\rho(z)$ and pulsed acoustic pressure $p(t)$. A mathematical

technique known as deconvolution is therefore needed to obtain a true space charge distribution profile.

3.2.2 LIPP method

The LIPP method [68] is one of the common techniques of PWP, and works on the same principle as PIPS. A laser pulse is aimed at a target attached to one side of a sample. The absorption of the laser energy results in a fast expansion of the target which produces a short but intense pressure wave into the sample, as shown in figure 3.2. As the very narrow compressed pressure pulse travels through the specimen at the velocity of sound, the current caused by the charge movement is directly proportional to charge distribution, i.e. $i(t) \propto \rho(z)$, where $i(t)$ is the displacement current detected in the external circuit and $\rho(z)$ is the charge density distribution along the sample thickness. Usually, a laser pulse with width 100ps~10ns from a Nd:YAG laser is used. This technique is applicable to both thin (10~100μm) and thick (1~20mm) specimens. A powerful laser pulse would result in a big current signal that is detectable without averaging the signal over a period to eliminate the system noise. An ideal set-up of a LIPP system could provide positional resolution as high as ~1μm. Because of the very fast laser, the initially compressed region in the sample is small and the profile of the current signal in the time domain is directly proportional to the charge distribution in space and no deconvolution is required [72]

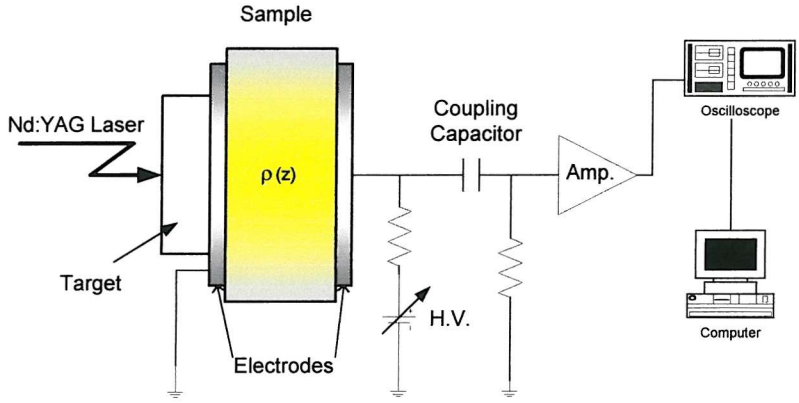

Figure 3.2 Schematic diagram of the LIPP method

3.2.3 PEA method

The PEA technique was developed in the early 1980s to measure the space charge distribution in dielectrics [73]. After twenty years of development and profiting from

progress in both measurement technology and data processing, this technique has become the most widely used for space charge measurements in solid dielectrics. A detailed description of the basic principle and relevant technique can be found elsewhere [74-77] and only a brief overview is given here.

Considering the plaque sample shown in figure 3.3. The space charge layer q_2, induces image charges q_1 and q_3 on the electrodes $(q_1 + q_3 = q_2)$. An external voltage pulse $v_p(t)$ applied across the sample produces an electric stress $e_p(t)$. The interacting between the pulsed electric stress and the charge layers will introduce a perturbation force p_1, p_2 and p_3 on the material where the charges are present according to Lorentz law and cause a slight movement of the material in the term of micro-scale. As a result, acoustic pressure waves proportional to the charge magnitudes will be launched in the dielectric material. A piezoelectric transducer detects the acoustic pressure waves and converts them into electrical signals, v_{s1}, v_{s2} and v_{s3}. Measurement of the time dependent voltage enables a profile to be obtained which is related to the amplitude of the space charge coincident with the propagating acoustic pulse.

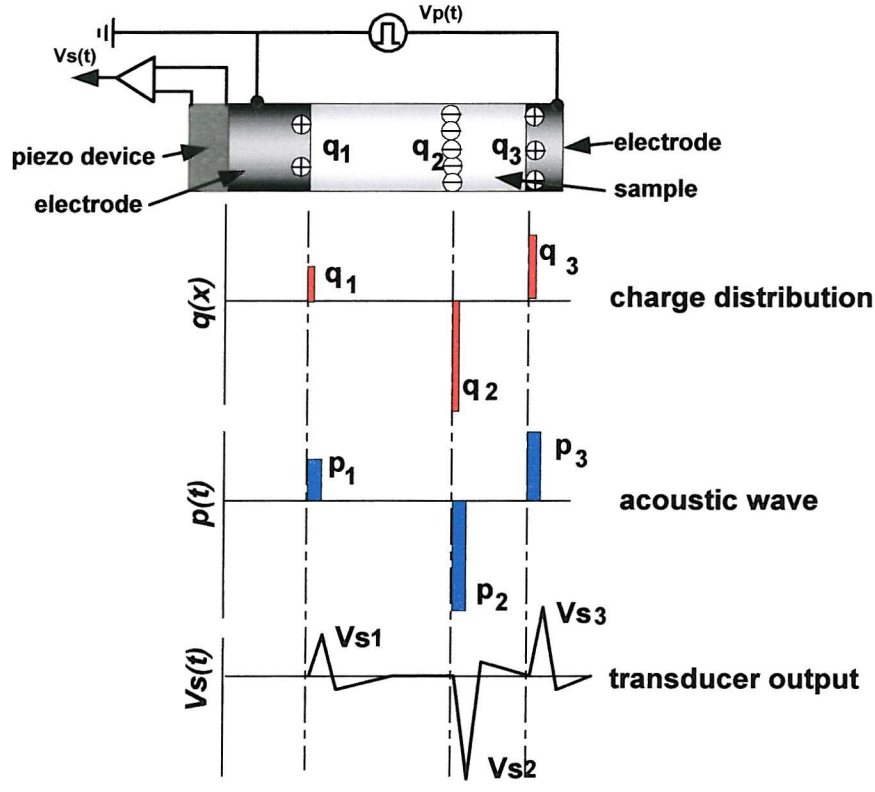

Figure 3.3 Basic principle of pulsed electro-acoustic (PEA) method

Figure 3.4 shows a schematic setup of the PEA system for space charge measurement in planar samples. The space charge profile contained in the output acoustic signal is extracted and calibrated through the use of digital signal processing. Normally, the frequency response of the piezoelectric device and its detection circuitry is not perfect over a wide frequency range. The output voltage signal $v_s(t)$, which contains the information of the space charge distribution may be deformed, so the deconvolution technique should be applied to recover the actual space charge distribution. This will be discussed specifically in chapter 4.

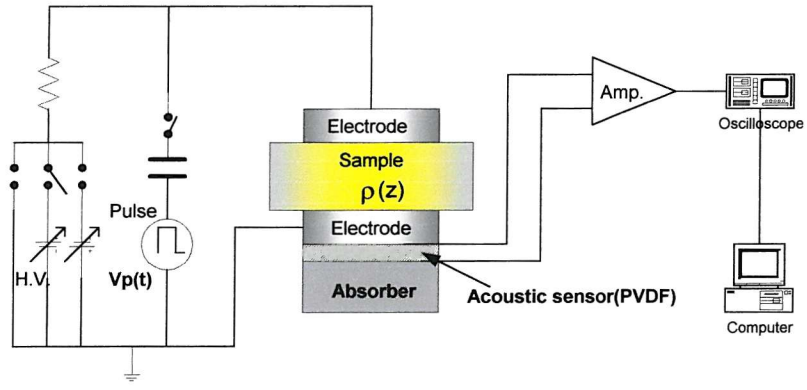

Figure 3.4 Schematic setup of PEA for plaque samples

3.3 Space charge measurement in plaque samples

With the benefit of developments in the space charge distribution measurement technology in solid dielectric materials, a considerable amount of research has been carried out on the space charge characteristics by taking measurement not only in sheet samples but also in coaxial cables. Because of the vital impact of the space charge accumulation on the polymer insulation system, about 80% of the publications on this subject have centred on polyethylene and polyethylene-based materials [78]. The emphasis of this research has been on the space charge development mechanism and the possible measures for suppressing it. The effects of the temperature, the electrode material, the interface status between different dielectrics and the residue (impurities) content on the space charge generation, migration and accumulation have been extensively studied. Fothergill [79] has demonstrated the "versatilities" of space charge measurements. Together with the current measurement, the information of free charge and bound charge on the electrode, conduction current, displacement current, power density and temperature increment in time and space can be obtained which may

provide a comprehensive way to study space charge and its effects on the dielectric properties.

Before the techniques measuring space charge distributions in solids were available, an abundance of investigations had been carried out to study the effect of the electrode material, as well as the different media interfaces on electrical conduction and charge injection in planar samples [37, 38, 62, 63, 80]. It has been shown conclusively that electron or "hole" injection from the electrode is a major source of electronic carriers in polymer insulation. The barrier height between electrode-polymer is generally as high as 2 to 3eV and the surface status affect the electrode injection [62]. In addition to the accumulation of space charges in the bulk material, charges may easily develop at the interfaces of polymer/electrode (metal or semiconductor) and polymer/polymer. With the aid of advanced measuring techniques, Chen and other researchers [81-85] have continued more precise research into space charge distribution in so far as their position and time evolution. For the common electrode materials used in either the laboratory or power cable industry, i.e. aluminium, gold and carbon-black-loaded-XLPE, the charge injection process takes place in all cases as soon as the applied electric stress exceeds a certain threshold. However, the amount of the injected charge and the dominant charge polarity is significantly dependent on the electrode material under the same applied electric stress [81].

The dependence of space charge accumulation upon the residues in XLPE (additives, oxidation products and by-products from the chemical reaction) has attracted a great attention of the researchers over the world [34, 35, 47, 86-89]. The research has covered the different material cross-linking method and the conditioning process after the manufacture. Comparison between two commonly used cross-linking reactions, e.g. dicumyl peroxide (DCP) and silane-based grafting has been made as they give different residue content to XLPE. The DCP method favours heterocharge whereas the silane-based grafting process favours the homocharge owing to the latter producing low residue concentration in XLPE [89]. By treating the newly prepared XPLE under different temperature or low-pressure conditions, or with combinations of both of them, some volatile residues may be removed from the samples. As a result, space charge accumulations have presented noteworthy variations. This suggests that the residue plays an important role in space charge accumulation in the volume of the polymer insulating material. Moreover, the pre-treating (degassing) conditions of

temperature and holding pressure had significantly different effects on space charge control [90].

Li and Takada [91] had experimentally observed charge transport and injection in XLPE sheet samples under external applied stress reversals. In their research, the charge was likely to transport more easily within the bulk than across the polymer /electrode interface under voltage reversal conditions.

On the basis of these extensive researches and fruitful achievements into the mechanism of space charge development, some researchers have attempted to describe the charging phenomena using a mathematical model [92, 93], in which the space charge density evolution was numerically simulated as a function of position, time and field. The results were compared with experimentally obtained profiles. However, the mechanisms of space charge dynamics are more complex than the parameters they considered, and a more sophisticated and comprehensive model containing all possible parameters can only be developed on the basis of further experiments.

At the same time, the PEA method was modified to measure very fast varying space charge distributions in sheet samples [94-96], which enabled synchronous space charge distribution measurements to be carried out in a planar sample under any shape of voltage application, such as step voltage or ac voltage at any frequency and any phase angle. In the system developed by Fothergill and See [95, 96], a high voltage (up to 4 kV) and narrow (5 ns) pulse was adopted to obtain good spatial resolution in charge distribution under rapidly varying voltage. Using this method, they have observed the formation and migration of charge packet in XLPE under dc voltage [97, 98]. As a common practice, very low frequency voltage, say 0.1Hz, is used when testing high voltage cable insulation integrity, but the space charge characteristics under low frequency ac is not yet clear. This modified PEA technique makes it possible to dynamically observe space charge evolution under ac voltage with different frequency. This has shown that space charge can develop and be accumulated in XLPE under a low frequency ac stress. As the frequency increases, the space charge density decreases. When the frequency is higher than 0.2Hz, measurement of space charge development and accumulation in XLPE becomes more difficult. All the above technology development on the space charge measurement has supplied the possibility of understanding the failure mechanisms of solid insulators under transient voltage, voltage polarity reversal and ac conditions. Ohki, Ebinuma and Katakai [99] have used the same technology to study the space charge formation in water-treed insulation. The

space charge generated in the vicinity of a tree tip was attributed to the interfacial polarization due to the high conductivity of a tree channel and the carrier injection from the tree tip at high electric stress. On the other hand, this technique has provided a method of clarifying the electrical properties of the water tree.

Most recently, some new efforts have been made on the measurement of three-dimensional space charge distributions and simultaneous measurement of TSC with charge distribution [100, 101]. These attempts could further enrich the method of space charge research.

3.4 Space charge measurement in specimens with cable geometries

Since Fukunaga made the first attempt to measure the space charge distribution in a coaxial cable using the PEA method [14], there have been quite a few researchers devoted to this subject using the PEA or the LIPP technique [21-24, 102, 103]. It is scarcely necessary to mention that the PEA method is still the favourable technique because of its low cost and its ease of operation. Figure 3.5 shows a typical arrangement of the electrode system for a coaxial cable PEA that was employed in the previous researches. This conventional design employs a curved ground aluminium (Al) electrode to maintain an intimate contact with the cable outer screen. A piezoelectric transducer (polyvinylidene fluoride PVDF) film is placed around the outside of the coaxial shape electrode. Additionally, a curve shaped absorber block is used to back the PVDF transducer and it is necessary to minimize unwanted reflections of acoustic waves at the interface. It is made from a material having similar acoustic impedance to the transducer, such polyethyl methacrylate (PMMA).

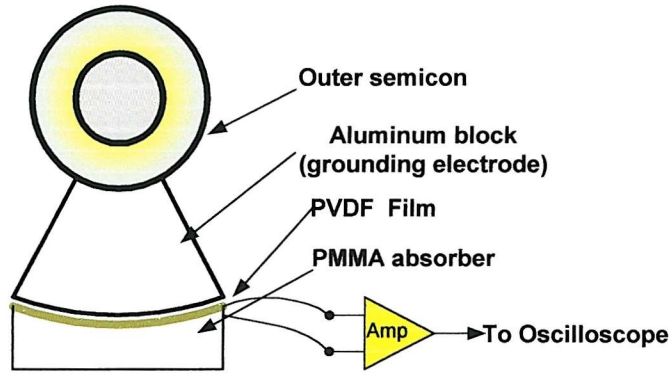

Figure 3.5 Schematic diagram of a conventional PEA for cable geometry

Hozumi *et al* measured space charge in cables at much higher electric stresses [21]. In their study, the cable sample was longer than several meters to meet the requirement of adequate termination for high voltage application. Its insulator could therefore no longer be regarded as a lumped capacitor. The pulsed voltage injected at the termination might be significantly distorted when it arrives at the test point. A specially designed electrode system was adopted in their research to solve this problem. Direct observation of time dependence of the space charge in an XLPE cable under different electric stresses showed that hetero-charge accumulation takes place mainly under low stress (~23kV/mm) and then tends to saturate. Under high stress (>100kV/mm), it was observed that heterocharge appeared soon after the application of the voltage, and was then followed by electron injection from the cathode. Afterwards, an intermittent injection of charge packet from the anode took place and propagated towards the cathode. The space charge consequently undergoes a kind of oscillation during the whole period of test time without stabilization. In another work of Hozumi *et al* [104], the same space charge behaviour in a cable sample under lower and higher stress was reproduced in sheet specimens of XLPE and LDPE. The effect of acetophenone, (one of main byproducts of the cross-linking process) on space charge generation was investigated by comparing the results of samples as-received (fresh) with dried (degassed) samples or samples dipped with acetophenone. It was found that the packet charge tended to occur when the electric stress was over 70kV/mm. This was thought to be related to the local ionization of impurities by the high field. Acetophenone was believed to assist the ionization of impurities.

Several research projects focusing on the effects of conditioning and external applied voltage polarity on space charge behaviour have been conducted in extruded polymer power cables [23, 89, 102]. Some valuable results for the development of dc cables have been obtained. The most remarkable one is that achieved by Takeda *et al* [105] and Terashima *et al* [106] on a newly developed ±250 kV XLPE dc full-size cable that has shown an excellent performance from the viewpoint of space charge suppression. Two kinds of modifed XLPE materials, which were loaded with polarized inorganic filler and conductive inorganic filler respectively, were used as insulations in two prototype dc cables. In addition to their satisfactory electrical, mechanical and long-term ageing performances, no significant space charge activity was observed in these two cable samples.

Using the LIPP method, HolbØll *et al* [103] investigated the space charge building up in an XLPE cable in which there was a non-uniform temperature distribution across the insulation. The core was heated by the Joule effect, while the outer sheath remained at the near ambient temperature. The temperature ranged from 20 to 80°C and the maximum temperature gradient across the insulation was up to 15°C. Except for the strong heterocharge accumulation at the cooler outer screen, the temperature dependency of space charge density across the cable insulation was not clearly observed. Due to the significant attenuation of the acoustic wave across the 5.5 mm insulation, the space charge profile near the inner electrode interface was not clearly presented.

Recently, space charge measurements have been used to investigate the water treeing in polymer insulated power cables [107]. It was found that the space charge distribution in and around the blue water tree is more harmful than the white tree. By examining this, it was revealed that an abundant space charge existed only at the tree tip, but not in the tree branch. This result indicated that the very high conductivity of the blue water tree is responsible for its harmfulness.

However, compared with the great amount of research on sheet samples, less attention is given to the space charge measurement in full sized cables and the development of the relevant technique. With the most commonly used curved electrode system, it is problematic to undertake measurements on cables with diverse radii, because the modification of electrode and transducer as well as the absorber is time consuming and difficult to carry out.

Moreover, several factors of data processing have not been tackled in the research so far described. Firstly, the acoustic wave propagation mechanism is still based on the plate-plate electrode system instead of one with a cylindrical geometry. The variation of the pulsed electric stress and acoustic pressure intensity along the radial direction is not considered. Secondly, in the case of a cable sample, the insulation can be several millimetres thick, so the attenuation and dispersion of acoustic waves travelling through the insulating material may be very significant. In order to obtain more accurate results both in charge density and position resolution, these effects should be taken into account. Finally, in the previous researches, only the electric stress at the electrode/insulation interface was determined. This was by comparing the peak height of the induced surface charge at the electrode with that obtained in the calibration. But

in practice, the maximum electric stress is likely to appear in the central part of the cable insulation, as homocharges appear. Additionally, the inhomogenity of the material and the non-uniform impurity distribution may lead to the development of packet charge in the bulk insulation and produce a complex electric stress distribution. Therefore, there is an essential requirement to obtain a whole electric stress profile across the cable insulation from space charge distribution measurements so that the effect of space charges on insulation performance can be thoroughly understood.

From the above review of research on space charge measurements both in planar geometries or in polymer insulated coaxial cables, it can be concluded that space charge generation and accumulation is still the main concern in high voltage dc cable insulation design. An effective method is therefore needed urgently to evaluate the space charge characteristics, especially in the prototype stage of dc cable development.

Chapter 4

Newly Modified PEA System and the Principle for Space Charge Measurement in Cable Samples

4.1 Introduction

As the PEA method is gradually being improved, more and more researchers in this field have been supplying valuable insights into the mechanisms of space charge formation, migration and accumulation in the dielectrics. Consequently, it has become possible and necessary to apply this technique to extruded polymer insulated power cables in the selection of insulating material. Hopefully in the near future, this method can also be used as a quality control measure in the process of polymer cable manufacturing.

As mentioned in Chapter 3, several researchers have applied this technique to extruded polymer insulated power cables, aiming to study the effects of thermal treatment and stress polarity on space charge evolution. However, without exception among these investigations, the same kind of PEA, i.e. a shaped outer electrode, transducer and absorber design has been used.

In order to overcome the intrinsic drawbacks of this PEA system as outlined in the preceding chapter, a new design adopting a flat electrode for coaxial cables is briefly introduced in this chapter. The transmission of an acoustic pressure wave through several interfaces between different media is analysed for this electrode configuration. Based on the theoretical discussion and the comparison of practical measurement results obtained from two systems, it is concluded that the new system is capable of

giving the same measurement results both in charge density and position resolution as that of the conventional design with the curved electrode arrangement.

In the previous work on the space charge measurement in sample of cable geometry, Liu *et al* [22] have comprehensively described the principle of the method used by those researchers, who adopted a curved ground electrode structure.

The theory of the modified PEA system with a flat electrode arrangement is outlined in this chapter. The relevant fundamental techniques, such as the data processing, calibration and deconvolution are also detailed.

4.2 Experiment setup

The schematic diagram of the new PEA system for the cable geometry is illustrated in figure 4.1. In this new design, the cable sample sits on an earthed flat Al electrode. The acoustic transducer (PVDF) is placed on the other side of the Al electrode. The interface between the outer screen of the cable sample and the earthed electrode is approximately in a line contact instead of an area contact as in old structure, and an intimate contact between the sample and the electrode is easily maintained in the new system.

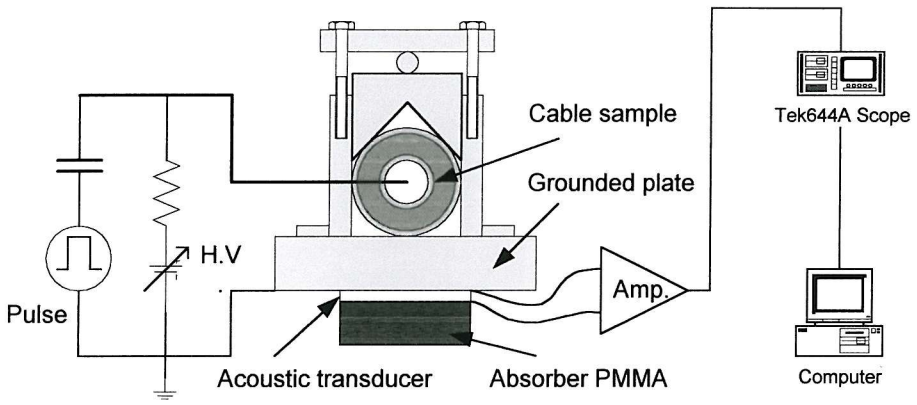

Figure 4.1 Schematic diagram of modified PEA system for cable samples

The whole setup consists of an electrical pulse generator, a dc high voltage power supply and a plate ground electrode under which an acoustic transducer (PVDF) and a wide band amplifier are assembled in a shielding box. The transducer signal is amplified and collected by a digital oscilloscope and the data is transferred through a general-purpose interface board (GPIB) to a personal computer for further processing. The whole data acquisition and processing is implemented in a program developed

under a graphical programming environment LabView™ (Laboratory Virtual Instrument Engineering Workbench).

The system is equipped with a ±100kV dc power supply and the polarity of the applied voltage can be easily changed. The electrical pulse generator produces a voltage with a width of 50ns and a range of amplitudes from 2kV to 8kV. Through the coupling capacitor bank, the pulse voltage can be applied to the core of the cable sample simultaneously with the external dc voltage. A 20kΩ resistor is connected in series with the external dc high voltage circuit to limit the current in the case of breakdown or flashover of the sample.

The photograph shown in figure 4.2 gives a general idea of the arrangement of the new PEA system for the cable geometry.

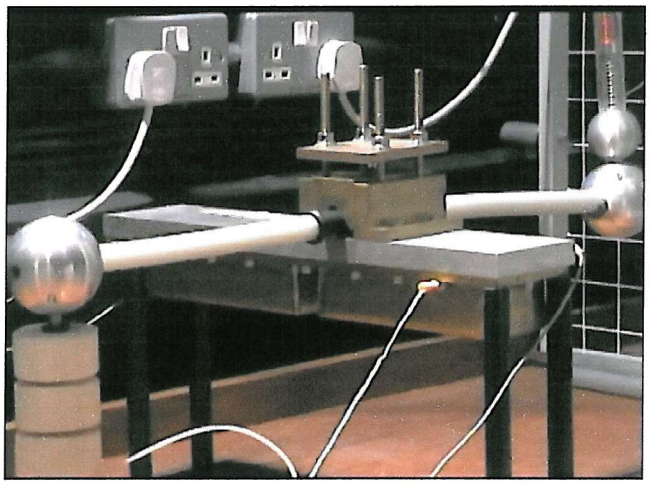

Figure 4.2 The photograph of the new PEA system for cable geometry

Cable specimens to be tested are normally prepared as shown in figure 4.3. The outer semiconducting layers at the two ends are sufficiently stripped back and removed to ensure the high voltage can be applied to the cable without surface flashover. Two stress relief rings are also built at the screen cuts to reduce the possibility of failure of the insulation over long term testing of the cable sample.

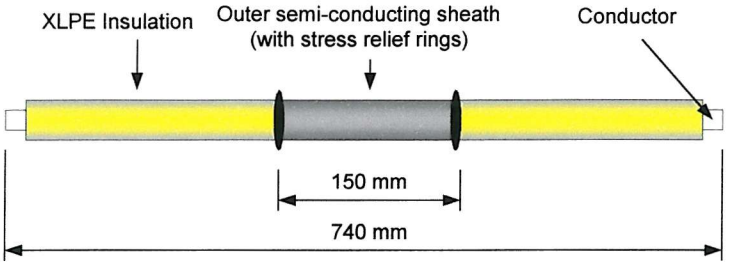

Figure 4.3 Illustration of prepared cable sample

4.3 Acoustic wave transmission through the interfaces and different media

In the conventional version of the PEA apparatus for cable samples which employs a curved ground electrode, acoustic transducer and absorber, the acoustic wave initiated inside the insulation propagates outwards through different media and interfaces, and impacts normally on the transducer's surface.

In the new modified system, however, the acoustic propagation is different due to its new configuration. It may be questioned whether the new system gives the desired sensitivity and spatial resolution. Therefore, a thorough understanding of the new system's acoustic characteristics is essential. The propagation of the acoustic wave in this new electrode configuration is schematically illustrated in figure 4.4. A detailed analysis of the wave travelling through the polymer, Al electrode and PVDF transducer film, as well as its action at each interface is presented in the following section.

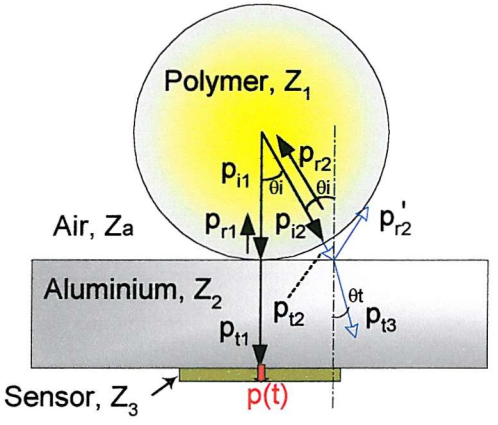

Figure 4.4 Acoustic wave propagation model in new PEA system

The four media subjected to the acoustic wave propagation have the following acoustic impedance: air z_a=415 rayls, polymer z_1=1.8×10^6 rayls, Al z_2=1.4×10^7 rayls [108] and PVDF sensor $z_3 \approx z_1$ respectively. p_{i1} and p_{i2} represent the acoustic pressure

wave amplitude travelling to the Al electrode at normal and oblique incidences respectively, and their corresponding reflection and transmission pressure wave amplitudes are denoted using subscript r and t.

In the case of a plane acoustic wave striking the plane interface between the polymer and the block electrode at normal incidence, the relationships between incident, reflected and transmitted waves pressure are given by [109]

$$\frac{p_{r1}}{p_{i1}} = \frac{z_2 - z_1}{z_2 + z_1} \tag{4.1}$$

and

$$\frac{p_{t1}}{p_{i1}} = \frac{2z_2}{z_2 + z_1} \tag{4.2}$$

When analysing the action of an acoustic wave interacting with a boundary across which there is a change of acoustic impedance between the two media, the process can be described in terms of the acoustic transmission and the acoustic reflection coefficient, α_t and α_r. For example, considering the normal incident acoustic wave at the interface between the polymer and the Al electrode, the transmission and reflection coefficient are given by [109]

$$\alpha_t = \frac{4z_1 z_2}{(z_1 + z_2)^2} \tag{4.3}$$

and

$$\alpha_r = \frac{(z_2 - z_1)^2}{(z_2 + z_1)^2} \tag{4.4}$$

Using the acoustic impedances listed previously, the values of α_t and α_r are 0.4 and 0.6 respectively at the interface between the sample material (polymer) and the metal electrode. These results suggest that 40% of the incident acoustic wave is transmitted to the second medium and 60% is reflected back when the outer surface of the cylindrical sample is in direct contact with the flat electrode.

In the case where the acoustic wave is at an angle of θ_i colliding with the Al electrode surface, the acoustic wave has to travel through the air gap formed between the outer surface of the cable sheath and the Al electrode first before arriving at the Al electrode. The acoustic wave transmitted into air from the polymer is defined as p_{t2} and that of the reflected pressure wave p_{r2}. Again from equation (4.3) (4.4) α_t and α_r are found to be 0.001 and 0.999 respectively. This implies that at the polymer/air interface

the acoustic wave is almost reflected back into the polymer medium and only a negligible fraction of the incidence can transmit. Even if this transmitted acoustic wave p_{t2} keeps propagating towards the Al electrode obliquely, there will be another significant reflection occurring at the interface of the air and the Al electrode. The expression for the acoustic waves transmitted and reflected at the air and Al interfaces for the incidence angle θ_i can be written as

$$\alpha_t = \frac{4z_a z_2 \cos\theta_i \cos\theta_t}{\left(z_2 \cos\theta_i + z_a \cos\theta_t\right)^2} \tag{4.5}$$

and

$$\alpha_r = \frac{\left(z_2 \cos\theta_i - z_a \cos\theta_t\right)^2}{\left(z_2 \cos\theta_i + z_a \cos\theta_t\right)^2} \tag{4.6}$$

In practice, we only consider the effective area covered by the transducer which normally is of width of 5mm, so θ_i is presumed small and $\cos\theta_i \approx \cos\theta_t \approx 1$. Substituting the corresponding values into equation (4.5) and (4.6) and noting $z_2 >> z_a$ yields $\alpha_t \approx 0$ and $\alpha_r \approx 1$. The result indicates that no acoustic wave travelling to the Al electrode surface in the angle θ_i will get into the Al electrode and reach the transducer.

From the above analysis, it can be concluded that only the acoustic wave propagating towards the Al electrode and transducer in the normal direction will partially travel through the interfaces of polymer/Al and Al/ transducer and can be detected by the transducer finally, although some reflection occurs at the interfaces. The acoustic wave radiating along the radial direction at an angle θ_i with the flat electrode surface is almost totally reflected at the interfaces of polymer/air and air/Al due to the air gap. Therefore, the transducer cannot sense the contribution of the acoustic wave from an oblique angle.

When the acoustic wave *p(t)* arrives at the transducer and propagates through it, a charge *q(t)* on the transducer surface is introduced due to the piezoelectric effect and this is given by [76]

$$q(t) = kp(t)S \tag{4.7}$$

where k is the piezoelectric strain constant of the transducer and S the area of the transducer.

Thus the potential difference across the transducer and the output voltage v_o in a open circuit can be found from the transducer's capacitance C_p.

$$v_o(t) = \frac{q(t)}{C_p} = \frac{kd}{\varepsilon_0 \varepsilon_r} p(t) \tag{4.8}$$

where $C_p = \varepsilon_0 \varepsilon_r S/d$. ε_0 the permittivity of free space and ε_r the relative permittivity of PVDF transducer, and d is the thickness of the transducer. In equation (4.8), it is apparent that the electric potential generated by the acoustic pressure wave $p(t)$ is dependent on the thickness d but independent of the area S of the transducer. A comparison between two electrode systems is simply illustrated in figure 4.5.

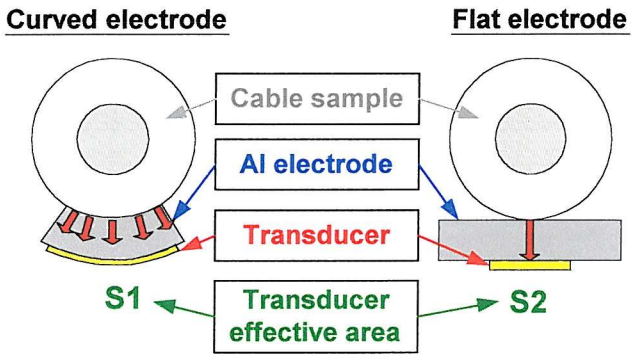

Figure 4.5 Illustration of curved and flat electrode system

The above analysis suggests that the output of the transducer is directly related to the magnitude of the pressure wave and transducer thickness but not the contact area. The implication of this conclusion is that the PEA system with a flat electrode and transducer arrangement can give the same detection sensitivity as that of the curved electrode system. The other components of the acoustic wave radiating in the oblique direction with the electrode surface, for instance along the routes of p_{i2}, p_{t2} and p_{t3} in figure 4.4, become negligible because of the two significant reflections occurring at the interfaces of polymer/ air and air/Al. Thus this part of the pressure wave will not affect the spatial resolution of the resultant measurement in spite of its relatively long route.

4.4 Practical comparison between the conventional and the improved system

No conventional PEA system was available in the laboratory, so the results of the space charge measurement in a 6.6kV XLPE power cable found in the literature [110] are quoted for comparison with the new system. The thickness of the cable insulation was 3.5mm and the outer radius of the insulation was 10mm, the externally applied dc stress at the inner and outer interfaces of the semiconducting layer and insulation were

approximated as 14.3kV/mm and 9.3kV/mm respectively when a 40kV calibration voltage was applied. As the measurement was carried out soon after the voltage application, only surface charges were introduced at the two interfaces. The measured charge density at the outer electrode was about 1.2C/m^3, with a half-peak height width (e.g. the resolution) of about 180μm.

The spatial resolution of space charge distribution in a given system is defined theoretically as the product of the pulse voltage width and the acoustic wave velocity in the polymer material. In this example, the applied pulse voltage width was 50ns and the acoustic wave travelling velocity in XLPE was considered as 2.2μm/ns, thus the best resolution of the system is estimated as 110μm. The difference between the theoretical resolution (110μm) and the practical value (180μm) was probably caused by the application of the mathematical deconvolution technique, which utilizes a low pass filter to remove the high frequency noise introduced by round-up errors and Gibbs oscillations at the point of discontinuity in the data processing [111].

In order to make the result comparable with that presented previously, a XLPE cable with 3.5mm thick insulation with inner and outer radii of 8.4mm and 11.9mm respectively was selected to carry out space charge measurement in our laboratory using the flat electrode PEA system. Similarly, when the 40kV dc voltage was applied to its central conductor the corresponding stress at the inner and outer interfaces were 13.6kV/mm and 9.6kV/mm respectively. The stresses are quite close to the values quoted in 6.6kV XLPE cable at the outer electrode/insulation interface in the literature. The space charge was measured at the beginning of the stressing voltage application, and no space charge accumulation was assumed in the bulk of the insulation except that induced surface charges by the external voltage at the electrodes, as shown in figure 4.6. The charge density at the outer electrode was measured as 1.2C/m^3 and half-peak height width was about 200μm. Obviously, the difference both in charge density and spatial resolution between these two sets of results obtained from different laboratories and different apparatus is not very significant. A comparison of the results is summarized in Table 4.1.

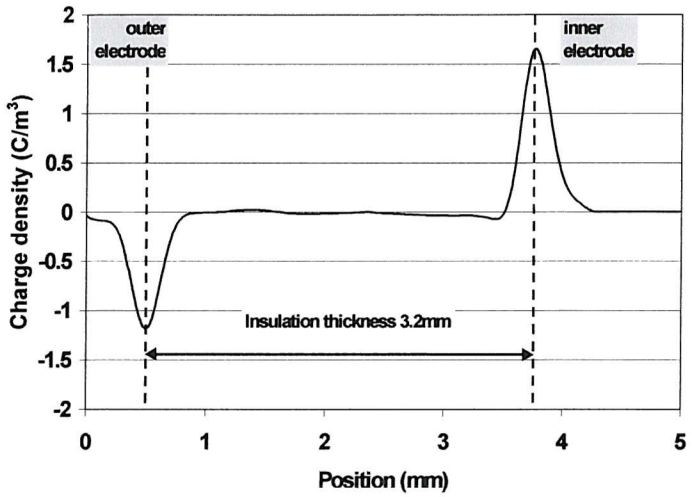

Figure 4.6 Space charge distribution obtained from new PEA system

Table 4.1 Comparison between two PEA systems

	Curved electrode	*Flat electrode*
Thickness of insulation	3.5mm	3.5mm
Electric stress (inner/outer)	~14.3 / 9.3 kV/mm	13.6/9.6 kV/mm
Charge density (inner interface)	~0.75 C/m^{3*}	1.7 C/m^3
Charge density (outer interface)	~1.2 C/m^3	1.2 C/m^3
Spatial resolution (inner interface)	~180 μm	200 μm
Spatial resolution (outer interface)	~400 μm*	200 μm

* No compensation was performed on the results from literature [110], so the peak representing the induced charge at the inner interface appeared lower and wider.

The results shown in figure 4.6 are after the geometric and propagation compensation. The ratio of charge densities on the inner and outer electrodes (*1.7/1.2≈1.4*) is in good agreement with the ratio of the externally applies electric stresses at these two interfaces (*13.6/9.6 ≈1.4)* if they are simply derived from the ac voltage in cable geometry.

In addition to the low pass filter adopted to improve the signal appearance after the deconvolution, a second filter was introduced to remove the noise produced from the data processing of the compensation algorithm for the geometry divergence and acoustic propagation attenuation and dispersion. All of these measures, however, in

turn will degrade the whole system's spatial resolution. This is the main reason that the spatial resolution in this example is reduced from the theoretical value of $110\mu m$ to about $200\mu m$ in practice.

4.5 Principle of the PEA method in the new electrodes arrangement

4.5.1 PEA system for cable geometry

Figure 4.7 illustrates the principle of the newly modified PEA system for space charge measurement in cable geometries. The cable consists of the central conductor, insulation, inner and outer semi-conducting layers, and is firmly held against the Al ground electrode. The PVDF transducer is attached on the other side of the ground electrode and is supported by a piece of acoustic wave absorbing material that has the same acoustic impedance as the PVDF. Much care is required to achieve an intimate contact between the electrode surface and the cable outer sheath to prevent acoustic wave loss and reflection.

In figure 4.7, it is assumed that a space charge distribution of density $\rho(r)$ exists in the cable insulation along the radial direction. According to the basic principles of the PEA technique described in chapter 3, a narrow pulsed voltage $v_p(t)$ is applied externally to the cable conductor via a coupling capacitor C. The pulsed electric stress $e_p(t)$ introduced by this voltage interacts with the space charge layer and a perturbation force is produced according to the Lorentz force. The pressure wave $p(t)$ resulting from this force propagates towards the central conductor and outer sheath of the cable. The acoustic wave arriving at the outer sheath is sensed by the piezoelectric transducer and is converted into an electrical signal. By detecting this output signal $v_s(t)$, and applying the necessary data processing techniques, the space charge distribution $\rho(r)$ can be obtained.

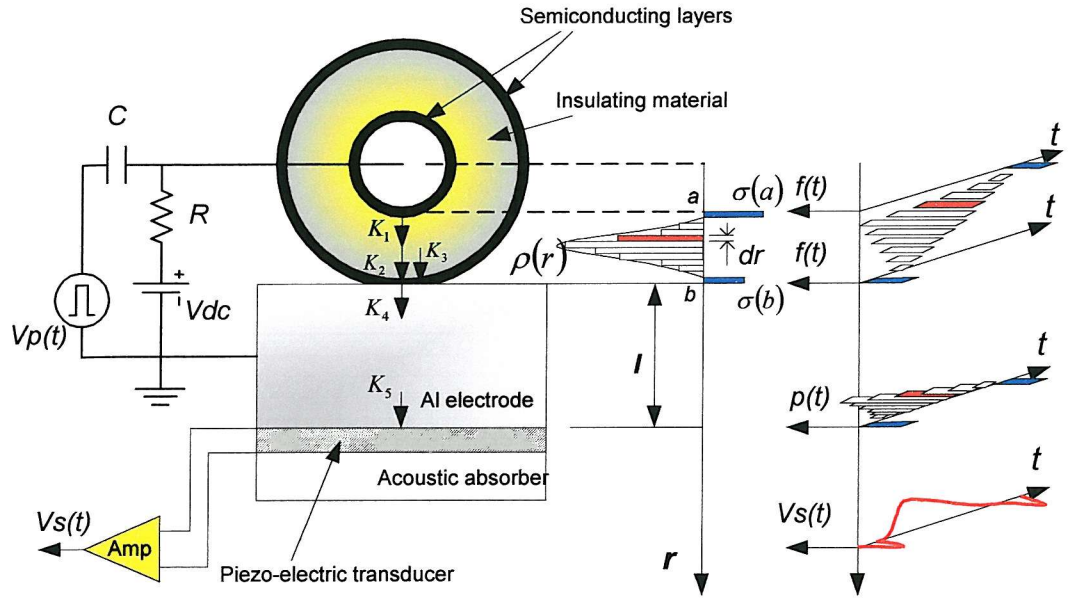

Figure 4.7. Principle of PEA method for coaxial cable sample

To simplify the description of the principles, we have to assume that the length of the cable is much greater than the thickness of the insulation and the material along the axial direction is homogenous. The space charge distribution is only changing in the radial direction within the insulation thickness. Therefore the acoustic pressure wave generated by the space charge density variation in this direction is also a one-dimension distribution depending only on the radial position.

It has to be pointed out that, in a non-dispersive medium, all the components of the pressure wave with different frequencies propagate with the same velocity. This fact is derived from the superposition principle and the pressure wave is viewed as a composition of harmonic components having the same speed. However, in a dispersive medium, the superposition principle is still applicable, but each harmonic component travels at its own speed [109].

4.5.2 Acoustic wave generation and detection

As shown in figure 4.7, the inner and outer radii of the cable insulation are *a* and *b* respectively. In the presence of space charge in the insulation with distribution $\rho(r)$, a small volume with thickness *dr* at position *r* has the elemental space charge $\rho(r)dr$.

According to Lorentz law, the force $\Delta f(r, t)$ induced by the pulsed electric field on this elemental charge is given by

$$\Delta f(t,r) = e_p(t,r)\rho(r)dr \tag{4.9}$$

where $e_p(t,r)$ is the applied pulse electric field, which varies through the thickness of the insulation and is expressed as

$$e_p(t,r) = v_p(t)/r\ln(b/a) \tag{4.10}$$

where $v_p(t)$ is the applied pulse voltage. To obtain a satisfactory spatial resolution for the space charge profile, the pulse voltage width should be as narrow as possible. Ideally, it should be described by the unit step function $u(t)$ in the following equation

$$v_p(t) = v_p[u(t) - u(t - \Delta T)] \tag{4.11}$$

v_p and ΔT are the amplitude and the width of the pulsed voltage.

Let $\sigma(a)$ and $\sigma(b)$ represent the induced surface charges at the inner and outer interfaces between the insulation and semiconducting layers, so the pulsed forces acting on these charge layers are

$$f(t,a) = \sigma(a)e_p(t,a) + \frac{1}{2}\varepsilon_0\varepsilon_r e_p^{\,2}(t,a) \tag{4.12}$$

at radius a, and

$$f(t,b) = \sigma(b)e_p(t,b) - \frac{1}{2}\varepsilon_0\varepsilon_r e_p^{\,2}(t,b) \tag{4.13}$$

at radius b. The interfacial charge densities $\sigma(a)$ and $\sigma(b)$ at the two interfaces are given as below

$$\sigma(a) = \varepsilon_0\varepsilon_r E(a) \tag{4.14}$$

$$\sigma(b) = \varepsilon_0\varepsilon_r E(b) \tag{4.15}$$

where $E(a)$ and $E(b)$ are the total static interfacial electric stresses at a and b, which are attributed to the applied dc voltage and the accumulated space charge in the bulk insulation. ε_r is the relative permittivity of the insulating material.

It is noticed that there are two terms in equations (4.12) and (4.13), the second term presenting the force due to the charge induced by the pulse voltage at the interfaces. Practically, the pulse voltage $v_p(t)$, is normally not higher than several kilovolt (e.g. in

the range of 2~8kV in this project and also with a very short duration). This is much smaller than the applied dc voltage which is of several tens of kilovolt, so the contribution from the charge caused by pulsed stress is much smaller than the first term and can be ignored.

During the application of the pulse voltage, the forces $\Delta f(t,r)$, $f(t,a)$ and $f(t,b)$ will cause the charge layers $\rho(r)dr$, $\sigma(a)$ and $\sigma(b)$to move slightly. This movement launches acoustic waves that propagate in two directions, one towards the electrode and the transducer and another in the opposite direction. The acoustic waves arriving at the transducer attached on the other side of the electrode will be detected and are represented by

$$p_s(t) = \frac{0.5K_3K_4K_5}{\ln(b/a)} \int_a^b \frac{\rho(r)}{(r)^{1/2}} v_p(t-\tau_s)dr \tag{4.16}$$

$$p_a(t) = \frac{K_1K_3K_4K_5}{(a)^{1/2}\ln(b/a)} \sigma(a)v_p(t-\tau_a) \tag{4.17}$$

$$p_b(t) = \frac{K_2K_4K_5}{(b)^{1/2}\ln(b/a)} \sigma(b)v_p(t-\tau_b) \tag{4.18}$$

where K_1 , K_2 are defined as the coefficients representing the ratio of the acoustic wave propagating towards the transducer to the total acoustic waves generated at the inner and outer interfaces between the semiconducting layers and the insulation respectively. If the acoustic impedances of the semiconducting layers and the insulation are the same, both K_1 and K_2 are 0.5. This is particularly true in XLPE cable where the semiconducting layer is also made of XLPE with certain additives. K_3, K_4 and K_5 are the pressure transmission coefficients of acoustic pressure at the interfaces of the insulation/semiconducting layer, the semiconducting layer/ground electrode and the ground electrode/transducer film (PVDF). Similarly, K_3 is approximately unity so $K_3=2K_1=2K_2$ if the acoustic impendence of insulation is the same as that of semiconducting material. τ_s , τ_a and τ_b represent the time required by the acoustic wave initiated at each charge layer to reach the transducer. Only the portion of the acoustic pressure wave propagating towards the outer sheath of the cable is considered, so a constant 0.5 is used in the equation (4.16). The terms of $(a)^{1/2}$ and $(b)^{1/2}$ in the equation derived from the effects of the cylindrical attenuation of the acoustic wave propagating through the cylindrical geometry. This will be considered in detail in the next chapter.

The total pressure sensed by the piezoelectric device (PVDF film) is the sum of $p_s(t)$, $p_a(t)$ and $p_b(t)$ and is given by

$$p(t) = p_s(t) + p_a(t) + p_b(t) \tag{4.19}$$

If we assume the bandwidth of the transducer response is much wider than the frequency spectrum of the pressure pulse generated by interaction between the charge layer and the pulsed electric stress, the induced charge $q(t)$ on the transducer surface due to the piezoelectric effect is linearly proportional to the pressure and the sensor area and is given by [76]

$$q(t) = kp(t)S \tag{4.20}$$

where k is the piezoelectric strain constant of the transducer and S the area. Otherwise, if the bandwidth of the transducer is less than that of the pulsed pressure, a deconvolution technique must be used to recover the space charge distribution. This case will be discussed later.

As described in the foregoing part of the chapter, the output voltage v_o from the transducer (in a open circuit) can be found from the transducer's capacitance C_p

$$v_o(t) = \frac{q(t)}{C_p} = \frac{kd}{\varepsilon_0 \varepsilon_r} p(t) = K_0 p(t) \tag{4.21}$$

where K_0 is a constant associated with the electro-mechanical coupling property of the transducer.

When the transducer is connected to an amplifier that has a frequency bandwidth wider than that of the input signal, then the amplified output voltage signal $v(t)$ will be proportional to the pressure pulse $p(t)$ too. It is given as

$$v(t) = GK_0 p(t) \tag{4.22}$$

G is the gain of the amplifier.

Considering the equation (4.16), (4.17), (4.18) and (4.19), we can obtain

$$\begin{aligned} v\ (t) = {} & \frac{K}{\ln(b/a)} \int_a^b \frac{\rho(r)}{(r)^{1/2}} v_p(t - \tau_s) dr + \frac{K}{(a)^{1/2} \ln(b/a)} \sigma(a) v_p(t - \tau_a) \\ & + \frac{K}{(b)^{1/2} \ln(b/a)} \sigma(b) v_p(t - \tau_b) \end{aligned} \tag{4.23}$$

in which $K=GK_0K_2K_4K_5$, because $K_3=2K_1=2K_2=1$ in XLPE cable.

4.5.3 Calibration of charge density

As the duration ΔT of the pulsed electric stress $e_p(t)$ is usually much shorter that the transit time of the acoustic wave through the cable insulation, $v_p(t)$ in equation (4.23) can be considered as a delta function with an amplitude V_p. Thus, $v(t)$ is directly proportional to the space charge distribution $\rho(r)$, as shown in the following equation

$$v(t)=K\left[\frac{\rho(u_{sa}t)}{(r)^{1/2}\ln(b/a)}V_p u_{sa}\Delta t+\frac{1}{(a)^{1/2}\ln(b/a)}\sigma(a)V_p+\frac{1}{(b)^{1/2}\ln(b/a)}\sigma(b)V_p\right] \quad (4.24)$$

where, u_{sa} is the velocity of acoustic pressure propagation in the insulation.

As the PEA technique is an indirect method of measuring space charge distribution in the dielectric material, the relationship between the piezoelectric transducer output and the charge density or the constant K has to be determined by calibration. To do so, a low dc voltage, under which no charge is introduced in the bulk of the material, is applied across the sample insulation. In this case, the first term of the equation (4.24) is zero and the following two components are regarded as the signal produced by the induced surface charges at the inner and outer interfaces and are represented by

$$v_{\sigma(a)}(t)=\frac{K}{(a)^{1/2}\ln(b/a)}\sigma(a)V_p \quad (4.25)$$

$$v_{\sigma(b)}(t)=\frac{K}{(b)^{1/2}\ln(b/a)}\sigma(b)V_p \quad (4.26)$$

where, $v_{\sigma(a)}(t)$ and $v_{\sigma(b)}(t)$ are the output voltages of the amplifier associated with the surface charges $\sigma(a)$ and $\sigma(b)$ resulting from the calibration voltage with low amplitude. Theoretically, both equation (4.25) and (4.26), or the induced charge at the inner and the outer electrode can be used to calculate the constant K as long as the acoustic attenuation and dispersion are negligible. However, in practice, the signal initiated at the outer interface, $v_{\sigma(b)}(t)$, is preferred because there is no attenuation and dispersion occurring. The outer semiconducting layer and the Al electrode is the common path for the acoustic waves initiated both from bulk charge and surface

charges, so the attenuation and dispersion occurring in all the acoustic waves are the same and can be cancelled out in the calibration procedure.

By integrating equation (4.26) within the region Δt, we get

$$\int_0^{\Delta t} v_{\sigma(b)}(t)dt = \frac{K}{(b)^{1/2}\ln(b/a)}\sigma(b)V_p\Delta t \tag{4.27}$$

The physical meaning of the left-hand term in equation (4.27) is the area under the voltage signal $v_{\sigma(b)}(t)$, which is proportional to the surface charge density at the outer electrode and is calculated in equation (4.15). Thus

$$K = \frac{(b)^{1/2}\ln(b/a)}{\sigma(b)V_p}\int_0^{\Delta t} v_{\sigma(b)}(t)dt \tag{4.28}$$

Substituting K into the first term of equation (4.24), the space charge distribution across the insulation of the cable can be expressed as

$$\rho(r) = \rho(u_{sa}t) = \frac{(r)^{1/2}v(t)\sigma(b)}{(b)^{1/2}u_{sa}\Delta t}\frac{1}{\int_0^{\Delta t} v_{\sigma(b)}(t)dt} \tag{4.29}$$

Figure 4.8 shows a typical calibration output voltage signal from a XLPE power cable with a wall thickness of 2.85mm when +25kV dc voltage was applied to the central conductor.

To verify that no space charge is formed in the calibration, the output signal was recorded after the removal of the calibration voltage, showing a straight baseline superimposed upon white noise from the system.

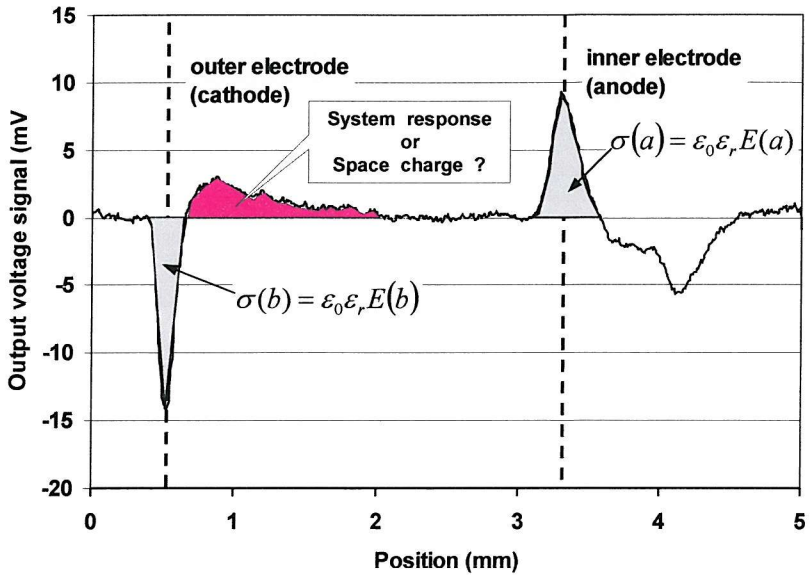

Figure 4.8. Calibration output signal from a XLPE cable at 25kV dc

4.5.4 Interfacial stress used for space charge density calibration

As the PEA technique is an indirect method of measuring the space charge distribution in the dielectric material, the relationship between the piezoelectric transducer output and the charge density has to be determined using a calibration procedure. A sufficiently low voltage is applied across the cable insulation for a short period of time which ensures no space charge is developed in the insulating bulk. The only charge present is the induced surface charge at the inner and outer insulation/electrode interfaces due to the external voltage, as shown in figure 4.8. The induced surface charges at the inner and outer electrodes are expressed in equation (4.14) and (4.15). In figure 4.8, the peak height or the area under each individual peak is proportional to the charge density at the electrodes. If we know the actual charge density at a given interface, the constant relating the output of the PEA system to the charge density will be determined by integrating the output signal throughout the peak duration. Here arrives another question, - how to determine the dc interfacial electric stress in sample of cable geometry?

It is known that the electric field distribution in an ac cable is dependent on the capacitance (or permittivity), whilst in dc cables it is governed by the conductivity of the insulating material. The variation of dielectric permittivity with either the temperature or electric stress is normally insignificant. In contrast, the conductivity is

dependent on the temperature and to a lesser degree on the electric stress. Discussion on the reasons for this dependence is however still limited on the empirical basis and no physical interpretation is available at the moment. Thus, it is difficult to predict the electric stress distribution across the cable insulation under dc conditions with the accuracy that can be achieved for ac cables [112]. As a result of the conductivity dependence with temperature and electric stress, in a fully loaded dc power cable the maximum electric stress will be at the outer semiconducting screen rather that at the conductor. Even without the temperature gradient across the cable insulation, as is the case with the present study which is being carried out at ambient temperature, the electric stress may also be influenced to an unknown extent by the non-uniformly distributed electric stress itself in the coaxial geometry. These characteristics, mainly limited to the oil-paper insulation, had been qualitatively analysed or described by the empirical formulae from the later 60's to 80's [112-116]. All the discussion was highly theoretical and the data were so scattered that Wiseman [116] indicated in his discussion that "There are no two papers in agreement when it comes to the influence of the applied voltage when there is a temperature gradient across the insulation". A literature search has found only very few reports on the dc electric stress distribution in polymer insulated power cables. It has been reported [117-120] that the conductivity in polymeric materials can be expressed empirically as

$$\gamma = \gamma_0 e^{\alpha T} E^p \tag{4.30}$$

γ_0 is the conductivity of dielectric material at reference temperature, α and p are the temperature and electric stress coefficients of the material, T is the temperature and E is the electric stress. The derived electric stress at a distance r from the centre of a cable conductor is given by

$$E(r) = \frac{\delta r^{(\delta-1)} U}{b^\delta - a^\delta} \tag{4.31}$$

where δ is a constant and is determined by the material, temperature difference across the cable insulation, and U is the applied voltage.

However, the constant δ in equation (4.31) suggested by Liu and MaAllister [117, 119, 120] is different from that by Tanaka [118]. According to their suggestion, in the case of a cable without a temperature gradient, δ takes the typical value of 2/3 and 1/2 respectively for XLPE insulated power cables. Consequently, the electric stress profiles

obtained for the different δ are significantly different. The ratio between the electric stresses at the inner and outer electrode is $(b/a)^{1/3}$ and $(b/a)^{1/2}$ respectively corresponding to different δ values. Obviously, they both differ from the electric field distribution derived from the expression governed by capacitance in the ac case, *i.e.*

$$E(r)=\frac{U}{r\ln(b/a)} \tag{4.32}$$

No matter which expression (equation (4.31) or (4.32)) is more precise in describing the actual situation, the electric stress distribution in a dc cable tends to be more uniform across the insulation in the absence of temperature gradient and space charge. However, the issue here is what value is used for the interface stress to determine the charge density in the calibration procedure. In view of the complexity of the above problem, the method suggested by Tanaka [118] has been adopted in this research to calculate the electric stress distribution in polymer insulation of a dc power cable when it is void of space charge. Thus the electric stress at the outer insulation/electrode interface is calculated from

$$E(b)=\frac{U}{2\sqrt{b}\left(\sqrt{b}-\sqrt{a}\right)} \tag{4.33}$$

The attraction of using the electric stress at the outer electrode is that a relatively small amount of attenuation and dispersion of the acoustic wave occurs at this point. Similarly, the stress at the inner semiconducting layer has the form of

$$E(a)=\frac{U}{2\sqrt{a}\left(\sqrt{b}-\sqrt{a}\right)} \tag{4.34}$$

and the ratio between the stress at the outer and inner interfaces is

$$E(b)/E(a)=\sqrt{a/b} \tag{4.35}$$

which differs from that obtained in the expression for the ac voltage, *e.g. a/b*. As mentioned previously, the induced surface charge is proportional to the interfacial stress, so the factor of $\sqrt{a/b}$ has to be adjusted to the acoustic signal originating from the inner electrode in the attenuation compensation scheme in next chapter.

Although the calibration based on the electric stress determined by $\delta=1/2$ is of some extent an approximation, it is the first time that the electric stress factor in a dc cable has been considered in space charge density measurements [14, 21-23]. If a more precise charge distribution is required, the δ values will need to be determined by a series of conductivity measurements.

4.6 Deconvolution of the raw signal

From the foregoing section, we know that the pressure waveform can realistically represent the space charge distribution both in spatial position and in quantity if the pulsed electric stress is sufficiently narrow. Nevertheless in some cases, the electric output signal from the piezoelectric transducer may be different from the actual space charge profile when the bandwidth of the transducer is not wide enough, or the detecting circuitry cannot give a perfect response to the piezoelectric device output. All the above factors may make it difficult to get the true space charge profile from the final signal output from the PEA system.

For instance, the waveform shown in figure 4.8 is a typical calibration signal with a very low dc voltage applied across the cable insulation. It is devoid of any trapped space charge except for the induced surface charges (indicated by grey shaded peaks). Any space charge in the bulk material would alter the voltage peaks and give rise to the voltage at the positions of trapped charge as shown in the shaded area in pink. However, in some cases the frequency response of the transducer and the amplifier can cause distortion of the output signal that can be wrongly interpreted as space charge. In other words, the output waveform without space charge could also look similar to the waveform shown in figure 4.8 as the pink shaded area [111, 121, 122].

To remove this effect, a deconvolution technique has to be employed to restore the original signal.

4.6.1 Frequency characteristics of the transducer

In section 4.5, we assumed that the frequency responses of both the transducer and amplifier are sufficiently wider to make the output linearly proportional to the charge distribution. The PVDF film used in the PEA has a very large bandwidth and a low Q and is believed to be superior to the ceramic transducer from the frequency response point of view [123]. If the transducer's thickness is d and the acoustic pressure travels through the transducer with a velocity u_p, then the transit time across the transducer is

$$\tau_a = \frac{d}{u_p} \tag{4.36}$$

τ_a is also known as the acoustic time. The transducer film used in our apparatus has a thickness of 52μm, so the acoustic transit time τ_a is 23.6ns if it is assumed that the acoustic pressure velocity in PVDF is ~2.2μm/ns. The cut off frequency of the transducer transfer function is about 42 MHz ($1/\tau_a$).

As the external pulsed electric field $e_p(t)$ has a duration of time Δt 50ns, its first zero point in the frequency spectrum after Fourier transformation is ~20 MHz. From this point of view, the frequency response of the transducer seems wide enough to cover the acoustic pressure wave.

However in practice, the frequency response of a transducer is much more complicated than described here, and may be influenced by the conditions of acoustic impedance match on both ends, in particular when it is sandwiched between two different materials [124]. This issue will be discussed together with the output circuit response in the following section.

4.6.2 Frequency characteristics of interface circuit and amplifier

In the PEA system, the piezoelectric transducer is directly connected to an amplifier with a finite input impedance, assumed to be dominated by the resistive input impedance R_a. Thus the output of the acoustic transducer can be modelled as a voltage source with an inherent capacitance C_p due to its geometry and permittivity. A first order Thevenin equivalent model of the electrical output network for the piezoelectric voltage in series with a single capacitor and resistor is shown in Figure 4.9. This one order high pass filter has a time constant $\tau_e = R_a C_p$, and the input capacitance of the amplifier is small in comparison with C_p and is neglected. The output voltage $v_0(t)$ across the resistor represents the transducer response to an acoustic pressure signal input.

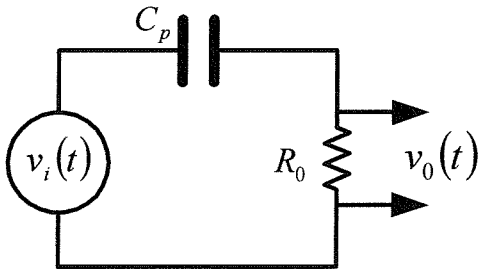

Figure 4.9 Equivalent output circuit of detector before the idea amplifier

The voltage signal detected by the amplifier is found by solving equation given by the Kirchhoff's Voltage Law (KVL):

$$\frac{1}{R_a C_p}\frac{dv_0(t)}{dt} + v_0(t) = v_i(t) \tag{4.37}$$

and the transfer function of this high pass filter in the frequency domain is

$$W(\omega) = \frac{V_0(\omega)}{V_i(\omega)} = \frac{j\omega\tau_e}{1 + j\omega\tau_e} = \frac{j2\pi f R_a C_p}{1 + j2\pi f R_a C_p} \tag{4.38}$$

The product of R_a C_p is called the electrical time constant τ_e of the detecting circuit. In our case, R_a is 50kΩ and C_p is about 310 pF (the PVDF transducer has ε_r=8, area 215mm^2 and thickness 52μm), thus the time constant of the input circuit is determined as 16μs, which is considered much longer than the transit time of the acoustic wave across the sample insulation. (For instance, in 5mm thick insulation, the transit time is ~2.5μs). The 3dB cut-off point of this high pass filter is ~63kHz, so that $W(\omega)$ can be regarded as having a flat frequency response over the relevant pass-band.

From the specification of the amplifier, its frequency response also has a wide band range from dc to 500MHz and should be able to respond accurately to the input signal. The transfer function of the amplifier is denoted as $A(\omega)$.

However, according to Bernstein [124], the transducer produces a frequency-dependent open circuit voltage by integrating the electric stress across its thickness which is then detected through the RC filter. The time-domain output is the convolution of these two functions. In the frequency domain, this transducer sandwiched between the Al electrode and the back absorber in a resonant configuration gives a large response to signal components over the frequency determined by τ_a^{-1}, but it attenuates the lower frequency components. This means that the transducer adopted in our setup cannot guarantee to give a flat response between the frequencies determined by the detection circuit's time constant τ_e, and the acoustic time τ_a, e.g. ~63kHz -42MHz. When an impulsive pressure excites the transducer, the final output from the whole system may look like the waveform shown in figure 4.8 due to this imperfect response. The pink shaded part was judged to be as the system's response and was ascertained by switching off the external voltage so that the output signal should return to the baseline since no space charge was developed under the calibration voltage.

4.6.3 Modelling of PEA signal system

From above description, we see that the signal containing the information about the space charge distribution can only be obtained after several conversions, e.g. the generation of the acoustic pressure by the interaction of the space charge layers and the pulsed electric field, the electric output as the acoustic pressure impinges on the piezoelectric device and the final output from the amplifier connected to the transducer. In practice, it is difficult to characterise each individual component, especially when they are connected together and influence each other.

Fortunately, from the engineering point of view, the issue concerned with the PEA application can be modelled as a simple, linear time-invariant system (LTI), from which a mathematical interpretation can be adopted to obtain the relationship between the exciting input (space charge distribution) and the response output (electrical signal). For simplicity, a LTI system takes an input signal *x(t)* and produces an output signal *y(t)* which is the convolution of *x(t)* and the indicial response *h(t)* of the system. The aim of the project is to obtain the space charge profile from the output signal of the PEA. To achieve this, a system has to be developed which is cascaded with the previous system (where the distortion happens during the signal transmission) to yield a replica of the desired signal. This system is known as an inverse system that carries out a deconvolution operation. The above two systems are shown in the cascade connection in figure 4.10

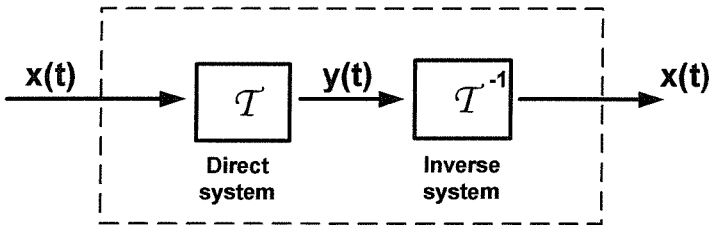

Figure 4.10 Invertible LTI system

In the PEA technique for the space charge measurement, the acoustic wave signal *p(t)* received at the transducer is converted into a voltage signal, which is then fed through an electronic interface to an amplifier. This conversion process can be described schematically in frequency domain form by the block diagram shown in

figure 4.11. The mathematical description of the above process with the final signal *v(t)* from the whole system is given in time domain as

$$v(t) = p(t) * s(t) * w(t) * a(t) \tag{4.39}$$

and

$$v(t) = h(t) * p(t) \tag{4.40}$$

where *s(t)*, *w(t)* and *a(t)* are respectively the unit impulse response of the transducer, the interface filter and the amplifier, and "*" denotes the mathematical operator of the convolution integral.

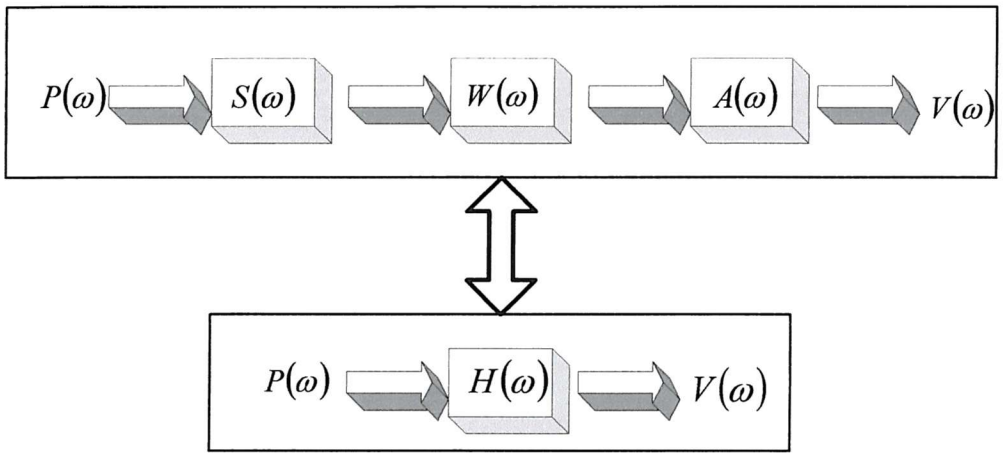

Figure 4.11 Equivalent LTI system in PEA

We can define *h(t)* as the unit impulse response of the overall PEA system which represents the total effects of all the transmitting steps from the piezoelectric effect to the electrical amplification of the signal. In the frequency domain, the previous relationship between the acoustic pressure wave *P(ω)* and the electric output *V(ω)* can be expressed in the following equation by introducing the transfer function of the whole system, *H(ω)*.

$$V(\omega) = H(\omega) \cdot P(\omega) \tag{4.41}$$

where *V(ω)* is obtained from the Fourier transform of the amplifier output *v(t)*. If the transfer function of the system *H(ω)* is known, the acoustic pressure wave in the frequency domain *P(ω)* can be determined. Consequently, with the following steps which use the inverse Fourier transform, the acoustic wave profile containing the information about the space charge distribution *ρ(r)* can be obtained. The

deconvolution method in the following part of the section is to determine the transfer function $H(\omega)$.

4.6.4 Concept of deconvolution

If the unit impulse response $h(t)$ of a continuous system is known, we can, in principle, work out the response of the system to any input $x(t)$. For instance, the input signal $x(t)$ shown in figure 4.12 can be approximated as a succession of rectangular pulses each of width $\Delta\tau$ and height $x(\tau)$, so that the area of a typical pulse centred at $t=\tau$ is $x(\tau)\Delta\tau$. If the pulse widths are assumed very small compared to the response time of the system under investigation, then each pulse can be modelled as an impulse of the form $A\delta(t-\tau)$, where the magnitude A of the impulse is equal to the area of the pulse and $\delta(t-\tau)$ is the unit delta function, the area under the delta function is finite and is equal to unity. Thus the signal $x(t)$ can be modelled as the continuous sum of impulses, each having the form of $[x(\tau)\Delta\tau]\delta(t-\tau)$. In the limit as the pulse with width approaches zero, $\Delta\tau$ can be replaced by $d\tau$, and $x(t)$ written as the integral

$$x(t) = \int_{-\infty}^{\infty} x(\tau)\delta(t-\tau)d\tau \tag{4.42}$$

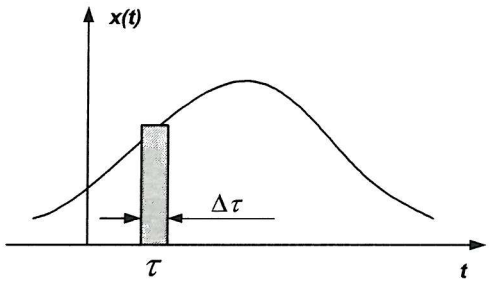

Figure 4.12 Illustration of the input (original) signal

Since we are dealing with a LTI system and we know that a unit impulse $\delta(t)$ gives rise to a response $h(t)$, then a scaled , time-shifted impulse will give rise to a similarly scaled and time shifted response. So using the principle of superposition we can likewise express the response $y(t)$ of the system to an input $x(t)$ as an integral summation of all the individual impulse response

$$y(t) = \int_{-\infty}^{\infty} x(\tau)h(t-\tau)d\tau \tag{4.43}$$

This integral is called the convolution integral and it defines the continuous convolution of x(t) and h(t).

$$y(t) = x(t) * h(t) = h(t) * x(t) \tag{4.44}$$

As we have previously shown in figure 4.10 that the direct system (known as a distortion system) yields an output *y(t)* which is the convolution of the input *x(t)* with the impulse response *h(t)*. The inverse system operation taking *y(t)* and producing *x(t)* is therefore called deconvolution.

4.6.5 Application of the deconvolution technique

In equation (4.43), $H(\omega)$ can be evaluated in the calibration procedure where a low dc electric stress is applied to the sample over a short duration of time to ensure no space charge is formed inside the insulation. The induced surface charge layers at both electrode interfaces are negligibly thin. In practice, it is impossible to get the charge in a line distribution due to the finite width of the pulsed voltage and the limitation of the whole system's spatial resolution. However, it is reasonable to assume the launched acoustic wave has a Gaussian distribution that is expressed in the following equation

$$p_1(t) = Ae^{-\alpha(t-\tau)^2} \tag{4.45}$$

A is the magnitude of the acoustic wave and is a constant for a given sample with a fixed thickness, dc stress and pulsed electric stress. α is a constant and is determined by the system's spatial resolution. Its frequency domain expression is $P_1(\omega)$. Correspondingly, its electric output in frequency $V_1(\omega)$ may also be given as

$$V_1(\omega) = H(\omega) \cdot P_1(\omega) \tag{4.46}$$

thus, the transfer function of the whole system is determined from the above equation. Finally, $P(\omega)$ in equation (4.41) can be obtained uniquely by the deconvolution technique.

To apply the deconvolution technique, we must firstly select the peak of the output signal, which contains the features of the whole system response. In figure 4.13, the curves in red and green colour represent the typical response of a system to the induced charges at the inner and outer interfaces. As there is no attenuation and dispersion at the acoustic signal from the outer electrode, the first peak and its follow-up exponential

overshoot response in figure 4.13 (the section between two dot-dashed lines) is selected as the reference signal to calculate the system transfer function.

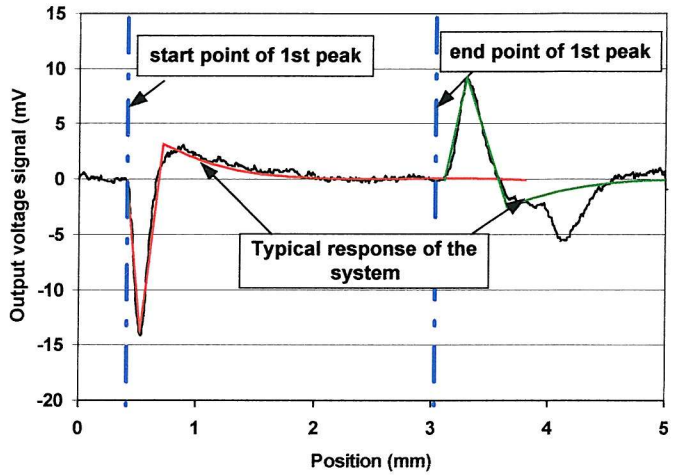

Figure 4.13 Response of the system and the definition of the reference peak

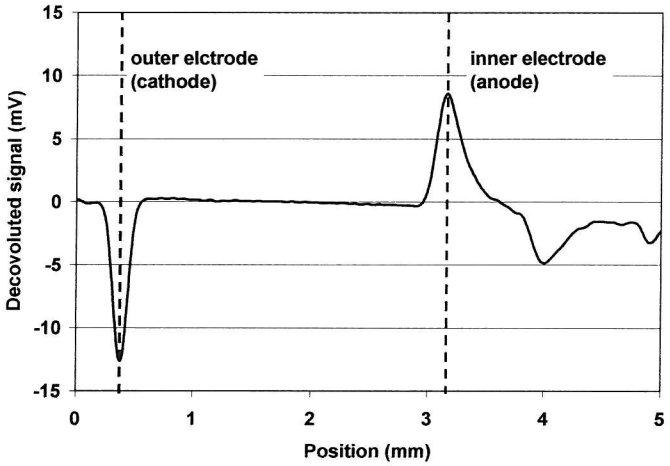

Figure 4.14 Deconvoluted signal

At the same time, a "unit impulse function" is generated by the software at the start point of the first peak (or the reference peak), which is expressed as $\delta(t-\tau)$ in a continuous-time system or $\delta(n-k)$ in a discrete-time system, where τ and k are the delay time or point of the first peak in continuous or discrete time system. Physically, this "unit impulse function" does not exist at all. So it is denoted here by $\gamma(t)$, a triangular function with a very short duration Δt [125]. Obviously, when $\Delta t \rightarrow 0$, $\gamma(t) = \delta(t)$.

Spectra of the so called unit impulse function $\gamma(t)$ and the reference output signal $v_1(t)$ at the outer electrode interfaces are obtained using a Fast Fourier Transform, and are given by

$$F(\omega) = \int_{-\infty}^{\infty} \gamma(t) e^{-j\omega t} dt = FFT[\gamma(t)] \tag{4.47}$$

$$V_1(\omega) = \int_{-\infty}^{\infty} v_1(t) e^{-j\omega t} dt = FFT[v_1(t)] \tag{4.48}$$

Thus the transfer function of the system from the acoustic pressure to the electric output signal is determined in the frequency domain by

$$H(\omega) = \frac{V_1(\omega)}{F(\omega)} \tag{4.49}$$

Similarly, applying the Fast Fourier Transform to the whole output voltage signal $v(t)$ and its frequency domain expression, $V(\omega)$ can be obtained. From equation (4.41), we have

$$P(\omega) = \frac{V(\omega)}{H(\omega)} \tag{4.50}$$

The acoustic pressure wave $p(t)$ containing the space charge distribution information (as described in equations (4.16)-(4.18) and (4.23)) can now be obtained by using a inverse Fast Fourier Transform. Finally, the real space charge profile is achieved from equation (4.24) in which the constant K is known from the calibration process. Figure 4.14 shows the voltage signal after the deconvolution. The result achieved at this stage can be further used to carry out charge density calibration. For the purpose of getting more accurate results, compensation for the geometry effect and propagation of the acoustic wave in the cable insulation will also be made on the basis of this waveform.

4.6.6 Deconvolution algorithm

The algorithm adopted in the research to perform the deconvolution is illustrated in figure 4.15.

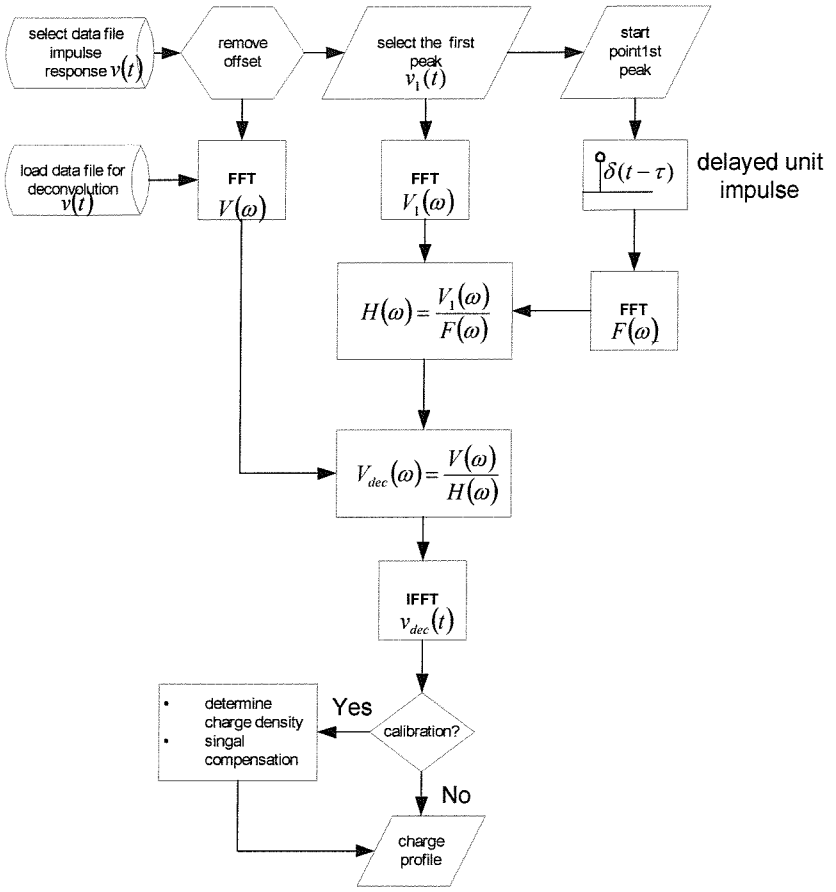

Figure 4.15 Flowchart of deconvolution

4.7 Summary

To overcome the inconvenience of the conventional PEA system in space charge measurement on cable samples, a newly modified system has been introduced in this research, which adopts a flat ground electrode. The new design offers several advantages such as ease of assembling the samples to maintain intimate contact at the interface of the cable sheath and the ground electrode. It is applicable to different sized cables without any modification to the electrode system.

In order to theoretically analyse the detection sensitivity and the position resolution of space charge measurement of this new PEA system, the acoustic wave propagation through all the media particularly the transmission property at the different interfaces has been discussed. The output of the piezoelectric transducer is proportional to both the pressure of the incident acoustic wave and the transducer thickness, but is independent of the contact area between the cable sheath and electrode or the effective

area of the transducer. Therefore the system which adopts a flat electrode can achieve the same detection result both in charge density and spatial resolution as that from the curved electrode configuration. This conclusion has been experimentally proved by the result obtained from the newly modified system in comparison with that obtained by a researcher [104] using the conventional PEA system.

The basic principle of this improved PEA system is described in detail from the signal conversion to the system's response. To acquire more reliable space charge distributions, the deconvolution technique is essential in order to remove improper responses of the system.

As a critical technique for the precise space charge measurement, the determination of the electric stress at the cable insulation and electrode interface used for charge density calibration is briefly discussed. Since the electric stress distribution in a dc cable is governed by the conductivity of the insulating material which is temperature and electric stress dependent, this introduces a complexity which throws the calibration of space charge densities in cable geometries into question: how does one determine the electric stress at electrode/insulation interface? The electric stress derived from ac voltage in a cable geometry used by all the researchers in charge density calibration is suspicious in the term of the accuracy in dc case. The electric stress at the outer sheath of the cable insulation is usually used for the charge density calibration and this is higher than the value obtained from the ac case. In particular, when the space charge is measured in the cable insulation with a temperature gradient to simulate the loaded cable, the error introduced by the calibration based on the ac voltage is even bigger. Two typical methods among the very limited advances in this area have been briefly discussed. One of them is adopted in this work for the purpose not only of improving the measurements, but most importantly for drawing more attention to the calibration technique required in space charge measurements in cable geometries.

Chapter 5

Geometry and Propagation Compensation to the Original Signal

5.1 Introduction

After the successful attempts to measure space charge in power cables by Fukunaga *et al* [14, 22, 104], there is a need to carry out measurements with more accuracy both in charge density and spatial resolution. For the PEA method, the above two measurement specifications are basically determined by the system design, for instance the width of pulsed voltage and the transducer thickness will directly influence the amplitude and the shape of the output signal. Additionally, the signal to noise ratio is another vital factor affecting the measurement result. In particular, when the method is applied to a full-sized power cable, the signal of interest may be significantly attenuated and broadened due to the attenuation and dispersion of the acoustic wave during its propagation through the thick insulation.

Moreover, owing to the coaxial geometry, the pulsed electric stress will vary across the cable insulation and the acoustic wave intensity will diverges along the radial direction of the cable insulation. Both factors will affect the finally detected signal at the piezoelectric transducer.

In this chapter, the above-mentioned factors are analysed in detail. To allow for all of them in the data processing, a compensation algorithm is developed to correct both for the geometry and propagation factor in the original signal in order to obtain a true space charge distribution profile across the cable insulation.

5.2 Compensation to the geometry factors

5.2.1 Divergence of the pulsed electric stress

Unlike the plaque samples across which a uniform electric stress distribution is assumed to be due to the external pulse voltage, the electric stress e_p for the coaxial geometry is given by the following equation:

$$e_p(t,r) = \frac{v_p(t)}{r\ln(b/a)} \tag{5.1}$$

where a and b are the inner and outer radii of the cable insulation respectively and $v_p(t)$ is the externally applied pulse voltage. This means that the pulsed electric stress decreases across the insulation from the inner electrode to the outer electrode. The PEA technique is based on the principle of detecting the acoustic pressure wave produced by the interaction between the pulsed electric stress and the charge layer. Thus, with the variation of the pulsed electric stress, the same space charge density near the inner electrode will give a higher acoustic signal than that close to the outer electrode. As a consequence of this non-uniform electric stress distribution, the acoustic pressure wave initiated by the above interaction will depend not only on the charge density but also on the position. Thus the variable distribution of the pulsed electric stress needs to be taken into account when a quantitative space charge distribution is sought in cable samples.

5.2.2 Divergence of acoustic waves in a coaxial geometry

As it is assumed that the space charge distribution only changes in the radial direction, the acoustic wave containing information about this space charge profile will depend only on the radial position. In this case the acoustic wave equation in cylindrical coordinate is given by [109]

$$\frac{1}{u_{sa}^2}\frac{\partial^2\phi(t,r)}{\partial t^2} = \frac{\partial^2\phi(t,r)}{\partial r^2} + \frac{1}{r}\frac{\partial\phi(t,r)}{\partial r} \tag{5.2}$$

where $\phi(t,r)$ is the velocity potential of vibrating motion in the medium, and u_{sa} is the velocity of the acoustic wave propagation. The solution of equation (5.2) is

$$\phi(r,t) = \frac{A}{\sqrt{r}} e^{j(\frac{\omega}{u_{sa}} r - \omega t)} \tag{5.3}$$

with $k = \omega / u_{sa}$, the above equation changes to

$$\phi(t,r) = \frac{A}{\sqrt{r}} e^{jk(r - u_{sa} t)} \tag{5.4}$$

where, ω is angular frequency of the acoustic wave, $\omega=2\pi f$, and A is a constant and is determined by the boundary condition.

Thus, the pressure wave per unit area at position r is [109]

$$p(t,r) = \mu \frac{\partial \phi(t,r)}{\partial t} = -\frac{j\mu u_{sa} Ak}{\sqrt{r}} e^{jk(r - u_{sa} t)} \tag{5.5}$$

where μ is the density of medium in which the acoustic wave is launched and travels. This equation describes the propagation of an acoustic wave in an elastic (or lossless) medium within a cylindrical geometry in the radial direction. According to this equation, the intensity of a pressure wave generated by the space charge will decrease along the radial direction causing a reduction in signal intensity when it travels to the outer sheath. This factor can be best described by the following equation

$$\frac{p(t + \Delta t, b)}{p(t,r)} = (r/b)^{1/2} \tag{5.6}$$

$p(t,r)$ and $p(t+\Delta t,b)$ are the acoustic waves produced at radius r and detected at the outer sheath b, and Δt is the time for an acoustic pulse travelling from position r to b. As the outer semiconducting layer is the common path for all the acoustic pressure wave produced within the bulk of the cable insulation (including the surface charge at the insulation/electrode interfaces), any divergence in this layer is neglected for the sake of simplicity.

The two divergent factors (pulse electric stress and acoustic pressure wave) are simply illustrated in figure 5.1.

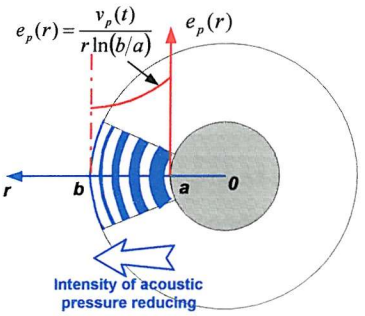

Figure 5.1 Divergent effects of pulsed electric stress and acoustic pressure

5.2.3 Correction to geometry divergences

Divergent effects due to cylindrical geometry can be explained in the following way. Assume that there are two charge layers with the same density at the inner and outer insulation/electrode interfaces. The acoustic pressure produced at the inner interface is (b/a) times higher than that at the outer interface because of the divergent distribution of the pulsed electric stress. On the other hand, the detected pressure wave at the outer sheath, originating from the inner interface, is $(a/b)^{1/2}$ times its originating value due to the acoustic transmission divergence, as described in equation (5.6). The resultant effect of the two factors will therefore suggest that the charge density at the inner interface is $(b/a)^{1/2}$ times that at the outer interface. In practice, the original signal after the deconvolution must be corrected by the geometry factor $(b/r)^{1/2}$ where r lies between the outer and inner electrode radii.

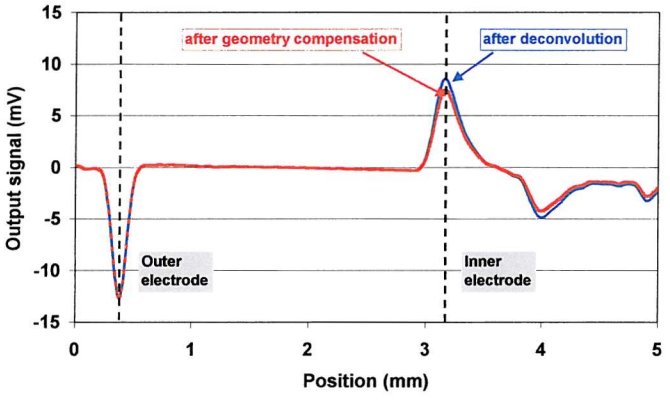

Figure 5.2 Output signal before and after geometry compensation

The signal in the blue colour in figure 5.2 is the original output after deconvolution (same as shown in figure 4.14), and the waveform in red shows the result after

geometry compensation. According to the factor $(b/r)^{1/2}$ introduced previously, the actual measured signal of the induced charge at the inner electrode can be 1.15 times higher than its true value, since the inner and outer radii of the cable insulation are 8.75mm and 11.55mm so $(11.55/8.75)^{1/2} = 1.15$. For some of the samples tested in the project, the outer radius of the insulation was twice the size of the inner radius, so the possible correction factor required can be as high as 1.4 ($\sqrt{b/a} = \sqrt{2} \approx 1.4$). Thus the error introduced in the measured value of the space charge in the vicinity of the inner electrode can be as high as ~40%. It is therefore necessary to implement a correction to the original signal to remove the influence of geometrical factors.

5.3 Compensation to attenuation and dispersion of acoustic wave

5.3.1 Attenuation and dispersion of acoustic wave in polymer insulation

So far, it has been assumed that the polymeric dielectric is an ideal medium for acoustic wave propagation, and neither attenuation nor dispersion is considered in the protocol of dealing with the acoustic wave propagation through the insulation. This assumption has been adopted by previous researchers on power cables [21-23, 102, 105] and may be valid for making space charge measurement on thin insulation or for comparing different materials. In full sized cables with thick walled insulation, the influence of the polymer characteristics on pressure wave propagation in the material is significant and can no longer be neglected if accurate results of charge density and distribution across the insulation are required. In this case, some measures must be taken to ensure the accuracy of the measurement result.

In the theory of elasticity, the stress and the strains in the medium are related by a constant [109], and the deformation process is completely reversible. However, it is known that most polymers exhibit an explicit departure from this type of behaviour and are regarded as being of visco-elastic or lossy. They are then dispersive media. Attenuation and dispersion may occur as acoustic waves propagate through. This phenomenon had already been observed in the early research where the acoustic waves were significantly attenuated and scattered during their propagation through the dielectrics, such as PE, XLPE and some other polymer insulating materials [75, 126, 127].

It is well known that if the medium is non-dispersive, acoustic waves with different frequencies propagate at the same velocity. The superposition principle therefore allows the possibility of a general wave being viewed as a composition of harmonic components having the same speed, which can also be called the phase velocity. When a medium is dispersive (as the polymeric material discussed here) the superposition principle still holds, but each harmonic component propagates with its own velocity [109]. Clearly, the location of wave packets within the pulse undergoes redistribution during propagation: faster ones travel to the front, while the slower ones move to the rear. The absorption and dissipation of acoustic wave energy into heat or other forms of energy are believed the major sources of attenuation [108].

Consider a plane harmonic pressure wave propagating through a solid elastic medium. It can be represented by

$$p(t,x) = p_0 e^{j(\omega t - kx)} \tag{5.7}$$

As noted earlier, the phase velocity u_{sa} is a constant and has a relationship of $k = \omega/u_{sa}$ with the wave number k, and ω as the angular frequency of acoustic wave.

In the linear visco-elastic medium, the real wave number k must be replaced by its complex generalization $k(j\omega) = \beta(\omega) - j\alpha(\omega)$. Substituting this relation into the above equation yields the wave propagation in a visco-elastic medium

$$p(t,x) = p_0 e^{i[\omega t - k(j\omega)x]} = p_0 e^{-\alpha x} e^{j(\omega t - \beta x)} \tag{5.8}$$

where α and β are defined as the attenuation and dispersion factor respectively. Both of them are functions of ω. The plane wave intensity is decaying (x>0, α>0) during propagation with a frequency-dependent decay rate governed by the imaginary part of the complex wave number $\alpha(\omega)$. The wave velocity is given by

$$u_{sa}(\omega) = \omega/\beta(\omega) \tag{5.9}$$

which is also frequency dependent and is governed by the real part of the complex wave number.

These two effects, which are referred to as wave attenuation and wave dispersion, constitute a radical difference between the behaviour of a purely elastic medium and that of visco-elastic medium. To appreciate the physical consequences of the above two effects, it is useful to imagine the propagation of a pulse in each of the above two media. In a perfectly elastic material the pulse does not suffer any distortion. On the

other hand, in a visco-elastic material the pulse decays due to the attenuation, and the waveform of the pulse is broadened since different harmonic components propagate with different acoustic velocities.

Real and imaginary parts of the complex wave number are not independent of one another. Their interdependence is determined by the Kramers-Kronig relationship [128, 129], further discussion of which is beyond the scope of this project.

5.3.2 Attenuation and dispersion factors in cable geometry

The attenuation and dispersion properties of the acoustic medium are characterised by the α and β functions of ω. As mentioned previously, they are interrelated by Kramers-Kronig relationship [128]. Mathematically, for a causal system, $\alpha(\omega)$ is related to $\beta(\omega)$ and vice versa. In practice, they can be determined experimentally in a given system.

By application of the Fourier transform, equation (5.8) in cylindrical coordinate is transformed into

$$P(\omega,r) = P(\omega,a)e^{-\alpha(\omega)(r-a)}e^{-j\beta(\omega)(r-a)} \tag{5.10}$$

where $P(\omega,a)$ and $P(\omega,r)$ are the Fourier transforms of the acoustic wave at radius of a and r respectively, and r is varying from a to b.

Equation (5.10) can be used to describe the propagation of an acoustic pressure wave in the visco-elastic medium in the frequency domain. If the attenuation factor $\alpha(\omega)$ and dispersion factor $\beta(\omega)$ are known, the propagation characteristics of the acoustic wave through the lossy and dispersive material can be determined. The transmitted acoustic wave at any position r is obtained by inverting the Fourier transform

$$p(t,r) = \frac{1}{2\pi}\int_{-\infty}^{\infty} P(\omega,r)e^{j\omega t}d\omega \tag{5.11}$$

In section 5.2, we have already solved the problem caused by the geometric divergence of the pulse electric stress and acoustic pressure along the radial direction. This means that to determine the attenuation and dispersion factor later on, there is no need to consider the geometrical factors any more.

Generally, the attenuation and dispersion factors α and β of acoustic waves can be determined from pressure wave measurements at two different positions within the medium, by making use of equation (5.10) [109].

In a practical application of the PEA technique to a cable sample, $\alpha(\omega)$ and $\beta(\omega)$ can be deduced from the measured values of the induced surface charges at the inner and outer electrodes in the calibration test. It is known that the magnitudes of the induced surface charge densities are linearly proportional to the interfacial electric stresses. The basic requirement of the calibration or the interfacial stress used for the calibration in dc cable case has been briefly discussed in section 4.5.4. Removing the geometry factor in the preliminary data processing converts the subject from the cylindrical geometry to the planar geometry. The induced charge peak at the inner interface is then regarded as attenuated and scattered result of the surface charge at outer interface after propagation across the cable insulation. Therefore the attenuation and dispersion properties of the cable insulation will be determined from these two peaks. The detailed procedure is described as below.

The frequency spectra of the acoustic pulse at $r=a$ and $r=b$ are given as

$$P(\omega,a)=|P(\omega,a)|e^{-j\phi(\omega,a)} \tag{5.12}$$

$$P(\omega,b)=|P(\omega,b)|e^{-j\phi(\omega,b)} \tag{5.13}$$

where $|P(\omega,a)|$ and $|P(\omega,b)|$ are the amplitude spectra for the waves at the inner and outer interfaces, and $\phi(\omega,a)$ and $\phi(\omega,b)$ are the phase spectra for the acoustic wave at the inner and outer interfaces respectively.

Substituting equations (5.12) and (5.13) into equation (5.10) and let $r=b$, the following equations can be obtained

$$|P(\omega,b)|=|P(\omega,a)|e^{-\alpha(\omega)(b-a)} \tag{5.14}$$

$$\phi(\omega,b)=\phi(\omega,a)+\beta(\omega)(b-a) \tag{5.15}$$

Considering the induced charge density proportionally connected to the external dc stress that has been discussed in section 4.5.4, the ratio of the electric stresses at the inner and outer electrode $\sqrt{a/b}$ has to be rectified to the acoustic signal from the inner electrode. Thus the attenuation and dispersion factors are obtained consequently

$$\alpha(\omega) = -\frac{1}{b-a}\ln\left|\frac{P(\omega,b)}{P(\omega,a)*\sqrt{a/b}}\right| \tag{5.16}$$

$$\beta(\omega) = \frac{1}{b-a}\left|\phi(\omega,b)-\phi(\omega,a)\right| \tag{5.17}$$

Hence, the relationship given in equation (5.10) between the initial acoustic pulse $P(\omega,a)$ and the transmitted pulse $P(\omega,r)$ is identified by $\alpha(\omega)$ and $\beta(\omega)$and the relevant acoustic transfer function at position r is given by

$$G(\omega,r) = \frac{P(\omega,r)}{P(\omega,a)} = e^{-[\alpha(\omega)+j\beta(\omega)](r-a)} \tag{5.18}$$

This transfer function can be used in the frequency domain to compensate for the attenuation and dispersion occurring during acoustic propagation at different positions r. Thus, the actual acoustic pressure profile across the cable insulation may be obtained by the inverse Fourier transform as given in equation (5.11).

5.3.3 Algorithm for the signal recovery

The algorithm for the signal recovery is illustrated in figure 5.3. It is worth pointing out that we are discussing the acoustic pressure attenuation and dispersion caused by a lossy and dispersive medium, so it is convenient to represent the acoustic pressure wave by the notation $p(t,r)$ or $P(\omega,r)$ in the time and frequency domains. However, in practice, the signal we deal with is the electrical output (voltage signal) from the transducer and the relationship between this and the pressure wave is given by equation (4.22). We also know that after the deconvolution of original signal, the acoustic wave profile is linearly proportional to the voltage output of the PEA system so from now on, the signal involved in the processing will be denoted as voltage, $v(t,r)$ in time domain and $V(\omega,r)$ in frequency domain.

In the discrete system, the signal compensation for the attenuation and dispersion in the frequency domain is detailed in the following steps.

In discrete form, the sequence of signals after deconvolution and geometry compensation is presented as

$$v(t,r_i) = [v(t,r_0), v(t,r_1), v(t,r_2), \ldots\ldots, v(t,r_N)] \tag{5.19}$$

N is the number of sampled points, $i=1$ to N. In the frequency domain, the signal after the fast Fourier transform (FFT) is expressed as

$$V(\omega, r_i) = FFT[v(\omega, r_i)] = [V(\omega, r_0), V(\omega, r_1), V(\omega, r_2), ..., V(\omega, r_N)] \quad (5.20)$$

$V(\omega,r_i)$ is the frequency spectrum of the signal at position r_i.

To remove the attenuation and dispersion effect, the transfer function obtained in equation (5.18) is applied correspondingly to each individual point (layer by layer). Thus the recovered signal corresponding to an individual point in the frequency domain is given in voltage form as

$$V'(\omega, r_i) = V(\omega, r_i) \cdot G(\omega, r_i) \quad (5.21)$$

The superposition principle is then applied to the thickness of the sample insulation and the total spectrum of the recovered signal is given as

$$V(\omega) = \sum_{i=1}^{N} V(\omega, r_i) \cdot G(\omega, r_i) \quad (5.22)$$

Finally, the Inverse Fast Fourier Transform (IFFT) yields the signal after the compensation in the time domain.

$$V(t) = v(r/u_{sa}) = IFFT[V(\omega)] \quad (5.23)$$

where u_{sa} is the velocity of acoustic wave travelling through the cable insulation.

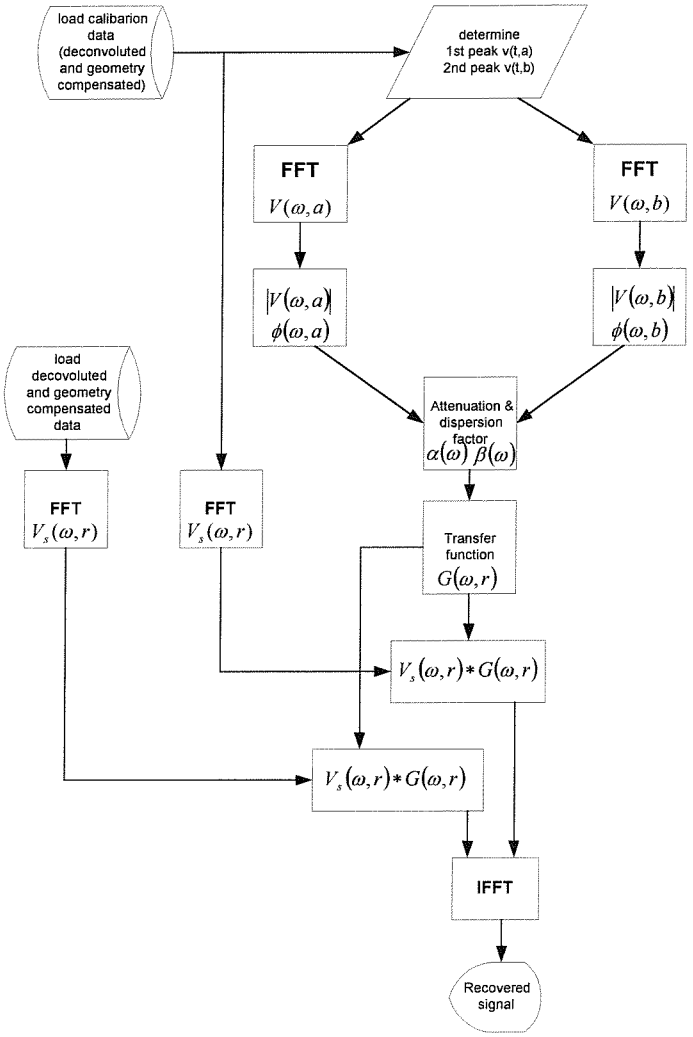

Figure 5.3 Algorithm for attenuation and dispersion compensation

Figure 5.4 represents the results before and after the attenuation and dispersion compensation. Two peaks that are selected by the vertical cursor lines in figure 5.4(a) are used to calculate the attenuation and dispersion factors. Diagram (b) is the final result after the data processing, for which the output has been converted to space charge density distribution by means of the calibration and the horizontal axis represents the location (in *mm)* within thickness of the cable insulation. Notice that the amplitudes of these two charge layers are consistent with the externally applied electric stresses at the two interfaces.

The interface appearance and the block diagram of the data acquisition and the processing program developed in LabView^{TM} environment is shown in appendix A.

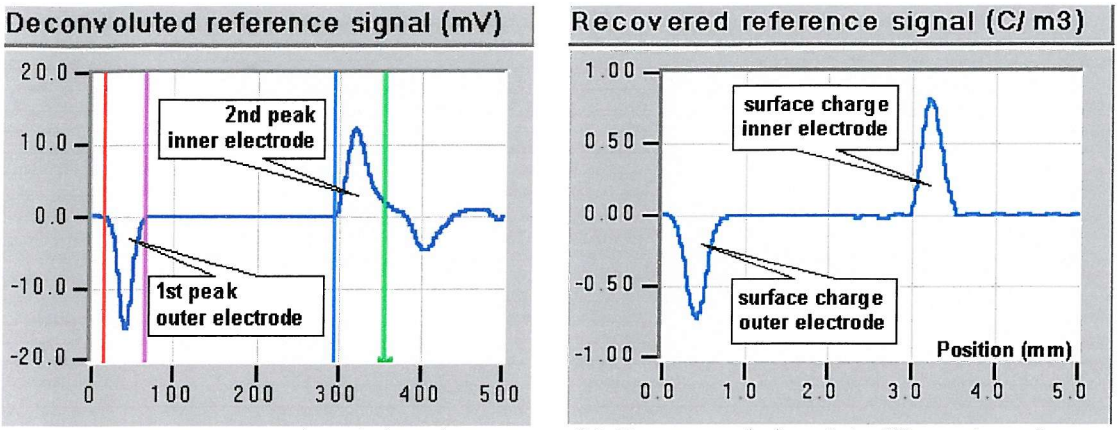

(a) Deconvoluted signal

(b) Recovered signal (calibrated to charge density)

Figure 5.4 Signals before and after recovery

5.4 Summary

Geometrical effects on the measurement of space charge in coaxial cables are fully analysed. Due to the cylindrical geometry, the pulsed electric stress varies across the insulation and so does the pressure of the acoustic wave as it propagates from the inner side to the outside. These two effects will make the measured space charge at position r to be $(b/r)^{1/2}$ times higher than the real value. The effect of these geometry factors has been removed in the subsequent data processing of the measurement of the space charge.

Acoustic wave attenuation and dispersion in polymeric cable insulation is briefly described. On the basis of this analysis, a method of determining the attenuation and dispersion coefficients from the experiment is suggested such that correct charge profiled can be obtained.

An algorithm has been developed in the project by taking all the effects such as geometry as well as the attenuation and dispersion from acoustic wave transmission into account. The result reported here from a XLPE cable measured at calibration voltage has proved the correctness of the compensation method.

Chapter 6

Modification of the Electric Stress by Space Charge

6.1 Introduction

The electric stress distribution modified by the space charge in cable insulation is the main concern in polymer-insulated dc power cable development. The presence of space charge in the cable insulation will result in the distortion of the initial electric field profile and causes localised electric stress enhancement. As a result, premature failure of the cable insulation may take place well below the anticipated or designed values. Takeda *et al* [106] estimated the electric stresses at the inner and the outer interfaces between the insulation and the semiconducting layer from the magnitude of the induced surface charges using the fact that the induced surface charge at the electrode is proportional to the interfacial stress. In most insulation systems, the interface is believed to be the weakest point where electrical breakdown is likely to occur. However, when space charges are present in the insulation the maximum electric stress does not always have to appear at the insulation/electrode interface. It may arise somewhere inside the bulk of the insulating material if distributed homocharges or irregular packet charges are present. Figure 6.1 graphically illustrates how accumulated space charge in a planar sample with parallel electrodes can distort the electric stress distribution. The appearance of the heterocharge causes the electric stress to be enhanced at the two interfaces and to be decreased in the centre part of the material, so the maximum electric field appears at the dielectric and electrode interface. The contrary situation exists in the case of the homocharge accumulation, in which the highest stress occurs in the bulk of the dielectric material.

For a full sized cable (especially that with a thick walled insulation) the heterogeneity of the insulating material may be inevitable because of the variation of molecular structure (crystalline degree) and distribution of cross-linking by-products and other additives in the material. Hozumi *et al* [104] have directly observed the packet charge formation and migration through the XLPE cable insulation due to the ionisation of impurities. This uneven and unpredictable charge distribution through the cable insulation thickness may change the local stress, and is likely to generate stress enhancement at certain regions of the insulation. With such a complex space charge profile, the electric field distribution distorted by the packet charge may become complicated and unpredictable throughout the whole insulation.

One of the most important tasks for research into extruded polymer insulated dc power cables is the accurate determination of the electric stress profile across the bulk insulation in the presence of bulk space charge. The reliability of the electrical insulation is still one of the most important factors determining the safe operation of the entire cable transmission system.

In this chapter, the method of determining the electric stress distribution across the cable insulation from the space charge profile is fully described. The total electric stress profile, which includes the externally applied divergent field and the component from the trapped charge in the bulk material, will be achieved by the method.

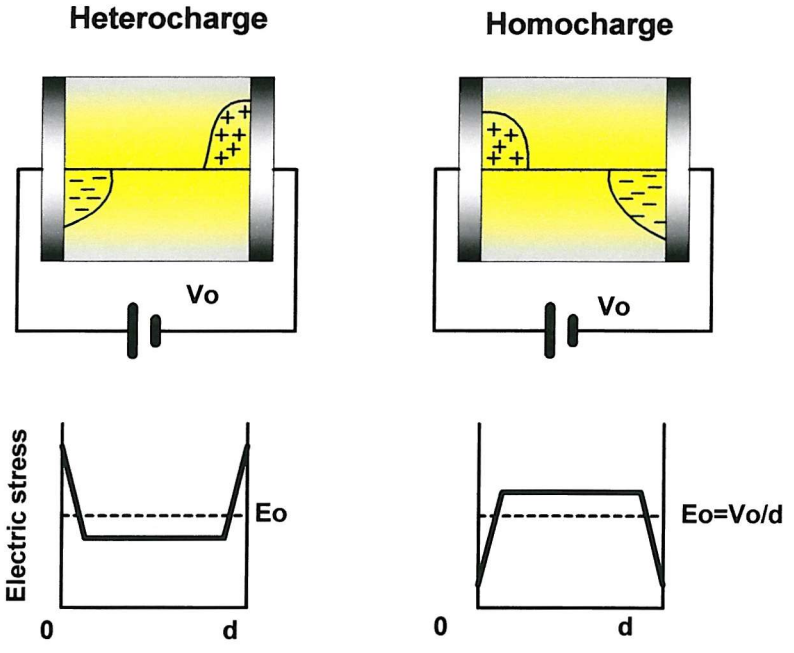

Figure 6.1 Illustration of electric field modified by space charge

6.2 Electric stress calculation in coaxial coordinates

The variation of the voltage potential distribution in a volume involving the space charge is generally described by Poisson's equation. Its general expression in cylindrical coordinate with charge density ρ is given as

$$\frac{\partial^2 U}{\partial r^2}+\frac{1}{r}\frac{\partial U}{\partial r}+\frac{1}{r^2}\frac{\partial^2 U}{\partial \phi^2}+\frac{\partial^2 U}{\partial z^2}=-\frac{\rho(r,\phi,z)}{\varepsilon_0\varepsilon_r} \tag{6.1}$$

where $\rho(r, \varphi, z)$ represents the charge density at point P in figure 6.2, ε_0 the permittivity of free space and ε_r the relative permittivity of the dielectric material in the volume.

It is assumed as before that the insulating material is homogeneous along the cable axial direction and the length of the cable sample is much bigger than its insulation thickness. The space charge distribution therefore only varies in the radial direction. So the charge density ρ can be regarded as dependent only on the cable insulation radius r. Thus, Poisson's equation (6.1) is reduced to

$$\frac{d^2 U}{dr^2}+\frac{1}{r}\frac{dU}{dr}=-\frac{\rho(r)}{\varepsilon_0\varepsilon_r} \tag{6.2}$$

or, by substituting $dU/dr=-E$ into equation (6.2), it becomes

$$\frac{dE(r)}{dr}+\frac{1}{r}E=\frac{\rho(r)}{\varepsilon_0\varepsilon_r} \tag{6.3}$$

This is a typical first order linear differential equation and its general solution is given by

$$E(r)=\frac{1}{\varepsilon_0\varepsilon_r r}\int_a^b r\rho(r)dr+\frac{1}{r}C \tag{6.4}$$

where C is a constant considered below.

The electric stress $E(r)$, including the contributions from both the applied voltage and accumulated space charge in the bulk of the cable insulation, is defined as the total electric stress $E_{total}(r)$ and is expressed as

$$E_{total}(r)=E_{charge}(r)+E_{applied}(r) \tag{6.5}$$

where $E_{applied}(r)$ stands for the externally applied electric stress. Its complex distribution across the cable insulation under dc voltage has been briefly described in section 4.5.4 on the charge density calibration. For the convenience of referring, the expression is re-stated:

$$E_{applied}(r) = \frac{\delta r^{\delta-1} U_{applied}}{b^{\delta} - a^{\delta}} \tag{6.6}$$

$U_{applied}$ is the externally applied voltage, and δ is a constant depending on the characteristics of the insulating material. For XLPE used in cable insulation, δ has the value 1/2. C in equation (6.4) is a constant and can be determined by considering the equal energy principle as expressed in equation (6.7). In practice, C is adjusted to make the area under the applied electric stress profile $E_{applied}(r)$ equal to the area under the modified electric stress due to the presence of the space charge $E_{total}(r)$. In other words, the algebraic sum of the area comprised under the electric stress profile attributed to the pure space charge $E_{charge}(r)$ must be zero.

$$\int_a^b E_{total}(r)dr = \int_a^b E_{applied}(r)dr = U_{applied} \tag{6.7}$$

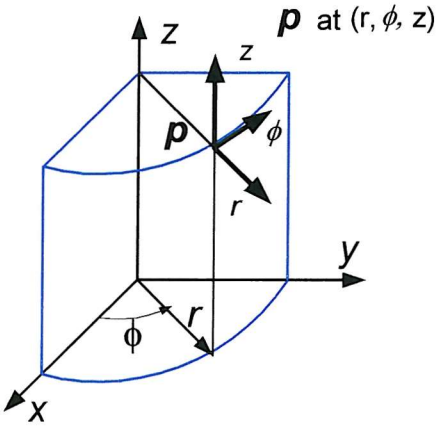

Figure 6.2 Cylindrical coordinate with space charge distribution $\rho(r, \phi, z)$

Implementation of the previously described procedures of electric stress calculation is schematically illustrated in figure 6.3. Two situations are discussed. Figure 6.3 (a) shows the measured result for a calibration procedure when no space charge is present in the bulk of the material. Figure 6.3 (b) deals with the case of space charge being present.

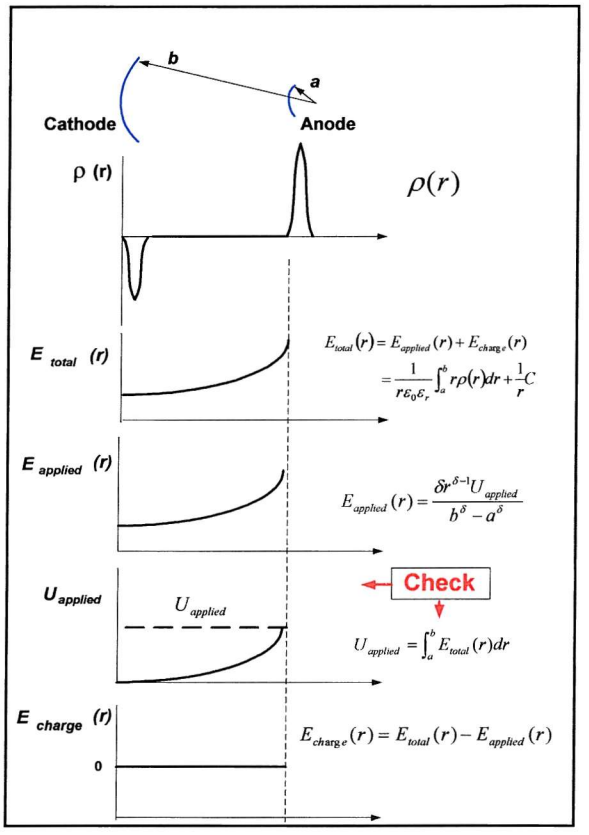

(a) Calculation of electric stress distribution without space charge

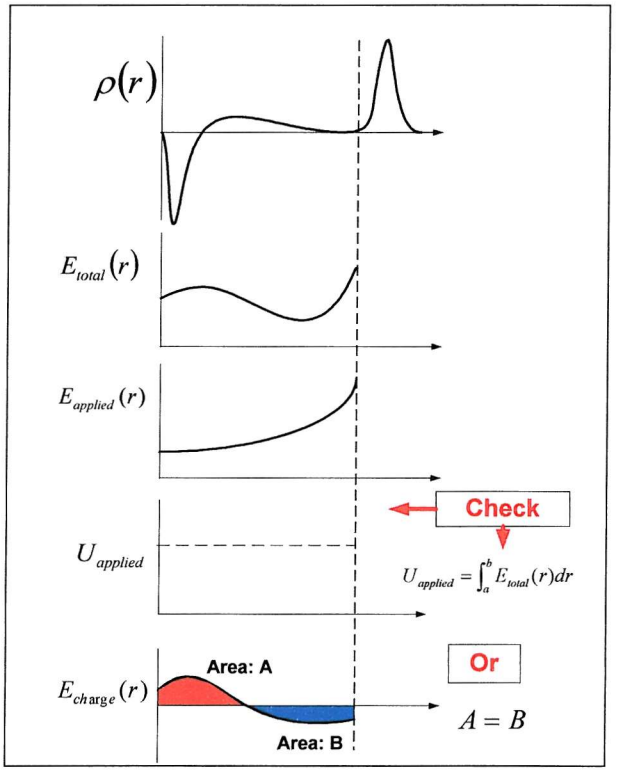

(b) Electric stress distribution with space charge

Figure 6.3 Procedure for computing of electric stress distribution (with bulk charge)

6.3 Practical calculation of electric stress distributions from space charge profiles

The electric stress distribution in a commercial ac XLPE power cable was practically calculated using the above method. One result was obtained under the calibration voltage when no space charge was developed in the bulk insulating material except for the induced surface charges at the two electrodes. The measured space charge is shown in figure 6.4 (a). Another result displayed in figure 6.5 (a) was obtained after the sample has been stressed at the dc voltage of +80kV for a period of time, in which a considerable heterocharge had been accumulated near the two electrodes.

The electric stress profiles derived on the basis of those space charge measurements are plotted in figure 6.4 (b) and figure 6.5 (b) respectively. For comparison, the electric stress distribution due to the external voltage (which is governed by the cable geometry) is also presented in the same diagram. Under the calibration voltage, there is no charge generated in the insulating material except the induced surface charge, so the total electric stress is only attributed to the calibration voltage. Its distribution is therefore determined by the cable geometry, as shown on the curve plotted in red. As expected, the electric stress distributions obtained from the space charge measurement (with only surface charge present) is in a good agreement with the externally applied stress.

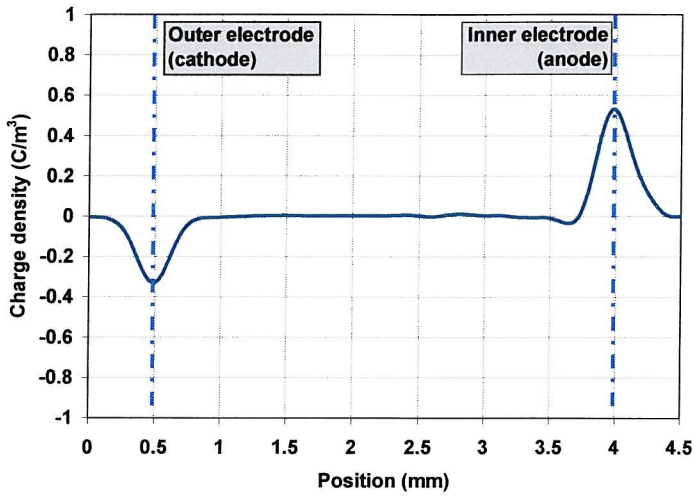

(a) Space charge distribution (calibration result)

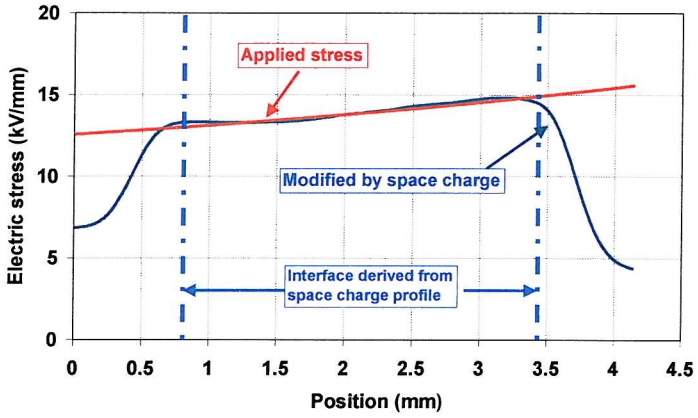

(b) Electric field distribution

Figure 6.4 Space charge and its modified electric field at calibration voltage

Obviously, the component of electric stress due to the bulk space charge is zero if the geometry-governed stress is subtracted from the total stress. As a check, the potential across the insulation is calculated from equation (6.7) by integrating the total electric stress throughout the cable insulation. The result gave just the value of the applied calibration voltage.

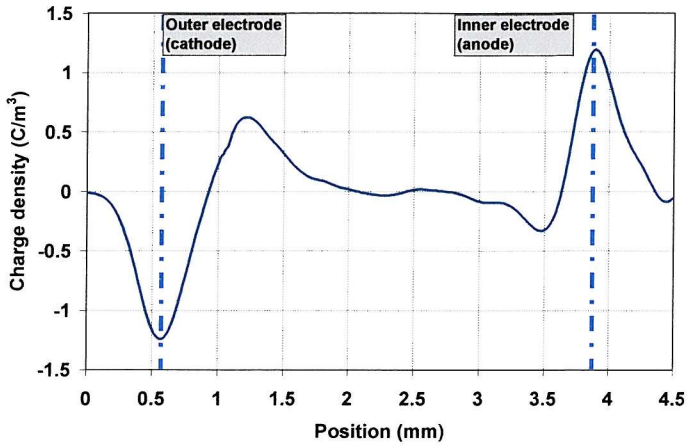

(a) Space charge distribution (80kV for 24hrs)

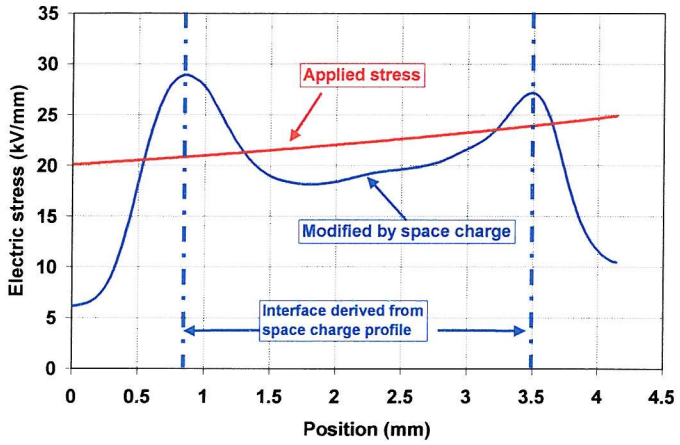

(b) Electric field distribution

Figure 6.5 Space charge and its modified electric field after a certain time ageing

Similarly, the electric stress distribution modified by the space charge in the same cable after a period of ageing is displayed in figure 6.5 (b). In this situation, the initial electric stress profile due to the external voltage has been considerably distorted by the space charge. As the heterocharges accumulated in the cable insulation, the electric stresses at the inner and outer electrodes are enhanced to about 27 kV/mm and 29 kV/mm respectively from their original values of 25 kV/mm and 20 kV/mm. On the other hand, the stress in the central part of the insulation is reduced by a certain extent as the electric field of these heterocharges counteracts the applied stress. In the same way in which the previous calculation was checked, the electric potential is calculated by integrating the electric stress across the insulation. The applied voltage value was obtained.

6.4 Improvement in method for electric stress determination

The method introduced above for calculating the electric stress distribution across the cable insulation is correct from the theoretical point of view, and has been used by many researchers working in sheet samples [6, 78, 130]. However, if we look at the results at the interfaces in figure 6.4 (b) and 6.5 (b), there may be some suspicions about its apparent position and the corresponding stress at these areas. Because of the limited spatial resolution in the space charge profile across the insulation, some errors may also be introduced into the result of electric stress calculation. Theoretically, if heterocharges are present as indicated by figure 6.5, the maximum value of the electric stress should appear at the two interfaces defined by the dashed lines in figure 6.5 (a). However, the actual position of the maximum electric stress formed by integrating the induced surface charge could only appear at the point of the surface charge peak returning back to zero. Therefore, the interface position indicated by the electric stress profile has shifted from both sides towards the centre of the insulating material.

Davies *et al* [131] proposed a method in the application of LIPP to the planar sample to overcome the above problem. It can be extended by analogy to cable geometries.

As the position resolution of the PEA system is limited, the magnitude of the charge density in the vicinity of an electrode is not accurate due to the overlap of the signals representing the surface charge and the bulk charge in the dielectric material. This difficulty can be somewhat solved by removing the stressing voltage to eliminate the surface charge at the electrode due to the external voltage, and leaving the bulk charge in the sample and its image charge at the interface. Figure 6.6 (a) shows a charge distribution in the same sample as that in figure 6.5 after the removal of the applied voltage. Figure 6.6 (a) is considered to be a good representation of the real space charge distribution over the region between lines ***c*** and ***d***. Integration of the charge density over this region will give the correct electric stress distribution due to the space charge alone.

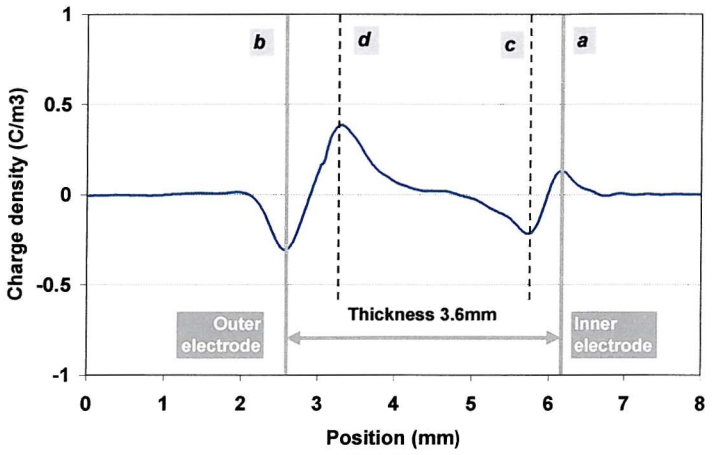

(a) Charge profile after voltage removal

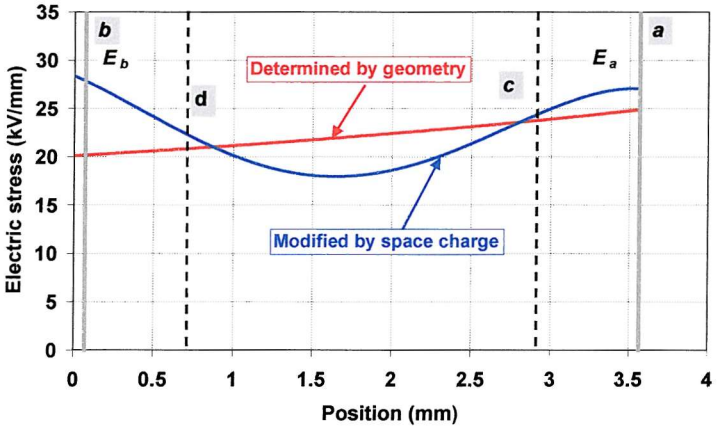

(b) Electric stress distribution

Figure 6.6 Electric stress distribution calculated by improved method

As noted previously, the surface charge density is linearly proportional to the interfacial stress, so the actual interface stresses E_a and E_b at the inner and outer electrodes can be determined from the amplitude of the surface charge at these two points when the external voltage is on. Specifically, as the interfacial stress and its induced surface charge amplitude under the calibration voltage is known, by comparing them with the surface charge under the test condition, the interfacial stresses, E_a and E_b, can be figured out. Knowing the electric stresses at the interfaces and the stress distribution in the middle of the sample and by using a higher degree polynomial to extrapolated a line from ***a*** to ***c*** and from ***d*** to ***b***, the electric stress over the whole thickness (between line A and B) can be mapped. Such a curve is presented in figure 6.6 (b).

The constant C in equation (6.4) is calculated according to the "equal energy" principle, *i.e.*

$$\int_a^b E_{total}(r)dr = \int_a^b E_{applied}(r)dr \qquad (6.8)$$

The graphical meaning of the above equation is that the area under the applied electric stress distribution $E_{applied}(r)$ is equal to the area under the modified electric stress profile $E_{total}(r)$.

Comparing figure 6.6 (b) with figure 6.5 (b), it is noticed that the two curves of electric stress distributions derived from different methods have almost the same shape. There might be some slight difference in the trend of the modified electric stress in the central insulation. This, however, may be attributed to the variation of space charge profile before and after the removal of the applied voltage. This suggests that the accuracy of the improved method of assessing electric stress from the space charge is limited to slow rates of charge change.

6.5 Summary

The calculation of the electric stress profile throughout the cable insulation from space charge measurements is firstly presented. Due to polymer materials' inhomogenities, the packet charge in the bulk material or the homocharge close to the electrode, the maximum electric stress appears to be somewhere in the insulation other than at the dielectric/electrode interface, like most researcher presumed. Knowledge of the electric stress distribution across the whole insulating material could lead to better understanding of the effects of space charges on polymer insulation characteristics in dc power cables.

The implementation of the method is introduced in detail by considering a XLPE cable sample in which electric stress profiles both under the calibration voltage and on ageing test voltage are derived from the space charge results. As a check, the integration of the electric stress through the cable insulation thickness has been found to give the calibration voltage and ageing voltage respectively.

In order to overcome the shortcomings brought in by the system's spatial resolution in measuring the space charge distribution and the subsequent determination of the electric stress profile, an improved method was adopted. The electric stress attributed to space charge is obtained by simply integrating the bulk charge within the insulating material as the external voltage is removed. The interfacial stress is determined from the amplitude of the surface charge peak, and the whole stress profile across the cable

insulation is then mapped by extrapolation using a high degree polynomial. This method may give more accurate results to the electric stress in the region close to the electrode if no fast charge accumulation is involved in the insulation.

Chapter 7

Space Charge Measurement in Cable Samples

7.1 Introduction

The aim of studying space charges in polymer insulation in electrical apparatus (e.g. extruded polymeric power cables), is to acquire better understanding of space charge behaviour in a practical structure. In particular, in an on-going project to develop a dc XLPE power cable, space charge measurements on a full sized cable sample can give insight into the effects of a number of features. These include the effects of the actual semiconductive layers, XLPE insulating materials actually being produced in the manufacturing process, and the divergent distribution of dc electric stress on space charge accumulation. It would also be convenient and realistic to investigate the effect of a temperature gradient across the insulation on the space charge distribution by heating the cable with an inducted current. This would create the exact situation of a loaded cable in service. As discussed in a previous chapter, the dc electric stress distribution in a cable insulation is governed mainly by the conductivity which is a rapidly increasing function of temperature and, to a great or less extent of the field strength [117-120, 132]. Therefore, the lowest electric stress in a fully loaded dc cable may appear in the insulation near the conductor because of the high temperature generated by Joule heat of the transmitted current, while the highest electric stress appears near the outer sheath.

In this chapter, the results of space charge measurements through the insulation of prototype cables incorporating different modified XLPE materials are presented and discussed. Attention is given to the material amendments on the fast space charge formation due to a voltage ramp, the charge build-up rate and decay speed, and the net

charge and its distribution. Moreover, each sample was tested separately before and after thermal treatment, and the space charge measurements showed significant differences between them. The removal of volatile residues by thermal treatment can considerably suppress space charge accumulation in these cable samples.

7.2 The experimental condition and cable samples

To ensure comparability among the different samples, measurements were conducted under almost similar temperature and externally applied electric stress conditions. Due to the large size of the cable samples, it was difficult to maintain a constant temperature during the experiments. The results discussed in this chapter were obtained under the room temperature ranging between 21 °C and 25 °C. The choice of electric stress and ageing time was determined on the basis of practical consideration, a literature review and preliminary space charge measurements in sheet and cable samples [9, 105, 133]. Of course, the limitation of the test facilities is another consideration.

The charging electric stress was chosen from what is encountered in practical dc power cable insulation. Hvdc cables with mass impregnated paper insulation currently operate at a stress of about 30kV/mm [41, 133]. The latest reported electric stress in a prototype product rated to ±250kV with XLPE insulation is only 25kV/mm [105]. Considering the capability of the testing rig in the current research, the electric stress for space charge measurement was therefore chosen from 10 to 30kV/mm, depending on the sample's insulation thickness.

It was found that the space charge in most samples could reach its steady distribution in 24 hours, so the space charge profile evolution within this ageing time only is discussed.

No measurement was carried out on cable insulation with a temperature gradient, because of the difficulty of precise control of the temperature through the thin insulation and the limited project time-schedule. However, such research is suggested for further work.

Three types of cable samples were investigated in the project and incorporated different modified XLPEs as insulating material. The comparison was conducted not only among different materials but also between the fresh sample and the sample subjected to heat conditioning (degassing) at 90°C for 100 hours to see the effect of

removing the residue produced in cross-linking on the space charge accumulation. The exact recipe of the modified materials is not known due to the commercial reasons. The cables made from three modified materials are labelled as 1491, 1494 and 1495.

7.3 Space charge measurement

7.3.1 Sample stressed under ramp voltage

In the space charge measurement on cable and plaque geometry, the sample was firstly stressed with a quick voltage ramp and the amplitudes of the induced charge peaks at the two electrode/insulation interfaces were recorded. There are two reasons for doing this ramp test. First, it is to see if there is any fast space charge formed during the process of the voltage increase. It is known that the induced charge at the electrode interface is linearly proportional to the interfacial electric stress. If there is no bulk charge with the insulating material, the interfacial stress is directly related to the external applied voltage, and the induced charge should also be proportional to the external voltage. If some space charge has been developed in the volume of the insulating material, the measured peak values of the induced charge deviate from the linear relationship (straight line) and their increases with the applied voltage will speed up or slow down depending on the space charge polarity, as the illustration in figure 7.1.

Second reason for the ramp test is to determine the threshold stress (or voltage) from which the space charge starts to build up. This value is used to check the validity of the calibration, which must be carried out below this voltage.

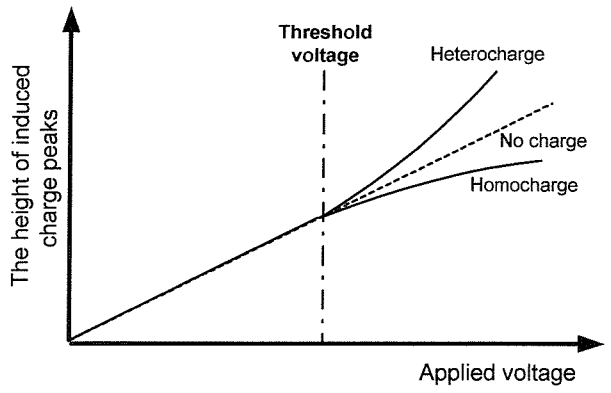

Figure 7.1 Illustration of ramp test

7.3.2 Cable 1491

Ramp test

The ramp test results of cable 1491 are shown in figure 7.2. When the applied voltage reaches 70kV, the relationship between the induced surface charge and the external voltage in the fresh sample starts to diverge from the linear tendency. As shown by the curves of figure 7.2(a), the induced surface charge at the cathode (outer electrode) is speeded up, whereas the charge at the anode (inner electrode) is slowed down as the voltage exceeds 70 kV. This un-proportional variation of the induced surface charges at the electrodes with the voltage increase implies that some positive charge has begun to accumulate in the bulk of the insulation as the applied voltage goes over 70kV. This space charge accumulation during the voltage ramp was also clearly observed from the space charge measurement after the voltage ramp test. This can be seen from the space charge profiles noted as "0 time" in figure 7.3 (a) and figure 7.4 (a), where a considerable amount of heterocharge (positive) at cathode has developed during the voltage ramp. On the contrary, no space charge was observed in the degassed sample during the voltage increase and the peak heights of the induced surface charge at two electrodes vary linearly with the applied voltage over the range from 0 to 80 kV, as shown in figure 7.2 (b)

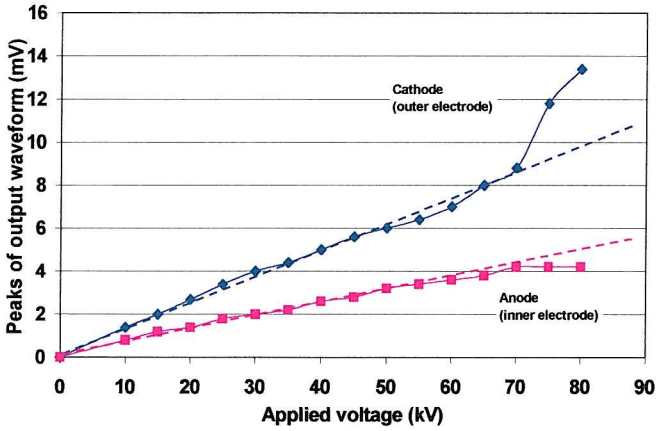

(a) Fresh sample

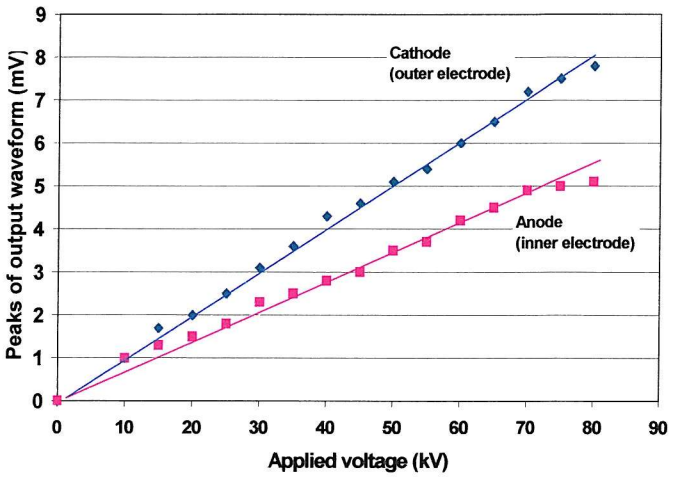

(b) Degassed sample

Figure 7.2 Interface charge variation with the external voltage in cable 1491

The inner and outer radii of the insulation were 5.62 mm and 11.50 mm respectively. The threshold stresses of the undegassed cable 1491 at the inner and outer interfaces are 14.5 kV/mm and 10.1 kV/mm corresponding to the voltage of 70 kV.

Space charge evolution

Figures 7.3 and 7.4 show how the space charges evolutes with the external voltage application over a period of time. The measurements were carried out under the conditions of both voltage on and voltage off.

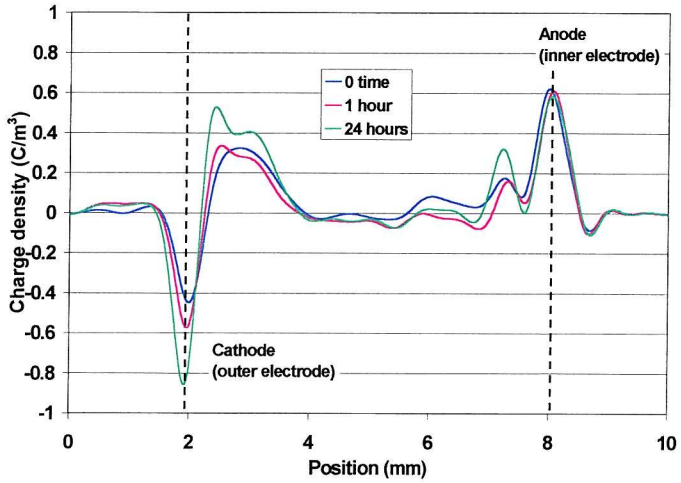

(a) Fresh sample

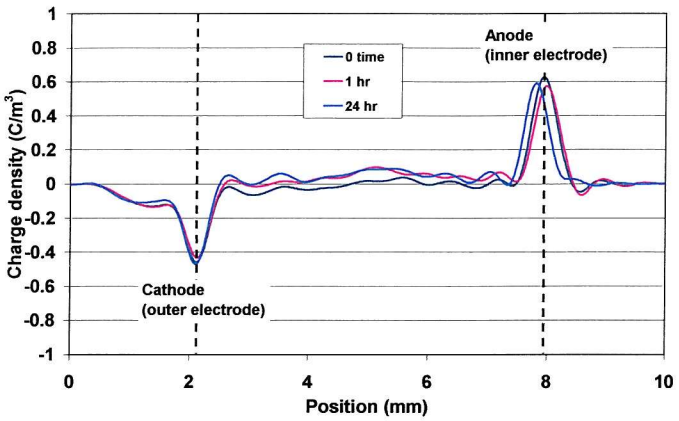

(b) Degassed sample

Figure 7.3 Space charge distribution of cable 1491 (volts on)

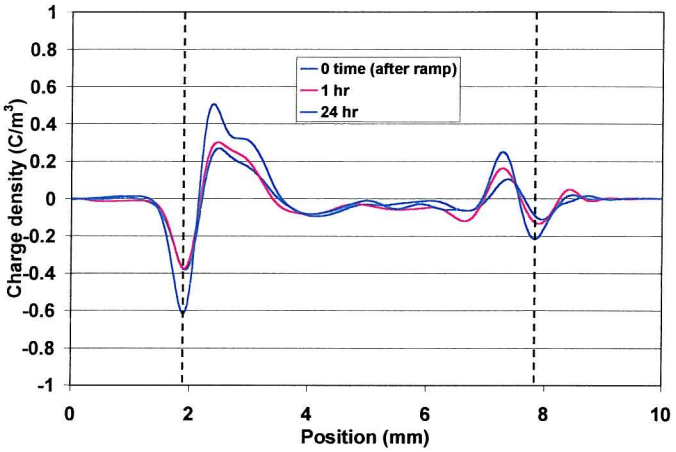

(a) Fresh sample

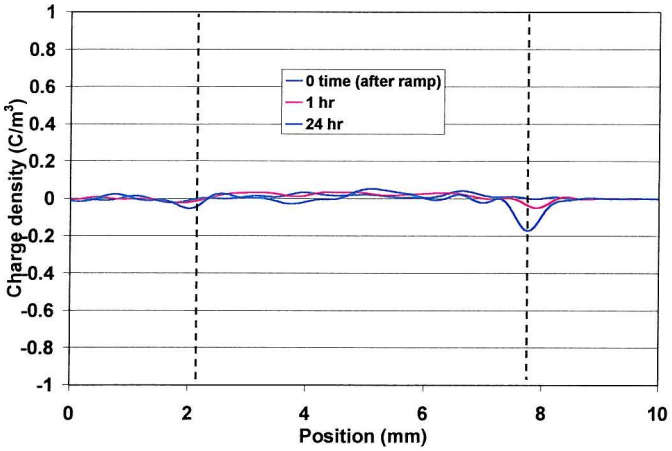

(b) Degassed sample

Figure 7.4 Space charge distribution of cable 1491 (volts off)

The curves denoted as "0 time" in these figures are the space charge measurement obtained soon after the end of the ramp voltage test which lasted about 5 minutes.

Obviously, a considerable positive charge has formed in the undegassed sample over this period of time, as shown in figure 7.3 (a) and figure 7.4 (a). After that, the packet positive charge gradually increases and accumulates near the outer electrode over the whole period of the ageing time. Simultaneously, a small positive charge is also generated adjacent to the inner electrode.

The space charge accumulations in the vicinities of the two interfaces are substantially different in this undegassed sample. It is noticed that a heterocharge (positive) has accumulated near the outer electrode (cathode), while a homocharge (positive) is near the inner electrode (anode). Furthermore, the former is much bigger than the latter in terms of the charge density. The location of the homocharge near the inner electrode is detached from the interface charge by a certain distance, rather than being adjacent to it. The heterocharge at the outer electrode and the packet shape of the positive charge close to the inner electrode indicates that the bulk effect of the ionization of residual impurities in the cable insulating material dominates the space charge accumulation in this situation.

From the results of the space charge initiation during the voltage ramp and the charge accumulation in the following ageing period, it is concluded that the space charge development, in particular for the heterocharge at the outer electrode, is very quick in the fresh cable 1491sample. As the heterocharge accumulation near the outer electrode in the voltage ramp procedure, it is believed that the interfacial electric stress has been enhanced; the higher electric stress in turn accelerates the ionization and results in a fast charge accumulation. The situation at the inner interface was in contrast because the interfacial stress was reduced by the positive charge. This might be the reason why the space charge density near outer sheath is higher than that close to the inner electrode even though the initial electric stress here is higher. No doubt, the distribution of residue concentration across the insulation may be another factor affecting the space charge distribution, but there is no available method to determine it.

By contrast, only a small net positive charge is found in the degassed sample with an even distribution through the cable insulation after 24-hour ageing time. The existence of these charges within the bulk insulating material can be discovered by the two small negative induced surface charges at the electrodes in the figure 7.4 (b). For this measurement the induced surface charge due to the external electric stress has been removed by turning off the applied voltage.

Space charge decay

After 24 hours of ageing, the external voltage was removed to carry out space charge decay tests with the outer sheath and the central conductor having been short-circuited. The space charge distribution was measured at certain intervals and the results are presented in figure 7.5.

Surprisingly, the space charge accumulated in the fresh sample also presented a fairly quick decay rate. Figure 7.5 (a) shows that a major amount of the space charge dies out within 4 hours of the voltage removal. On the other hand, the charge in the degassed sample is quite stable despite its very low density, as shown in figure 7.5 (b). It is hard to see the variation among the results obtained over 8 hours in the decay process.

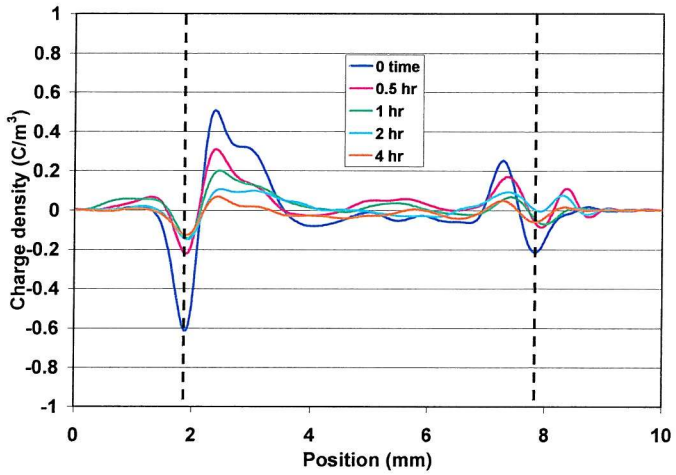

(a) Fresh sample

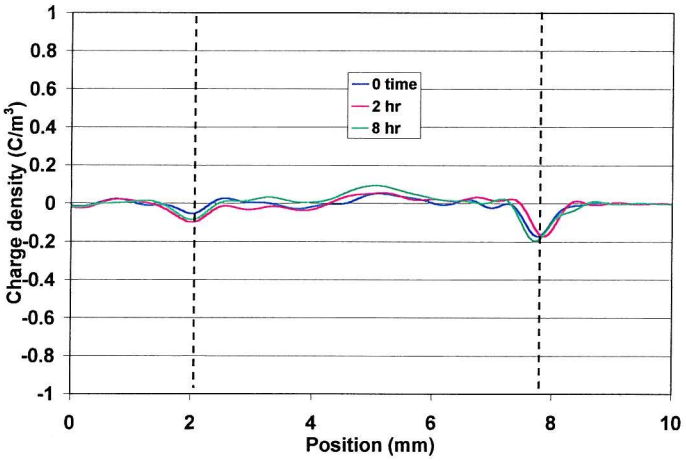

(b) Degassed sample

Figure 7.5 Space charge in decay process (cable 1491)

7.3.3 Cable 1494

Undegassed cable 1994 and 1495 were received in large coils without any wrapping to prevent natural degassing. The results reported here were obtained after the sample has been left exposed to the air for about one month.

Ramp test

Following the same procedure as carried out on the previous sample, the cable 1494 was firstly stressed with the ramp voltage from 0 to 80kV. The relationship between the peak height of the induced surface charge at the insulation/semiconductor interface and the applied voltage is plotted on figure 7.6. From the linear relationships, it can be concluded that no space charge appears in the bulk of the insulation either in the fresh or the degassed cable within this voltage range.

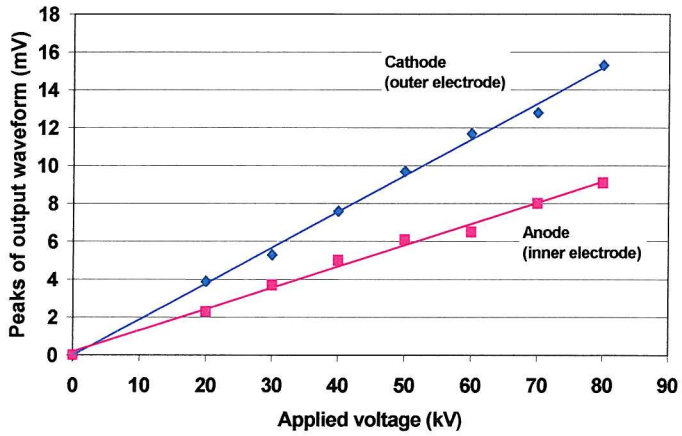

(a) Fresh sample

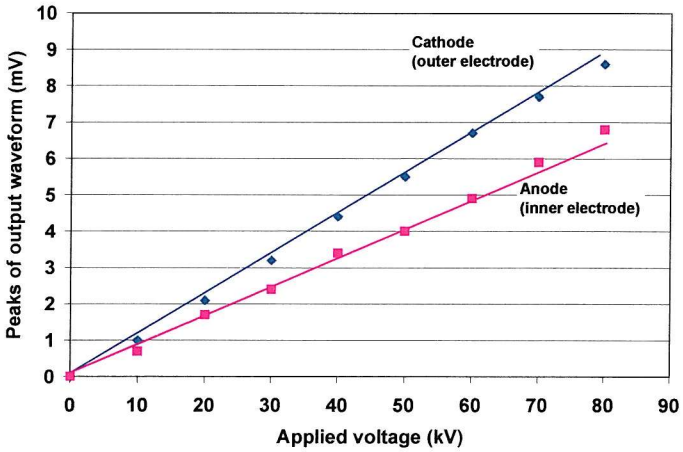

(b) Degassed sample

Figure 7.6 Interface charge variation with the external voltage in cable 1494

Space charge evolution

Space charge distributions in both the fresh and the degassed cable 1494 were measured under the conditions of volts on and volts off throughout a 24 hour ageing term. The results are exhibited in figurs 7.7 and 7.8.

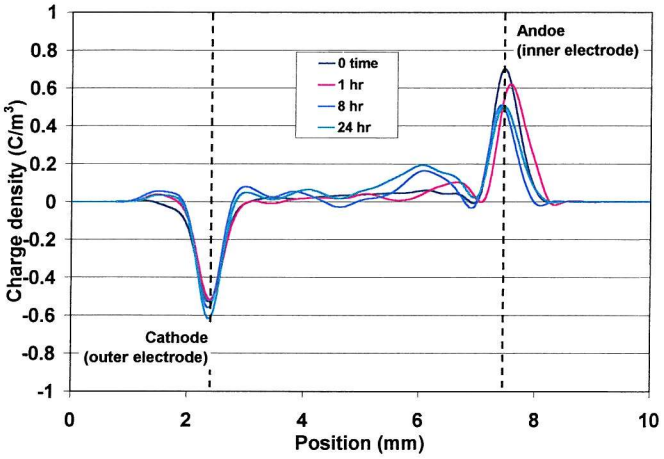

(a) Fresh sample

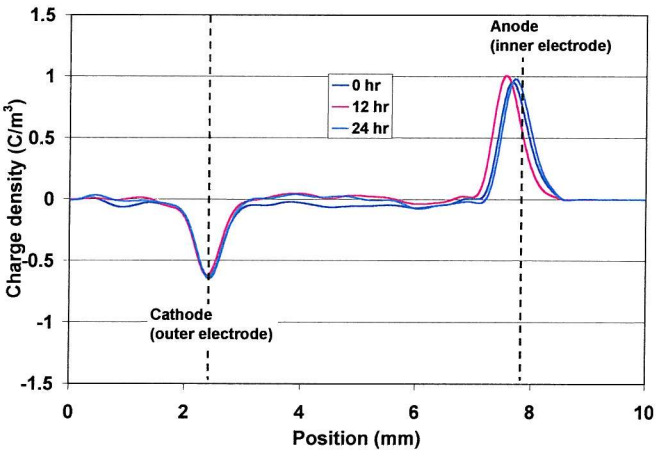

(b) Degassed sample

Figure 7.7 Space charge distribution of cable 1494 (volts on)

In the undegassed cable, a positive packet charge slowly accumulates close to the inner electrode (anode) and reaches saturation within about 4 hours. Similar to the situation in undegassed cable1491, this packet positive charge is also separated from the inner electrode (anode) as shown in figure 7.7 (a). The result suggests again that the charge accumulation in material containing residues is due to the bulk effect of ionization of impurities. The interface effect or electrode injection might be quite weak in comparison with the bulk effect. The quick initiation of the positive charge near the

anode in turn would diminish the interfacial stress and subsequently weaken the charge injection. Unlike the space charge distribution in cable 1491, figure 7.7 (a) and figure 7.8 (a) show no space charge accumulating in this sample in the insulation close to the outer electrode.

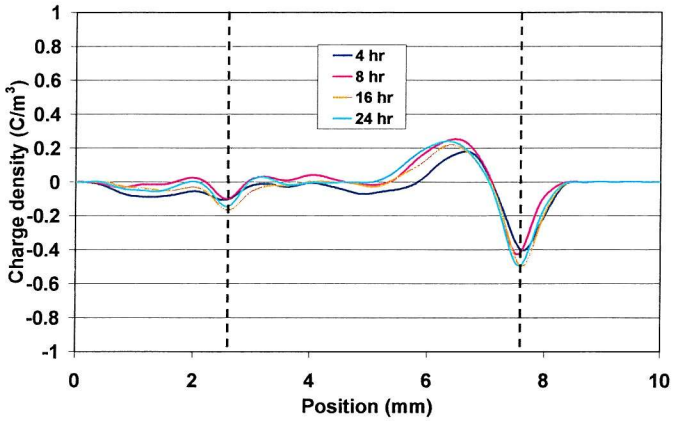

(a) Fresh sample

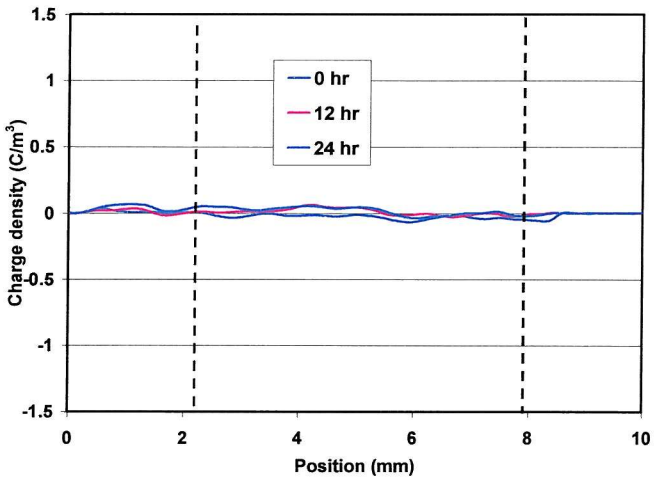

(b) Degassed sample

Figure 7.8 Space charge distribution of cable 1494 (volts off)

The removal of the volatile residues by heating the cable at 90°C for 100 hours has virtually stopped the space charge accumulating. The measurements made on the degassed cable 1494, as presented in figure 7.7 (b) or figure 7.8 (b), show almost no space charge appearance in the cable insulation throughout the entire ageing period.

Space charge decay

The tendency for space charge decay in the undegassed cable 1494 is illustrated in figure 7.9. In comparison with the cable 1491, the decay rate in the fresh sample is

fairly slow. Change of the space charge over 12 hours is hardly visible. As no space charge is shown in the degassed cable, no decay test was carried out.

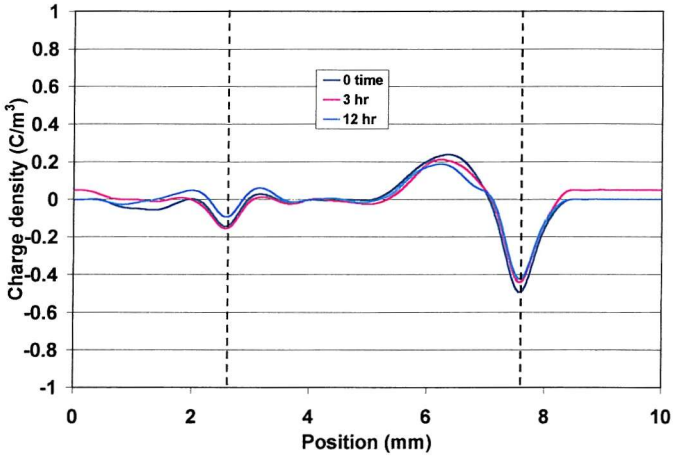

Figure 7.9 Space charge in decay process (undegassed cable 1494)

7.3.4 Cable 1495

Ramp test

Like cable 1494, no space charge is formed in the bulk insulation due to the application of the ramp voltage on either the fresh or the degassed cable 1495 samples. This conclusion is evident from the linear relationship between the height of the induced surface charge peaks and the external voltage over the range from 0 kV to80 kV, as shown in figure 7.10.

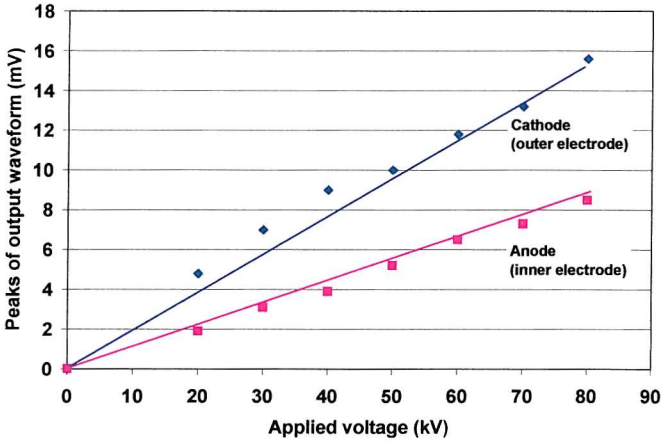

(a) Fresh sample

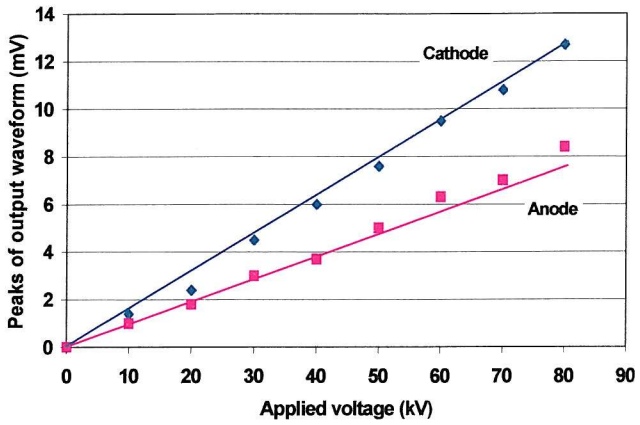

(b) Degassed sample

Figure 7.10 Interface charge variation with the external voltage in cable 1495

Space charge evolution

Figures 7.11 and 7.12 show the space charge evolution over the 24-hour ageing period in the fresh and degassed sample under the conditions of the external voltage on and voltage off. In both figures, the curves signified by "0 time" present the space charge distribution after the ramp test, and show no space charge accumulation in the bulk material. On the other hand figure 7.11 (a) shows that a bulk of positive charge (heterocharge) is gradually accumulated near the outer electrode in the fresh cable over the subsequent ageing process. By contrast, figure 7.11 (b) shows only a small packet positive charge being developed in the central insulation of the degassed cable within the same period of time. A space charge accumulation in both fresh and degassed sample is clearly seen in figure 7.12 (a) and (b), where there are no induced surface charges due to the external voltage on the electrode.

Whether cable 1495 is fresh or degassed, the final space charge distribution is an accumulation of positive net charge in the bulk insulation. Degassing this sample has only reduced the charge density to a certain extent without eradicating it completely. A manifest feature of the space charge generation in this cable is its constant increasing speed. Unlike the space charge observed in undegassed cables 1491 and 1494 which saturates very quickly, the space charge in cable 1495 builds up gradually and accumulates at an almost constant speed over the entire ageing term.

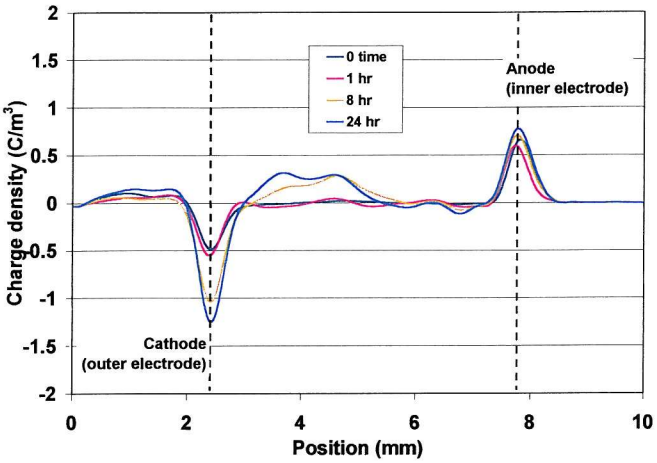

(a) Fresh sample

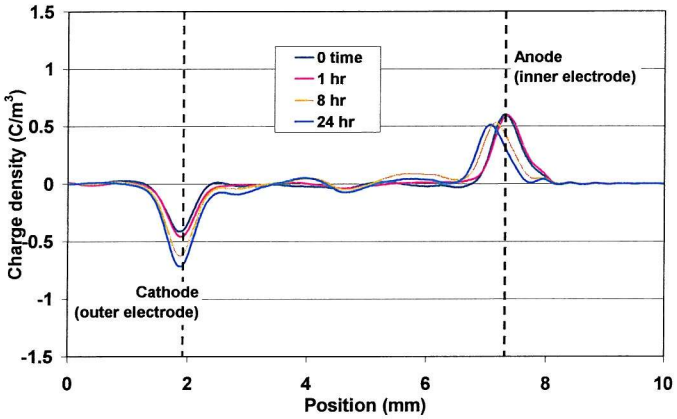

(b) Degassed sample

Figure 7.11 Space charge distribution of cable 1495 (volts on)

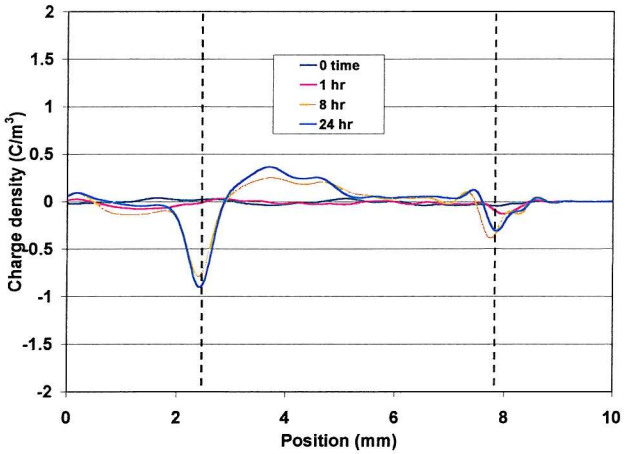

(a) Fresh sample

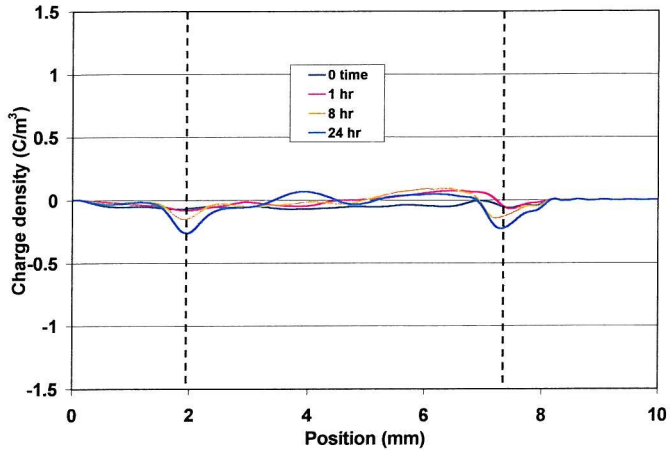

(b) Degassed sample

Figure 7.12 Space charge distribution of cable 1495 (volts off)

Space charge decay

The space charges formed in both fresh and degassed sample of cable 1495 are extremely stable compared with that in cables 1491 and 1494. In figure 7.13 it is hard to notice the variation of the space charge profiles over the 48 hours decay time as.

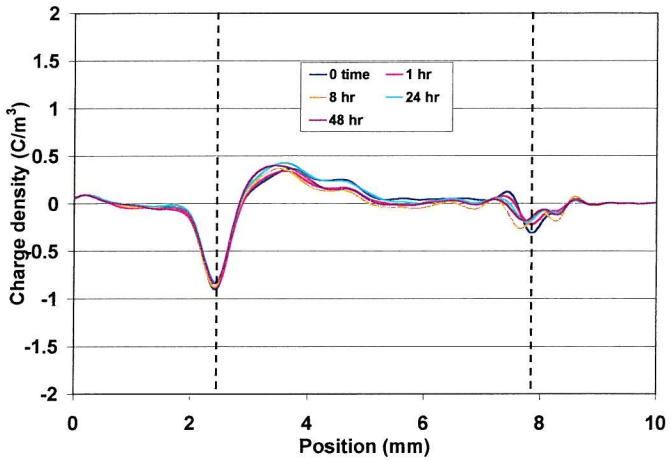

(a) Fresh sample

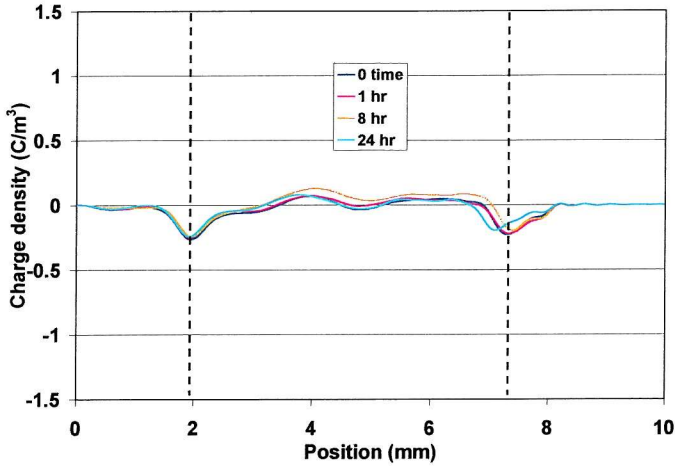

(b) Degassed sample

Figure 7.13 Space charge in decay process (cable 1495)

7.3.5 XLPE ac power cable with different inner and outer semiconducting layers

Space charge measurements were also carried out on a commercially available XLPE ac power cable with insulation 2.8mm thick, and different semiconducting materials at the inner and outer screens. To identify the effect of the semiconducting material on the space charge characteristics, the space charge measurements were carried out either with positive or negative voltages applied to the central conductor. The approximate interfacial stress corresponding to an external voltage of 80kV is 30.7kV/mm and 26.7kV/mm respectively at the inner radius (8.75mm) and the outer radius (11.55mm) in the absence of space charge in the bulk insulation.

The ramp test results showed a linear relationship between the induced surface charge and the external dc voltage at both positive and negative polarities. This result indicates that no space charge is formed in the bulk material at the stress below 30.7kV/mm in the short period of time like the voltage ramp process. This is in accordance with what is expected. As a commercial cable has to be subjected to the whole manufacturing process including the final stage of degassing, the majority of volatile byproducts of the cross-linking may have been removed from the cable insulation. As a result, no fast-accumulated charge will be built up over the ramp test.

However, throughout the following long ageing period, a packet homocharge gradually accumulated adjacent to the outer electrode and another bulk heterocharge (also corresponding to the outer electrode) is formed beside it. Figures 7.14 (a) and (b)

show the space charge evolution over a 30 hour ageing time when the central conductor is energised either with a positive or a negative voltage respectively.

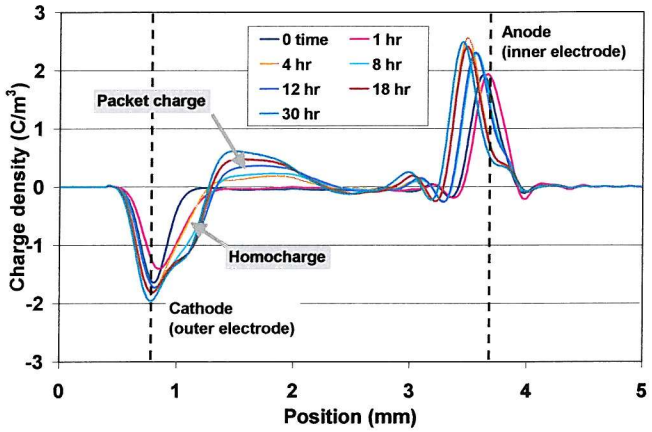

(a) Positive at the central conductor

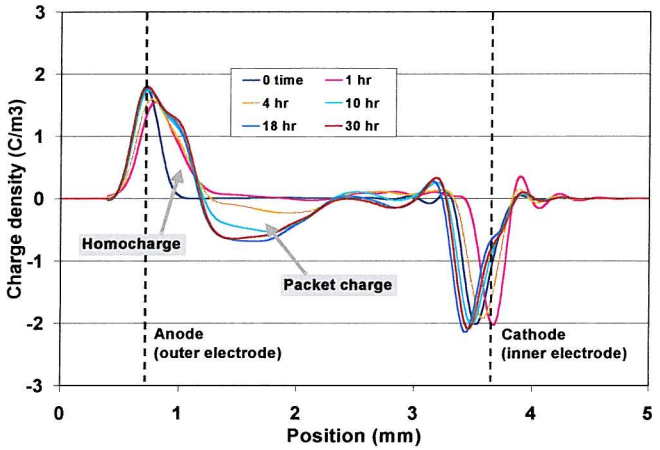

(b) Negative at the central conductor

Figure 7.14 Space charge distributions in a XLPE cable with reduced insulation

It is interesting to notice that the space charge distributions under positive and negative voltage have almost the same shape except for the opposite polarities. Even the charge densities across the insulation thickness and the charge build-up speeds are similar under the two opposite voltage polarities. The same phenomenon has been reported in the literature [23, 89] and is defined as a "mirror image effect" by Bambery *et al* [89]. The results presented here clearly indicate that the outer semiconductive layer made of LM0531 has a charge injection property which is different from that of the inner semiconductive layer, LE0590. The former probably has a strong charge carrier injection ability both at the anode and cathode, while the latter does not, even though the electric stress near the inner electrode is higher.

Due to the limitation of the spatial resolution in the measurements, the homocharge adjacent to the outer electrode is coalescing with the induced surface charge and is rather difficult to distinguish (see the left hand peaks in figures 7.14 (a) and (b)). After the removal of the external voltage, and its induced surface charges at the electrodes, only the homocharge remains and is clearly shown on the results of the decay test as presented in figure 7.15.

Space charge decay

The decay of these so called "mirror image" accumulated space charge under positive and negative voltage conditions are illustrated in figure 7.15 (a) and (b) respectively, and both of them decay extremely slow. The central conductor and the outer sheath of the sample tested under positive voltage was short-circuited for as long as 48 hours for the charge decay test, but the space charge variation over this period of time is hardly visible.

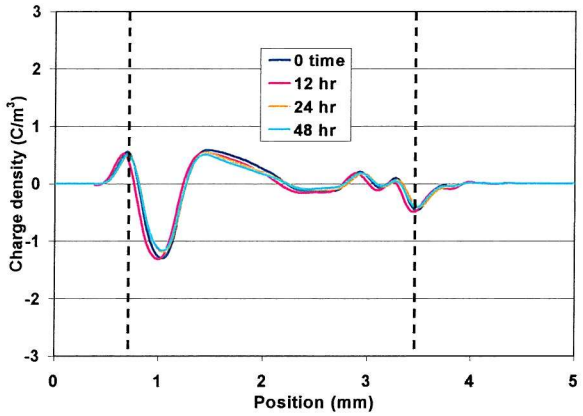

(a) After positive stressing

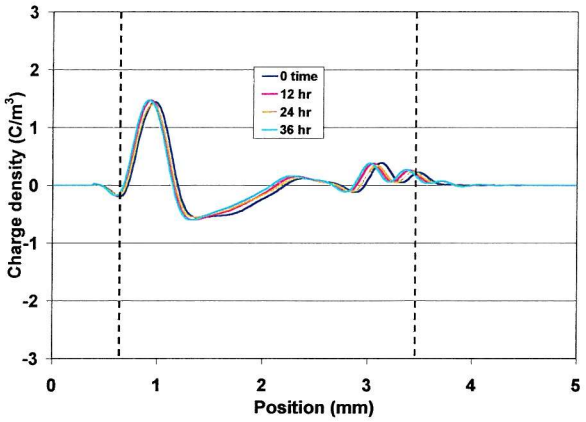

(b) After negative stressing

Figure 7.15 Space charge decay of XLPE cable with reduced insulation

7.4 Discussion

7.4.1 Space charge accumulation characteristics

Except for the undegassed cable 1491, none of the cable samples have shown a fast space charge accumulation in the voltage ramping process. These results cannot be compared with those obtained from the plaque samples made of the same material, which will be dealt with in chapter 8. It is believed that the electric stress in the cable geometry is far less than that in the plaque sample, in which the uniformly distributed stress could be as high as 36kV/mm even in the thickest sample (1.9mm) with 70kV external voltage, whereas the applied electric stress in the cable specimen is around 20 kV/mm at the inner electrode at the test voltage. Additionally, the divergent electric stress distribution across the cable insulation also makes it difficult to compare the space charges in plaque and cable samples.

However, the measured results have exhibited a big variation among these cable samples both of space charge generation and distribution, and some valuable information could be obtained to evaluate the effect of material modification in controlling space charges in dc polymer power cables.

The basic characteristics of space charge accumulation in the tested batch of cables are summarised in Table 7.1.

From the space charge profiles presented in the section 7.3 and the summary in table 7.1, it is seen that the difference in space charge activity in the fresh sample and the degassed sample is significant. After being thermally conditioned, all the samples have very small space charge accumulations or do not possess space charge activity at all in some samples. Even for some degassed samples in which small charge developed (such as cable 1491 and 1495), charge build-up and decay speeds are extremely slow. All these results suggest that the residues inside the XLPE insulation play a key role in space charge accumulation but they can be removed by simply heat treatment.

According to the literature [34, 51, 133], a fresh sample with residual impurities will in general generate heterocharges, while the degassed sample will produce homocharges after a long period of stressing. The results obtained in the present work from the cable samples generally agree with this rule too, particularly for the undegassed sample. However, in degassed cable samples no homocharge was actually observed in the vicinities of the two electrodes, but in some cases, such as 1491and

1495, a small packet charge was slowly developed in the volume of the insulation. The externally applied electric stress in these experiment was within the range between ~12 kV/mm and ~18kV/mm, which is believed to be much lower than the stress in plaque samples where it ranged from 36kV/mm to 42kV/mm for the thickest and thinnest samples.

Table 7.1 Charge formation in ramp test and final charge polarity after 24 hour ageing

Cable sample		Fast charge during ramp	Space charge after 24hr ageing	Charge building-up	Charge decay
1491	**Fresh sample**	Heterocharge at cathode Homocharge at anode	Large heterocharge at cathode; Small homocharge at anode	Fast	Fast
	Degassed	No appearance	Small positive charge in the central insulation	Slow	Slow
1494	**Fresh sample**	No appearance	Large homocharge at anode	Moderate	Slow
	Degassed	No appearance	Small charge appearance		
1495	**Fresh sample**	No appearance	Large heterocharge at cathode; Small homocharge at anode	Moderate	Slow
	Degassed	No appearance	Small positive charge in the central insulation	Slow	Slow

Electron and/or hole injection at the electrode-dielectric interface is believed to dominate the space charge accumulation in the degassed XLPE or the pure LDPE [32, 39], and the injection is mainly controlled by the applied voltage (or stress) for a given dielectric and electrode interface. Therefore, the charge injection effect at the electrode and dielectric interface may be too weak to develop noticeable homocharges within the ageing time and with an electric stress similar to those in the cable experiments. Alternatively, for an appreciable space charge accumulation under the lower stress, a relatively long ageing time may be required. Sanden [133] had observed in a degassed XLPE planar sample under the applied stress of 40kV/mm that the initially formed heterocharge near the cathode was gradually replaced by a homocharge after about 2000 hours of ageing. This example on the other hand implies that the effect of the bulk

and interface on space charge generation may occur at the same time but the homocharge resulting from interface injection needs higher stress or longer stressing time. This may also be the reason for no fast charge appearing in a degassed plaque sample during the ramp test, but finally coming out after a certain time of stressing.

The small packet charge within the volume of the degassed insulation in a cable sample may be attributed to the ionization of remaining traces of impurities after the degassing.

Consider now the undegassed cable samples, most of them displayed a much more active space charge process than the degassed sample. Throughout the ageing term, there was dominant heterocharge (positive) formation near the cathode in cables 1491 and 1495. At the same time a packet of positive charge was formed at the place close to but not adjacent to the anode in cable 1491. This also occurred in cable 1494. However, no space charge formation was found at the cathode of cable 1494 or at the anode of cable 1495. The main reason for these asymmetric and uneven space charge distributions may be the uneven concentration of impurities in the polymer. The non-uniform electric stress across the insulation may be another reason.

7.4.2 Charge build-up speed

In practice it may be difficult to compare the rate of space charge accumulation in the different samples because of charges in each cable have distributions which are different in both position and charge polarity, especially when the divergence of electric stress and the residue distribution throughout the cable insulation become the major factors influencing the space charge development.

In this research, we use the concept of "relative speed", which is defined as the time needed by the space charge to reach its maximum density. The maximum space charge can be positive or negative, and can also be anywhere in the insulation. This comparison should give a more general judgment on the effect of different XLPE modifications in controlling space charges. The space charge accumulation in the degassed samples is too small for this comparison, so figure 7.16 illustrates only the maximum charge density variation with ageing time in the undegassed cables.

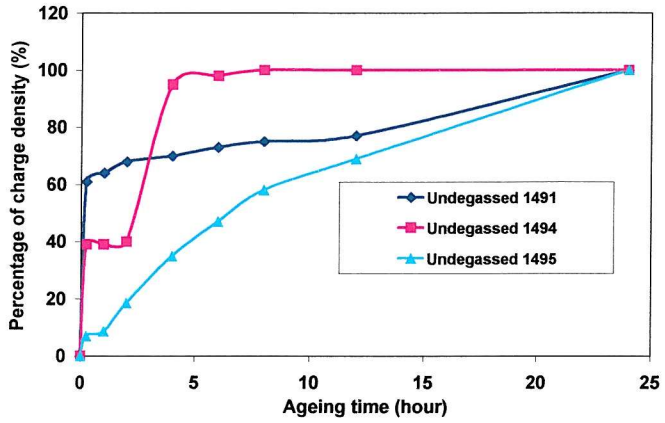

Figure 7.16 Percentage of charge built up by 24 hours in undegassed cable

Amongst these samples, the space charge accumulation in cable 1495 was much slower compared with the others and maintained a constant accumulating rate throughout the whole ageing process. On the other hand, the space charges in cables 1491 and 1494 accumulated very quickly in the first few hours and then slowed down to a relatively low speed. Particularly, in cable 1491, an appreciable charge had already been generated during the voltage ramp, but in the following ageing hours the rate of charging was fairly slow.

7.4.3 Maximum space charge density

The bar-chart of figure 7.17 shows the maximum space charge density in different cables under fresh and degassed condition. Cable 1494 exhibits a low maximum charge density both before and after the degassing, while samples 1491 and 1495 have relatively high charge densities. As the space charge in cable 1495 remains comparatively stable after it has built up, it is much more harmful than that in the other two samples. This situation should be avoided in dc cable insulation design [132].

The effect of degassing on space charge generation in the material is confirmed once more by these results. No matter how high is the space charge density in a fresh sample, heat treatment can significantly reduce the space charge accumulation. Whether the degassing process can completely stop the space charge generation in cable insulation is not yet certain. It needs to be investigated by long term ageing tests.

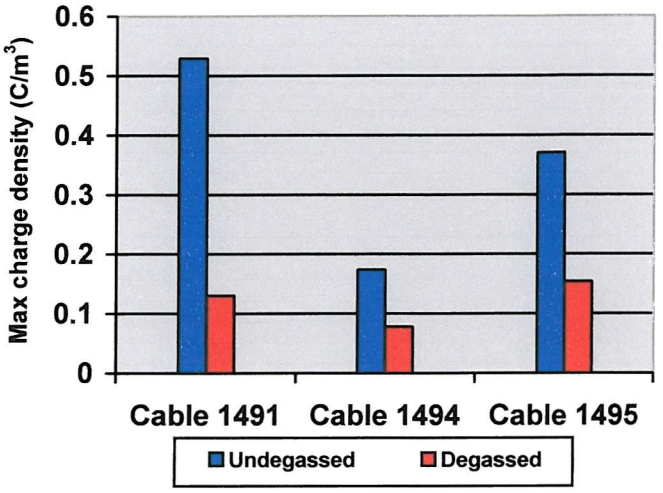

Figure 7.17 Maximum space charge density after 24-hour ageing

7.4.4 Space charge decay speed

The rate of space charge decay in the undegassed cables can be quantified by the ratio of the total charge after certain time of decay to the initial value. The decay rate for each cable is presented in figure 7.18. It is easy to see that cable 1491 has an extremely fast decay rate, like it has a fast build-up speed. On the other hand, the space charge in undegassed cable 1495 is so stable that it is difficult to see any charge dieing off over the whole decay time. Just as it has a lower decay rate, so also does it exhibit a slow space charge accumulation speed in the ageing process.

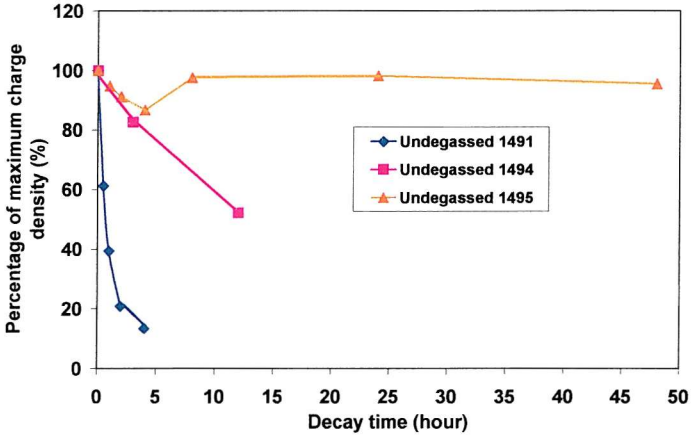

Figure 7.18 Space charge decay speeds of different cables

In spite of small charge accumulation in the degassed sample, its decay speed is extremely slow in comparison with that of the corresponding fresh sample. It has been mentioned previously that the space charge in the degassed sample possesses a low

accumulation rate. A preliminary conclusion can therefore be reached from the above results that the faster the space charge builds up, the faster it decays, and vice versa. This phenomenon will also be observed in chapter 8 for the plaque samples.

7.4.5 Space charge distribution shapes

Space charge distributions in power cables are not similar in form to those observed in most polymer film samples where homocharges or heterocharges are accumulated mainly in the region near the electrodes. Instead, most space charges in cable samples exhibit a packet shape located elsewhere across the insulation. For instance, a small packet charge developed in the central part of the insulation in degassed cable 1495; and two positive bulk charges were near the anodes in undegassed cable 1491 and 1494. Similar space charge distributions of packet shape were also found across the cable insulation in the researches of Wang *et al* [23], Fleming *et al* [82] and Lim *et al* [134]. There may be two reasons causing these differences between sheet samples and cable samples. One is material's homogeneity. Due to the relatively small thickness of the sheet sample, it is easy to make the material homogeneous and get an even distribution of impurities, if there are any. In the thick insulation of a power cable, however, the material may easily remain inhomogeneous both in morphology and impurity distribution. These factors will directly influence the space charge distribution across the insulating material. Another reason, of course is the non-uniform applied electric stress which initiates the space charge at different locations by different amount.

Some power cables may employ different materials for the inner and outer semiconducting layers, such as the ac XLPE power cable tested previously. From measurement of its space charge, it has been found that these two semiconducting materials have considerably different capabilities for space charge generation in the adjacent insulation. The homocharge was always found at the vicinity of the outer semiconductive electrode under both the positive and negative voltage, but not at the inner electrode, although the initial electric stress here was higher than that at the outer sheath. Moreover, a large heterocharge (to the outer electrode polarity) was generated just beside the above-mentioned homocharge. In view of the similar charge densities adjacent to the outer sheath under the two opposite polarities, it seems that the material used for the outer semiconductive layer possesses equal ability for electron injection

and hole injection (or electron extraction) to or from the XLPE insulation. On the other hand, the material used for the inner electrode causes little charge injection under the same condition, i.e. of electric stress and interface with the XLPE material tested here.

7.4.6 Origin of the "mirror image effect"

The reason for the "mirror image effect" in space charge distribution in the commercial ac XLPE power cable is explained below.

As stated in Chapter 2, space charge accumulation in XLPE is generally considered to be the result of electron injection or extraction at the electrode/insulation interface, and/or the ionization of impurities in the bulk material by electron or ion separation.

When the cable insulation is first stressed with a positive voltage at the central conductor, electron injection from the cathode occurs simultaneously with the ionization of impurities in the bulk material. Although some volatile byproducts of cross-linking may be removed by the thermal treatment during manufacture, some organic or inorganic impurities may still remain in the insulation [23]. Ionization of these impurities under electric stress inevitably results in the bulk space charge [32, 35, 87] in the insulation. At the interface (say the outer electrode, the cathode) if the electron injection rate at the cathode exceeds the electron migration rate, a negative space charge begins to accumulate adjacent to the cathode in the insulation. This accumulation of homocharge will, in turn, increase the height of the barrier through which the electrons must travel to enter the insulator, and consequently the injection will decline. On the other hand, this newly injected negative charge layer will enhance the electric field strength in the material between this homocharge and the anode. As a result, the bulk effect of ionization will be advanced.

The same event may occur at the anode when the negative voltage is applied to the central conductor. Positive charge will begin to accumulate adjacent to the outer electrode (anode) due to the electron extraction or hole injection into the dielectric material.

According to Lewis [135], electron transfer by tunnelling through an electrode/insulator interface, no matter the direction, will involve only a narrow "window" of combined donor and acceptor states in the insulation, centred on the Fermi level and the states within the same energy range in the electrode. For a given

electrode (same material), the equilibrium barrier heights and widths for electron extraction and injection must be equal.

The interface injection effect in this situation will finally arrive at equilibrium due to the decline of the interfacial stress as the homocharge is formed at the outer electrode. Since the height and the width of a given barrier depends on the local electric stress, in the present case the equal amount of negative and positive charge close to a given electrode will be obtained under two opposite voltage polarities. This leads to the same but opposite charges being generated near the outer electrode at two opposite stressing polarities.

The bulk effects on the space charge generation within the volume of the insulating material will be the same under two opposite stress polarities. Packet charges in the central material are generated by the ionization of impurities and are normally assumed to have negligible mobility so, under the opposite polarity stresses of equal strength, they are reckoned to give the "mirror image" distribution too.

This discussion also applies to the situation of heterocharge development if the material has a high charge migration. Under two opposite stressing polarities, a corresponding sequence of events and similar equilibrium condition will occur except when the voltage is reversed. The previously formed charge is quickly transported to the electrode with opposite polarity before being neutralized by the new local charge.

This test was conducted on two pieces of cables stressed with different voltage polarities separately. Space charge with the "mirror image" pattern was also obtained in a cable which was stressed at one voltage polarity until equilibrium was reached and was then switched to the voltage of opposite polarity. Results of this test will be presented and discussed in chapter 9.

7.4.7 Electric stress distribution modified by the space charge

Accumulation of space charge in the insulation of power cable under dc electric stress increases the field stress at some places, and decreases it at others. The increased field stress may exceed the "threshold electric stress" above which electric ageing takes place in the insulation. This could lead to premature failure of the cable.

The distorted electric stress distribution across the cable insulation due to the space charge is calculated by the method introduced in chapter 6. Some results are presented

in figure 7.19, where the electric stress is derived from the final space charge distribution after the cables have been aged for a certain time.

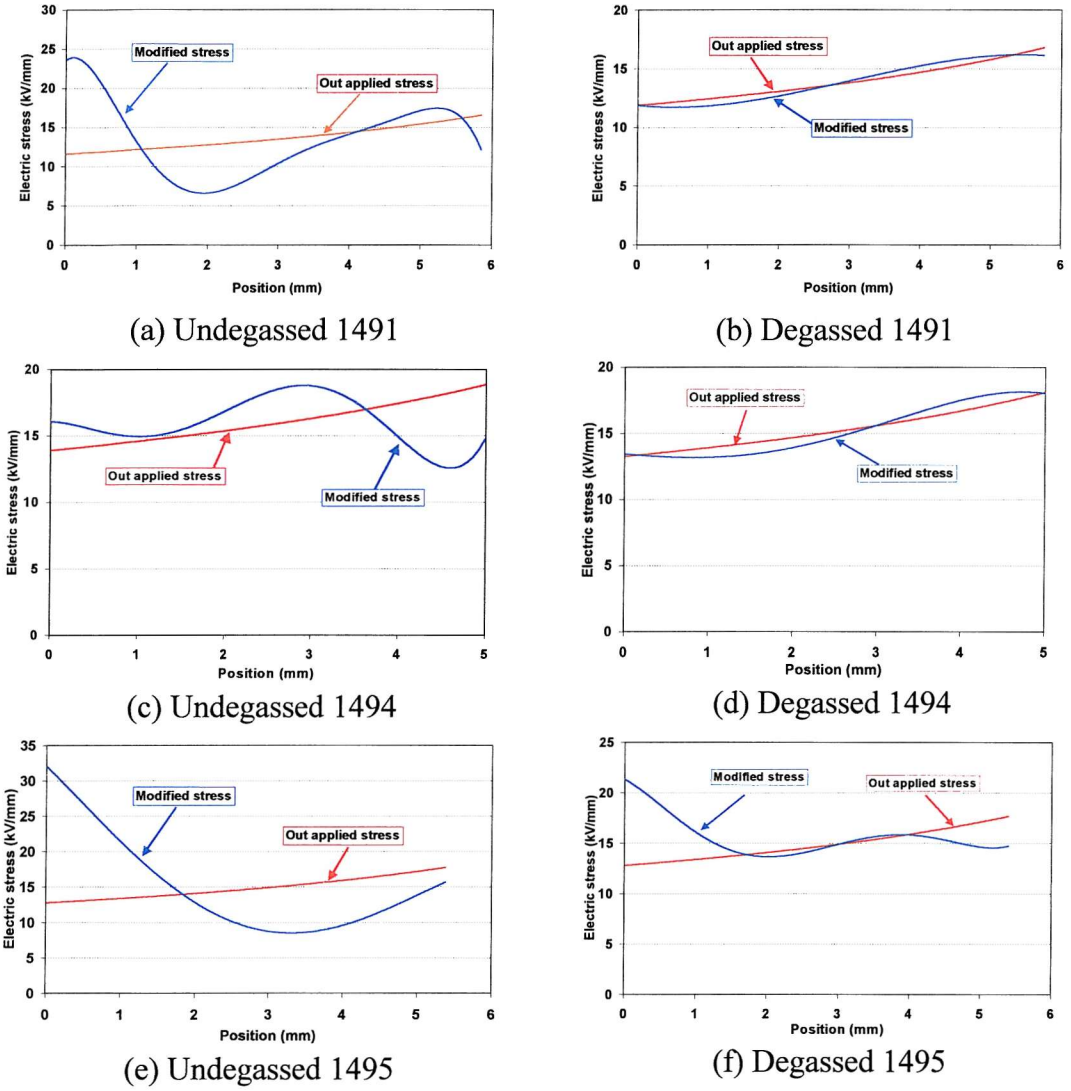

Figure 7.19 Electric stress distribution across the cable insulation after 24hr ageing

Figure 7.19 shows that the externally applied electric stress in the undegassed cable has been crucially distorted by the space charge appearance. The worst situation occurred in undegassed cable 1491 and 1495, where a large bulk of positive charge (heterocharge) had formed close to the outer sheath (cathode) and resulted in a significant increase of interfacial stress at that location. The stresses at the outer sheath in these two cables reached 24kV/mm and 31kV/mm respectively, much higher than the designed values for the cable geometries. On the other hand, in the central part of the insulation and in the region near the inner electrode, the stress has been reduced to a certain extent.

Due to the positive charge adjacent to the inner electrode (anode) in the undegassed cable 1494, the electric stress in the region near the inner electrode is appreciably reduced. At the same time, the stress within the region from the position of the positive packet charge to the outer sheath is enhanced. The highest electric stress appears in the central part of the cable insulation with the value about 18kV/mm.

With the exception of cable 1495, most of the degassed samples didn't show very significant space charge accumulations in their insulations, so the electric stress distributions derived from the space charge measurements agree well with those calculated from the geometries. In the case of degassed cable 1495 some net positive charge has formed with a relative even distribution along the cable insulation. As a consequence, the electric stress at the inner interface of the electrode/insulation is reduced, while enhanced at the outer interface.

7.5 Conclusions

Space charge measurements have been carried out on three types of prototype power cables which employ different modified XPLE insulations under both fresh and degassed conditions. The characteristics of the space charge within these materials are studied in term of the accumulation speed, distribution profile and decay property. Tests were also conducted on a commercial XLPE power cable, with different semiconducting materials at the inner and outer electrodes. Based on the above results, the following conclusions may be drawn.

Firstly, degassing treatment removes the residues after the cable manufacture and can considerably reduce the space charge accumulation. For the same cable insulation in a fresh condition, a considerable charge could develop within 24 hours of ageing although the charge profiles differ from sample to sample. Conversely, the charge accumulation in the degassed sample was much less active or even non-existent over the whole period of ageing. These results show that the byproducts of the cross-linking and other additives play an important role in the space charge accumulation in XLPE.

Secondly, amongst the results from different cables, no two samples showed similar space charge distribution shapes. Even in the same sample, the space charge at the inner and outer interfaces of the electrode-insulation also possessed quite different charge accumulation. In addition to the influence of the non-uniform applied electric stress, the inhomogenity of the insulating material (which includes the morphology and

impurity distribution) is the main reason for the asymmetric space charge distribution through the cable insulation, unlike that which is found in the film sample.

Thirdly, the differences between the space charge behaviours in these prototype cable samples are very significant. In the undegassed condition, cable 1491 showed the most active space charge accumulation. Even in the voltage increasing procedure, a considerable heterocharge formed in the vicinity of the cathode. This cable also held the highest space charge density, $0.52C/m^3$, amongst all of the samples. Cable 1495 also had a strong ability for space charge accumulation. After ageing for 24 hours at 80kV, a broadly distributed heterocharge (positive) had generated near the cathode in the undegassed sample. The highest charge density in the bulk of the material has reached $0.37\ C/m^3$. However, the difference among the degassed samples is not very substantial except for the formation of small positive packet charge in the centre of the insulating materials of cables 1491 and 1495.

These samples also displayed large difference in space charge build-up rate. In undegassed cable 1491, the space charge built up quickly at the beginning of the application of the external voltage. During the ramp test, the space charge had reached approximate 60% of its maximum density at the end of the ramp and then gradually arrived at its maximum value in the following steady state. Cable 1494 also showed a relatively high charge-accumulating rate. Surprisingly, it was noticed that the space charges in these two samples also possess a relatively high decay speed. On the contrary, the space charge decayed extremely slowly in cable 1495, just as its charge accumulation speed was slow. In view of these results, it can be concluded that the space charge build-up speed and the decay speed accord with one another, i.e. the faster the space charge develops, the faster it dies out, and vice versa.

The electric stress distribution derived from the space charge measurement has supplied a direct and quantitative way of understanding the impact of the space charge on dc cable insulation. Clearly, the appearance of space charges in the undegassed cable seriously distorts the geometry-governed electric stress (so called the designed electric stress). The electric field strength at some positions in the insulation is reduced, but in other places is dreadfully enhanced. For instance, in cables 1491 and 1495 the electric stress at the outer sheath is doubled due to the heterocharge near the electrode. The positive packet charge in the undegassed cable 1494 causes the highest electric stress to occur in the central part of the insulation instead of at the interfaces.

Based on the above results, the "recipe" used in cable 1494 seemed to have a favourable property from the space charge suppression point view. The material used in cable 1495 has a high charging ability even after degassing, and a stable charge distribution. These are weaknesses in comparison with others.

Finally, it is concluded that the "mirror image" effect in the space charge distribution under two opposite stressing polarities is likely to be a common phenomenon in XLPE insulation within the electric stress range discussed in the project. This conclusion is drawn from the present work and from other papers in the literature [23, 89]. The result from the XLPE cable with different semiconductive layers suggests that the material used at the outer sheath has a higher charge injection (or extraction) ability than that used at the inner electrode. It indicates that the semiconductive layers also play an important role in the formation of space charge in the material.

Chapter 8

Space Charge Measurement in Thick Planar Samples

8.1 Introduction

Research into the space charge characteristics in insulated dc cables is time consuming and costly because of the difficulty of the prototype cable preparation, many experiments still need to be carried out on plaque samples to investigate the effect of insulating material modification. The planar samples for this test can be made of different modified materials and semiconductive electrodes, and can be prepared exactly in the same processing procedure as the cable manufacture. A sample made for this research is usually thicker in order to reduce the surface effect of the tin film samples. Therefore, in the application of the PEA system for thicker plaque samples, a relatively high voltage has to be applied across the sample to obtain an adequate stress for the space charge formation. Of course, the attenuation and dispersion of the acoustic wave propagation through the thick sample is another concern in the precise measurement of the space charge distribution.

In this chapter, the PEA system suitable for thick plaque samples and the relevant data processing technique are briefly introduced.

To investigate the effect of the modification to XLPE insulating materials on space charge characteristics, a batch of thick plaque samples made of different amended XLPEs were tested using this system. The space charge results among these samples have shown a great variation in the fast charge initiation in the voltage ramping process, in the charge accumulation over the ageing term and in the space charge decay

after the removal of the applied voltage. Unsurprisingly, the space charge generation in the sample is obviously affected by the degassing conditioning. To obtain more informative insight into this issue, the samples subjected to different degassing treatment (i.e. at the conditions of fresh (undegassed), partially degassed (0.5% residue) and thoroughly degassed) were also studied in terms of space charge accumulation and decay.

8.2 Set-up of the PEA system and data processing for thick plaque samples

8.2.1 PEA system for plaque samples

The photograph in figure 8.1 shows a view of the PEA system for thick planar samples and is of the same principle as illustrated in figure 2.4. The embedded coupling capacitor bank consists of three individual capacitors in series, each one with a rating voltage of DC 40kV and a capacitance of ~2700pf. To satisfy the requirement of a relatively high stressing voltage across the sample, besides the application of voltage bushing on the high voltage electrode, adequate flashover distance is also required for the sample along its surface from the upper electrode (high voltage) to the ground electrode, thus a bigger sample in size is required in the test. This makes it difficult to maintain an even contact between the sample and the electrode insulator surfaces. Some air gaps may inevitably be formed between them. As a result, the flashover voltage across the sample is significantly reduced. At the beginning of the test, this problem frequently occurred through this air gap path over the surfaces of sample at a voltage over 50kV. This difficulty was successfully solved by smearing some silicone grease around the embedded semiconducting electrode of the sample. The PEA system enables a dc voltage as high as 100kV to be applied across the sample.

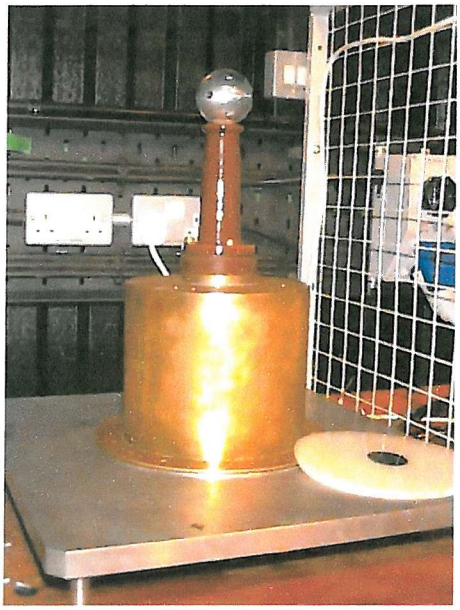

Figure 8.1 Photograph of the PEA electrodes system for the thick plaque sample

8.2.2 Data processing

Chapter 5 discussed acoustic wave propagation in cable insulation and showed the significance of the attenuation and dispersion of the acoustic wave. This will also be significant in the thick plaque samples and will give a lower detecting sensitivity and poorer spatial resolution of the charge layer in the sample far away from the transducer. A similar data compensation algorithm to that used in cable sample was developed to correct the effects caused by the acoustic pressure travelling through the planar sample. The program interface and its block diagram are presented in Appendix B. Diagrams in figure 8.2 (a) and (b) show an example of the space charge distribution at the calibration voltage before and after compensation for the acoustic signal propagation. The attenuation and dispersion effect of the acoustic wave is clearly indicated in the peaks of the induced surface charges at the two electrodes in figure 8.2 (a). The signal from the upper electrode (the peak on the right hand) appears lower and wider when it arrives at the transducer after transmission through the sample thickness. Owing to the uniform distribution of the electric stress throughout the planar sample, the induced surface charges at two electrodes should have the same charge density if there is no bulk space charge present in the volume of the dielectric material, like the profile shown in figure 8.2 (b), two surface charges have the same density and distribution. Similarly, due to system response, the previously discussed deconvolution technique also has to be applied in this system.

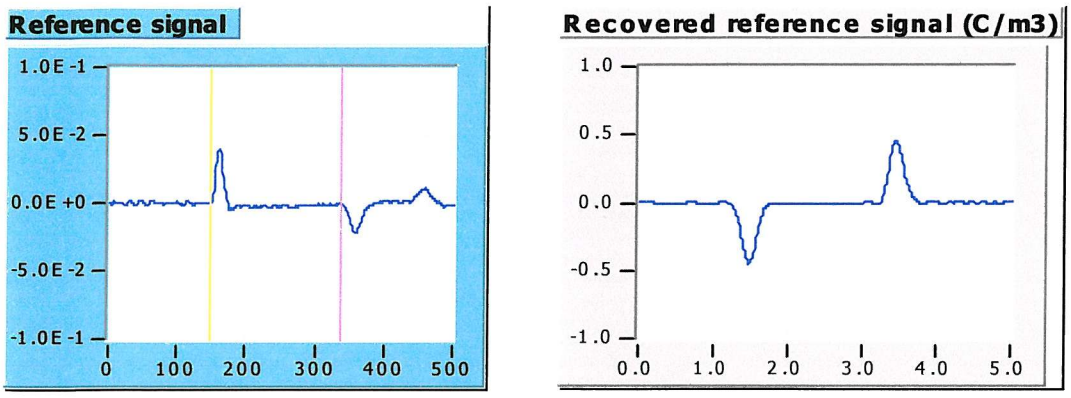

(a) Raw data of calibration signal (b) True space charge distribution

Figure 8.2 Space charge profile (in calibration) before and after attenuation and dispersion compensation

8.3 Sample preparation and test procedure

8.3.1 Samples

The samples tested in the research are reference XLPE and modified XLPEs. All have the same semiconducting electrodes made of crossing-linked polyethylene with carbon black and other additives. In order to understand the influence of the residue on the space charge formation, samples having been subjected to different treatment containing a variety of cross-linking byproducts were also tested. Figure 8.3 illustrates a sample's dimensions and its cross section.

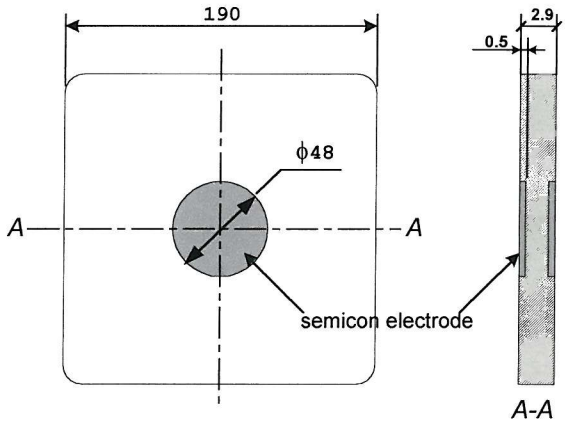

Figure 8.3 Sample dimension and its cross section

Apart from the flashover problem mentioned in the preceding section, several samples from the first batch failed due to electrical breakdown occurring at the edge of the semiconducting electrode in the voltage ramp procedure or during the ageing test. For this reason, one more sample was sectioned through the test region to check the attachment between the semiconducting electrode and the bulk insulating material, the condition of the insulation and the profile of the electrode. No significant defect or poor quality was observed in the insulation except for the sharp inner edge of the semiconducting electrode. This is believed to be the main reason for the electrical failure of the sample as it raising the stress in the vicinity of the edge. The photograph in figure 8.4 shows the sharp electrode edges and an electrical breakdown path running through the sample insulation from the upper electrode to the ground. A semiconducting electrode with a rounded edge was used in the subsequent samples.

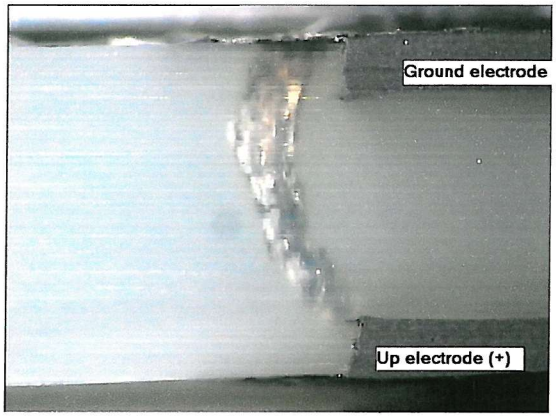

Figure 8.4 Image of breakdown path through the sample

Commercial confidentiality denied us knowledge of the composition of the modified XLPE and its processing procedure except for the thermal treatment. The plaque samples tested are therefore coded and listed in Table 8.1. There were two specimens of each sample, and both were tested with good reproducibility.

8.3.2 Experimental procedure

Space charge measurements on each sample started with the ramp with an applied voltage ranging from low to the required value of 70kV. As mentioned in Chapter 7, the intention of this experiment is to find the threshold voltage above which a bulk charge starts to accumulate in the sample. The calibration voltage must be lower than this value.

The space charge measurement was then carried out over a certain period of ageing time with the external voltage continuously applied. The space charge distribution in most of the samples reached its equilibrium within 24 hours, and some them even sooner. At the end of the ageing test, the space charge decay test was conducted by recording the space charge profile at different time intervals as the applied voltage was removed and the conductor and the outer sheath was short-circuited.

Table 8.1 Plaque sample's code, series number and treatment

	Undegassed	Partially degassed (0.5% residue)	Degassed
P3 (Reference XLPE)	✗ (Flashover)	✓	✗ (Failed in ramp)
	✗ (Flashover, retested)	✓	✓
P28 (Modified XLPE)	✓	✓	✗ (Failed at 1.5 hrs)
	✗ (Failed at 4 hrs)	✓	✓
P29 (Modified XLPE)	✓	✓	✓
	✗ (Failed at 12 hrs)	✓	✓
P30 (Modified XLPE)	✓	✓	✓
	✓	✓	✓
LDPE (No peroxide)		✓	

8.4 Space charge measurement results

8.4.1 Ramp voltage test

The voltage ramp test results from different samples are presented in figure 8.5, in which the variation of the induced charge at the two electrodes with the external applied voltage is plotted. In order to minimize the influence of the stressing time on the charge formation, the measurement at each voltage value had to be carried out quickly. Hence, only the peak heights of the induced surface charges at the upper and the ground electrodes were read directly from the oscilloscope in units of voltage. Due to the attenuation of the acoustic signal across the sample, the peak height of the upper

electrode (away from the transducer) is lower than those from the ground electrode. However, its measured variation with the external applied voltage is exactly presented.

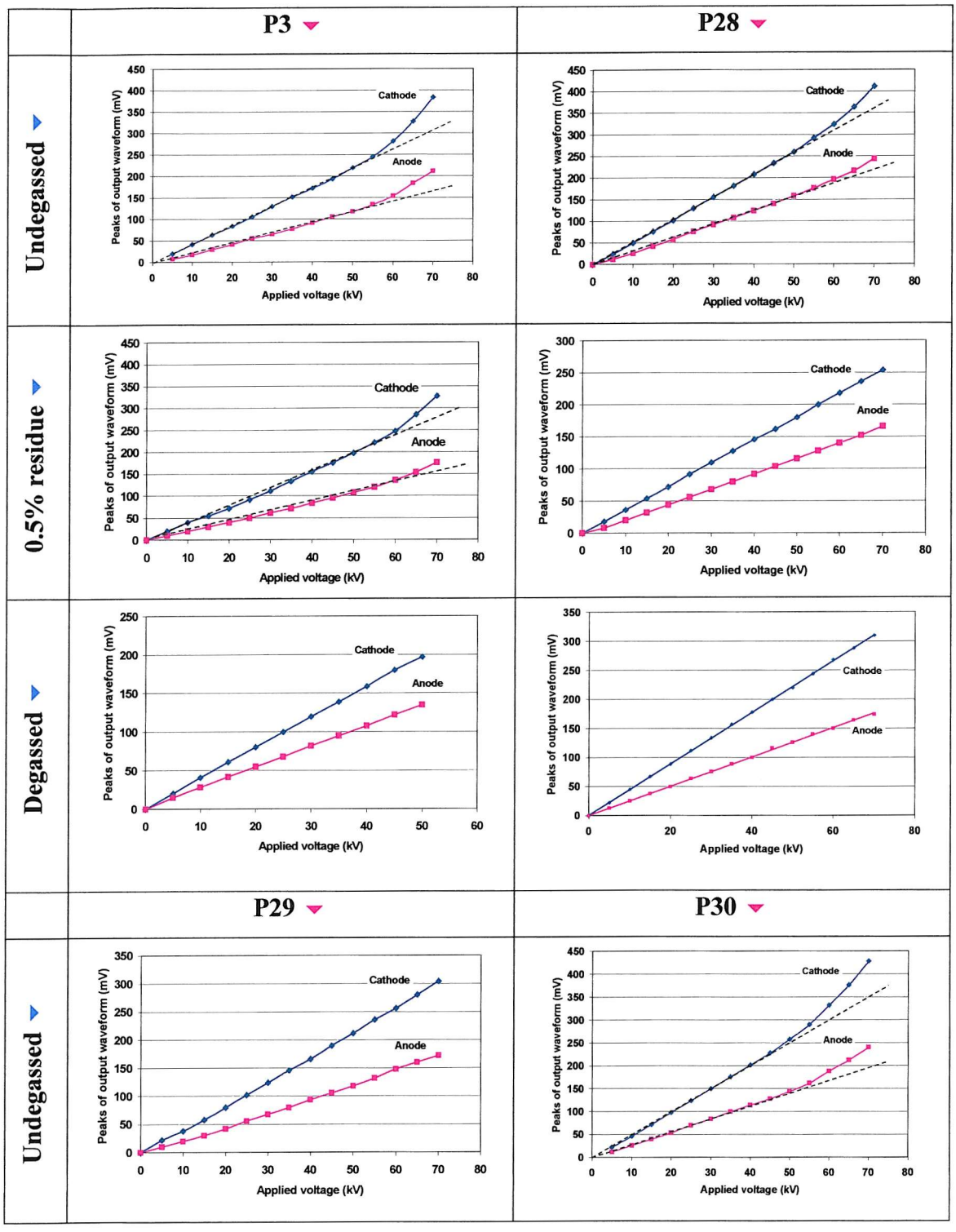

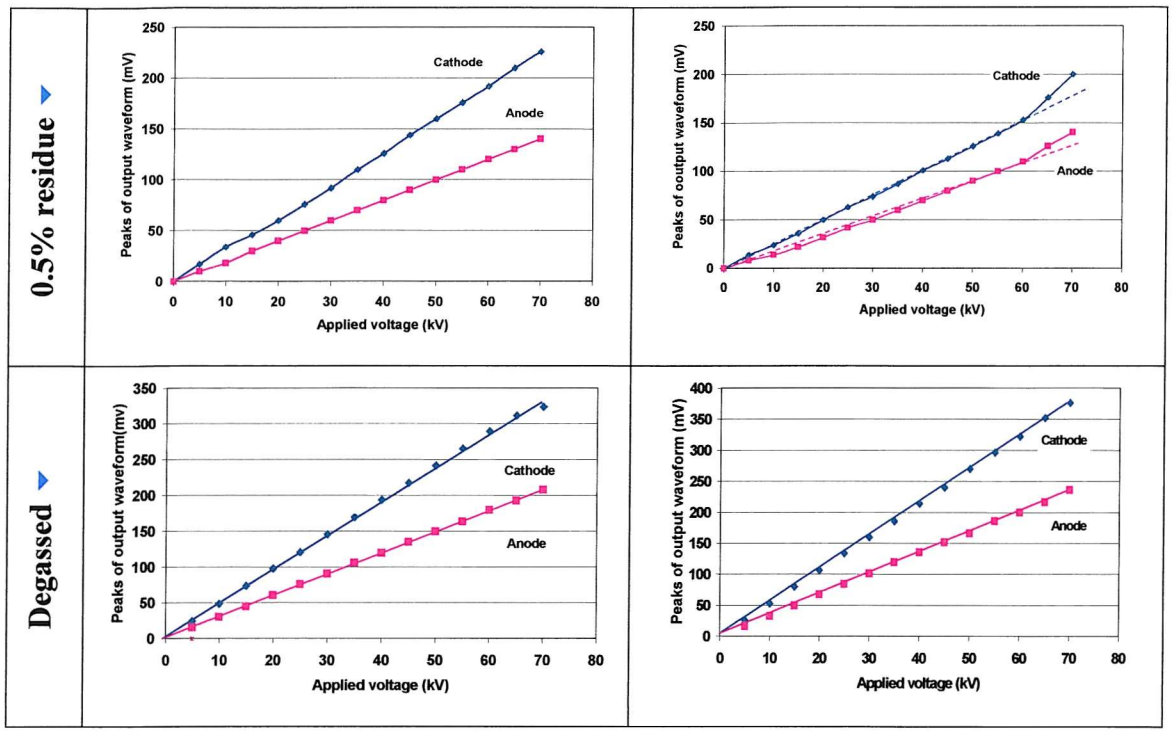

Figure 8.5 Relationship between the induced surface charge and the external voltage

The first degassed sample P3 failed during the voltage ramping, so the ramp test on the second sample was terminated at 50kV. In order to avoid any other failure in this sample, the space charge distribution was initially measured at 50kV for 24 hours and the result showed no space charge accumulated at this voltage. After that, the ageing voltage was upgraded to 70kV for another 24 hours. In the next batch of samples, the inner edge of the semiconducting electrode had been improved to reduce the electric stress concentration. With the aid of silicone grease smeared on the sample surface around the semiconducting electrode, flashover never happened in the subsequent experiments at voltages as high as 70kV.

From the ramp results presented in figure 8.5, it is noticed that for all the degassed samples and the two samples with 0.5% residue a linear relationship exists between the external voltage and the induced charges at the electrodes. These results indicate that no space charges are accumulated over a short time in the bulk materials at voltage between 0 kV and 70 kV. On the other hand in almost all of the fresh samples and in some partially degassed samples, space charge accumulation in the bulk material was initiated when the applied voltage reached about 50kV. As a result, the induced surface charge density at the electrodes started to deviate from its linear tendency as illustrated

by the dotted line. These results have also validated the charge density calibrations, which were carried out at 25 kV on all the samples.

8.4.2 Space charge evolution during the long-term ageing

The space charge measurement results from all the planar samples are presented in this section. Ageing tests as long as 24 hours were conducted by taking space charge measurements at intervals over the ageing term. The charge profile titled "0 time" in each diagram stands for the result obtained soon after the voltage ramp process, and indicates the total space charge accumulation during the voltage ramp.

8.4.2.1 Sample P3

Sample P3 is made of reference XLPE material. Samples were subjected to three different treatments, i.e. degassed at 90°C in an oven for three days, partially degassed with 0.5% of residue and not degassed respectively. Owing to the failure of the first degassed sample in the ramp test, the other one was tested at 50 kV for 24 hours to acquire some data in the case of electrical breakdown happening again before the voltage was increased to 70 kV. However, under neither voltage was there any space charge formed in this degassed sample.

Volts on

Figure 8.6 shows the space charge distribution and progression among the samples with different residue contents. From the results of the undegassed sample and the partially degassed samples, it is seen that the influence of the residue content on the charge distribution is not very significant. In figure 8.6 (a) and (b), two samples almost have similar space charge distributions after 1 hour stressing. However, the charge accumulation speed is obviously affected by the residue in the sample. In the ramp test of the undegassed sample, a quite considerable charge had built up, whereas in the sample with 0.5% residue, most of the charge formed in the following one hour ageing after the voltage ramp. Due to the flashover occurring along the surface of the undegassed sample from the semiconducting electrode to the ground, no further data after one hour of ageing could be obtained as the test was terminated. Figure 8.6 (c)

displays the results of the degassed sample being aged at 70 kV for 24 hours. Even though the sample had been aged at 50 kV for 24 hours and another 24 hour at 70 kV, no space charge appeared.

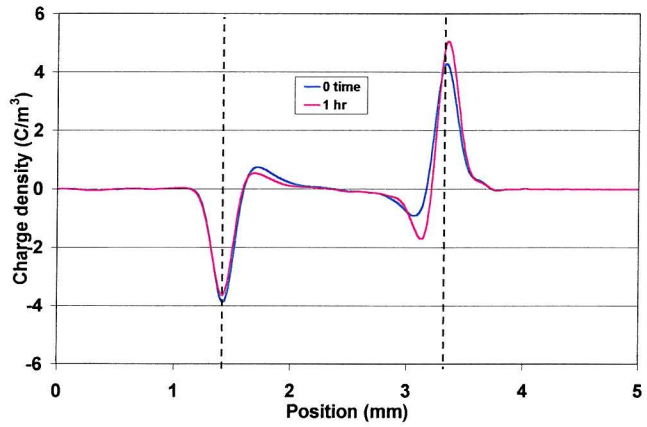

(a) Undegassed sample

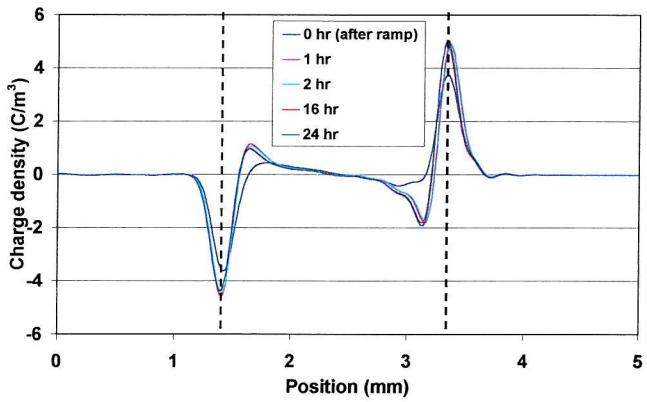

(b) Partially degassed sample with 0.5% residue

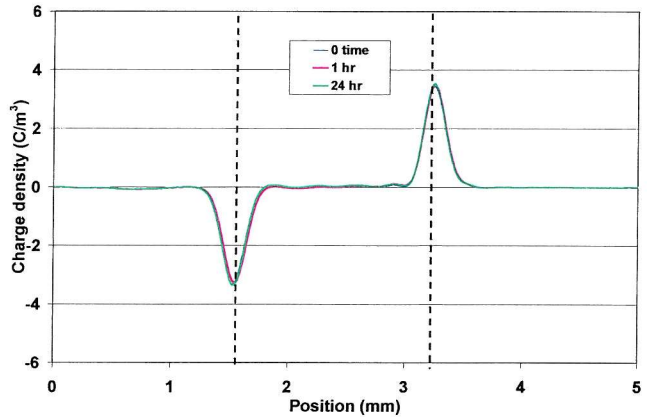

(c) Degassed sample

Figure 8.6 Space charge profiles of sample P3 (volts on)

As a remedial measure, the undegassed sample was retested two weeks later after the burnt track of the flashover had been removed and the silicon grease had been smeared around the electrode. The result is plotted in figure 8.7. As calibration was required before the retest, the sample had to be left short circuited to release any previously formed charge. Natural degassing of the sample was unavoidable during this time. So the space charge distribution is much lower than that in the last experiment.

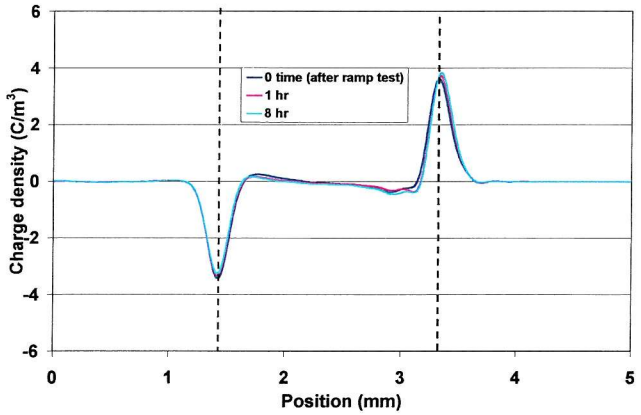

Figure 8.7 Re-tested result of the undegassed sample P3

Volts off

Space charge distributions were also measured at the different times over the ageing term after removal of the external voltage to check the homocharge, which may be merged into the surface charge due to the external voltage. The results are shown in figure 8.8.

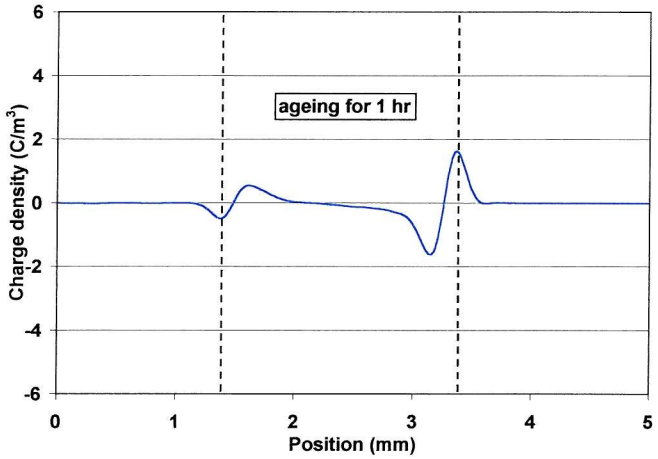

(a) Undegassed sample

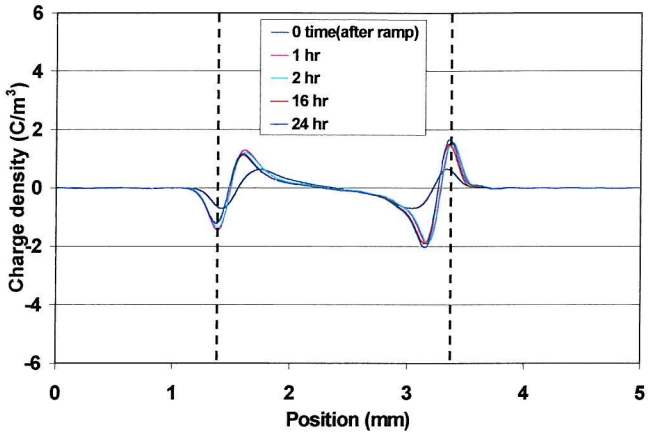

(b) Partially degassed sample with 0.5% residue

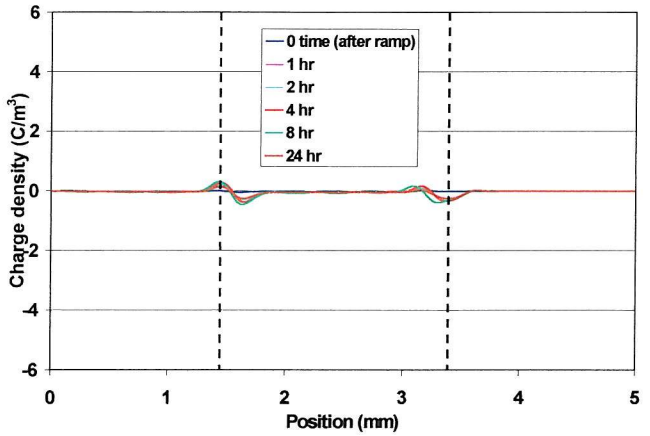

(c) Degassed sample with homocharge accumulation

Figure 8.8 Space charge profiles of sample P3 (volts off)

Results from the volts on and off tests have shown the same space charge distribution in the bulk of the material except in the degassed sample, in which a very small homocharge was developed but was not observed when the voltage was on. In the absence of the induced surface charge due to the external stressing voltage, the homocharge in the degassed sample is clearly observed, as shown in figure 8.8 (c).

Charge decay

Space charge measurements on each sample were followed by space charge decay tests, in which the two electrodes were kept short circuited after the removal of the voltage. The space charge profiles measured at different times are plotted in figure 8.9, where the charge diminution characteristics are displayed. It must be pointed out that the results reported in 8.9 (a) from the undegassed sample are from the second experiment with a comparatively low space charge density in the volume of the material. After the

flashover in the first test, no decay test was carried out since the pulse voltage could not be applied across the sample.

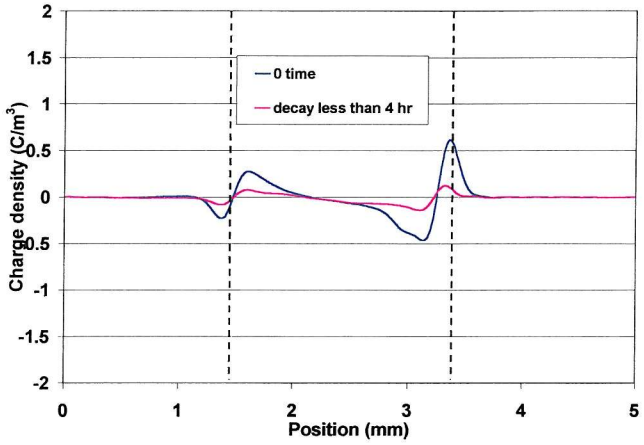

(a) Undegassed sample

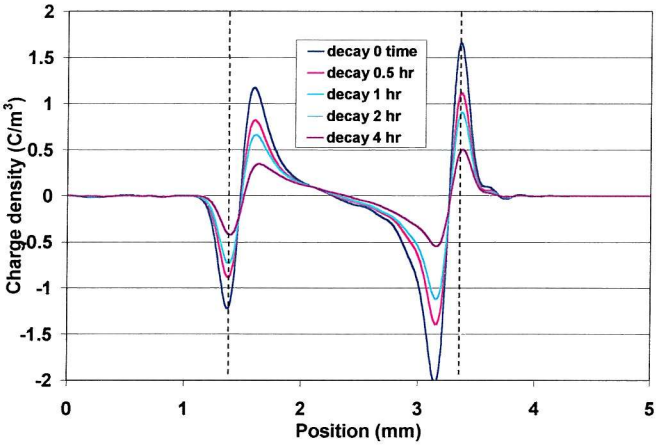

(b) Partially degassed sample with0.5% residue

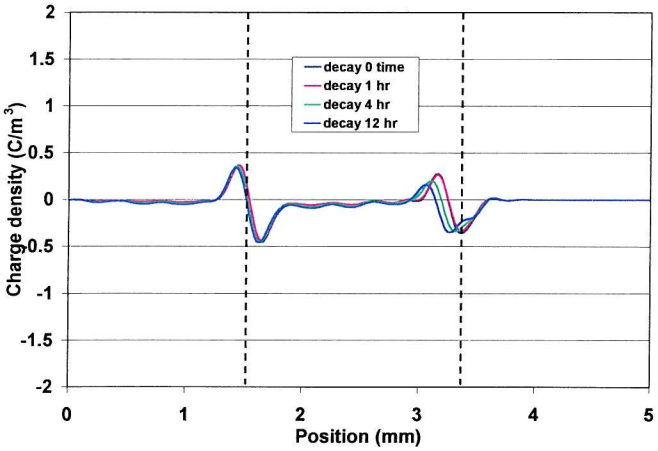

(c) Degassed sample

Figure 8.9 Space charge decay of sample P3

As the undegassed sample and the sample with 0.5% residue have a heterocharge accumulation, they possess a fast space charge decay speed in comparison with that of the degassed sample with a homocharge.

8.4.2.2 Sample P28

Volts on

Space charge measurements in sample P28 with the external voltage applied are shown in figure 8.10.

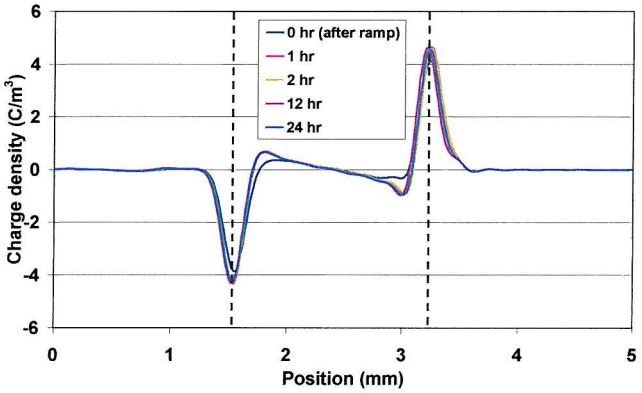

(a) Undegassed sample

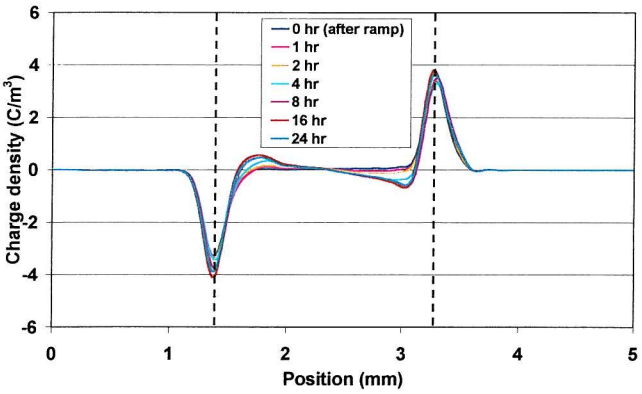

(b) Partially degassed sample with 0.5% residue

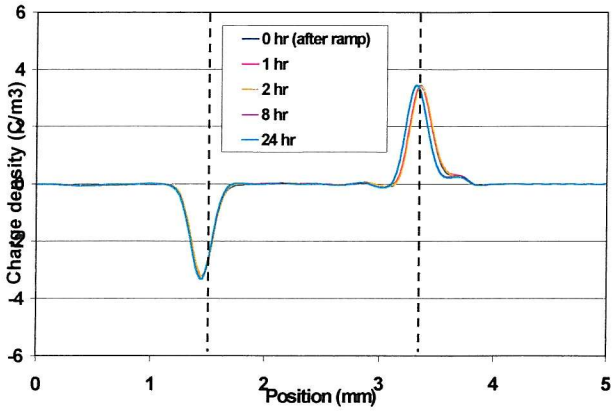

(c) Degassed sample

Figure 8.10 Space charge profiles of sample P28 (volts on)

Without exception, the undegassed sample possesses a relatively fast charge generation speed, as shown in figure 8.10 (a). After the fast heterocharge accumulation in the voltage ramp, the space charge distribution through the sample almost reached saturation within the one hour in the ageing term. In the sample with 0.5% residue, the space charge accumulation slowly progressed and saturated in about 8 hours. The space charge evolution in this sample over the whole ageing period is displayed in figure 8.10 (b). The final charge distributions between these two samples are very comparable after 24 hours ageing. Unlike in the P3 material under the degassed condition, no space charge was observed in the P28 material over the whole ageing time.

Volts off

In the same way, to determine the space charge development in the bulk material, the measurements were also conducted as the applied voltage was switched off. The results are presented in figure 8.11. The amount of charge in the undegassed sample is higher than that in the sample with 0.5% residue. The lack of space charge accumulation in the degassed sample is plain from figure 8.11 (c), where a straight base line is shown when the voltage was removed after 24 hour ageing.

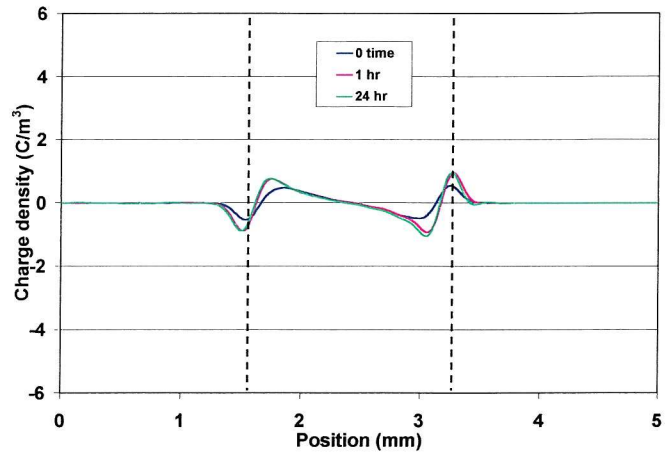

(a) Undegassed sample

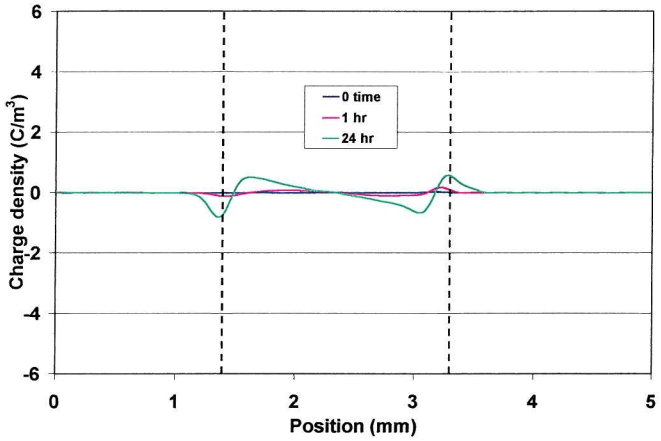

(b) Partially degassed sample with 0.5% residue

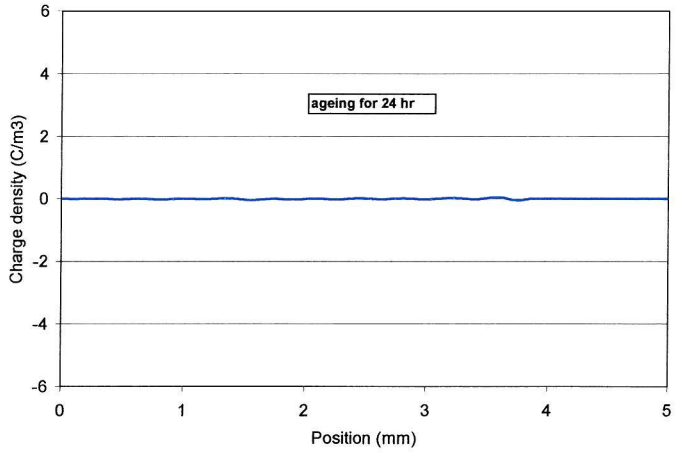

(c) Degassed sample

Figure 8.11 Space charge profiles of sample P28 (volts off)

Space charge decay

As in the undegassed sample P3, the space charge in P28 also possesses a fairly high decay speed. In figure 8.12 (a), the massive heterocharge in the bulk material has died

off within two hours after the electrodes were short-circuited, whereas the sample with 0.5% of impurities displays a completely different charge decay property. The space charge generated in this sample is so stable that no significant variation is observed from the charge profiles presented in figure 8.12 (b) over an 8-hour decaying time. No decay test was carried out in the degassed sample because of the absence of the charge.

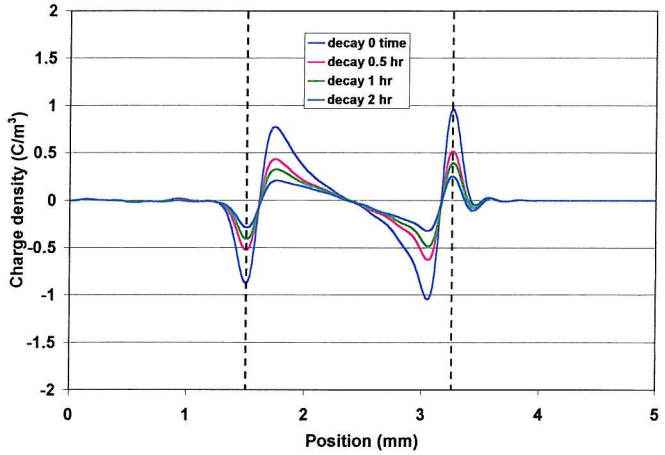

(a) Undegassed sample

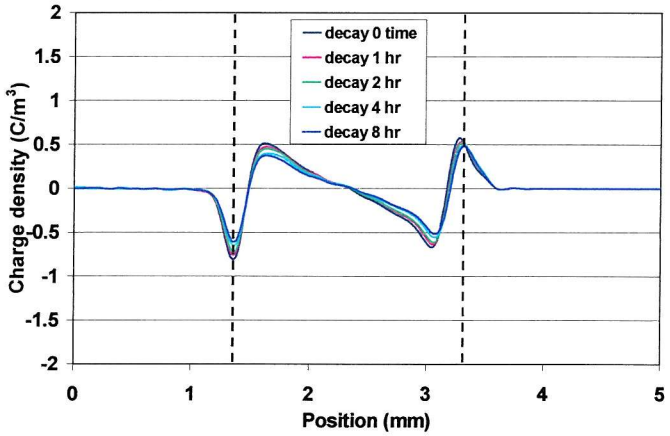

(b) Partially degassed sample with 0.5% residue

Figure 8.12 Space charge decay of sample P28

8.4.2.3 Sample P29

Space charge measurements on P29 were conducted following the same process as in the previous samples.

Volts on

Space charge accumulation activity was much less in this modified material compared with the reference material and the sample P28. As shown in figure 8.13 (a) and (b), small and slow heterocharge was developed in the sample under fresh or partially

degassed conditions over the entire ageing time. In figure 8.13 (c), as expected, no space charge accumulation in the degassed sample is observed.

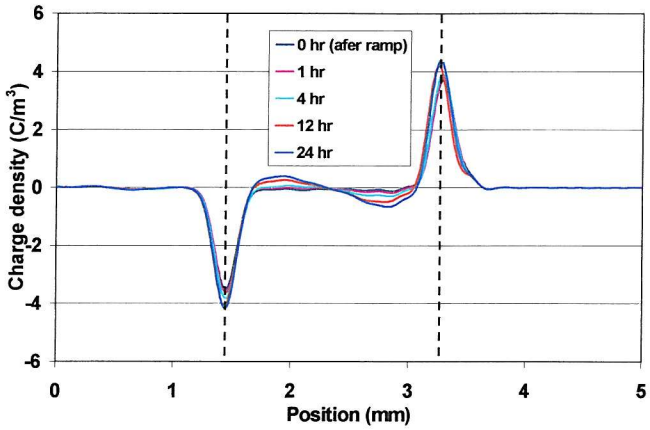

(a) Undegassed sample

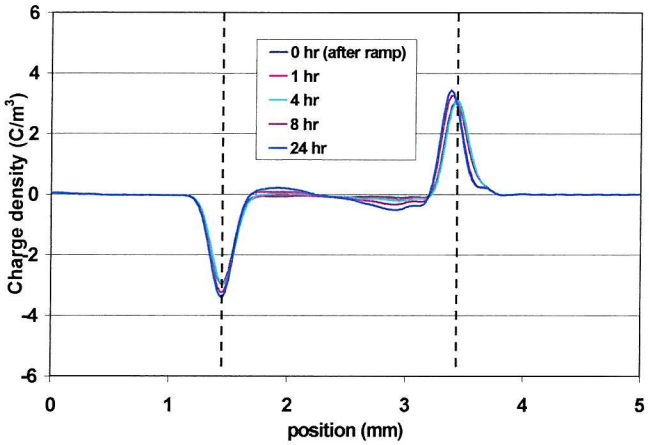

(b) Partially degassed sample with 0.5% residue

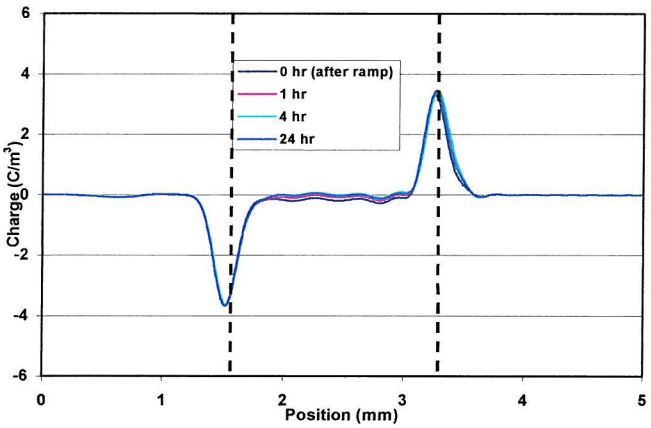

(c) Degassed sample

Figure 8.13 Space charge profiles of sample P29 (volts on)

Volts off

The space charge evolutions in this bunch of samples are displayed in figure 8.14 when no induced surface charges appear due to the external voltage. Again, the amount of charge I the bulk in the undegassed sample is higher than that in the sample with 0.5% residue. The result in figure 8.14 (c) clearly indicates no homocharge accumulation in the sample under the degassed condition over the whole ageing time.

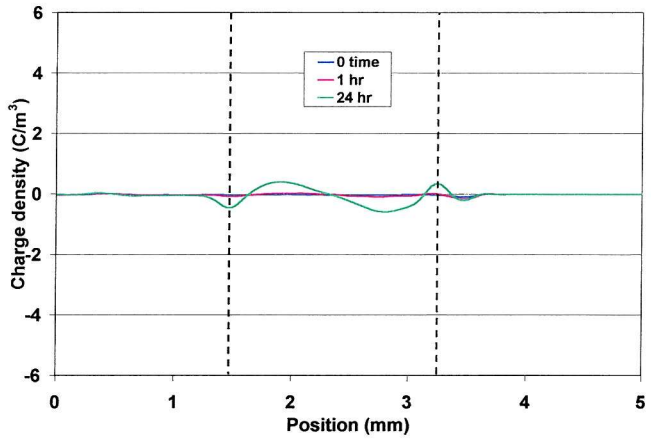

(a) Undegassed sample

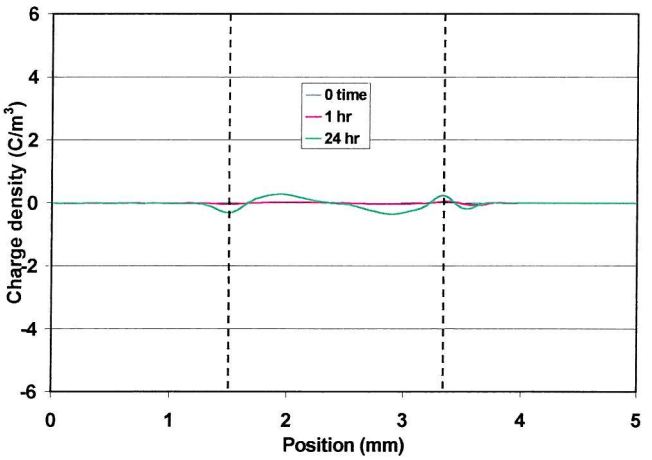

(b) Partially degassed sample with 0.5% residue

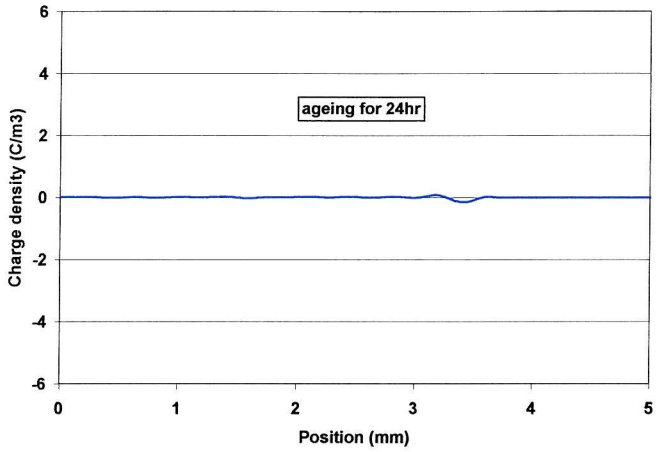

(c) Degassed sample

Figure 8.14 Space charge profiles of sample P29 (volts off)

Space charge decay

After the stressing test, the sample was left for the space charge to decay for as long as 12 hours and the results are shown in figure 8.15. Surprisingly, the space charges in both the fresh sample and the sample with 0.5% residue are very stable, although they are of low charge density. Decay tests were not carried out on the degassed sample because of no charge appearance.

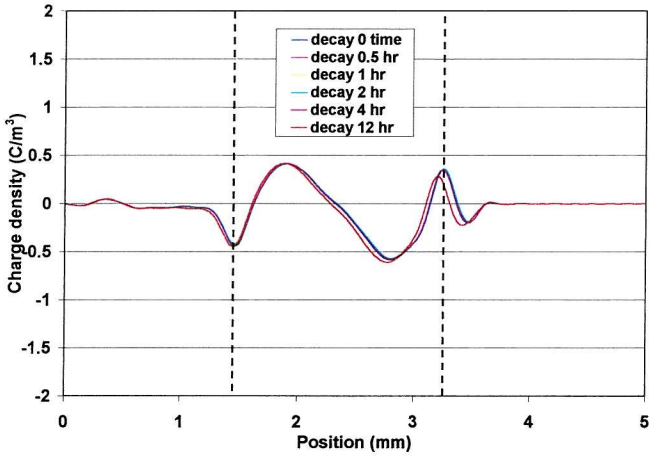

(a) Undegassed

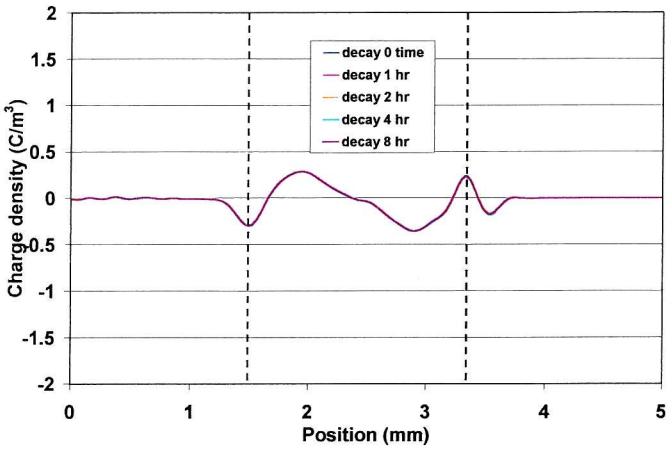

(b) 0.5% residue

Figure 8.15 Space charge decay of sample P29

8.4.2.4 Sample P30

Volts on

Another modified XLPE sample is P30. Despite the modification to the material, space charge accumulation in the undegassed and partially degassed sample is still very active. This is clearly shown in figure 8.16 (a) (b). In both cases, a considerable amount of heterocharge was formed during the voltage ramp test, and then reached its equilibrium state within about one hour in the following ageing process. The fresh sample has a slightly higher charge density than the sample with 0.5% residue. For the degassed sample, it is hard to discern any changes of charge formation under the applied external voltage from the result shown in figure 8.16 (c).

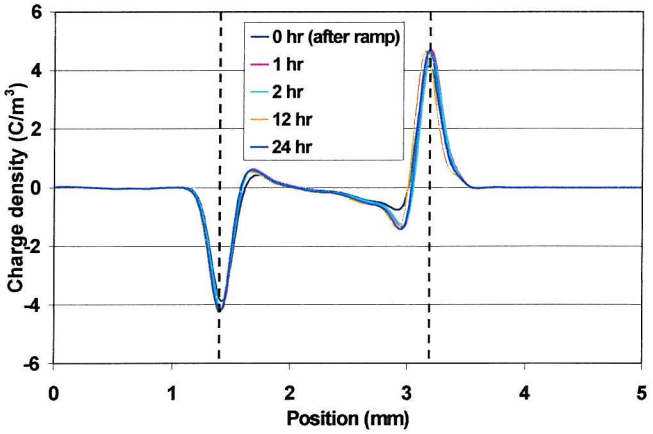

(a) Undegassed sample

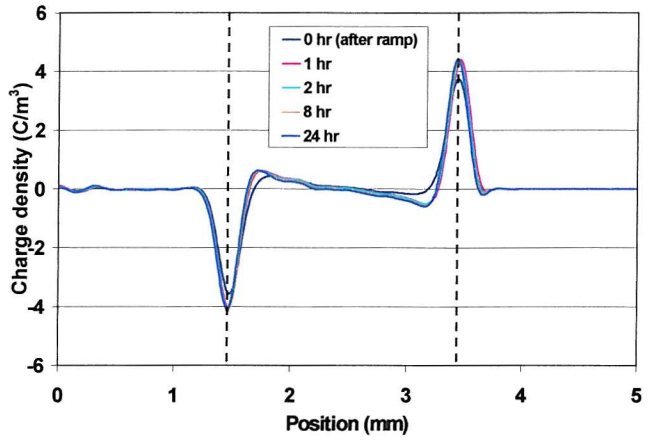

(b) Partially degassed sample with 0.5% residue

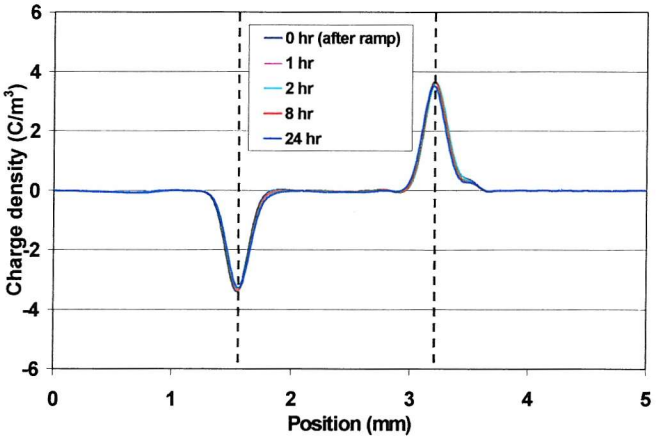

(c) Degassed sample

Figure 8.16 Space charge profiles of sample P30 (volts on)

Volts off

The results in figure 8.17 with no applied external voltage show the same space charge evolution in the ageing test except for the case of the degassed sample. A small homocharge is revealed in figure 8.17 (c).

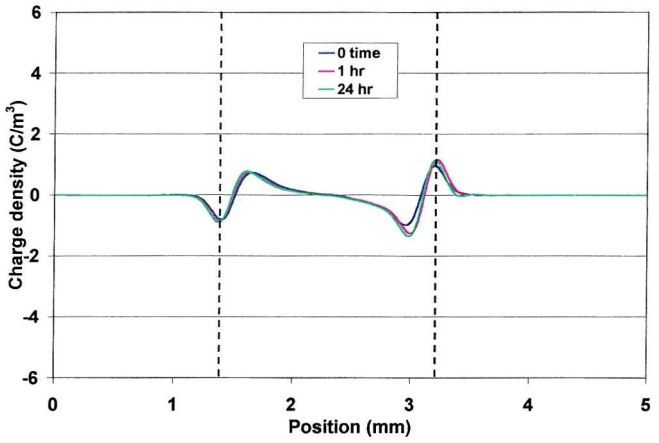

(a) Undegassed sample

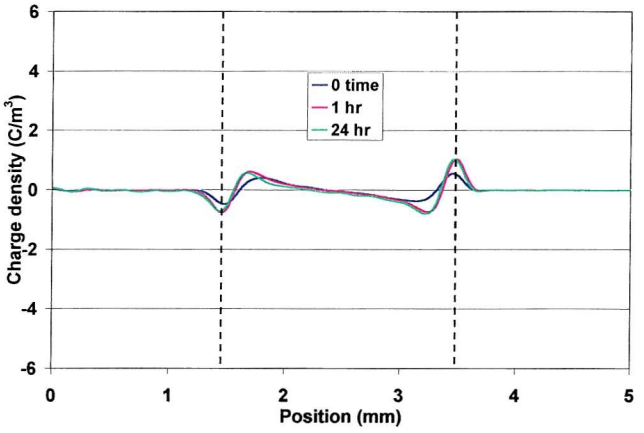

(b) Partially degassed sample with 0.5% residue

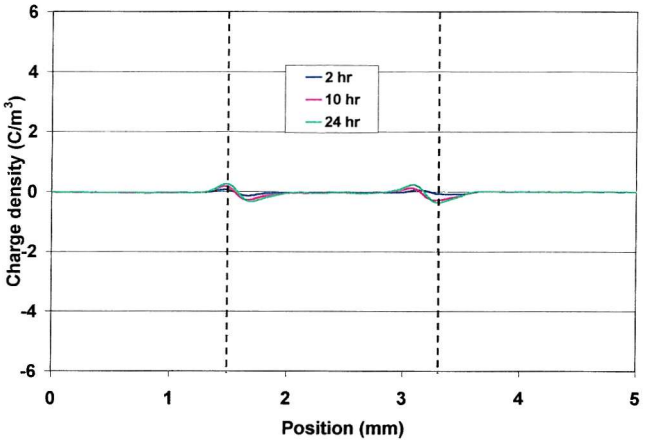

(c) Degassed sample

Figure 8.17 Space charge profiles of sample P30 (volts off)

Space charge decay

The space charge decay of sample P30 is plotted in figure 8.18. Both the fresh and the partially degassed sample exhibit a fairly high decay rate, as seen by the profiles in

figures (a) and (b), whereas the homocharge generated in the degassed sample possesses a high stability after the external stressing voltage was removed.

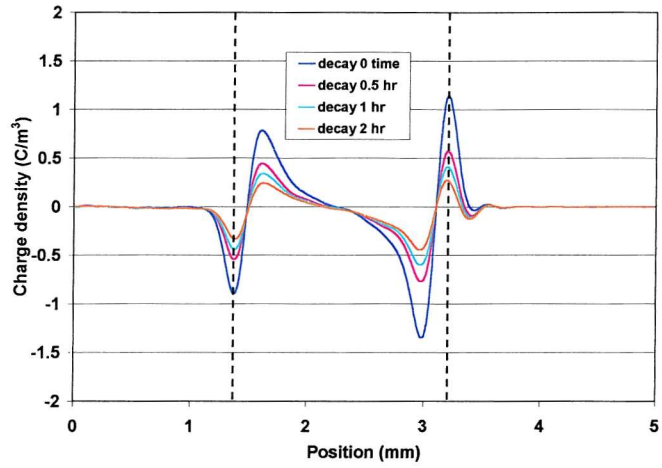

(a) Undegassed sample

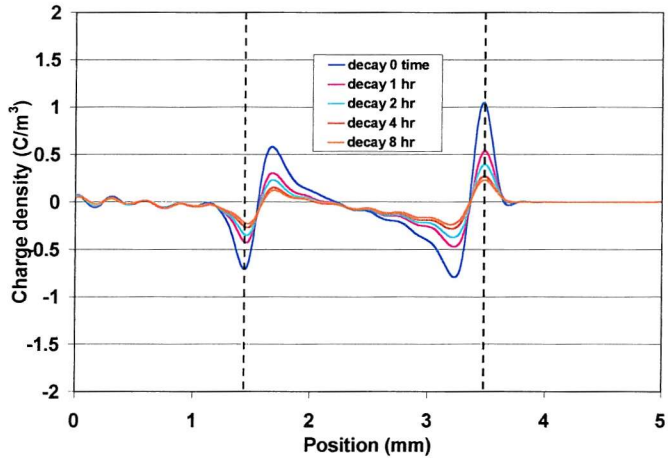

(b) Partially degassed sample with 0.5% residue

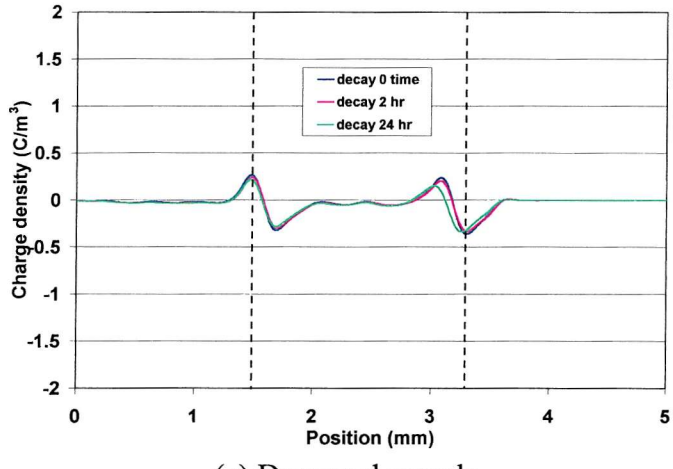

(c) Degassed sample

Figure 8.18 Space charge decay of sample P30

8.4.2.5 Sample LDPE

For reference, the space charge distribution and its development were also measured on a low-density polyethylene (LDPE) sample. This has been prepared by thermal pressing, and no peroxide was added to the sample. The test pursued the same experimental procedure as the modified XLPE samples.

From the ramp test result shown in figure 8.19 (a), the linear relationship between the induced surface charge and the external voltage suggests no space charge appearing in the voltage increasing process. Within the following ageing period, homocharges gradually accumulated in the bulk insulation at the vicinities of electrode, as shown in figure 8.19 (b) and (c). The latter one shows more clearly the presence of homocharge in the sample. Like all the homocharges observed in the previous degassed XLPEs, the homocharge in this LDPE sample also showed a very slow decay speed, as illustrated in figure 8.19 (d).

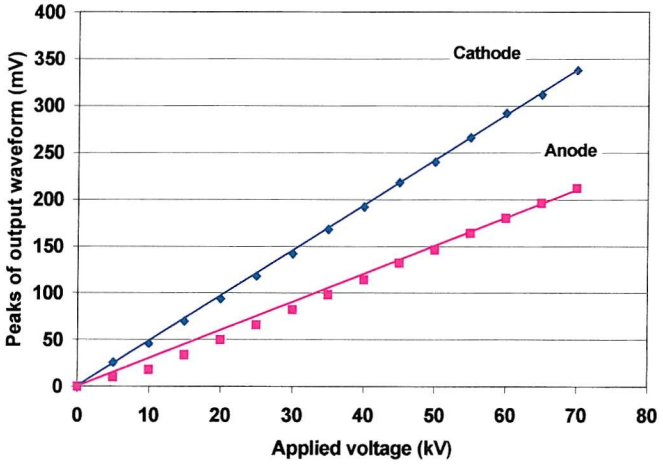

(a) Ramp test

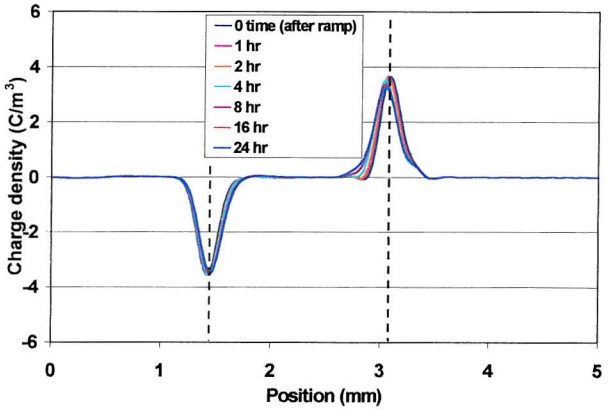

(b) Space charge profile (volts on)

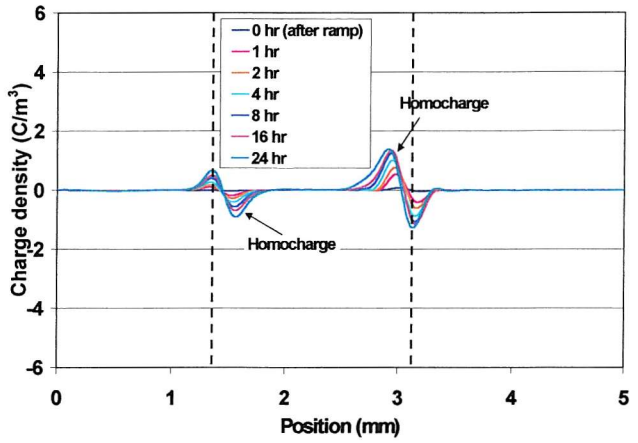

(c) Space charge profile (volts off)

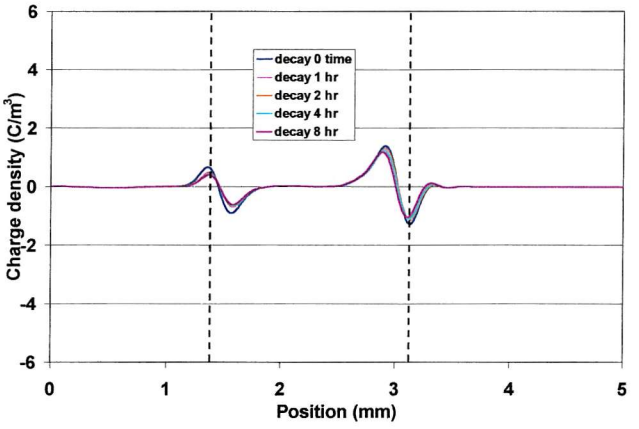

(d) Space charge decay

Figure 8.19 Space charge behaviour of LDPE sample

8.5 Discussion

8.5.1 Threshold stress for the fast charge formation in ramp test

The ramp test results presenting the relationship between the induced surface charge and the external voltage in figure 8.5 show that almost all of the undegassed XLPE samples (except sample P29) have a heterocharge accumulation during the voltage ramp process. As a result, the surface charge induced at the dielectric material and the electrode interface increases more rapidly with the external voltage due to the interfacial stress enhancement. This fact is clearly presented in the non-linear relationship between the induced surface charge and the stressing voltage. The heterocharge formation during the voltage ramp in two other partially degassed samples (P3 and P30) was also observed in the same way. The threshold stress, above which space charge starts to generate, is determined by dividing the corresponding voltage by

the sample's thickness. The specific threshold stress of each individual sample for the space charge initiation is listed in table 8.2. For those specimens having no observed charge in the voltage ramp test, the thresholds are described by the term "higher than" (>) the stress determined by the maximum stressing voltage, e.g. 70kV.

Table 8.2 Threshold stress (kV/mm) of space charge formation

	Un-degassed	0.5% residue	Degassed
P3	28	31	>40
P28	33	>37	>38
P29	>40	>35	>41
P30	25	31	>42
LDPE		>42	

Obviously, in the undegassed samples (except for P29) space charges are initiated at a relatively low electric stress compared with those of the corresponding partially degassed or degassed samples. Amongst the undegassed samples, P30 has the lowest threshold stress and its value is even smaller than that of the reference material XLPE (P3). To assess the space charge behaviour at this stage, it seems that the modification to the material of specimen P28 and P29 has achieved positive effects in suppressing space charges. On the other hand, the modification of the material for sample P30 did not show any improvement in space charge accumulation compared with that in the reference material P3.

If the same materials are degassed by the thermal method to remove the volatile impurities, the space charge accumulation can be suppressed to some extent or even eventually stopped. For instance, the threshold stresses of samples P3 and P30 had been increased from 28kV/mm and 25kV/mm respectively in the fresh samples (with maximum residue content) to the values of 31 kV/mm in the sample with 0.5% residue. If they are further degassed to remove all the cross-linking byproducts (the degassed sample), no space charge at all may be quickly formed in the voltage ramp process. Sample P28 behaved in a similar way after the degassing treatment. As in all the degassed specimens, no space charge was observed in the LDPE sample when the voltage ranged from 0 to 70kV, as the sample had no added peroxide or any other additives.

From the above results, it could be simply concluded that the ionization of the cross-linking residue in the XLPE insulation may take place at a relatively low electric stress. This may be the main contributor to the fast space charge at low stress. This

demonstrates the leading role of impurities in governing space charge accumulation in the bulk material.

8.5.2 Space charge polarity after 24hr ageing

From the above test results, it is evident that specimens with different modified insulating materials and thermal treatments (degassing) have different space charge development speeds and final charge distributions. In particular, samples with and without residues may have space charge of opposite polarities in the volume of the material adjacent to the electrode. Table 8.3 details the final space charge polarities of these samples under different conditions.

Table 8.3 Space charge polarity of samples after 24hr ageing

	Undegassed	0.5% residue	Degassed
P3	Hetero	Hetero	Homo
P28	Hetero	Hetero	Not observed
P29	Hetero	Hetero	Not observed
P30	Hetero	Hetero	Homo
LDPE		Homo	

The results presented in this table clearly indicate that the residue or the impurity, no matter how high its content, is the main source of the heterocharge. In samples like pure LDPE or those from which impurities have been removed by degassing treatment, it is very difficult to develop heterocharge under the electric stress applied in this test, except for the small homocharge accumulation in some samples, such as LDPE, P3 and P30. From the results of the degassed samples, one can therefore easily conclude that the modifications to materials P28 and P29 are helpful in suppressing the space charge accumulation in XLPE. Of course, the effect of the modification to XLPE on other space charge characteristics, such as charge building up and decay speed, and charge amount are other considerations to be taken into account in the material selection process.

Additionally, the fact of the longer time requirement for the small homocharge to develop in the degassed sample or LDPE sample may suggest that homocharge formation is more difficult than heterocharge [132-133]. The former case may need higher electric stress or longer time under the same electrode and dielectrics arrangement in order to develop same amount of space charge.

8.5.3 Space charge building up speed

As discussed in a preceding chapter, the time for the space charge to reach its saturation status is the most practicable way to describe the space charge building up speed. It has been observed that degassing treatment can radically influence the space charge generation in these XLPE materials, so the comparison is made among different samples, as well as different treatments.

The results shown in figure 8.20 reveal that for the samples having residual impurities (which normally develop heterocharges as discussed in the previous section) have shorter space charge saturation times than the degassed samples in which homocharges appear. Among these samples, P3 and P30 display quite similar features of space charge accumulation. In both of them in the undegassed or the 0.5% residue condition, the space charge could reach its saturation distribution within 1 hour. The development of homocharge in the degassed specimen was fairly slow.

As an exception, sample P29 shows a relatively slow space charge building up speed in the undegassed sample and in the sample with 0.5% residue. Similar to the degassed sample, thermally pressed LDPE has also shown a very low charge accumulation speed.

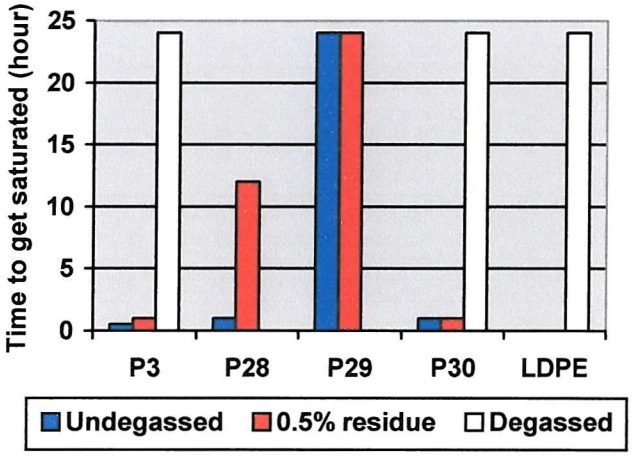

Figure 8.20 Saturation time of different samples

8.5.4 Maximum space charge density

To compare the charging ability of different samples, the maximum space charge densities after 24 hour stressing are illustrated in figure 8.21.

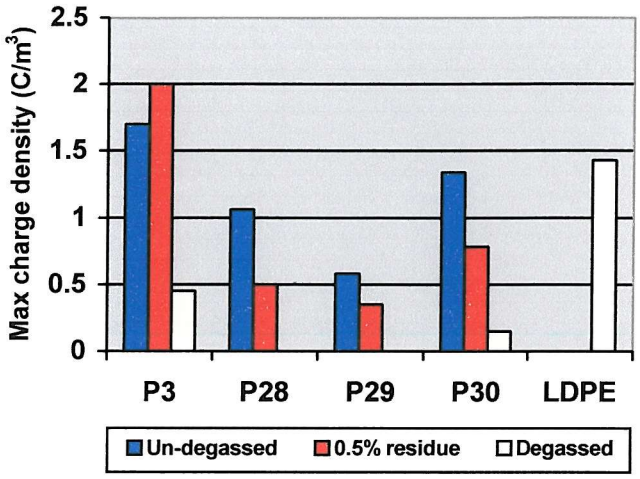

Figure 8.21 Maximum space charge density in different samples

Among the four types of XLPE sample, irrespective of the concentration of the residue within the material, P3 and P30 show higher charge densities than the other two modified materials. In each type of XLPE, degassing treatment significantly reduces the charge density, and even change the charging mechanism such as the formation of homocharge in degassed P3 and P30.

By comparing the space charge densities in LDPE and degassed XLPEs, the former material is seen to exhibit a much higher homocharge density than the other four degassed XLPEs. On the assumption that no impurities remain in the thermally pressed LDPE and degassed XLPE sample and provided the same electrode material is used, the above results suggest that the cross-linked structure of the polymer has actually suppressed the space charge accumulation.

8.5.5 Space charge distribution shape

In addition to the difference in the space charge polarity, building up speed and charge density among the samples of different materials and residue concentration, a notable difference also exists between the space charge distribution outline of sample P29 and that of the other samples. In most samples, the space charge tended to accumulate in the vicinity of the dielectric material and electrode interface, while in P29 the space charge had a flat distribution and a deep location inside the sample away from the dielectric and the electrode interface. The charge profile shown in figure 8.22 (a) is a typical result of those found in most samples with certain amount of residue. The charge locates dominantly in regions adjacent to the electrode. On the other hand, the space

charge in P29 has a broader distribution through the sample thickness, as shown in figure 8.22 (b).

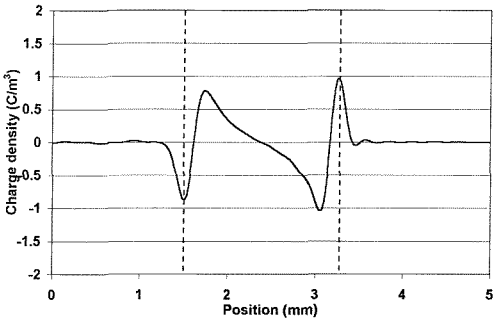

(a) Charge close to electrode (undegassed P28)

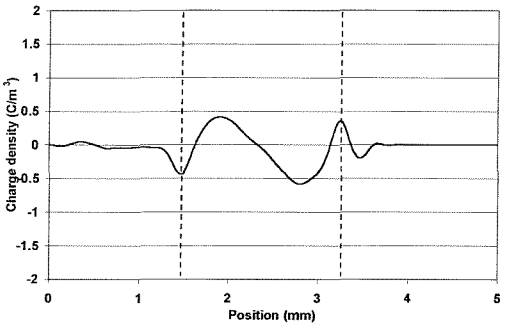

(b) Broader charge distribution in undegassed P29

Figure 8.22 Comparison of space charge distribution between P29 and other samples

This distinctive distribution of space charge in P29 is also found in the sample with 0.5% residue. This feature must therefore be related to the unique nature of the residue produced in the material processing. Mizutani *et al* [137, 138] and Kaneko *et al* [139] have reported a similar finding in two types of LDPE (polymerised with a conventional high-pressure method and a metallocene method respectively) but with the appearance of homocharge. The space charge in one sample was closer to the electrode, and in the other was spread away from the electrode. It has been suggested that injected carriers in the material with a deeper charge distribution have a higher mobility. It is possible to draw an analogy between their discovery and the case of P29. If the electron carrier is liberated mainly by the bulk effect of instead of by electrode injection and has a relatively low mobility, the positive charge, for instance, will have little chance to transport to the cathode side and most of the carriers will reside where they are initiated, so producing a broad distribution. In the same way, if the negative charge carrier is fastened in the bulk material on other side of the material due to its low migration, a flat negative charge layer will be formed close to the anode electrode. The charge distribution, on the other hand, may also reflect the reside distribution in the material. The low charge carrier mobility in the fresh or partially degassed samples of P29 can also be proved indirectly by its low charge decay speed.

8.5.6 Space charge decay rate

Space charge decay rates of different samples presented in section 8.4 have shown a big variation associated with the different materials and different degassing conditions. They are summarised and discussed as below.

Firstly, in most cases the space charge decay speed corresponds to its building up speed, in that the faster the space charge accumulates, the faster it decays, or vice versa. Typical results which lead to this conclusion are presented in figure 8.23 where P30 and P28 are regarded as typical fast charging and slow charging examples respectively.

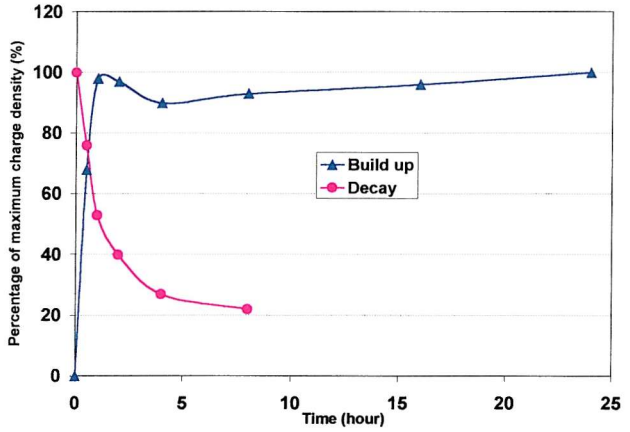

(a) Fast charge build up and decay in P30

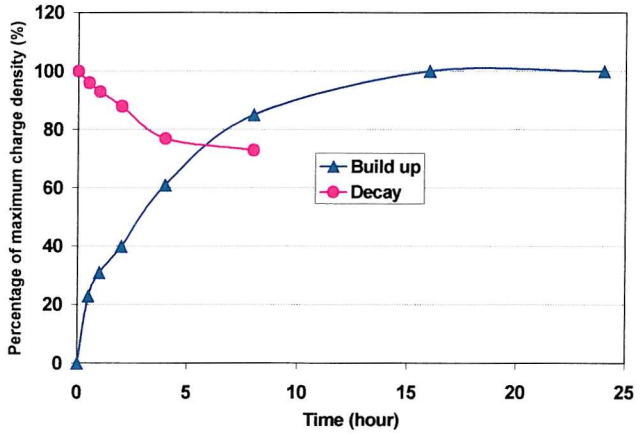

(b) Slow charge build up and decay in P28

Figure 8.23 Space charge accumulation rate in accordance with decay rate

As shown in figure 8.23 (a), space charge built up very quickly in the sample P30 (with 0.5% residue) and almost reaches saturation in one hour. Correspondingly, space charge also decayed very quickly when the applied voltage was removed. Only ~20% of initially accumulated charge was left when the sample was short-circuited for 8

hours for discharge. On the other hand, in the sample P28 (0.5% residues, see figure 8.23 (b)), the space charge built up gradually and reached its equilibrium in about 15 hours after the ageing started. After leaving the sample electrodes short-circuited for 8 hours for the space charge to decay, there was still a high percentage of space charge residing in the sample. The charge decay speed was fairly slow. The space charge in samples P3 and P29 showed the same characteristics in the accumulation and the decay process.

Secondly, homocharge in the degassed sample decays much more slowly than does heterocharge in the undegassed sample. As shown in figure 8.24, heterocharge in the undegassed sample P30 had a very high decay rate. After 3 hours, the maximum charge density decayed to about 20% of its original value, while the homocharge accumulated in the degassed sample was relatively stable. Of course, if we refer back to the section 8.4, we know that homocharge also has a very slow building up speed, which agrees with the conclusion about the building up and the decay speed discussed previously.

Space charge evolution and decay in figure 8.19 (c) and (d) also show the same features for the LDPE sample.

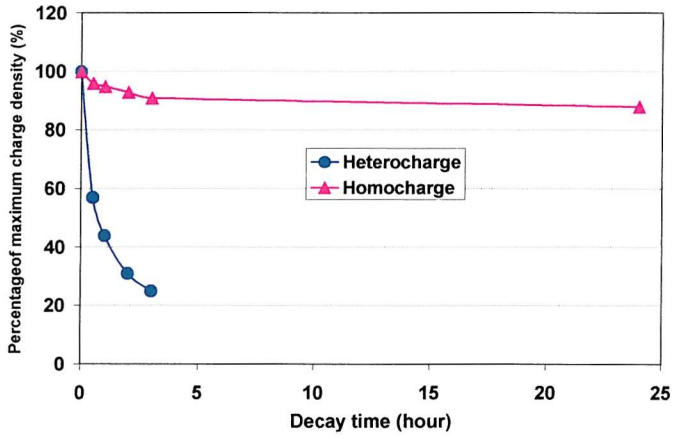

Figure 8.24 Comparison of homo and hetero charge decay speed

For the degassed sample, the removal of residue means that the homocharge is mainly contributed by electron injection at the cathode and extraction at the anode and it accumulates because of the mobility of electrons in the material is low. The homocharge due the trapped electrons and the left holes is more stable and as a consequence the charge will decay slowly if the external voltage is removed.

8.5.7 Electric stress distribution modified by the space charge

As a consequence of space charge accumulation in the insulation material, the external applied electric field will be detrimentally distorted. To actually understand this effect in the planar geometry, the modified electric stress distribution across the bulk of the insulating material was drawn from the final space charge profile after a certain period of ageing. The results are presented in figure 8.25, in which the evenly distributed applied electric stress is also plotted for the convenience of comparison.

The method employed here to calculate the electric field is the same as that introduced in chapter 6. in which the component attributed to space charge is derived from the integration of the bulk charge along the sample thickness while the interface stress is determined by the induced charge density.

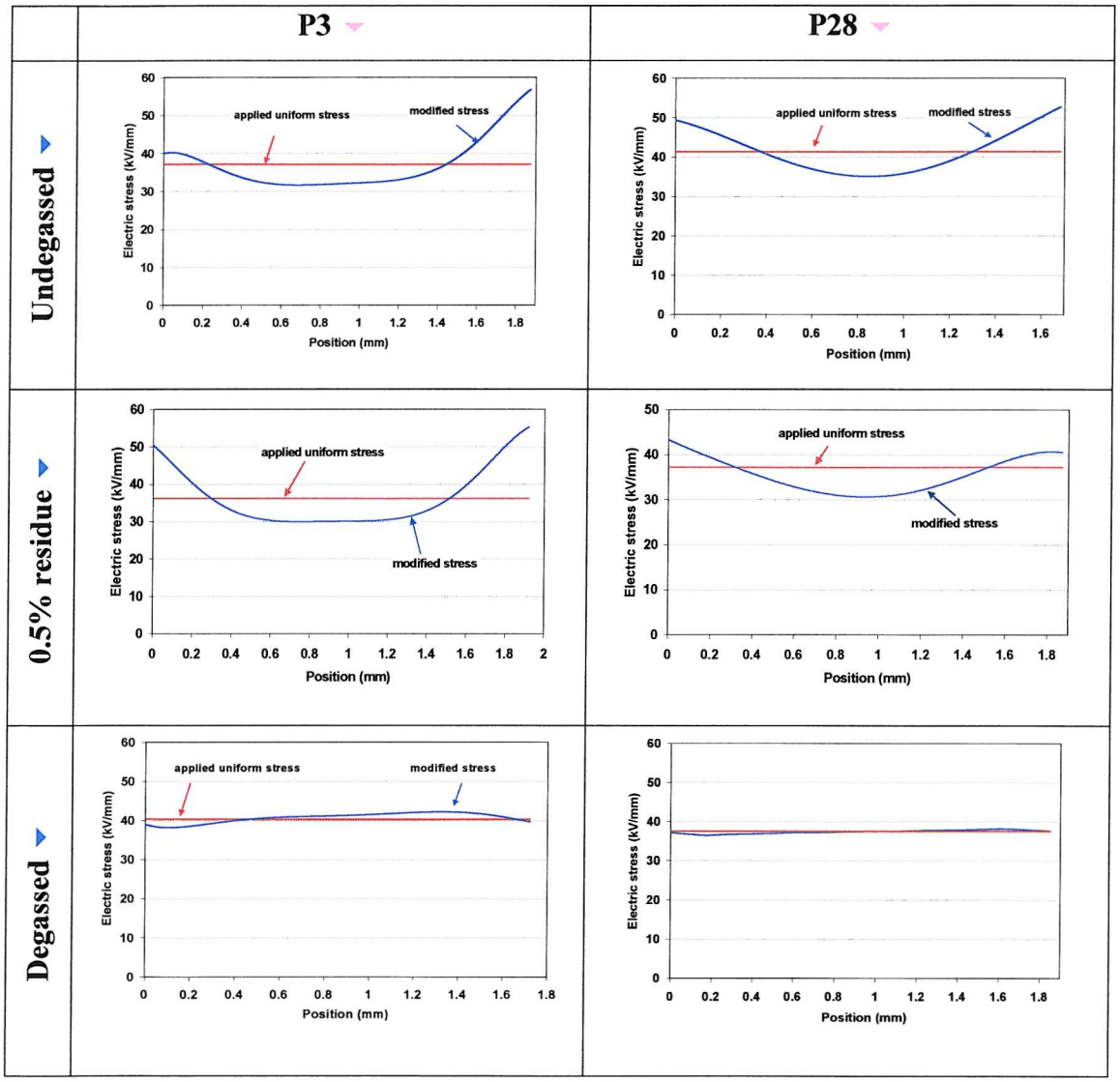

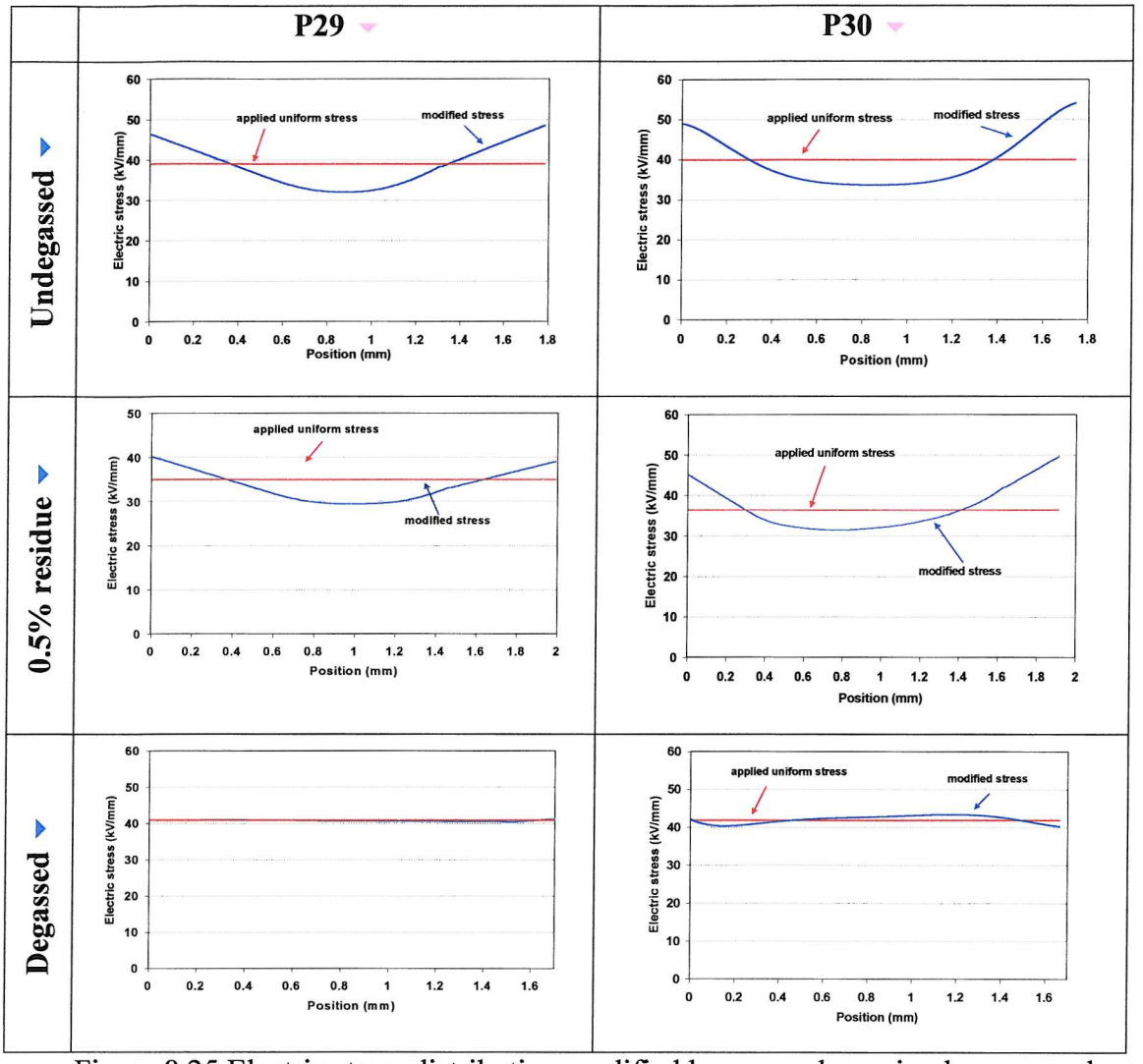

Figure 8.25 Electric stress distribution modified by space charge in plaque samples

As expected, the uniform electric stress distribution due to the externally applied voltage is significantly distorted because of space charge in the fresh sample or in the sample with some residues. As seen in the figure 8.25, the heterocharge has resulted in the enhancement of the interfacial stress and in a stress reduction at the specimen centre. In both fresh or partially degassed samples of P3 and modified P30 the large bulk charge accumulation adjacent to the electrode causes the interfacial electric stress at the anode to be increased from its applied value of ~36kV/mm to ~57kV/mm. No charge was accumulated in the degassed samples P28 and P29, so the electric stress distribution calculated from the space charge profile actually agreed with the externally applied stress. Due to the small homocharge in P3 and P30, the electric stress in the central area of the insulation has been slightly enhanced.

The influence of homocharge on the electric stress distribution is illustrated very well by the LDPE sample because of its comparatively high charge density, and is seen

in figure 8.26. As described previously, the interfacial stress between the insulation and the electrode is actually reduced whereas the stress in the central material is enhanced.

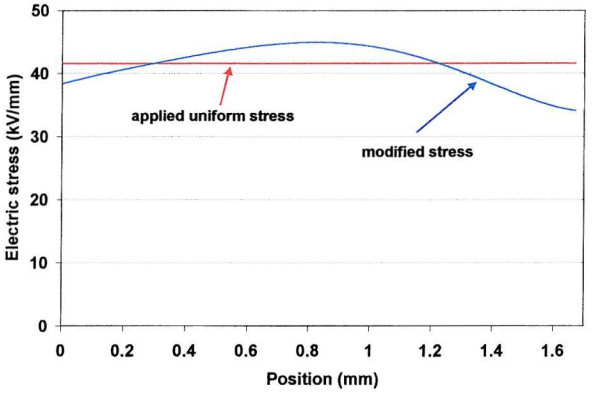

Figure 8.26 Space charge modified electric stress distribution in LDPE sample

To evaluate the effect of the modification on each material, a comparison was conducted among the modified XLPEs from the aspect of the maximum electric stress resulting from space charge accumulation. Figure 8.27 shows the maximum modified electric stress in each sample through the insulation. The values here have been normalised to the initial stress when no space charge was present.

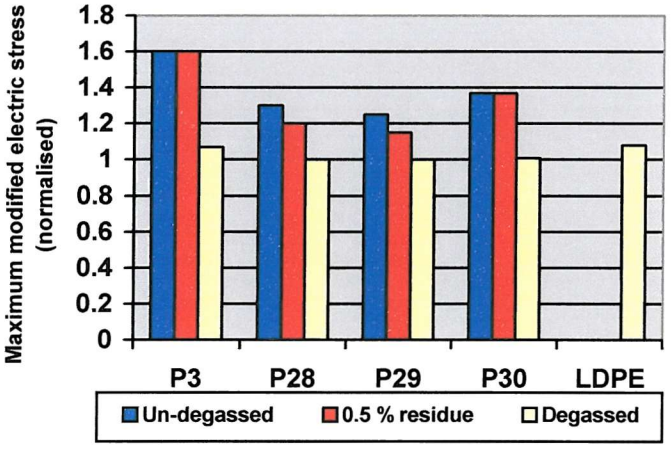

Figure 8.27 Comparison of maximum electric stresses among different samples

Owing to a large amount of charge accumulation in reference XLPE P3 and modified XLPE P30, the electric stress at the interface of the insulation and the electrode is ~1.4-1.6 times its original value. Modification in samples P28 and P29 obviously suppresses the space charge formation, but the final space charge distribution still enhances the electric stress at the interface to some extent.

The homocharge in the LDPE sample has enhanced the stress in the central material to about 1.1 times its externally applied stress.

8.5 Conclusions

A brief introduction to the application of the PEA system for space charge measurements in thick plaque sample is given in this chapter. Actual resultsof space charge distributions from a batch of modified XLPEs and reference materials are presented and discussed. Based on this research, the following conclusions may be drawn.

Firstly, the PEA system introduced here is ideal for measuring space charge in thick plaque samples which can be prepared exactly following the production of the polymeric cable. It can be viewed as a necessary method for studying and selecting materials for polymer insulated dc power cables.

Secondly, space charge results have revealed significant differences between the different XLPEs and the reference materials. They have proved the effectiveness of the modification to the XLPE in suppressing space charges in dc insulation systems. Amongst these modified XLPEs, the materials of samples P28 and P29 are the most effective in preventing space charge formation. Neither sample displayed any space charge formation when stressed at ~40kV/mm for 24 hours after being subjected to the degassing treatment. Even in the fresh condition or with 0.5% of residue, these two materials showed a lower space charge generating ability than the sample P30 and the reference material (sample P3).

Thirdly, the by-products of cross-linking or the residual impurities play an important role in the space charge accumulation in XLPE. For instance in sample P28 and P29, the modification to the material has reduced the space charge accumulation to a certain extent in comparison with the reference XLPE (sample P3) in the fresh condition, but a considerable amount of charge was still generated. When they were partially degassed leaving 0.5% of residue in the sample, the space charge density was impressively reduced. In the fully degassed sample, no space charge appeared in the testing condition. In the other two degassed samples, P3 and P30, a small homocharge was built up in the vicinity of the electrode. At this stage, space charge accumulation is governed by the charge injection from the electrode.

Amongst the samples in the undegassed and partially degassed condition, sample P29 displayed the lowest space charge accumulating rate and, the heterocharge maintained an increase over the whole ageing period. In the sample of P3, P30 and undegassed P28, the space charge almost reached saturation in the first two hours.

However, the homocharge appeared in some degassed sample and in the LDPE showed a fairly slow formation speed.

The space charge accumulation speed corresponds well with the decay speed. In other words, the faster the space charge accumulates, the quicker it decays. It is also found that homocharge in degassed material decays much more slowly than the heterocharge in the same undegassed material.

Finally, the distortion of initial external applied electric stress caused by space charge is significant. The highest electric stress in reference XLPE due to the appearance of heterocharge reaches 1.6 times its original value.

Chapter 9

Space Charge Distribution and Its Modified Electric Stress Profile under the Applied Voltage Reversal

9.1 Introduction

Most dc transmission schemes in existence are provided with bi-directional power flow capability. This is necessary and a quite usual operation in dc transmission system. The power flow direction conversion is controlled by the exchanging roles of rectifier (sending end) and inverter (receiving end). Thus to achieve a change in the direction of the power flow, the voltage polarity is reversed too.

When the insulation of XLPE power cable is subject to a dc stress, and space charge may form after a certain period of time. If such a space charge cannot move in response to a sudden dc voltage polarity change, there may be a danger of insulation failure as the localised electric stress can be very high. Such a problem may also be encountered when the dc system suffers from transient overvoltage, which may be caused by malfunction of the converter or by the intrusion of lightning surges.

In this chapter, the space charge behaviour within the XLPE cable under the influence of external voltage reversal is investigated. The motivation for performing these experiments is briefly summarised as follows:

- How does the space charge behave when there is a voltage polarity reversal?
- How does the rebuilding up speed of the space charge after the voltage reversal differ from that under the previous polarity?

- What will the modified electric stress across the insulation look like when the voltage polarity is changed?

9.2 Experiment procedure

The tests were conducted on two commercially available ac XLPE power cables with insulation thickness of 3.6mm and 2.8mm respectively. After the space charge calibration, each sample was initially stressed from a low stress which was then gradually ramped up to the required value. Space charge measurements were carried out over the whole period of a subsequent ageing time under each polarity in turn to observe the space charge evolution.

As soon as the space charge got stable, the external applied dc voltage was turned off and the insulation of the cable sample was short-circuited for short time to release the surface static charge. Finally, the dc supply was switched to the opposite polarity and connected back to the sample again. The above implementation was finished within about 90 seconds. The voltage of the new polarity was then stepped up to the desired value, and the space charge distribution was measured at this reversed voltage in the following time. The experimental procedure and the voltage application method are illustrated in figure 9.1.

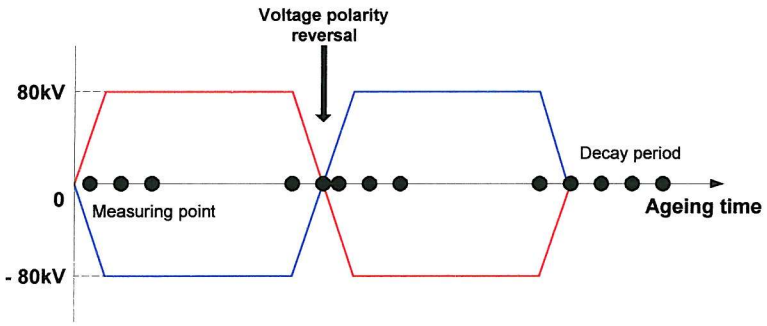

Figure 9.1 Voltage application form

9.3 Experimental results

9.3.1 Test of XLPE power cable with 3.6mm insulation

Space charge accumulation with positive voltage at central conductor

After the space charge calibration at +30kV, the externally applied dc voltage was stepped up to +80kV and the space charge was measured at each voltage. From the

results shown in figure 9.2, it is noticed that no space charge accumulated in the voltage ramping process (see the profile indicated as "0 time"). However in the following ageing test, heterocharge gradually accumulated in the vicinities of the inner and outer electrodes and reached a stable distribution in about 90 minutes.

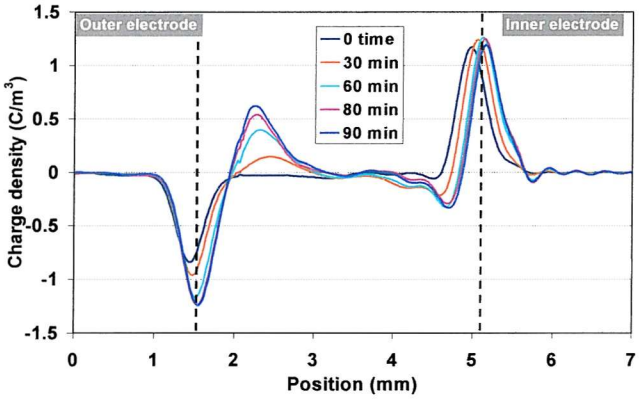

Figure 9.2 Space charge accumulation with ageing time (+80kV at central conductor)

Space charge evolution after voltage switched from positive to negative

As described in the previous section, following the first round test under the positive voltage, the applied voltage polarity was switched to negative. The variation of the space charge distribution during the voltage change is presented in figure 9.3. In these results, the previously formed charge (positive near the outer sheath, indicated in ***b***) remains almost the same when the voltage starts from –30kV. The induced charge at the outer electrode (peak ***a***) increases linearly with the external voltage as no fast charge is developed during the voltage ramping process with the negative polarity. However, the surface charge ***a*** is significantly suppressed by the remaining positive charge ***b***.

After the voltage reached –80kV, the heterocharge began to accumulate in the bulk of the insulation again, see figure 9.4. The previously accumulated heterocharge (positive) near the outer electrode was gradually neutralised by the newly formed heterocharge (negative) at the same position, and resulted in the reduction of positive charge. The final result of the neutralisation was the accumulation of the new heterocharge (negative) and the induced surface charge at the outer electrode/insulation interface increase. It took another 90 minutes for the sample at negative voltage to get the same charge density as that at positive voltage.

When the applied voltage polarity was reversed, the heterocharge accumulated near both the inner and the outer electrodes under the previous polarity had to be neutralised first. It was therefore generally expected that the charge would take a longer time to reach its new saturation state or the same charge distribution as that in the first round of test. However, the experiment showed that a similar space charge distribution to that at positive voltage was rebuilt up within 90 minutes. The space charge near the inner electrode/insulation interface took about 30 minutes to reach its highest charge density at the reversed voltage. This was even faster than the charge near the outer electrode.

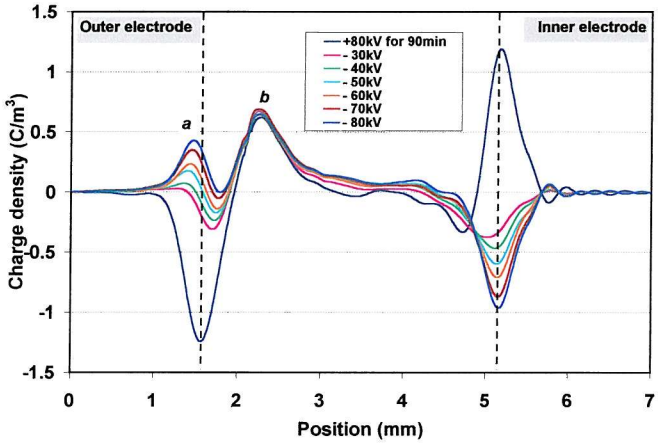

Figure 9.3 Space charge response to the reversed voltage amplitudes

The final space charge distributions at two opposite stressing polarities are displayed in the figure 9.5 which was obtained as the externally applied voltage was removed. A "mirror image" charge distribution is observed again after ageing for the same time at the positive and the negative voltages.

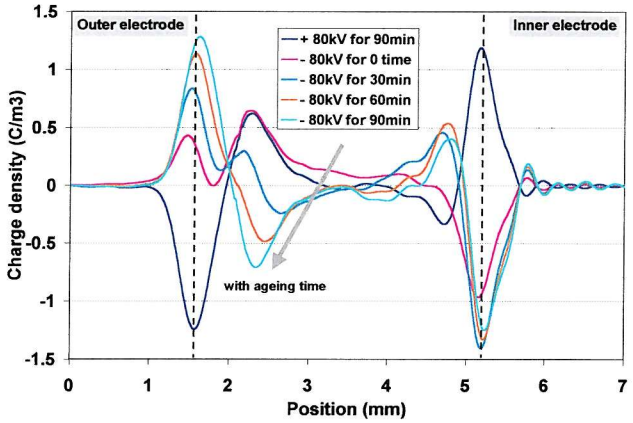

Figure 9.4 Space charge accumulation with reversed voltage application time

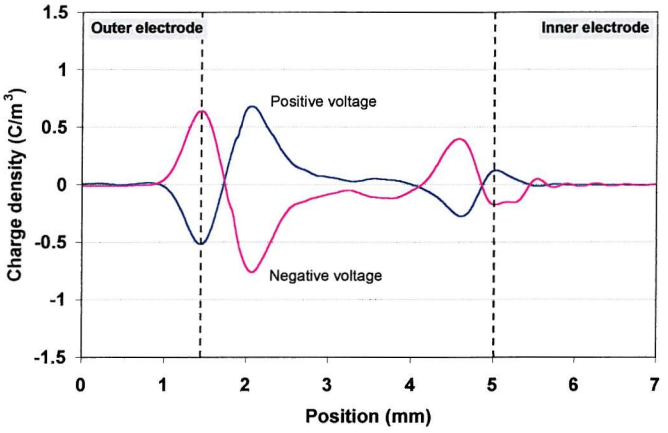

Figure 9.5 Comparison between the charge aged for 90 min and that under reversed voltage for another 90 min

9.3.2 Test of XLPE cable with 2.8mm insulation

Space charge accumulation with positive voltage at central conductor

The same test was carried out on another XLPE power cable with 2.8mm thick insulation. First, the evolution of space charge distribution at +80kV over 20 hours is exhibited in figure 9.6. In the first 4 hours after the stressing voltage reached +80kV, a small amount of positive charge (peak ***a***) began to develop adjacent to the inner electrode (anode). In the following hours, a large "lump" of positive charge accumulated in the central region of the insulation (peak ***b***). The result obtained at 20 hours shows its saturated state. It is seen that the charge close to the inner electrode reached steady state much more quickly than the packet charge in the central insulation.

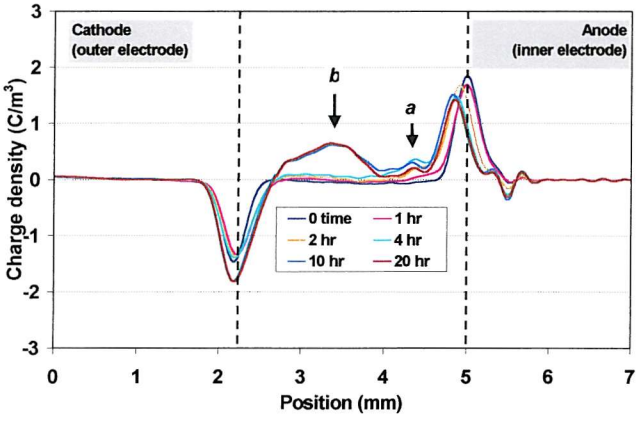

Figure 9.6 Space charge accumulation with ageing time (+80kV)

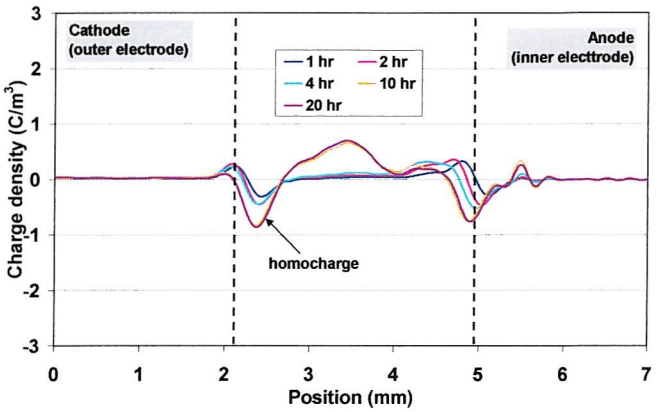

Figure 9.7 Space charge accumulation with time (+80kV off)

To check the homocharge adjacent to the electrode, the measurements after the removal of the external voltage are shown in figure 9.7. The homocharge is clearly displayed at the outer electrode in the absence of the induced surface charge due to the applied voltage. In fact, the unsymmetrical shape of the peak at the outer electrode suggests the existence of this homocharge in figure 9.6.

Space charge evolution after the voltage switch from positive to negative

When the voltage amplitude was stepped up from 30kV to 80kV after the polarity reversal, the space charge profile in the bulk remained the same as what had been built up previously, as shown in figure 9.8. The homocharge and the positive charge in the central material remains unchanged, and the induced surface charges at the two electrodes increase linearly with the negative voltage amplitude. With the bulk charge in the central part of the insulating material, the induced charge at the outer interface was obviously suppressed while heightened at the inner electrode.

As the application of negative voltage continued, the space charge profile started to redistribute across the cable insulation. The variation of charge distribution with ageing time is presented in figure 9.9.

It is notable again that the space charge re-distribution was faster than its development in the first round of test at the positive voltage. The space charge distribution after 4 hours of ageing is already comparable with that obtained at the positive voltage for 20 hours. With continuous application of the reversed voltage, the

negative packet charge in the middle of the material increased at a steady rate, and its density became higher than that at the earlier voltage polarity.

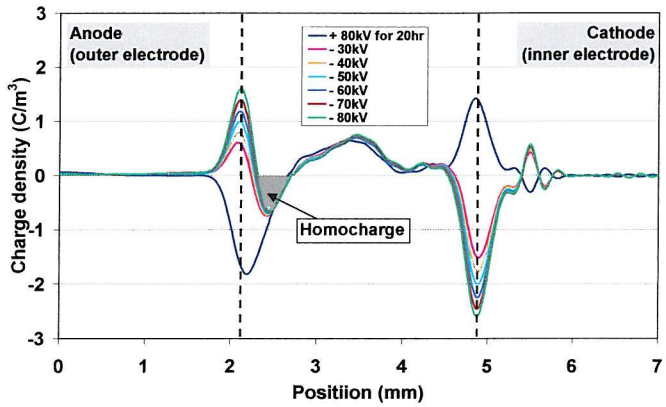

Figure 9.8 Space charge response to the reversed voltage amplitude

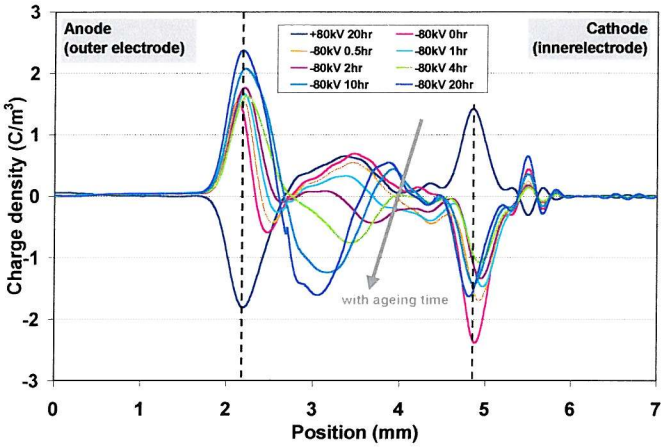

Figure 9.9 Space charge evolution under the reversed voltage

As in the situation under positive voltage, a homocharge near the outer electrode (anode) was developed again under the reversed voltage. This can be distinguished from the unsymmetrical shape of the induced charge at the outer electrode or from the result after the applied voltage is removed, as shown in figure 9.10.

Unlike the 11kV XLPE cable with the "mirror imagine" space charge distribution under two opposite voltage polarities, the results in this sample after the same hours of ageing at the positive and the negative voltages are quite different, as the profiles shown in figure 9.10.

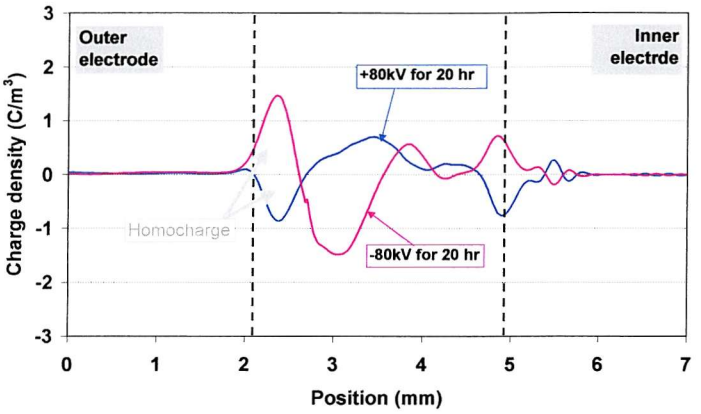

Figure 9.10 Comparison between the charge aged for 20 hours and that under reversed voltage for another 20 hours

9.4 Discussion

9.4.1 Space charge accumulation under opposite voltages

The above two cable samples were subjected to an electric stress at one polarity until space charge equilibrium was reached, then the polarity was changed. In these two stressing tests, some noticeable features of space charge accumulation have been identified both in the process of voltage reversing and in the following ageing time.

Firstly, it seems that for both samples under the reversed voltage, a shorter time is needed for the space charge to reach the same charge distribution as required under the previous polarity. It can also be said that space charge under reversed voltage possesses higher accumulation speed. For a better description of this fact, the total space charge within a unit length of cable was obtained by integrating the space charge density distribution across the insulation thickness. Its variation against ageing time is plotted in figures 9.11 and 9.12 respectively for the two cable samples. The total charge here stands for the sum of the absolute values of the positive and negative charges within the volume of the insulation.

As seen in figure 9.11 (a) and 9.12 (a), the space charges in these two samples accumulate a constant speed when the voltage is first applied. They then accumulate more slowly until they reach equilibrium after about 70 minutes and 12 hours respectively in the two cables.

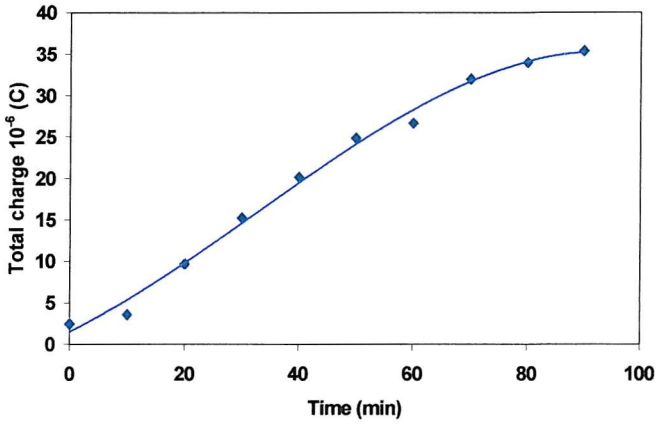

(a) At initial polarity (positive)

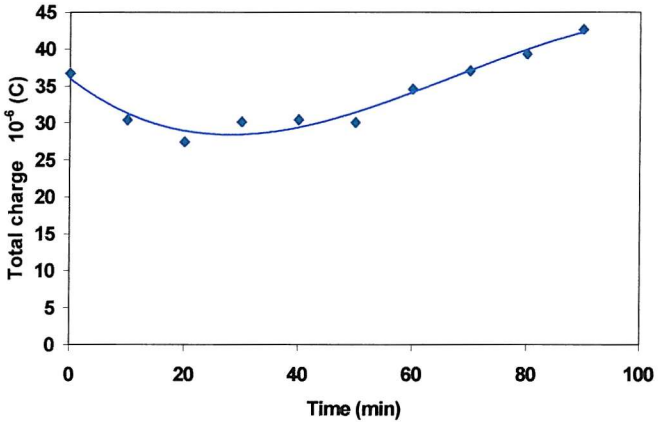

(b) At reversed polarity (negative)

Figure 9.11 Space charge accumulations at initial and reversed polarities in XLPE cable with 3.6mm insulation

As noticed in the previous section, the space charge distributed under the first voltage is fairly stable at the moment of the voltage reversal and under voltage amplitude ramping. In other words, the response of the space charge to the voltage polarity reversal is very sluggish. As soon as the voltage is reversed, the total charge across the cable insulation starts to reduce slightly in the cable with 3.6mm insulation, but more quickly in the cable with 2.8mm insulation (see the curves in figures 9.11 (b) and 9.12 (b)). However, the reduction of the total charge in these two cables stops at 20 minutes and 2 hours respectively. The total charge does not appear to reduce to zero due to the neutralisation of the original charges by the newly formed ones. Instead, before the total charge arrives at the zero, it starts to build up again in the ageing time.

Under the reversed voltage, more space charge accumulates than that before the polarity reversal in the same period of ageing.

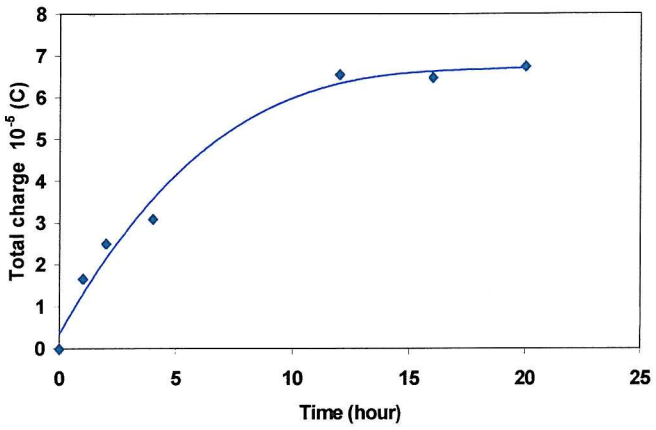

(a) At initial polarity (positive)

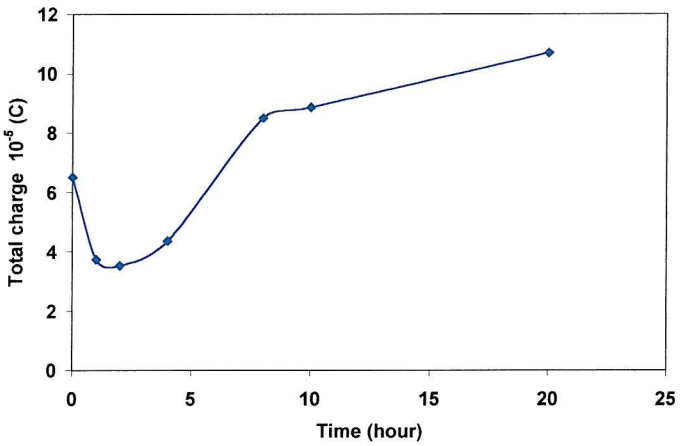

(b) At reversed polarity (negative)

Figure 9.12 Space charge accumulations at initial and reversed polarities in XLPE cable with 2.8mm insulation

The second feature of the space charge variation under the reversed voltage is seen in figures 9.4 and 9.9, in which some packet charges (negative) are initiated from the central insulation and then migrate towards the outer electrode as the result of the neutralisation with the previously formed positive charge. The reason for the opposite polarity of the charge initiated from this location may be the enhancement of the electric stress at this region due to the applied voltage reversed. The detailed electric field stress distribution will be discussed in the following section. On the other hand this result may imply that under reversed stress polarity, space charge accumulation may not start in the same place as the space charge under the previous voltage

application, but from another location having a higher electric stress. Thus the newly accumulated space charge will not be able to cancel out the old charge completely. In particular, in these two cables whose insulation has relatively low charge migration properties, the space charge distribution is fairly stable, because only adjacent charges with opposite polarities can be neutralised. In the meanwhile, new charges will be formed at locations where they cannot be cancelled by old charges. This may be the reason for the total charge not approaching zero when the applied voltage was reversed.

9.4.2 Electric stress distribution during and after the voltage reverse

As introduced at the beginning of the chapter, the electric stress distribution during and after the reversal of the applied voltage is one of the main concerns of space charge research in polymer insulated cables. Under the influence of the modified electric stress, the space charge initiation and development may be different under the reversed voltage, as discussed previously. To understand the relation between the electric field variation and the space charge re-distribution during the voltage polarity reversal, the electric field profiles were calculated on the basis of the space charge distribution, and the results are presented in figure 9.13 and figure 9.14.

Consider the cable with 3.6mm insulation after 90 minutes application of +80kV at the central conductor. A considerable heterocharge has accumulated in the vicinities of the outer and inner interfaces. As a result, the interfacial stresses at the outer and inner interface have been increased from the applied values of 20.5kV/mm and 25.3kV/mm to 30.3kV/mm and 27.3kV/mm respectively. The electric stress in the central part of the insulation is reduced to a certain extent.

Immediately after the applied voltage is reversed and stepped to the desired voltage of –80kV, the originally accumulated charge retains almost the same distribution due to its relatively stable characteristic. The electric stress in the central part of the insulation is significantly enhanced because of the contribution of the electric stress from the space charge. The maximum stress in this region is about -30kV/mm, which is much higher than the applied value of -25.3kV/mm at the inner interface in the absence of the space charge. This is the region where the negative charge initiates and accumulates in the subsequent ageing time after the negative voltage is applied. On the other hand, the stresses at the inner and the outer interfaces reduce to about 20kV/mm and 10kV/mm

respectively because the electric stress contributed by the previous heterocharge, which has now become a homocharge, counteracts the applied stress.

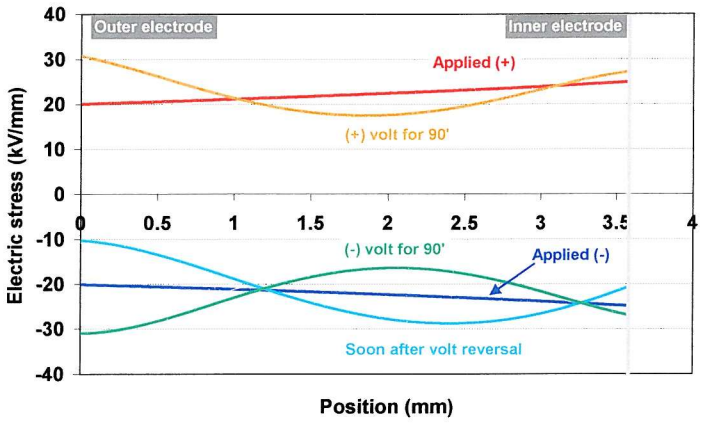

Figure 9.13 Electric stress distribution of 11kV cable before and after external applied voltage reverse

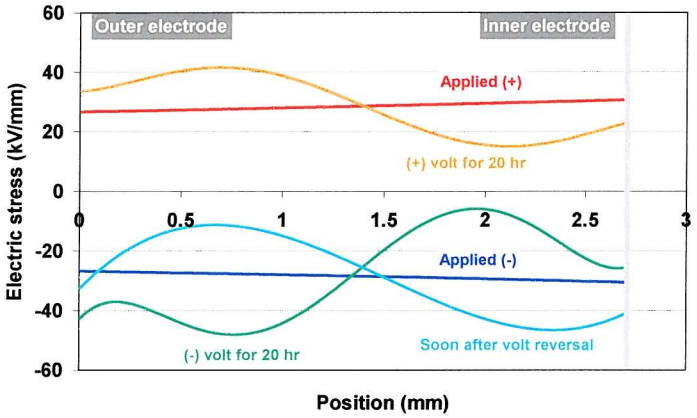

Figure 9.14 Electric stress distribution of 2.8mm insulation cable before and after external applied voltage reverse

In the following ageing period after the voltage reversal, the space charge within the insulation is progressively re-distributed. Since the final distribution of space charge under the negative voltage is very similar to that before the voltage reversal (except for the opposite signs) the modified electric stress profile also has a similar shape as that obtained under positive voltage ageing. The stress at the interface area is strengthened, but is reduced in the central insulation.

The situation in the cable with 2.8mm insulation is a bit different from the above example. The electric stress variation caused by the voltage polarity reversal is illustrated in figure 9.14. Because of the large packet charge (positive) accumulated in the centre of the insulation under the previous voltage polarity, the electric stress near

the anode electrode is obviously reduced. In the region near the cathode, the large lump of positive charge has resulted in the enhancement of stress close to the outer electrode and the highest stress is over 40kV/mm. As the applied voltage polarity is switched from the positive to the negative and the amplitude is ramped up to –80kV, the previously accumulated charge remains unchanged from that of figure 9.8. Therefore, the electric stress attributed to the space charge has almost the same profile at negative and positive voltages. However, as the applied voltage is switched to negative at the central conductor, the stress near the inner interface is enhanced to about 47kV/mm, which is much higher than the applied stress at the inner electrode/insulation interface in the absence of any space charge. This lump of positive charge has caused a reduction of stress in the area between it and the outer electrode.

After 20-hour stressing with negative voltage at the central conductor, a large negative packet charge accumulates in the volume of the material near the outer electrode. As a result of this space charge distribution, the electric stress is excessively strengthened in this region. From figure 9.14, it is noticed that the highest stress could be as high as 50kV/mm, which is much higher than the designed value at the inner interface. In contrast, the stress in the region between this packet charge and the inner electrode is considerably reduced.

9.5 Conclusions

Space charge accumulation in the process of the reversal of the external voltage polarity and then under the reversed voltage has been experimentally studied in two XLPE ac power cables. In order to understand the impact of the space charge on the cable insulation as the voltage polarity in a dc system is switched, the electric stress distributions have been calculated from space charge profiles measured during the process of polarity reversal and in the ageing period following the voltage reversal. The following conclusions can be obtained from these results.

Firstly, as soon as the space charge is accumulated in the cable insulation, its response to the externally applied voltage change may be slothful. This is regarded as the dangerous moment for dc power cable insulation as the pole polarity is reversed, as the electric stress is likely to have a complex distribution due to the formerly accumulated space charge. In the experiment, the voltage reversing process took about 90 seconds, which is much longer than the time by a real dc transmission system. Even

so, the change of the space charge lags greatly behind the voltage reversal. This slow response of the space charge is well illustrated in the space charge profiles obtained during the voltage inverting and ramping process, as is shown in figures 9.3 and 9.8.

Secondly, as a consequence of the slow response of the space charge to the external voltage change, any previously formed charge may make the electric stress distribution through the cable insulation very complicated. Some localised stress will be much higher than the designed values. Specifically in the first XLPE cable sample, the former heterocharge appeared as a homocharge at the moment of the polarity change. The electric stress in the central region of the material was strengthened to about 30kV/mm, which was already much higher than the designed value at the inner interface. The worst situation occurred in another cable sample in which a large lump positive charge had previously been formed. When the applied voltage at the central conductor was reversed from the positive to the negative, the electric stress close to the inner interface of the insulation and the semiconducting layer reached about 50kV/mm, which was much higher than the applied stress under the space charge free conditions. Owing to the homocharge (negative) near the outer electrode before the voltage reversal, the large positive packet did not cause any significant change in electric stress at the outer interface when the polarity was reversed. However, the stress between the homocharge and the lump positive charge was reduced.

In the same process on the second sample, a larger negative packet charge gradually built up in the volume of the insulating material close to the outer electrode, and resulted in the enhancement of the electric stress around this region to about 50kV/mm.

Thirdly, space charge development under two opposite voltage polarities may have different rates, and is actually governed by the new electric stress distribution when the voltage polarity is reversed. As the electric stress distribution is changed by the reversed voltage, space charge may initiate and accumulate in the region where there is a higher electric stress. Therefore, the formerly formed charge will not be completely neutralised by the newly developed charges. This phenomenon is clearly displayed in figure 9.9, in which a packet charge is initiated in the central part of the material and eventually migrates towards the outer electrode as the charge density increases. At the same time, the former positive charge is gradually cancelled out by this new bulk charge. Before the original space charge is neutralised, a considerable amount of new charge has already been developed elsewhere.

Finally, over the same stressing time under the reversed polarity, similar or even bigger space charge densities are obtained in the two cables. Considering that part of the newly formed charge neutralizes the previous charge, it can be concluded that space charges accumulate at a greater rate after the polarity reversal than they do when the previous voltage is switched on from zero.

Chapter 10

Investigation of Two Problems Encountered in Space Charge Measurement in Cable Samples

10.1 Introduction

The space charge measurements reported in foregoing chapters show that the peak of the induced surface charge at the inner electrode shifts towards the outer electrode in the first few hours of ageing and this sometimes continues over the whole ageing term. This peak shift shows little regularity. The same phenomenon, however, has also been found by other researchers [14, 51] but with no further explanation. At the beginning of this research, it was simply attributed to electrically induced mechanical strain in this type of highly elastic material, e.g. XLPE, leading to the insulating material contracting. In particular, it is believed that the induced mechanical stress may be greater when space charges appear. Subsequently, the mechanical stress due to the applied electric field and the space charge formation results in compression of the polymer insulation. Since Stark and Garton discussed the electromechanical breakdown [140] more than 40 years ago, the existence of this phenomena has been be proved by growing evidence and the related theory is thoroughly discussed [141, 142]. However, according to the value suggested by Lewis *et al* [142], the electrically induced mechanical stress could contribute to mechanical fatigue and ageing only when the electric field stress exceeds 100kV/mm. This implies that in our research, mechanical deformation caused by the electric stress cannot be big enough to be observed.

In the initial trial stages of the space charge measurements in cables, a short length of semiconducting screen was left as the outer electrode. This was in direct contact with the ground aluminium electrode. With this configuration, a pair of peaks always exists in front of the induced surface charge at the outer electrode. This might influence space charge measurements if it is too close to the signal of interested.

The true reasons for above problems were investigated experimentally and some proper measures were taken in the subsequent research to avoid them.

10.2 The reason for the shift of the inner induced charge peak

An XLPE cable sample with 2.8mm thick insulation was firmly held in the PEA test system and the tightness of the clamp holding the cable was carefully controlled by a "Torqueleader^{TM}", which could supply a controlled tightening torque.

The waveform representing the space charge distribution across the cable insulation was then obtained under three conditions. First, no dc voltage was applied to the sample over the entire testing period except at the time of taking a measurement. The cable insulation only bore mechanical stress from the clamping element in the test. Space charge distribution (actually only the induced charge at the two interfaces) was measured several times by turning on the dc voltage (30kV) and pulsed voltage for a short period of time. The distance between the two induced peaks, i.e. the thickness of the insulation was recorded each time. In this way, neither the electric stress nor the space charge can influence the position of the induced charge peaks, since the application times of dc voltage was too short to generate space charges in the insulation. In the next two conditions, 30kV and 80kV of dc voltage were applied across the cable insulation continuously over the test period to study the influence of the electric stress on the distance between the two peaks. The pulsed voltage was only switched on when measurements were taken. In the same way, the thickness of the insulation (or the distance between the two induced surface charges) was recorded against ageing time.

Due to the big size of the PEA system for cable samples and the use of the high voltage, the measuring temperature was not controlled in the above experiment. However, the ambient temperature in each round of test was recorded to check the effect of any temperature change. The whole test procedure is schematically illustrated in figure 10.1.

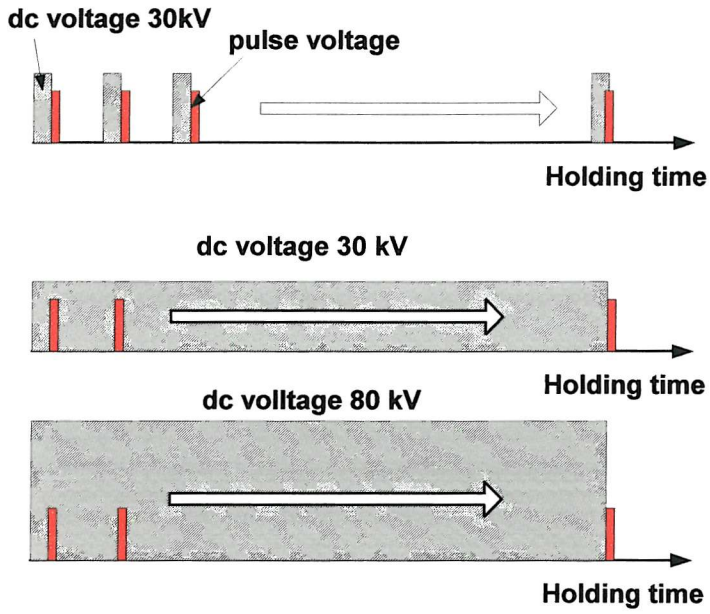

Figure 10.1 Schematic diagram of the voltage application

The variation of the distance between the two induced peaks against cable holding time under each test condition is presented in figure 10.2. With no applied electric stress, the shift of the induced charge peak at the inner electrode is still represented by change of the distance between the two induced surface charge peaks. This variation takes about 20 hours to get stable. In the tests which followed with the application of 30kV and 80kV dc voltage applied separately for certain periods of time, no significant change of the distance between two induced peaks was observed while the heterocharge was gradually building up except for a small random change with test time.

These results clearly show that the position of the right hand peak is not directly related to the external voltage. When the dc voltage was applied, the distance between two peaks showed some deviation around the value of 2.82mm. This was obtained after the cable had been held for a certain period of time without the electric stress. However the ambient temperature was observed to change within the range from 21°C to 24°C throughout the experiment time. To verify the effect of temperature, the variation of the insulation thickness is plotted in figure 10.3 against the temperature. Surprisingly, the apparent thickness of the cable insulation measured from the space charge profile is closely connected with the ambient temperature.

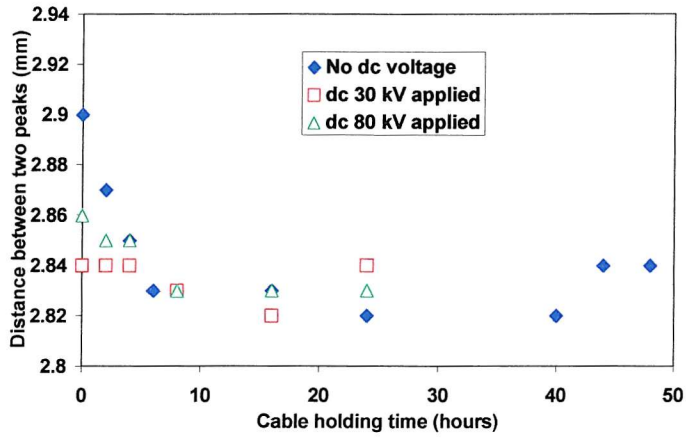

Figure 10.2 Distance between the induced surface charge peaks changing with the test time under three conditions

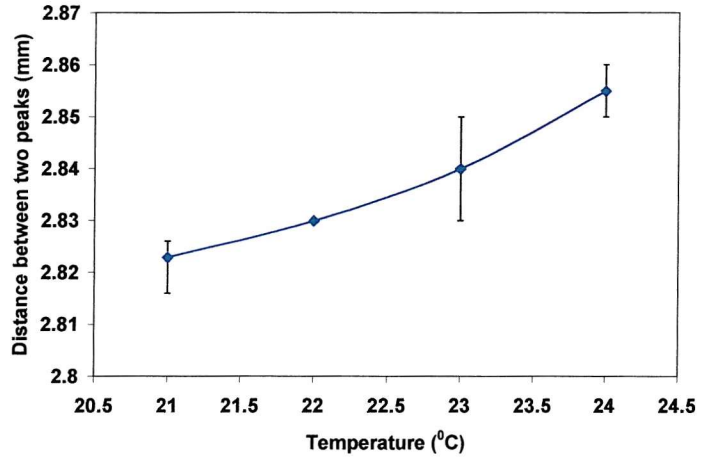

Figure 10.3 Distance between the induced surface charge peaks as a function of the ambient temperature

Based on the above experimental results, the reasons for the shift of the induced surface charge peak at the inner electrode can be discussed and summarised as follows.

First, the applied electric stress across the cable insulation in the experiment was far lower than that suggested by researchers [141, 142] at which mechanical strain may be induced. If in our situation there was some electrically induced mechanical stress in the insulating material, its magnitude might be too small to be acknowledged. This has been proved in the test on the sample which was stressed by the external voltage and no systematic variation of the insulation thickness was observed, in spite of an appreciable space charge having accumulated in the bulk insulation.

Second, the most significant reduction of the distance between the two peaks happened in the first few hours after the sample was loaded onto the PEA electrode

system. From figure 10.2, it is seen that the apparent thickness of the sample insulation varied between 2.90mm and 2.83mm within the first 6-hour without any externally applied electric stress. Therefore, the shift of the induced charge peak at the inner electrode (i.e. the apparent reduction of the insulation thickness) can be attributed to the creep property of the polymeric material itself [143] instead of the electrically induced mechanical strain. A polymer having visco-elastic properties undergoes stress relaxation when it is hold in a stiff clamping apparatus. The strain stays constant and the stress decays slowly with time until it reaches its steady state. The creep property of a polymer can be described by the exponentially decaying function [143]

$$\kappa = \kappa_0 \exp(-t/\tau_0) \qquad (10.1)$$

where κ_0 is the initial stress when load is firstly applied, and τ_0 is the relaxation time. As the holding time increases, the inner stress in the cable insulation gradually becomes smaller and smaller due to the relaxation. After a certain period of time, when the completely relaxed or unstressed state is approached, the material will give a smaller apparent dimension. This pattern is consistent with the phenomena observed in the experiment over the first 24 hours during which the distance between two peaks or the insulation thickness reduced gradually.

Moreover, from figure 10.3 we can see that the distance between the two peaks is also directly dependent on the ambient temperature. Apart from the effect of creep and thermal expansion, the other factor which will influence the distance between the peaks is the effect of the temperature on the acoustic wave speed [144]. HolbØll [145] has reported a big variation of the inner electrode peak position in his research where a higher temperature was introduced in the sample.

10.3 The interference peak from the semiconducting screen

Throughout the work described in this thesis, a short length of the outer semiconducting screen around the cable was directly in contact with the ground electrode. With this configuration, a pair of peaks was always found to appear in front of the waveform of the induced surface charge at the outer interface between the semiconducting sheath and the insulation. This is shown in figure 10.4. The distance between them is just the thickness of the semiconducting sheath. It is confirmed that these peaks are launched from the outer surface of the semiconducting layer.

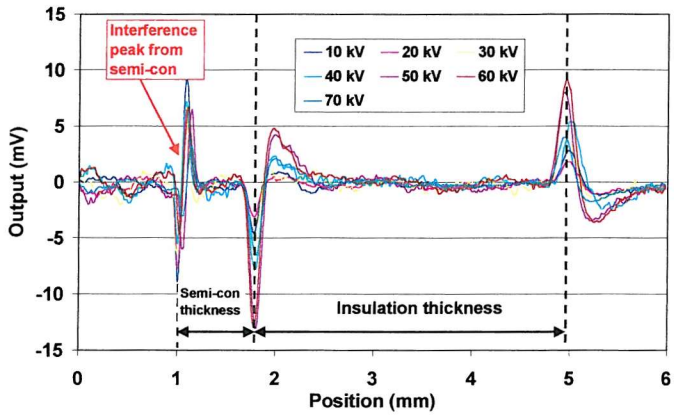

Figure 10.4 Interference peaks produced from the outer surface of the semiconducting sheath

It has been shown that the magnitude of these two peaks is directly proportional to the magnitude of the pulsed voltage but is almost independent of the applied dc voltage. As shown by the waveforms plotted in figure 10.4, the height of the interference peaks remain almost the same when the external applied dc voltage increases from 10kV to 70kV, while the height of the peaks of the induced surface charges at the inner and the outer electrode vary linearly with dc voltage. In order to verify the independence of the interference peaks on the pulsed voltage, the measurement obtained without the dc voltage is presented in figure 10.5. The same pair of peaks appears. This clearly indicates that these peaks are caused by the pulsed voltage at the outer surface of the cable's semiconducting sheath.

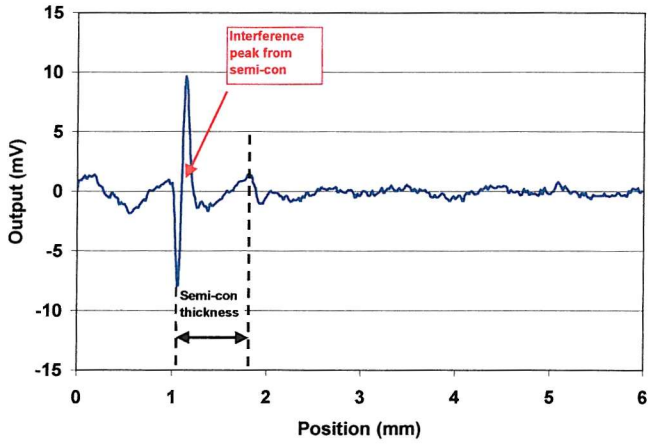

Figure 10.5 Interference peaks induced by the pulsed voltage at the outer surface of the semiconducting sheath

In practice, we are only interested in the signal from within the insulation's thickness, *e.g.* the signal in the region bounded by the two peaks of the induced charge at the two electrodes. If the semiconducting layer is thick enough, the peak resulting from the pulse voltage appears well in advance of the first peak due to the induced charge on the outer electrode. The ensuing voltage oscillation can be neglected in the processing of the data generated by the space charge distribution within the insulation. However, when the semiconducting layer is thin, the voltage oscillation from the interference peaks may still be present in the segment of interest in the whole waveform. It may then interfere with the measurement of surface charge or the bulk charge in the cable insulation.

The reason for the interference peaks caused by the outer semiconducting sheath is simply attributed to the stray capacitance between the ground electrode and the semiconducting screen, as shown in figure 10.6. It is believed that the pulsed voltage produces a surface charge on the outer surface of the semiconducting sheath due to its high resistivity at high frequency. This generates the initial voltage oscillation in the output waveform as shown in figure 10.5. The time difference between the signal due to the stray capacitance and the dc voltage induced charge on the semiconductor/insulation is just equal to the time for the acoustic wave to propagate through the outer semiconducting layer.

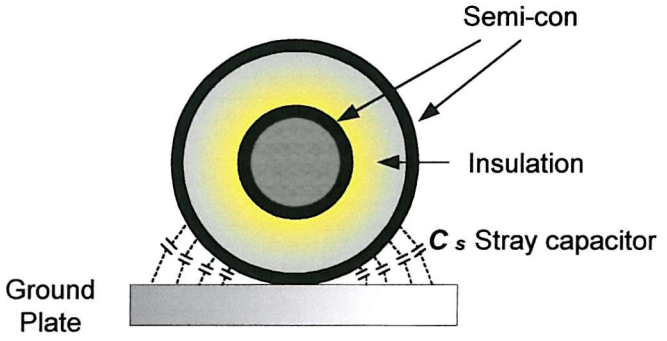

Figure 10.6 Stray capacitance between the outer sheath and the ground plate

To reduce the effect of this stray capacitance, the outer semiconducting layer was wrapped with 10μm thick aluminium foil. The improvement in the output waveform is seen in figure 10.7 (blue line). It is noticed that peaks produced by the pulse voltage at the outer surface of the semiconducting sheath is reduced tremendously. This method was therefore promptly adopted in all the subsequent space charge measurements.

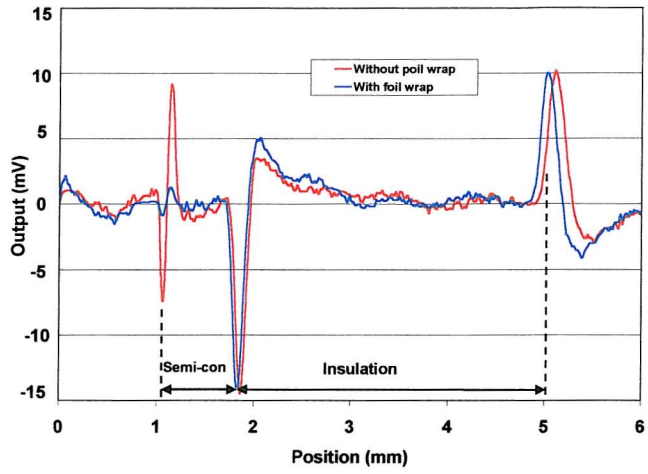

Figure 10.7 Improvement of output waveform by foil wrap

10.4 Summary

Two problems have been studied experimentally in this chapter: (a) the variable distance between the two peaks of the induced surface charges at the electrodes which seems to indicate a change in the cable insulation thickness, (b) the influence of the interference peaks caused by the pulse voltage at the outer surface of the semi-conducting sheath.

A common phenomenon in space charge measurements in polymer dielectrics (in particular in the thick sample such as the full sized power cables) is the shift of the peak due to the induced surface charge as the test time passes. If this was due to a change of the cable insulation thickness, it could be attributed to the creep property of the polymeric material under a given strain. In the PEA system with a flat ground electrode, the stress borne by the cable insulation at the contacting point is relatively higher than that in a conventional design, and the variation in the distance between the induced peaks from the two electrodes is more significant. Another reason explaining this problem may be the temperature change which results in either the expansion or contraction of the material or a change of the acoustic wave velocity through the insulation.

It should be noted that the low electric stress levels in the experiments were insufficient to generate any mechanical stress. As a counter-argument to this, the fact of the mechanical stress induced by the electric field and the space charge in the material is not observed in the research because of the low electric stress.

Under the very fast voltage pulse, the high resistivity of the semiconducting material may introduce a surface charge on the outer surface of the semiconducting screen. This surface charge may cause some interference to the space charge measurement in the cable insulation if the semiconducting layer is too thin. The signal from this surface charge can be very significantly reduced by wrapping the outer sheath with a thin aluminium foil.

Chapter 11

Conclusions and Suggested Future Work

11.1 Conclusions

This thesis presents the technique and practical application of the PEA method of space charge measurement in polymer insulated power cables under dc voltage.

A newly revised PEA system has been introduced which adopts a flat electrode and greatly facilitates space charge measurements in coaxial geometry cable samples. There are obvious disadvantages inherent in the conventional PEA system, such as the difficulty of maintaining good acoustic coupling between the cable sample and the ground electrode, and the inconvenience of testing cables with different sizes. These have been successfully overcome by the new design of the electrode system.

The acoustic wave propagation in this new PEA system, particularly the transmission at certain interfaces between different media has been analysed. The cable sample is clamped to a flat electrode with only a small area (a narrow line-contact) between the outer screen and the aluminium ground electrode. The analysis concludes that the only acoustic wave which is finally sensed by the transducer is that which propagates in a direction normal to the ground electrode having passed (partially) through the different media and across the interfaces between them. The portion of acoustic wave which travels to the electrode in an oblique direction is almost totally reflected back by the air gap between the cable outer screen and the ground electrode. This part of the acoustic pressure, propagating in a longer route than that in the normal direction, will not degrade the system's spatial resolution. The output from the piezo-electric transducer depends on its thickness but not on its area, so even if the outer sheath of the cable is in nearly-line contact with the ground electrode and the

effective transducer area is relatively small, the whole piezo-electric system will still have a satisfactory detecting sensitivity. The above analysis shows that the flat electrode and transducer arrangement is capable of giving the same charge density and position resolution as that of the curved electrode system. This conclusion has been confirmed by comparing the space charge measurements obtained in the two PEA systems.

The fundamental techniques of space charge measurement, including the charge density calibration and the deconvolution of the original signal have been fully described. Despite the careful selection of wide band frequency response and a high input impedance amplifier, the deconvolution of the original signal is still necessary because of the resonant response of the transducer sandwiched between the Al electrode and the acoustic wave absorber.

Calibration is an essential part of the precise measurement of space charge distributions in cable sample, and the technique was carefully considered in this project. The charge density calibration is based on the induced charge at the interface of the insulation and the electrode under the known externally applied dc electric stress. This must be low in amplitude and short in duration so that no bulk charge is developed in the volume of the dielectric material. This technique is easily implemented in a plaque sample, in which the external electric stress is of uniform distribution throughout the dielectric. However, the charge density calibration in a coaxial cable geometry is much more complex in comparison with the plaque sample, as the dc electric stress distribution in the cable insulation is controlled by the dielectric material conductivity which is a complex function of the temperature and the electric stress. Even if there is no temperature gradient across the cable insulation, the original variation of the dc stress makes the stress distribution unpredictable, so the actual determination of the interfacial stress used for the calibration is difficult. Therefore, the electric stress derived from the ac voltage in cable geometries used by all the previous researchers in their calibration process is of dubious accuracy in the dc case. Two methods among the very limited advances in this area have been briefly reviewed in this thesis and one of them is adopted not only for improving measured results, but most importantly to draw attention to the calibration technique in space charge measurements in cable geometries.

The coaxial geometry of the cable sample causes a divergent distribution of the pulsed electric stress and a divergent propagation of the acoustic pressure from the

inside to the outside of the insulation. The output of the system is therefore not merely dependent on the space charge distribution, but also on the position from which the acoustic signal originates. Furthermore, the polymer insulating material, such as PE or XLPE, in the power cable cannot be regarded as an ideal medium for acoustic pressure wave propagation. Its visco-elastic property will cause some attenuation and dispersion of the acoustic wave as it travels through it. This loss of the acoustic wave amplitude and the scattering of the acoustic pulse may give a poor space charge measurement, both of density and position resolution. In particular, when the PEA technique is applied to thick walled cable insulations, this effect may become more significant. To achieve a precise space charge measurement, a compensation algorithm has been developed by taking into account the above geometric and acoustic wave propagation factors in the data processing. This applies corrections to the original signal.

A comprehensive program including the functions of data acquisition, deconvolution, charge density calibration and geometry and propagation compensation was developed under the LabView^{TM} environment. This makes the quantitative measurement of space profiles in polymer cables more effective and more accurate.

The method of determining the electric stress distribution across the cable insulation in the presence of space charges has been systematically introduced. The method of integrating the whole space charge (inclusive of the induced surface charges at interfaces) throughout the cable insulation would give correct results for the electric stress magnitude, but the limited resolution of the space charge profile gives less accuracy in the electric stress distribution at the interfaces. An improved method was therefore introduced by only integrating the bulk charge within the insulating material in the absence of an induced surface charge from the externally applied stress. The interface stress was estimated from the amplitudes of the induced surface charges under the calibration and test voltages respectively. Extrapolation was used to pad the points between the integrated curve and the boundary values using a higher order polynomial.

Space charge measurements in a group of cable samples have shown a remarkable difference between the different modified XLPE materials and those with different residue content. Comparison of the results from fresh and degassed samples shows that the degassing treatment significantly affects the space charge activity in XLPE insulation. Upon removing the volatile residue through the degassing treatment, the space charge density was tremendously reduced and the charge distribution was greatly

changed. This result has confirmed again that the crosslinking by-products and the additive residues play an important role in the space charge accumulation.

The space charge activity in the undegassed prototype cable sample 1491 was so vigorous that an appreciable space charge was accumulated during the voltage ramp process. Cable 1495 showed a strong charging ability. A broad space charge distribution was developed after 24 hours of ageing at 80kV with the charge density reaching as high as $0.37C/m^3$. Except for the formation of a traceable positive packet charge in the centre of the insulating material in cables 1491 and 1495, the differences between the degassed samples, however, are not very significant.

Due to the presence of the space charge in the undegassed cable, the geometry governed electric stress was greatly distorted. For instance, at the outer sheath in undegassed cable 1491 and 1495 the electric stress had been doubled due to the heterocharge near the electrode.

In view of the above results, it seems that the modified materials used in cables 1494 possesses the favourable property for space charge suppression. From the viewpoint of dc power cable insulation design, the material used in cable 1495 has the weakness of stable charge distribution besides having the high charging ability even after degassing.

A further study of the effect of material modification was carried out on a set of thick planar samples. The effect of the crosslinking by-products on the space charge development was clearly shown from the measurements. In the two fresh materials P28 and P29, the modification effectively reduced the space charge accumulation but it did not thoroughly prevent it. When the volatile residue in the sample was partially removed by degassing, the charge density was correspondingly decreased. However, in completely degassed material some limited charge generation may still occur.

The polarity of the space charge is also directly related to the residues in the material. In all the samples with residues, no matter how high the residue concentration, the heterocharge was developed, while in at least two completely degassed samples (such as P3 and P30, and LDPE without peroxide), small amounts homocharge accumulation were found. In the latter situation, charge injection from the electrode may dominate the charge development.

The results from both the cable sample and the plaque sample show that the space charge building up speed and decay speed correspond well. That is to say that the faster the space charge develops, the faster it decays, or vice versa. It is also noticed that

homocharge in degassed materials develops with greater difficulty than the heterocharge in the same material in the undegassed condition. The former initiates at the higher electric stress and requires longer time, and is, of course, more stable as long as it is formed.

Space charge distribution and evolution in cable samples when the voltage polarity is reversed showed that the change of the space charge from its stationary distribution logs greatly behind the voltage change. During the voltage reversing and ramping process, the initially formed charge remained the same both in density and location. A more complex electric stress distribution might therefore, be found across the cable insulation. Some localised stress could get unexpectedly higher than the initially designed value.

Finally, as a clarification experiment, the reason for the shift of the peak of the induced sheet charge at the inner electrode has been investigated. It is concluded that the creep property of the polymeric material results in stress relaxation after a certain period of time when the sample is held. The material in the free state has smaller dimensions in comparison with its stressed condition. Moreover, a temperature change causes material expansion and contraction and a slight change of the acoustic wave velocity in the material. This is another reason for the apparent change of the cable insulation thickness during the test. The electrically induced mechanical stress may be too small to have any effect in these experiments because of the relatively low electric stress.

12.2 Suggested future work

In this thesis, the space charge distributions of cable samples employing different modified XLPEs under ambient temperature have been discussed. However, the space charge behaviour of these materials at high temperatures was not examined. The temperature gradients which exist in the real dc cables in service will make the space charge distribution more complex. Studies of the space charge evolution within the cable insulation in this situation will give a direct insight into the material characteristics of polymer insulated dc power cables. The actual electric stress distribution which is dependent on geometry, space charge distribution and temperature (conductivity) is supposed to be determined.

It is noticed that the space charge accumulation in the XLPE was dominated by the charge injection at the dielectric and electrode interface in the degassed sample. Actually this effect must occur at the same time as impurity ionisation (bulk effect). If we consider the ionisation of the residue as a consuming process, after a long-term ageing the charge injection should finally overwhelm the bulk effect and gives a homocharge distribution for the material with the residue. To verify the above hypothesis, the space charge evolution over a long-term ageing should be investigated on these modified materials both with and without the residue.

Further investigations are required into the formation and the slow build-up and decay rates of homocharge in degassed samples when the external voltage polarity is reversed. Long-term ageing tests are required.

References

1 B. M. Weedy, *Electric power system*, 3rd edition, John Wiley & Sons Ltd, Great Britain, 1987

2 R. Arrighi, " From impregnated paper to polymeric insulating materials in power cables", IEEE Trans. on EI. Vol. EI-21, pp.7-18, 1986

3 P. K. Watson, "The Transport and Trapping of Electrons in Polymers", IEEE, Trans. on DEI, Vol. 2, pp.915-924, 1995

4 T. Takada, "Space Charge Formation in Dielectrics", IEEE Trans. on EI., Vol. 21, pp.873-879, 1986

5 T. Takada, "Acoustic and Optical Methods for Measuring Electric Charge Distribution in Dielectrics", IEEE Trans. on DEI, Vol. 6, pp.519-547, 1999

6 T. Takada, Y. Tanaka, N. Adachi and X. Qin, "Comparison between the PEA Method and the PWP Method for Space Charge Measurement in Solid Dielectrics", IEEE, Trans. on DEI, Vol. 5, No. 6, pp.944-951, 1998

7 P. Laurence, G. Dreyfus and J. Lewiner, "New principle for the determination of potential distribution in dielectrics", Phys. Rev. Lett., Vol. 38, pp-46-49, 1977

8 C. Alquie, G. Dreyfus and J. Lewiner, "Stress wave probing of electric field distribution in dielectrics", Phys. Rev. Lett., Vol. 47, pp.1483-1487, 1981

9 Y. Li and T. Takada, "Experimental observation of charge transport and injection in XLPE at polarity reversal", J. Phys. D: Appl. Phys. Vol. 25, pp704-716, 1992

10 T. Doi, Y. Tanaka and T. Takada, "Measurement of space charge distribution in acetophenone coated low-density polyethylene", IEEE Annual Report of CEIDP, pp.32-35, 1997

11 T. Takada, N. Hozumi, H. Suzuki and T. Okamoto, "Factor of space charge generation in XLPE under dc electric filed of 20kV/mm", Proc. of ICPADM-97, pp.137-141, Seoul, Korea, 1997

12 K. Fukunaga and T. Maeno, "Measurement of the internal space charge distribution of an anti-electrostatic discharge polymer", IEEE Trans. on DEI, Vol. 2, pp.36-39, 1995

13 Y. Li, T. Takada, H. Miyata and T. Niwa, "Observation of charge behaviour in multiply low density polyethylene", J. Appl. Phys., Vol. 74, pp.2725-2730, 1993

14 K. Fukunaga, H. Miyata, T. Takahaashi, S. Yoshida and T. Niwa, "Measurement of Space Charge Distribution in Cable Insulation Using the Pulsed Electroacoustic Method", Proc. 3rd Int. Conf. on Polymer Insulated Power Cables, Versailles, France, pp.520-525, 1991

15 Y. Tanaka, Y. Li, T. Takada and M. Ikeda, "Space charge distribution in low-density of polyethylene with charge-injection suppression layers", J. Phys. D: Appl. Phys, Vol. 28, pp.1232-1238, 1995

16 K. S. Suh, J. Y. Kim, H. S. Noh and C. R.Lee, "Interfacial charge in polyethylene/ethylene vinylacetate laminates", IEEE Trans. on DEI, Vol. 3, pp. 758-764, 1996

17 H. Kon, Y. Suzuoki, T. Mizutani, M. Ieda and N. Yoshifuji, "Packet-like space charge and conduction current in polyethylene cable insulation", IEEE Trans. on DEI, Vol. 3, pp. 380-385, 1996

18 K. S. Suh, J. H. Koo, S. H. Lee, J. K. Park and T. Takada, "Effects of sample preparation conditions and short chains on space charge formation in LDPE", IEEE Trans. on DEI, Vol. 3, pp. 153-160, 1996

19 A. Yokayama, H. Miyata and T. Takahashi, "Effect of minute amount of impurities on conductivity and space charge formation in polyethylene", Trans. IEE Japan, Vol. 117-A, pp.754-760, 1997

20 S. Muramoto, K. Tanaka, M. Fukuma, M. Nagao and M. Kosaki, "Effect of acetophenone on electric breakdown and space charge formation in low-density polyethylene film", Trans. IEE Japan, Vol. 118-A, pp. 654-659, 1998

21 N. Hozumi, H. Suzuki, T. Okamoto, K. Watanabe and A. Watanabe, "Direct Observation of Time-dependent Space Charge Profiles in XLPE Cable under High Electric Fields", IEEE Trans. on DEI, Vol. 1, pp.1068-1076, 1994

22 R. Liu, T. Takada and N. Takasu, "Pulsed Electro-acoustic Methode for Measurement of Space Charge Distribution in Power Cables under both DC and AC Electric Fields", J. Phys. D: Appl. Phys. Vol. 26, pp.986-993, 1993

23 X. Wang, D.Tu, Y. Tanaka, T. Muronaka, T. Takada, C. Shinoda and T. Hashizumi, "Space Charge in XLPE Power Cable under dc Electrical Stress and Heat Treatment", IEEE Trans. on DEI, Vol. 2, pp.467-474, 1995

24 T. Takeda, N. Hozumi, H. Suzuki *et al*, "Space Charge Behavior in Full-size 250kV DC XLPE Cables", IEEE Trans. on PD, Vol. 13, pp.28-39, 1998

25 T. Maeno, T. Futami, H. Kushibe and T. Takada, "Measurement and Simulation of the Space Charge Distribution in Electron-beam Irradiated Polymers", J. Appl. Phys. 65, pp.1147-1151, 1989

26 C. Alquie and J. Lewiner, "The Measurement of Internal Fields in Insulation for High Voltage Cables", Jicable, B1 Direct Current Cables, Part 2, pp.81-90, 1987

27 R. Gerhardt-Multhaupt, "Analysis of Pressure Wave Method for Non-destructive Determination in Dielectrics", Physical Review B, Vol. 27, pp.2494-2503, Feb. 1983

28 R. Gerhardt-Multhaup, "Electrets: Dielectrics with Quasi-permanent Charge or Polarization", IEEE Trans. on EI, Vol. EI-22, pp.531-554, 1987

29 A. R. Blythe, *Electric properties of polymers*, Cambridge university press, UK, 1980

30 S. Wu, D. Xie, S. Chen and B. Yu, *Electrical insulating material science and engineering*, Xian Jiaotong University press, China, 1996 (in Chinese)

31 F. H. Kreuger, *Industrial high voltage*, Volume 3, Delft university press, Netherlands, 1991

32 K. S. Suh, C. R. Lee, J. S. Noh, J. Tanaka and D. H. Damon, "Electrical Conduction in Polyethylene with Semi-conductive Electrodes", IEEE, Trans. DEI., Vol. 1, pp.224-230, 1994

33 D. McAllister, *Electric cables handbook*, Granada, 1983

34 K. S. Suh, S. J. Hwang, J. S. Noh and T. Takada, "Effect of Constituents of XLPE on the Formation of Space Charge", IEEE Trans. on DEI., Vol. 1, pp1077-1083, 1994

35 K. S. Suh, J. H. Koo, S. H. Lee, J. K. Park and T. Takada "Origin of Heterocharge in Polyethylene", 4th ICPADM, Brisbane, Australia, 1994

36 C. C. Ku and R. Liepins, *Electrical Properties of Polymers, - Chemical Principles*, Hanser Publisher, Munich, 1985

37 M. Ieda, "Electrical Conduction and Carrier Traps in Polymeric Materials", IEEE Trans. EI., Vol. EI-19, pp.162-178,1984

38 T. Takada, "Space Charge Formation in Dielectrics", IEEE Trans. on EI., Vol. EI-21, pp.873-877, 1986

39 M. Ieda, "Carrier injection, space charge and electrical breakdown in insulating polymers", IEEE Trans. on EI., Vol. EI-22, pp.261-267, 1987

40 K. Suh, J. Tanaka and D. Damon, "What is TSC", IEEE Electrical Insulation Magazine, Vol. 8, No. 6, pp.13-20, 1992

41 B. Sanden, *XLPE Cable Insulation Subjected to HVDC Stress: - Space Charge, Conduction and Breakdown Strength*, PhD Thesis of Norwegian University of Science and Technology, 1996

42 L. A. Dissado, J. C. Fothergill, *Electrical Degradation and Breakdown in Polymers*, Peter Perrginus Ltd. On behalf of the Institution of Electrical Engineers, 1992

43 A. Garton, J. H. Groeger and J. L. Henry, "Ionic impurities in cross-linked polyethylene cable insulation", IEEE Trans. on EI, Vol. 25, pp.427-434, 1990

44 Y. Miyashita and H. Kato, "Cross-linking reaction of LDPE and the behaviour of decomposition products from cross-linking agents", Proc. of 21st Symposium on Electrical Insulating Materials, pp.259-262, 1988

45 D. Marsacq, P. Hourouebie, L. Olmmedo, and H. Janah, " Effect of physical and chemical defects of polyethylene on space charge behaviour", IEEE Annual Report- Conf. on Electrical Insulation and Dielectric Phenomena, 1995

46 P. Hourouebie, D. Marsacq, B. Vallayer and L. Olmmedo, "Trapping and Detrapping of Electrical Charges in Polymers", IEEE Annual Report- Conf. on Electrical Insulation and Dielectric Phenomena, 1996

47 R. Nath and M. M. Perlman, "Effect of crystallinity on charge storage in polypropylene and polyethylene", IEEE Trans. on EI, Vol. 24-EI, pp. 409-412, 1989

48 G.A. Carthwrigth, A.E. Davies, S. G. Swingler and A.S. Vaughan, "Effect of an antioxidant on morphology and space charge characterisation of low-density polyethylene", IEE Proc. Sci. Meas. Tech., pp. 26-34, 1996

49 G. Blaise and W. J. Sarjeant, "Space Charge in Dielectrics, Energy Storage and Transfer Dynamics From Atomistic to Macroscopic scale", IEEE Trans. on DEI, Vol. 5, pp.779-808, 1998

50 C. Lavergne, C. Lacabanne, "A Review of Thermo-stimulated Current", IEEE Electrical Insulation Magazine, Vol. 9, No. 2, pp. 5-11, 1993

51 Y. Suzuoki, K. Yasuda, T. Mizutani and M. Ieda, " The Influence of Oxidation on Thermally Stimulated Current from Trapped Carriers in High Density Polyethylene", J. Phys. D: Appl. Phys., Vol.10, pp.1985-1990, 1977

52 N. Hozumi, T. Takeda, H. Suzuki and T. Okamoto, "Space Charge Behaviour in XLPE Cable Insulation Under 0.2-1.2MV/cm dc Field", IEEE, Trans. DEI, Vol.5, pp.83-90, 1998

53 N. Hozumi, Y. Muramoto and M. Nagao, "Estimation of Carrier Mobility Using Space Charge Measurement Technique", CEIDP, 1999

54 P. Eyerer, "Charge Storage and Transport During Crosslinking, Melting, Softening, and Permeation Process in Polymers", 5th Intern. Symp. On Electrets, Heidelberg, pp.482-487, 1985

55 T. Tanaka and A. Greenwood, *Advanced power cable technology*, Vol. 2, CRC Press Inc. Florida, 1983

56 Y. Zhang, J. Lewiner, C. Alquie and N. Hampton, "Evidence of strong correlation between space charge build up and breakdown in cable insulation", IEEE Trans. on DEI, Vol.3, pp.778-783, 1996

57 N. Hozumi, J. Tanaka, A. DeReggi and N. Nagurinivas, "Effect of dc Tests on Induced Space Charge2, Conf. Rec. on the 1990 IEEE Intern. Symp. on EI, Toronto, Canada, pp.332-334, 1990

58 T. Hibma, H. R. Zeller, P. Pfluger abd Th. Baumann, "A model for Space Charge Injection in Dielectrics", 1985 Ann. Rep. Conf. on Electr. Insu. Dielectr. Phenom., IEEE Report No. 85 CH2165-9, pp.259-265, 1985

59 J. J. O'Dwyer, "The Role of Space Charge in the Theory of Solid-Dielectric Breakdown", IEEE Trans. on EI, Vol. 19, pp1-9, 1984

60 G. Yianakopoulos, J. Vanderschueren and J. Niezette, " Influence of Physical Aging Process on Electrical Properties of Polymers", Proc. Of the 3rd Intern. Conf. on Conduction and Breakdown in Solid Dielectrics, Trondheim, Norway, pp.197-201, 1989

61 Z. Liu, R. Liu, H. Wang and W. Liu, "Space Charge and Initiation of Electrical Trees", IEEE Trans. on EI, Vol. 24, pp.83-89, 1989

62 M. Ieda, "Carrier injection, space charge and electrical breakdown in insulating polymers", IEEE Trans. on EI, Vol. 22, pp261-267, 1987

63 S.B. Lang and D. K. Das-Gupta, "Polarization and Space Charge Distribution in Thermally Poled Polyethylene and a Comparison with Polyvinylidene Fluoride", IEEE Trans. on EI, Vol. 21, pp.399-403, 1986

64 Y. Makekawa, A. Yamaguchi, C. Ikeda, Y. Sekii and M. Hara, "Research and Development of dc XLPE Cables", Proc. 3rd Intern. Confe. On Polymer Insulated Power Cables, pp. 562-569, 1991

65 R. E. Collins, "Measurement of Space Charge Distribution in Electrets", Rev. Sci. Instrument., Vol. 48, pp.83-91, 1977

66 A. Cherifi, M. A. Dakka and A. Toureille, "The Validation of the Thermal Step Method", IEEE Trans. on EI, Vol. 27, pp.1152-1158, 1992

67 S. B. Lang and D. K. Gupta, "Laser Intensity Modulation Method: A Technique for Determination of Spatial Distributions of Polarization and Space Charge in Polymer Electrets", J. Appl. Phys., Vol. 59, pp.2151-2160, 1986

68 P. Laurenceau, G. Dreyfus and J. Lewiner, "New principle for the detection of potential distribution in dielectrics", Phys. Rev. Lett., Vol. 38, pp. 46-49, 1977

69 R. Gerhard-Multhaupt, "Analysis pf pressure wave method for the nondestructiove determination of spatial charge or field distributions in dielectrics", Phys. Rev. B, Vol. 27, pp.2494-2503, 1983

70 M. Haardt and W. Eisenmenger, "High resolution technique for the measuring charge and polarization distribution in dielectrics by piezoelectrically induced pressure step waves", 1982 Annual Report, CEIDP, pp.46-51, 1982

71 F. Chapeau, C. Alquie and J. Lewiner, "The Pressure Wave Propagation Method for the Analysis of Insulating Materials: Application to LDPE Used in HV Cables", IEEE Trans. on EI., Vol. 21, pp.405-410, 1986

72 N. H. Ahmed and N. N. Srinivas, "Review of Space Charge Measurement in Dielectrics", IEEE Trans. on DEI, Vol. 4, pp.644-656, 1997

73 T. Takada and T. Sakai, "Measurement of Electric Field at a Dielectric/Electrode Interface Using an Acoustic Transducer Technique", IEEE Trans. on EI, Vol. 18, pp.619-628, 1983

74 T. Maeno, T. Futami, H. Kushibe, T. Takada and C. M. Cooke. "Measurement of Spatial Charge Distribution in Thick Dielectrics Using the Pulsed Electroacoustic Method", IEEE Trans. on EI, Vol. 23, pp.433-439, 1988

75 Y. Li, M. Yasuda and T. Takada, "Pulsed Electroacoustic Method for Measurement of Space Charge Accumulation in Solid Dielectrics", IEEE Trans. on DEI, Vol. 1, pp.188-195, 1994

76 Y. Li, M. Yasuda and T. Takada, "Pulsed Electroacoustic Method for Measurement of Space Charge Accumulation in Solid Dielectrics", IEEE Trans. on DEI, Vol. 1, pp.188-195, 1994

77 T. Maeno and K. Fukunaga, "High-resolution PEA charge distribution measurement system", IEEE Trans. on DEI, Vol.3, pp.754-757, 1996

78 K. Fukunaga, "Industrial Applications of Space Charge Measurement in Japan", IEEE Electrical Insulation Magazine, Vol. 15, pp.6-18, 1999

79 J. C. Fothergill, "Space charge in dielectrics: old theories and new measurements", 8th International Conference on Dielectric Materials, Measurements and Applications, pp.1-8, Edinburgh, UK, 2000

80 T. J. Lewis, "Electrical effects at interfaces and surfaces", IEEE Trans. on EI, Vol. EI-21, pp.289-295, 1986

81 G. Chen, T. Y. G. Tay, A.E.Davies and T. Takada, "Electrode and charge injection in low-density polyethylene", IEEE Trans. on DEI, in press, 2001

82 R. J. Fleming, M. Henriksen and J. T. Holbøll, "The influence of electrodes and conditioning on space charge accumulation in XLPE", IEEE Trans. on DEI, Vol. 7, pp.561-571, 2000

83 K. S. Suh, E. J. Kim, M. K. Han and T. Takada, "Charge accumulation characteristics in XLPE with heat treated semiconductive electrodes", Proc. of Inte. Conf. on Solid Dielectrics, pp.418-422, Sestri Levante, Italy, 1992

84 K. S. Suh, J. J. Lee, J. Y. Kim, and T. Takada, "Charge formation in PE/Ethylenen-base copolymer laminates", 8th Int. Symp. On High Voltage Engineering, pp. 111-114, Tokohama, Japan, 1993

85 K. S. Suh, J. Y. Kim, C. R. Lee, and T. Takada, "Charge distribution in polyethylene/ethylene vinylacetate laminated and blends", IEEE Trans. on DEI, Vl. 3, pp.201-206, 1996

86 Y. Li, M. Masataka and T. Takada, "Influence of spatial charge distribution of across-linking agent residues in XLPE", Proc, of 3rd Int. Conf. on Properties and Applications of Dielectric Materials, pp.1210-1213, Tokyo, Japan, 1991

87 K. S. Suh, J. H. Koo, S. H. Lee, J. K. Park and T. Takada, "Effects of sample preparation conditions and short chains on space charge formation in LDPE", IEEE Trans. DEI, Vol. 3, pp.153-160, 1996

88 Y. Suzuoki, T. Furuta, H. Yamada, S. O. Han, T. Mizutani, M. Ieda and N. Yoshfuji, "Study of space charge in polyethylene by direct probing: effect of oxidation", IEEE Trans. on EI, pp.1073-1079, 1991

89 K. R. Bambery and R. J. Fleming, "Space charge accumulation in two power cable grades of XLPE", IEEE Trans. DEI, Vol. 5, pp.103-109, 1998

90 R. J. Fleming, M. Henriksen and J. T. HolbØll, "Space charge formation in XLPE –the influence of electrodes and pre-conditioning", 10th Int. Symp. On Electrets, pp.19-22, 1999

91 Y. Li and T. Takada, "Experimental observation of charge transport and injection in XLPE at polarity reversal", J. Phys. D: Appl. Phys. 25, pp. 704-716, 1992

92 J. M. Alison and R. M. Hill, "A model for bipolar charge transport, trapping and recombination in degassed crosslinked polyethylene", J. Phys. D: Appl. Phys. 27, pp1291-1299, 1994

93 K. Kaneko, T. Mizutani and Y. Suzuoki, "Computer simulation on formation for space charge packet in XLPE films", IEEE Trans. on DEI, Vol. 6, pp.152-158, 1999

94 A. Omori, T. Miyazaki, Y. Tanaka, T. Takada and T. Maeno, "Time Dependence of Interface Charge in Polypropylene Laminated Paper under DC Voltage", IEE Japan, Vol.119-A, pp100-105, 1999

95 J. C. Fothergill, L. A. Dissado, J. Alison and A.See, "Advanced pulsed electro-acoustic system for space charge measurement", 8th International Conference on Dielectric Materials, Measurements and Applications, pp.352-356, Edinburgh, UK, 2000

96 A. See, J. C. Fothergill, L. A. Dissado and J. M. Alison, "Measurement of space-charge distribution in solid insulators under rapidly varying voltage using the high-voltage, high-speed pulsed electro-acoustic (PEA) apparatus", Institute if Physics Publishing, Meas. Sci. Technol, 12(2001), pp.1227-1234, 2001

97 A. See, L. A. Dissado, J. C. Fothergill, G. Teyssedrre, C. Laurent, G. C. Montanari and F. Palmieri, "The relationship between charge distribution, charge

packet formation and electroluminescence in XLPE under dc", 7th International Conference on Solid Dielectrics, pp.97-100, Eindhoven, the Netherlands, 2001

98 A. See, L. A. Dissado and J. C. Fothergill, "Electric field requirements for charge packet generation and movement in XLPE", 7th International Conference on Solid Dielectrics, pp.232-235, Eindhoven, the Netherlands, 2001

99 Y. Ohki, Y. Ebinuma and S. Katakai, "Space charge formation in water-treed insulation", IEEE Trans. on DEI, Vol. 5, pp.707-712, 1998

100 Y. Imaizumi, K. Suzuki, Y. Tanaka and T. Takada, "Three-dimensional space charge distribution measurement in electron beam irradiated PMMA", Trans. IEEJ, Vol. 116-A, pp.684-689, 1996

101 Y. Tanaka, H. Kitjima, M. Kodaka and T. Takada, "Analysis and discussion of conduction current based simultaneous measurement of TSC and space charge distribution", IEEE Trans. on DEI, Vol. 5, pp.952-956, 1998

102 F. N. Lim, R.J. Fleming, "The temperature dependence of space charge accumulation and dc current in XLPE power cable insulation", Int. Conf. on Electrical Insulation and Dielectric Phenomena, pp.66-69, 1999

103 J. T. HolbØll, M. Henriksen and J. Hjerrild, "Space charge build-up in XLPE-cable with temperature gradient", Int. Conf. on Electrical Insulation and Dielectric Phenomena, pp.157-160, 2000

104 N. Hozumi, T. Takada, H. Suzuki and T. Okamoto, "Space charge behaviour in XLPE cable insulation under 0.2-1.2MV/cm dc fields", IEEE Trans. DEI, Vol. 5, pp.82-90, 1998

105 T. Takeda, N. Hozumi, H. Suzuki *et al*, "Space Charge Behavior in Full-size 250kV DC XLPE Cables", IEEE Trans. on PD, Vol. 13, pp.28-39, 1998

106 K. Terashima, H. Suzuki, M. Hara and K. Watanabe, "Research and development of ±250kV dc XLPE cables", IEEE Trans. on Power Delivery, Vol. 13, pp.7-15, 1998

107 G. Katsuta, A. Toya, Y. Li, M. Okashta, F. Aida and Y. Ebinuma, "Experimental investigation on the cause of harmfulness of blue water tree to XLPE cable insulation", IEEE Trans. on DEI, Vol. 6, pp.887-891, 1999

108 D. D. Reynolds, *Engineering Principle of Acoustics: Noise and Vibration Control*, Allyn and Bacon, Inc, Boston

109 A. I. Beltzer, *Acoustic of Solids*, Springer-Verlag, Berlin Heidelberg, 1988

110 T. Mureonaka, Y. Tanaka, T. Takada, S. Maruyama and H. Mutou, "Measurement of Space Charge Distribution in XLPE Cable Using PEA System with Flat Electrode", IEEE Annual Report- Conf. on Electrical Insulation and Dielectric Phenomena, San Francisco, pp.266-269, 1996

111 A. V. Carazo, *"Space Charge Measurement Using Pulsed Electroacoustic Technique and Signal Processing"*, Internal report of the University of Southampton, 1997

112 C. C. Barnes, *Power Cables, Their Designs and Installation,* Chapman and Hall Ltd., London, UK, 1966

113 B. M. Weedy, *Electric Power System, 3rd edition,* John Wiley & Sons, Norwich, UK, 1987

114 B. M. Weedy, and D. Chu, "HVDC extruded cables – parameters for determination of stress", IEEE Trans. on PAS, Vol. PAS-103, pp662-667, 1984

115 J. M. Oudin, M. Fallou, and H. Thevenon, "Design and development of dc cables", IEEE Trans. on PAS, Vol. PAS-86, pp.304-311, 1967

116 F. H. Buller, "Calculation of electrical stresses in dc cable insulation", IEEE Trans. on PAS, Vol. PAS-86, pp.1169-1178, 1967

117 Z. Liu, *Electrical Insulation Design, -Power Cables*, Mechanic Industry Press, Beijing, China, 1981 (in Chinese)

118 T. Tanaka, and A. Greenwood, *Advanced power cable technology, Volume I,* CRC Press Inc., USA, 1983

119 I. W. McAllister, G.C. Crichton, and A. Pedersen, "Charge accumulation in dc cable: a macroscopic approach", Conf. Record of the 1994 IEEE International Symposium on Electrical Insulation, Pittsburgh, PA USA, pp.212-216, 1994

120 I. W. McAllister, G.C. Crichton, and A. Pedersen, "Space charge field in dc cables", Conf. Record of the 1996 IEEE International Symposium on Electrical Insulation, Montreal, Canada, pp.661-665, 1996

121 M. Fu, G, Chen and A. E. Davies, Y. Tanaka and T. Takada, "A Modified PEA Space Charge Measurement System for Power Cables", 6th Intern. Conf. on Properties and Applications of Dielectric Materials, Xi'an China, pp.104-107, 2000

122 A. E. Davies, G. Chen and A. Vazquez, " Space Charge Measurement in Dispersive Dielectrics", 5th JICABLE, Versailles, France, pp.733-738, 1999

123 T. Takada and Y. Li, "Pulsed Electroacoustic Techniques to Characterize Charge Accumulation Properties", 6th Int. Conf. on Dielectric Materials, Measurements and Applications, Manchester, UK, pp.104-107, 1992

124 J. B. Bernstein, "Analysis of Electrically Stimulated Acoustic-wave Method for Observing Space Charge in Semi-insulating Material", Physical Review B, Vol. 44, pp.804-814, 1991

125 Y. Zhu, D. Tu and T. Takada, "Mathematical Analysis and Interpretation of Pulsed Electro-acoustic System", 6th Intern. Conf. on Properties and Applications of Dielectric Materials, Xi'an China, pp. 63-66, 2000

126 Y. Li, M. Aihara, "Space Charge Measurement in Thick Dielectric Materials by Pulsed Electro-acoustic Method", Rev. Sci. Instrum, Vol. 66, pp.3909-3916, 1995

127 K. S. Suh, J. J. Lee, J. Y. Kim and T. Takada, "Charge Formation in PE/Etylene-based Copolymer Laminates", 8th ISH, Yokohama, Japan, pp.111-114, 1993

128 M. O'Donnell, E. T. Jaynes and J. G. Miller, "Kramers-Kronig Relationship Between Ultrasonic Attenuation and Phase Velocity", J. Acoust. Soc. Arm. Vol. 69, pp.696-701, 1981

129 W. Sachse and Y. Pao, "On the determination of phase and group velocities of dispersive waves in solids", J. Appl. Phys. Vol. 49, pp.4320-4327, 1978

130 Y. Tanaka, H. Tanaka, T. Takada, Y. Murooka and N. Tomita, "Observation of Charge Accumulating Process in PMMA under Electron Beam Irradiation", 8th Inter. Conf. on Dielectric Materials, Measurements and Applications, Edinburgh, UK, pp.63-67, 2000

131 A. E. Davies, G. Chen, N. Hampton, S. J. Sutter and G. Swingler, "Calculation of charge density and electric stress in XLPE compounds", 5th Inter. Conf. on Insulated Power Cables, Versailles, France, pp.728-732, 1999

132 T. Tanaka, A. Greenwood, *Advanced power cable technology, Volume II,* CRC Press Inc., USA, 1983

133 B. Sanden, E. Ildstad and R. Hegergerg, "Space charge accumulation and conduction current in XLPE insulation", 7th Inter. Conf. on Dielectric Materials, Measurements and Applications, Bath, UK, 1996

134 F. N. Lim, R. J. Fleming and R.D. Naybour, " Space charge accumulation in power cable insulation", IEEE Trans. on DEI, Vol. 6, pp. 273-281, 1999

135 T.J. Lewis, "Electrical effects at interfaces and surfaces", IEEE Trans. on EI, Vol. EI-21, pp. 289-295, 1986

136 T. Fukuyama, T. Nakui, Y. Sekii and T. Maeno, "The influence of additives on the space charge formation and charge profiles in XLPE", Proc. of 6th International Conference on Properties and Applications of Dielectric Materials, pp.51-54, Xian, China, 2000

137 T. Mizutani, K. Shinmura, K. Kaneko, T. Mori, M. Ishioka and T. Nagata, "Space charge behaviours near the interface between different low-density polyethylene" Proc. of 6th International Conference on Properties and Applications of Dielectric Materials, pp.59-62, Xian, China, 2000

138 T. Mizutani, "High voltage dc insulation and space charge", Proc. of 6th International Conference on Properties and Applications of Dielectric Materials, pp.18-23, Xian, China, 2000

139 K. Kaneko, H. Semi, T. Mizutani, T. Mori and M. Ishioka, "Charge transport and space charge formation in low-density polyethylene", Proc. of 6th International Conference on Properties and Applications of Dielectric Materials, pp.71-74, Xian, China, 2000

140 C. G. Garton and K. H. Stark, Nature 176, pp. 1225-1226, 1955

141 L. A. Dissado, and J. C. Fothergill, *Electrical degradation and breakdown in polymers,* Peter Perigrinus, Stevenage, 1992

142 T. J. Lewis, J. P. Llewellyn and M. J. Van der Sluijs, "Electrically induced mechanical strain in insulating dielectrics", IEEE Annual Report, Conference on Electrical Insulation and Dielectric phenomena, 1994

143 R. J. Young and P. A. Lovell, *Introduction to polymers*, Chapman & Hall, London, UK, 1991

144 T. Bourbie, O. Coussy and B. Zinszner, *Acoustic of porous media*, Gulf publishing company, 1987

145 J. T. Holboll, M. Henriksen and J. Hjerrild, "Space charge build-up in XLPE-cable with temperature gradient", Conference on Electrical Insulation and Dielectric Phenomena, 2000

Appendix A Interface of data acquisition and processing program – cable geometry

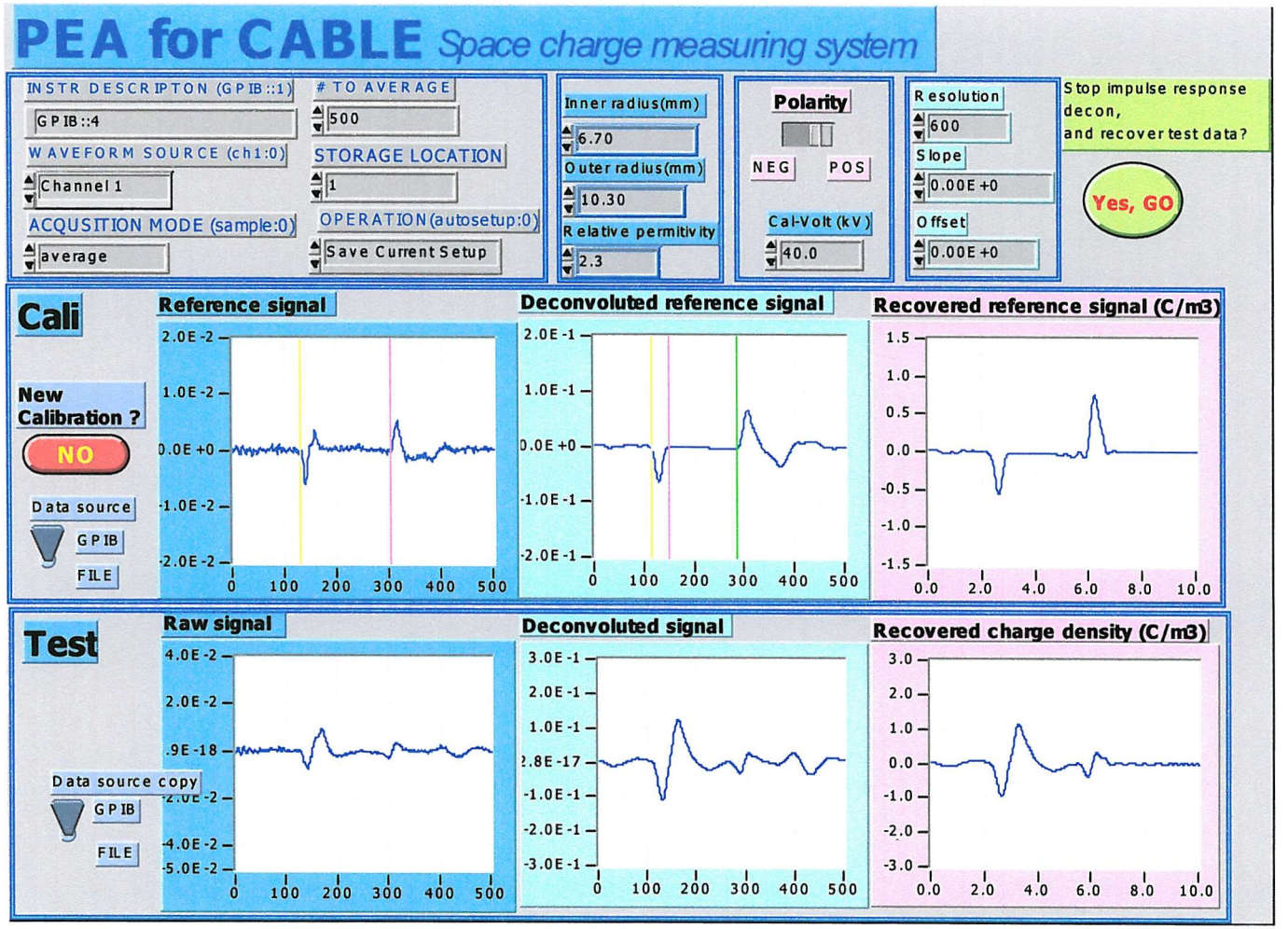

Appendix A Block Diagram of data acquisition and processing – cable geometry

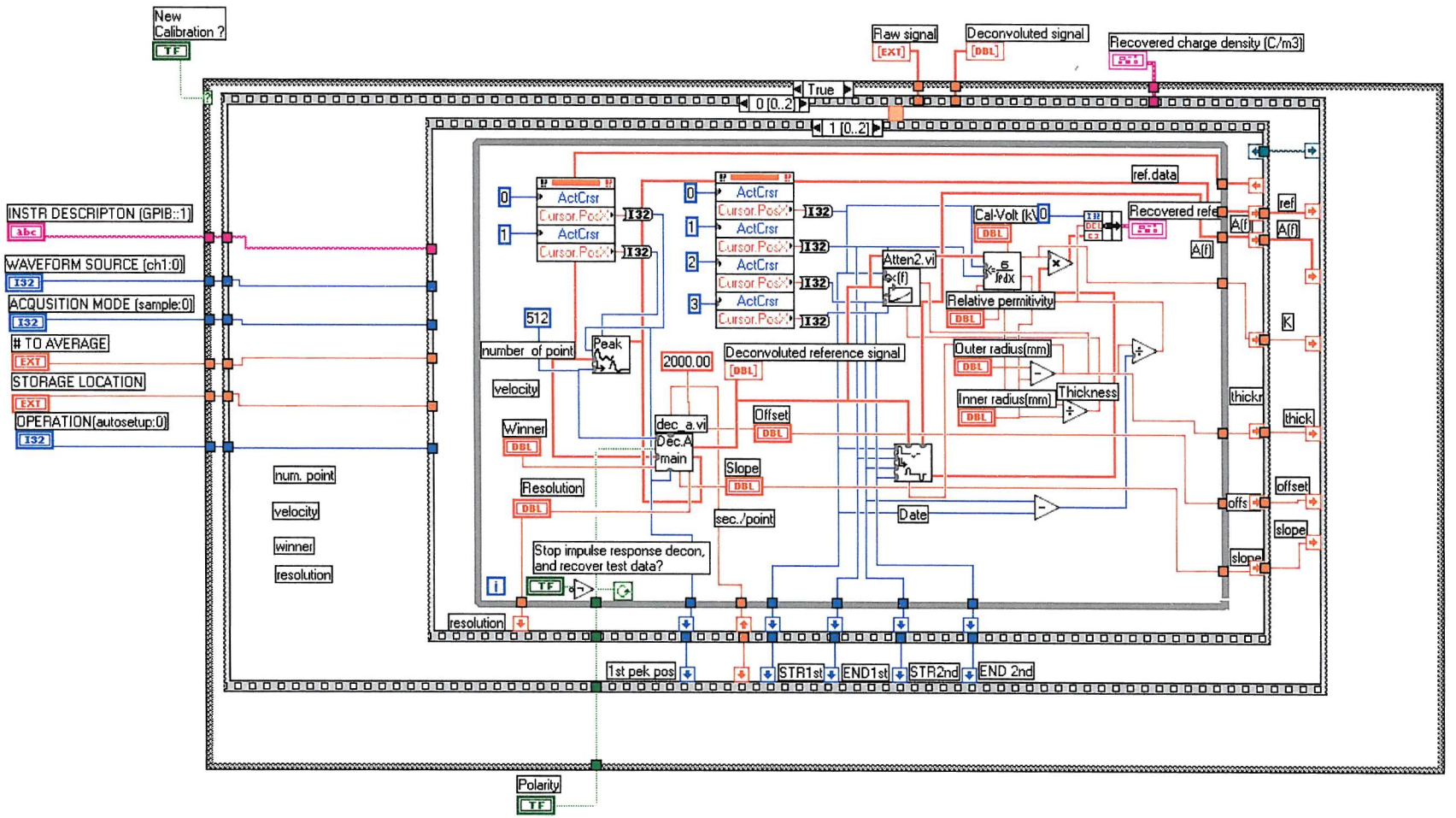

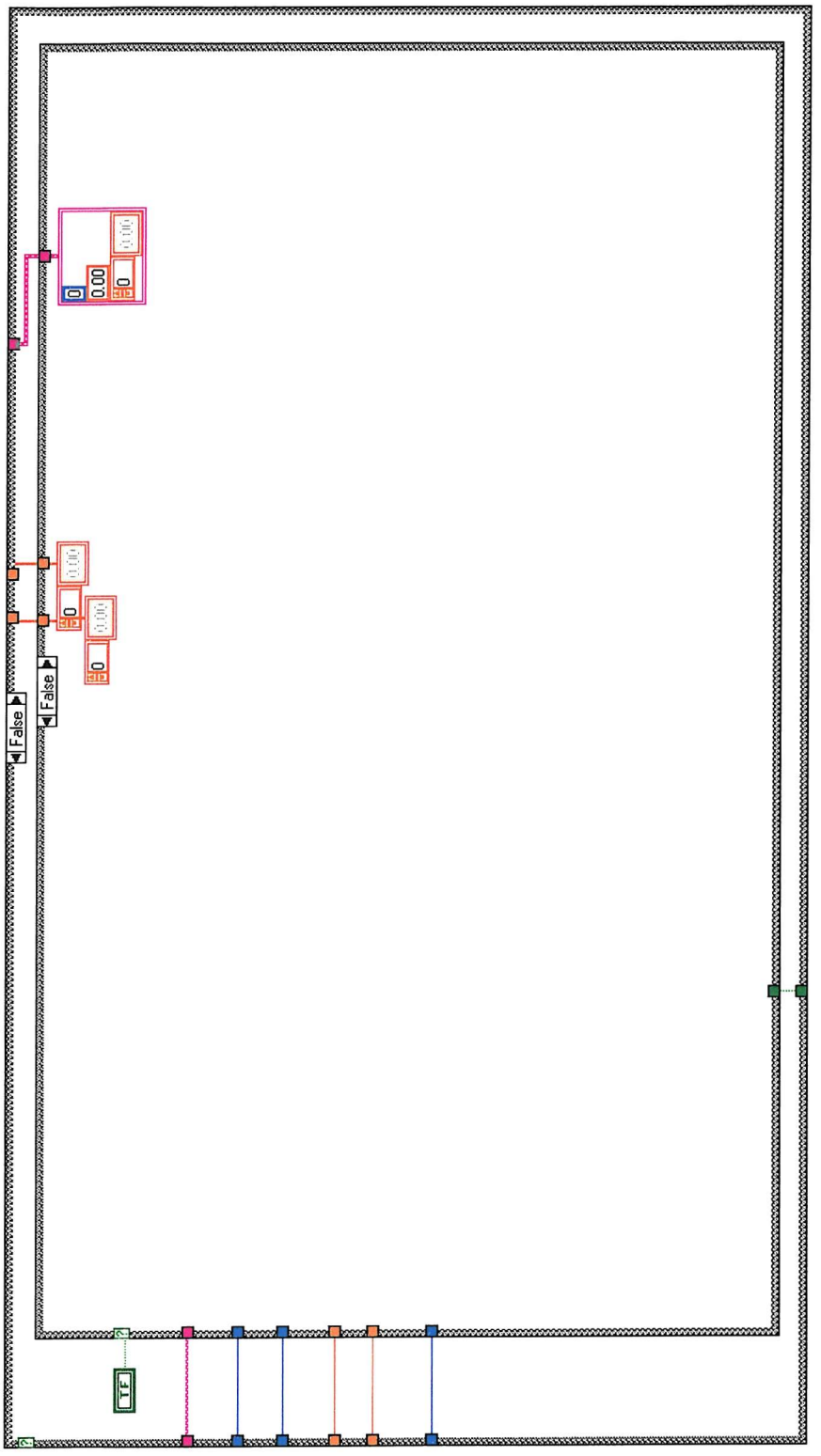
0
0.00
0
0
0
0
False
False
TF

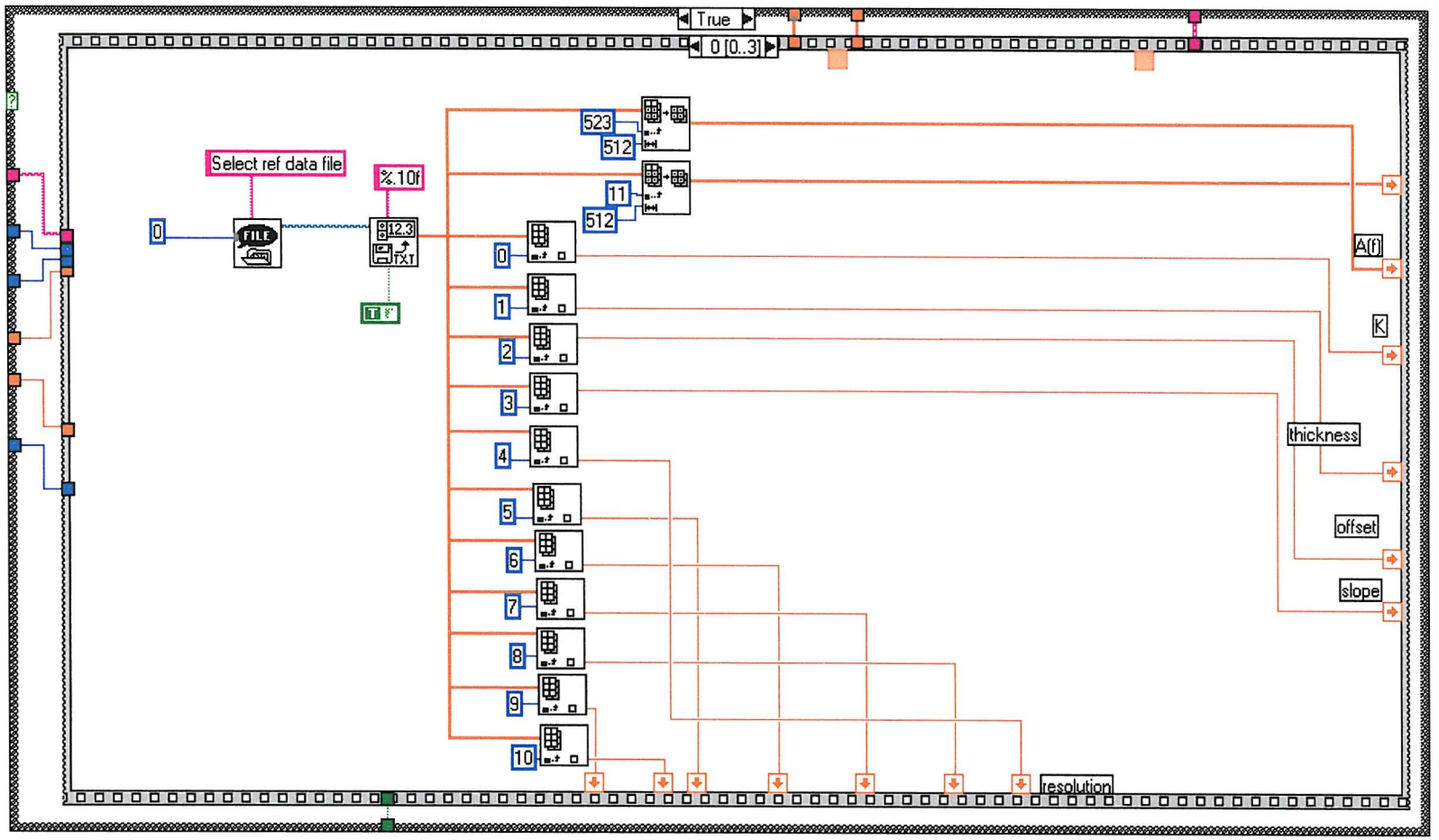
True
0 [0..3]
Select ref data file
%.10f
0
FILE
12.3
TXT
523
512
11
512
0
1
2
3
4
5
6
7
8
9
10
A(f)
K
thickness
offset
slope
resolution

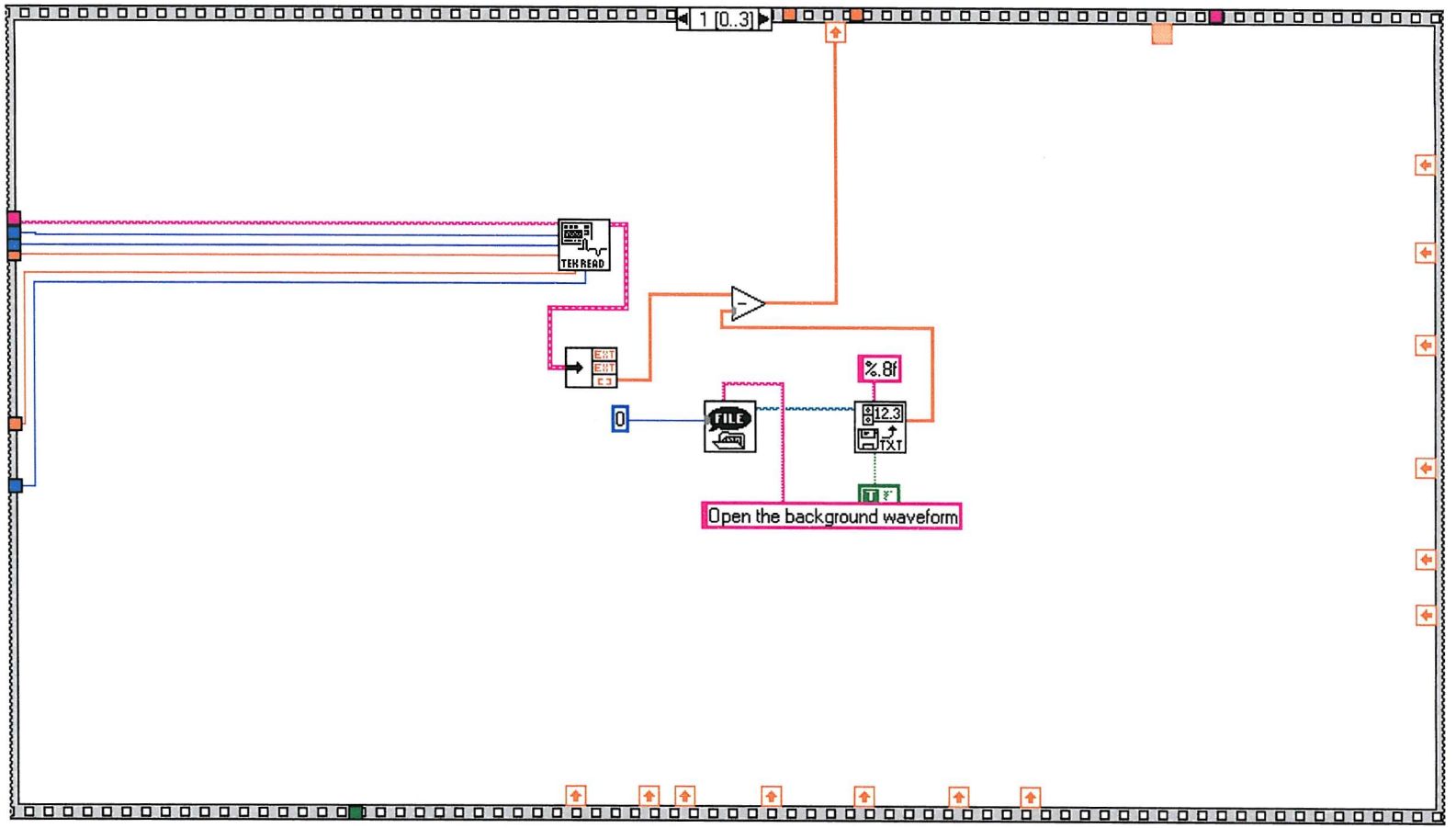
1 [0..3]
TEK READ
%.8f
0
FILE
12.3
TXT
Open the background waveform

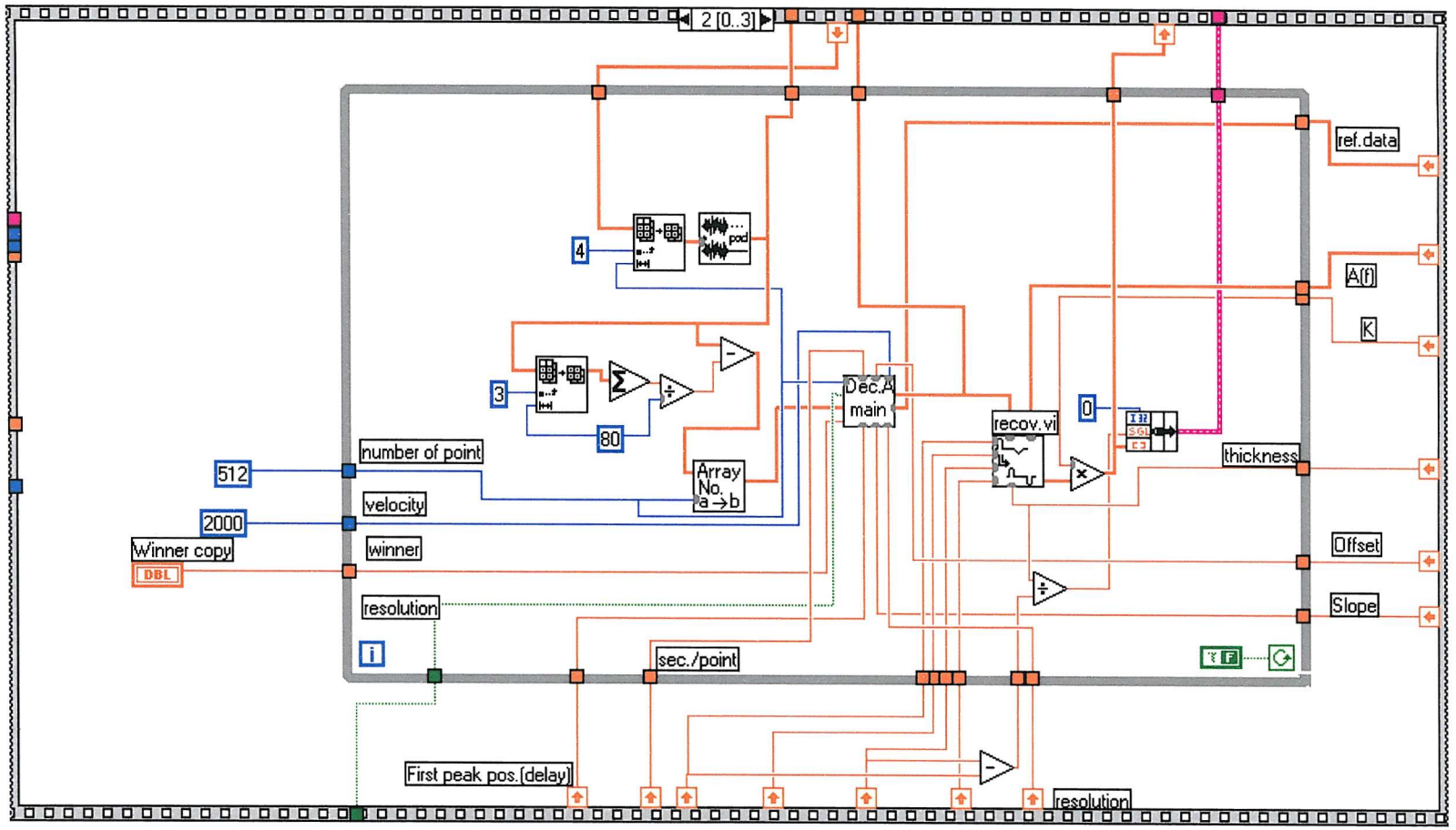
2 [0..3]
ref.data
A(f)
K
4
3
80
Dec.A
main
recov.vi
0
thickness
number of point
512
velocity
2000
winner
Winner copy
DBL
Array
No.
a→b
Offset
Slope
resolution
i
sec./point
First peak pos.(delay)
resolution

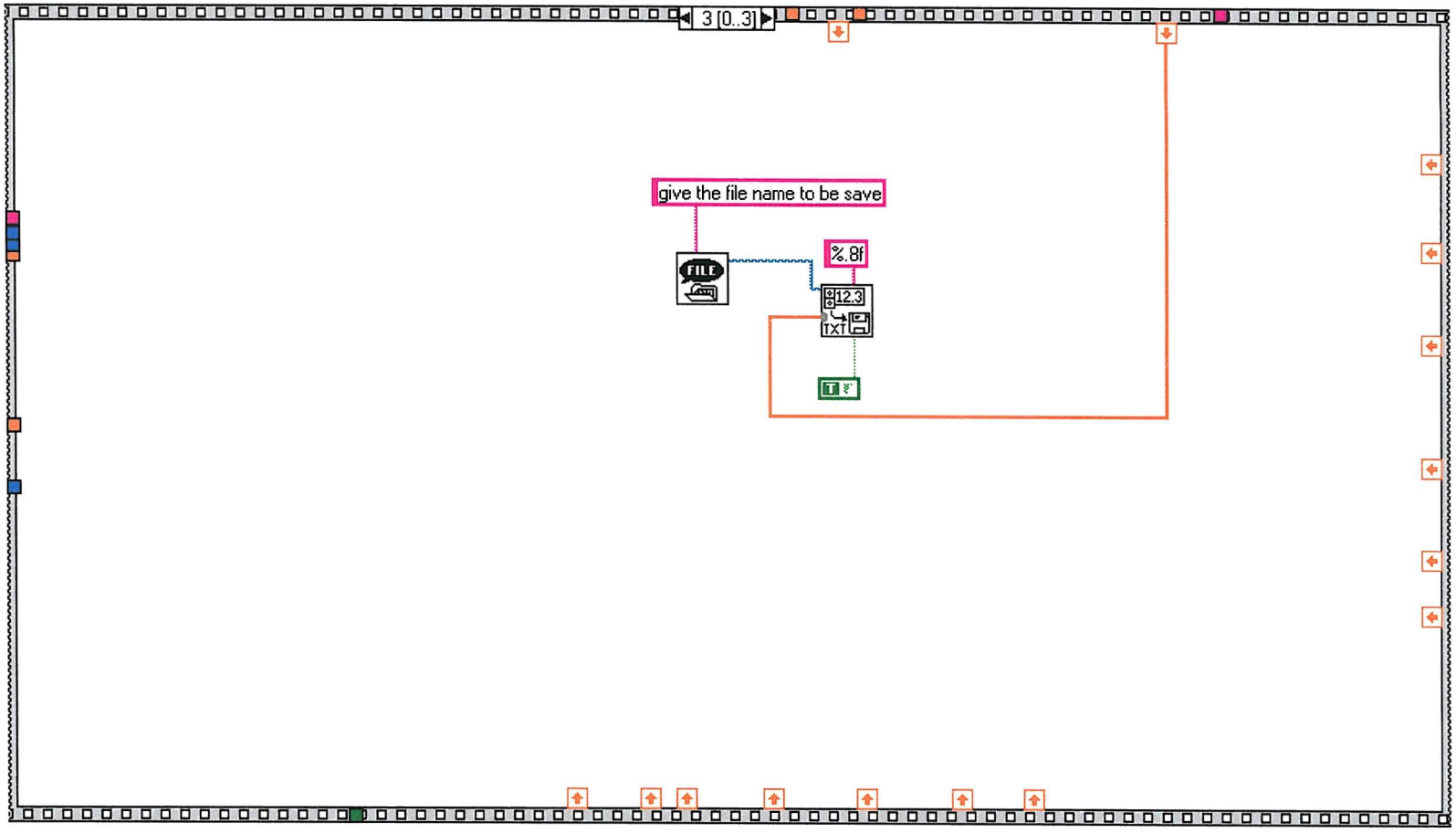
3 [0..3]
give the file name to be save
%.8f
FILE
12.3
TXT

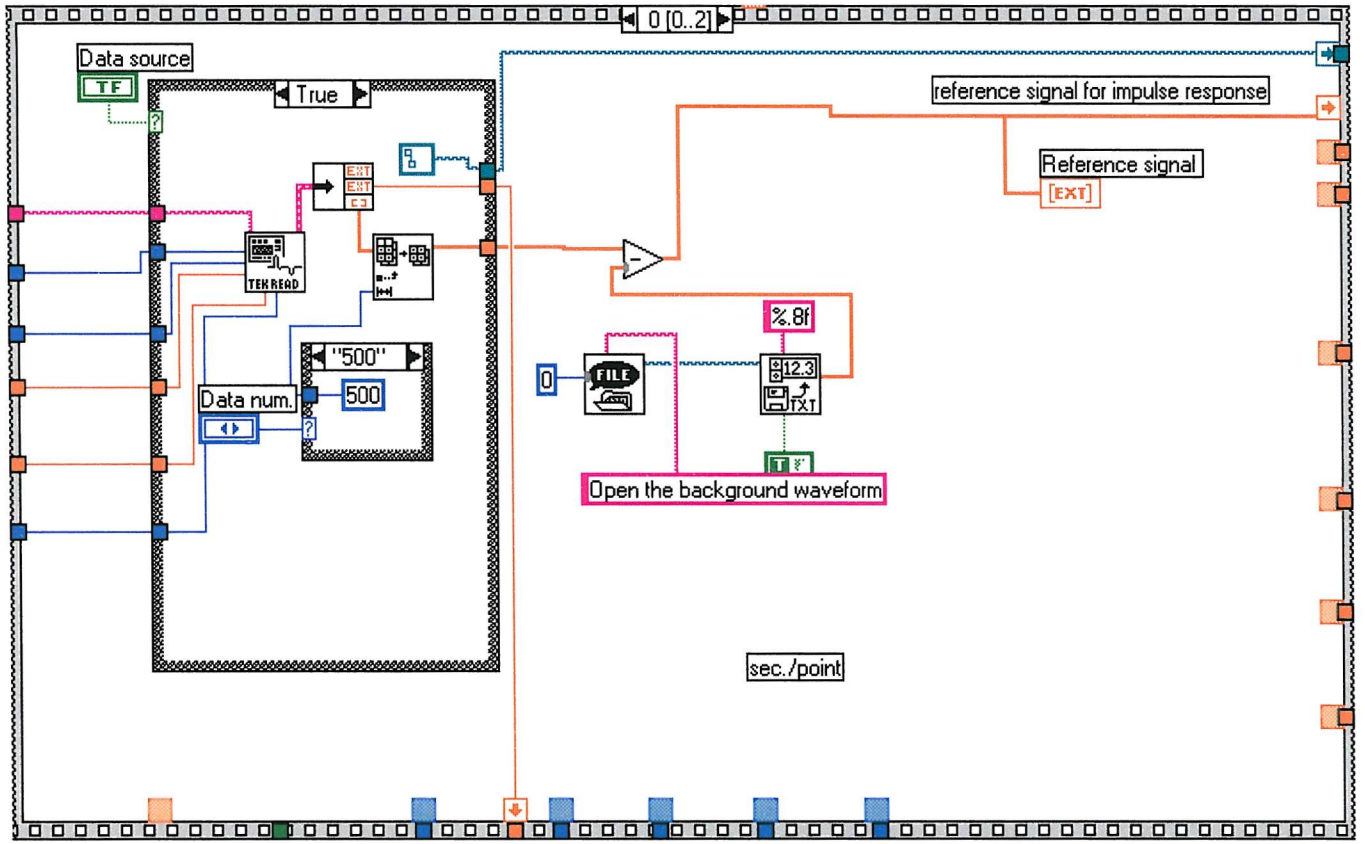
0 [0..2]
Data source
TF
True
reference signal for impulse response
Reference signal
[EXT]
TEK READ
"500"
Data num.
500
%.8f
0
FILE
12.3
TXT
Open the background waveform
sec./point

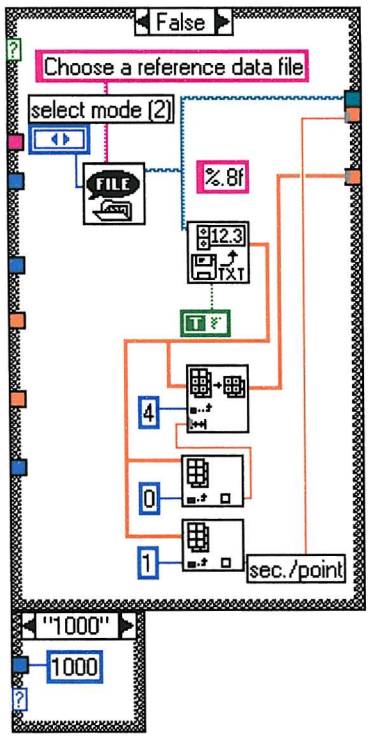
False
Choose a reference data file
select mode (2)
FILE
%.8f
12.3
TXT
4
0
1
sec./point
"1000"
1000

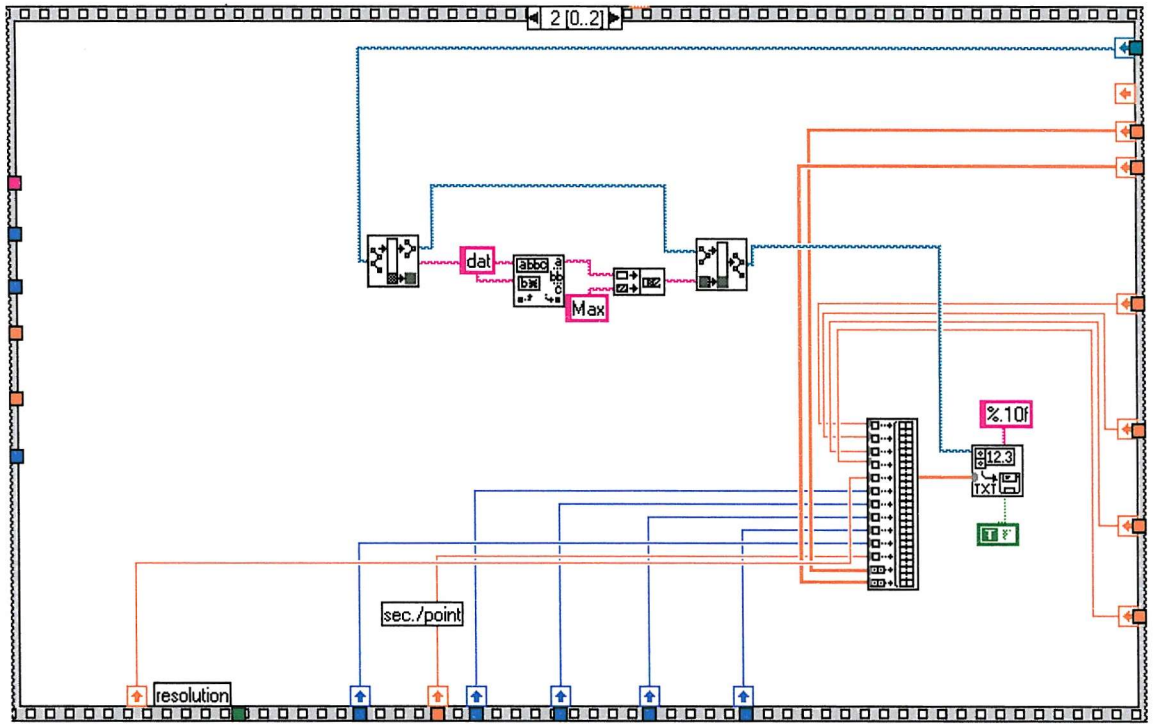
2 [0..2]
dat
Max
%.10f
12.3
TXT
sec./point
resolution

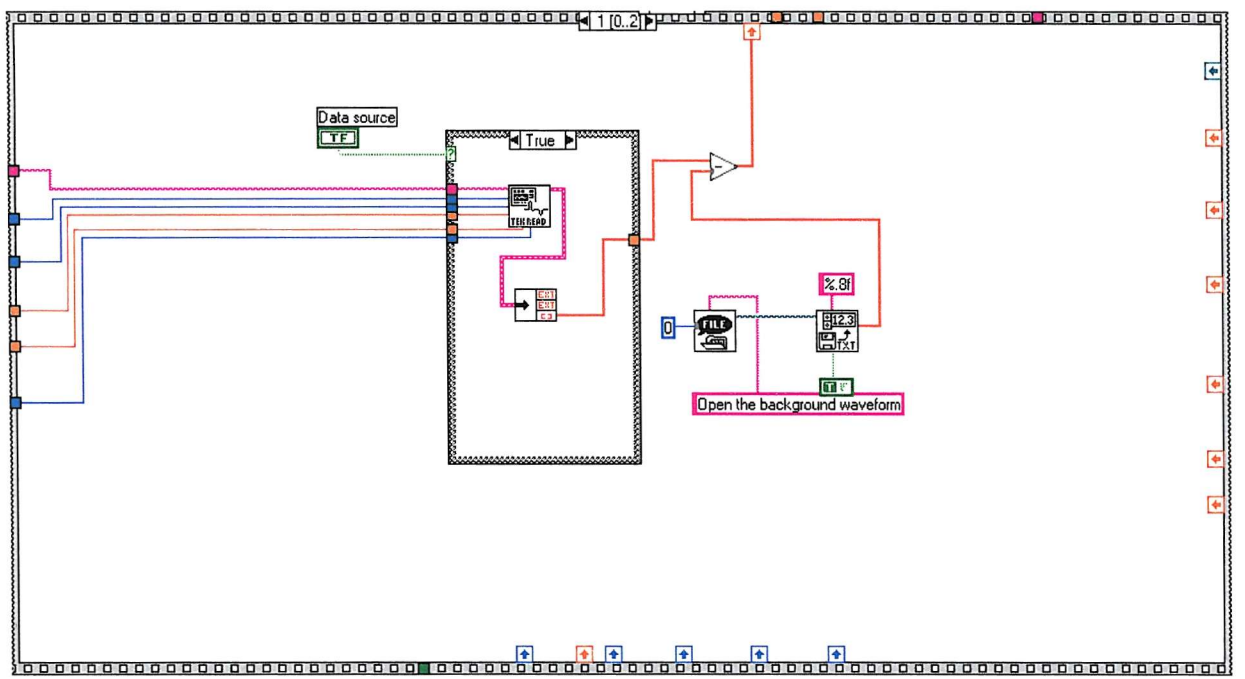
1 [0..2]
Data source
TF
True
TDR READ
%.8f
0
FILE
12.3
TXT
Open the background waveform

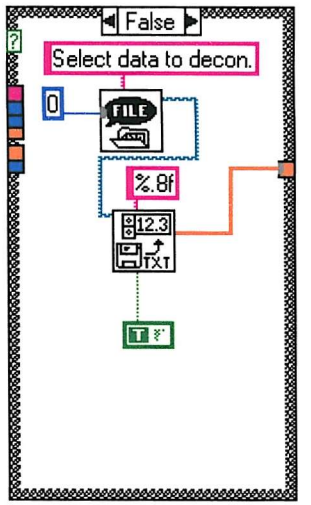
False
Select data to decon.
0
FILE
%.8f
12.3
TXT

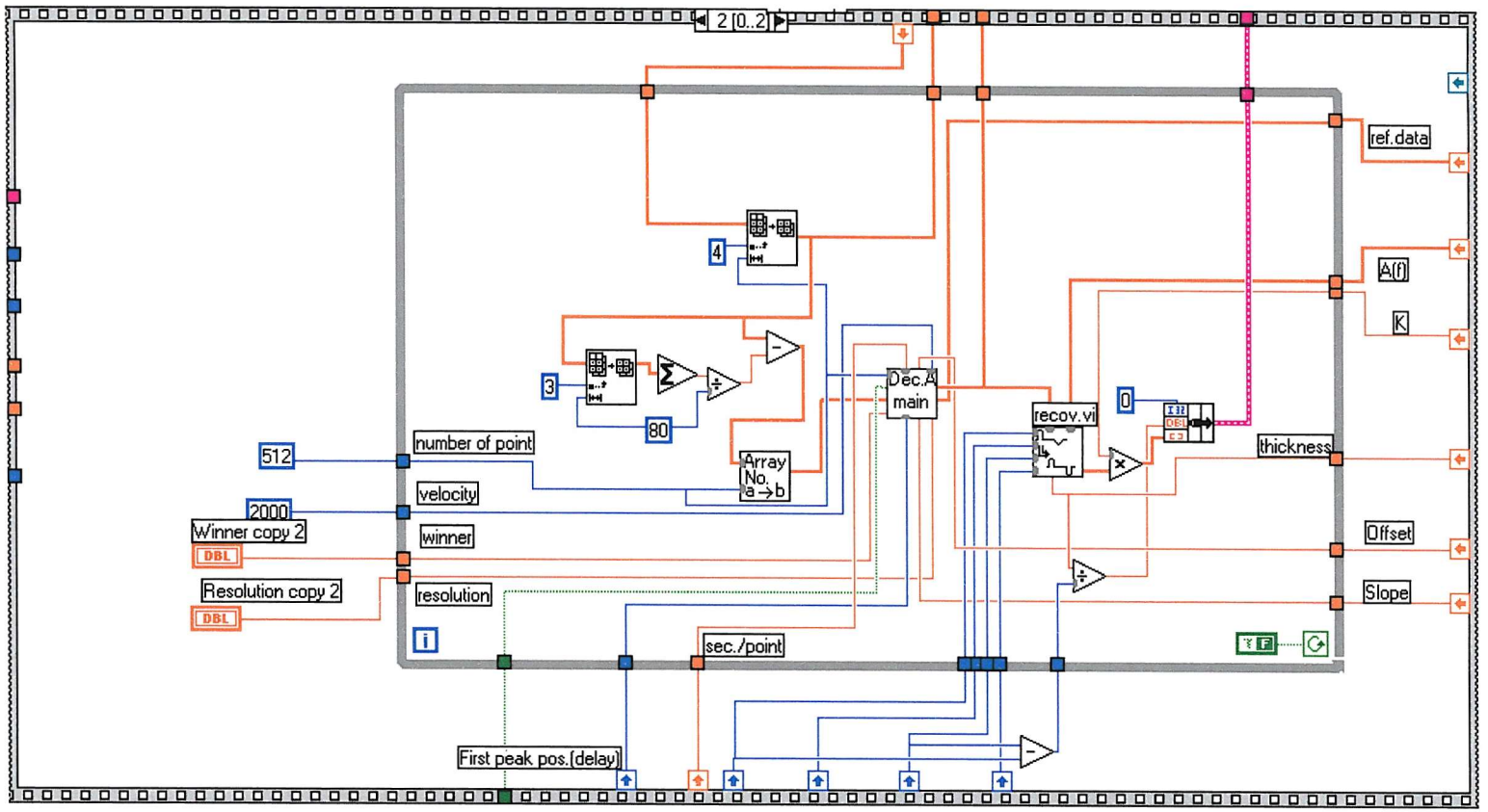
2 [0..2]
ref.data
4
A(f)
K
3
80
Dec.A
main
recov.vi
0
thickness
512
number of point
Array
No.
a→b
velocity
2000
Winner copy 2
DBL
winner
Offset
Resolution copy 2
DBL
resolution
Slope
i
sec./point
First peak pos.(delay)

Appendix B Interface of data acquisition and processing program – planar geometry